EFFECTIVENESS OF POLYMER FIBERS FOR IMPROVING THE DUCTILITY OF MASONRY STRUCTURES

By

THOMAS P. C. HERVILLARD

A thesis submitted in partial fulfillment of
the requirements for the degree of

MASTER OF SCIENCE IN CIVIL ENGINEERING

WASHINGTON STATE UNIVERSITY
Department of Civil and Environmental Engineering

DECEMBER 2005

To the Faculty of Washington State University:

The members of the Committee appointed to examine the thesis of THOMAS P. C. HERVILLARD find it satisfactory and recommend that it be accepted.

_____
Chair

_____

_____

ACKNOWLEDGMENTS

I would like to acknowledge the financial support provided by the Northwest Concrete Masonry Association, the Masonry Industry Promotion Group of Spokane Washington, and the W.R. Grace & Co.-Conn.

I would like to thank Dr. David McLean for serving as chair of my committee, particularly for his invaluable help, patience, and guidance throughout my project and my graduate curriculum. I would like to thank him for giving me a chance to join Washington State University and for allowing me to live such a wonderful experience in the United States. I would like to thank Dr. Cole McDaniel for serving on my committee and for his valuable assistance throughout this project. I also would like to thank Dr. William Cofer for serving on my committee, for his advice, and also for his perpetual jokes that made the time spent at Sloan Hall such a good one.

I would like to give a very special acknowledgment to Dr. Marie-Pierre Laborie who helped me to first come to Washington State University for an internship under her guidance, introducing me to Dr. McLean and making this happen for me.

I would like to thank the staff of the Civil and Environmental Engineering Department and the members of the Wood Materials and Engineering Laboratory for their support, especially Karl Englund for his precious explanations on statistics. I would like to acknowledge Matt Snook and Karl Olsen for their help when I needed it.

Finally, I would like to thank Blandine Valle for her constant support throughout my undergraduate and graduate curriculum, and thanks to my parents for everything they have done for me.

EFFECTIVENESS OF POLYMER FIBERS FOR IMPROVING

THE DUCTILITY OF MASONRY STRUCTURES

Abstract

by Thomas P. C. Hervillard, M.S.
Washington State University
December 2005

Chair: David I. McLean

Provisions in the 2005 MSJC *Building Code Requirements for Masonry Structures* establish limits on the amount of flexural reinforcement for use in masonry structures. These limits are based on material strain capacities and specified drift limits and are intended to provide ductile response. The effect of these provisions has been to restrict the use of masonry systems for many traditional applications. Previous research has demonstrated that steel confinement plates and seismic reinforcement combs can be placed in the masonry mortar joints to increase the masonry compressive strain capacity and, thereby, improve ductility. The goal of the present research is to investigate the effectiveness of adding polymer fibers into the grout as a technique for improving the ductility of masonry.

The research presented in this thesis investigated the stress-strain behavior of fiber-reinforced masonry piers subjected to compressive loading. Thirty masonry piers were constructed: fifteen of concrete block masonry and fifteen of clay brick masonry. The cells of the masonry in the piers were grouted solid, with one-third of the piers containing grout with no fibers, one-third with grout containing fibers at a dosage of 0.12% by weight, and one-third with grout containing fibers at a dosage of 0.20% by weight. The pier specimens were loaded in compression to failure under a controlled rate of displacement. Average stress-strain curves were

determined for each material type and level of fiber dosage. A statistical analysis was conducted at a 90% confidence level to determine whether or not the fibers had an effect on the peak stress values, the corresponding strain values and the strains at 50% of the peak stresses of the compressive piers. Results showed that the fibers increased the ductility of masonry piers made of concrete blocks and clay bricks, but the improvements were lower than those observed when other types of confinement reinforcement were used, namely the steel plates and the seismic combs.

The Modified Kent-Park model was used to characterize stress-strain curves for masonry with and without fibers in the grout. The model was also used to characterize results from previous studies using steel plates and seismic combs as masonry confinement reinforcement. Previous shear walls tests were modeled with commercial software using material properties obtained from the Modified Kent-Park models. Moment-curvature analyses provided predictions of the load-displacement response for each wall. Comparisons between results from previous tests on shear walls and the analytical results of this study were performed. It was found that the fibers, as well as the other forms of confinement reinforcement previously studied, provided only modest increases in ductility and drift capacity for masonry shear walls. The ductilities obtained are likely to be less than what would be expected for the design of reinforced structural elements in seismic areas.

TABLE OF CONTENTS

LIST OF FIGURES

LIST OF TABLES

CHAPTER ONE: INTRODUCTION

1.1 BACKGROUND

Older masonry structures have experienced damage and even collapse during seismic events. Research during the past three decades has resulted in significant improvements, and modern masonry structures have performed very well in recent earthquakes. Past research has investigated the compressive behavior of piers made of concrete block masonry and clay brick masonry in order to better understand the stress-strain behavior of these materials and the effects of different types of confinement reinforcement. Several studies on confined piers with steel plates or seismic combs incorporated in the mortar joints have shown increases in compressive strain capacity.

As a result of recent changes in the masonry building codes, there is interest in utilizing these confinement techniques to improve the performance of masonry structures during seismic events, particularly in regard to improving the performance of masonry shear walls. The behavior of shear walls during earthquakes is mainly influenced by inelastic deformation mechanisms in shear and flexure. Previous studies have shown that the modes of failure are different depending upon whether the response is primarily due to shear or flexure. In the first case, the failure is brittle, while it is more gradual in the second case. The amount of flexural reinforcement and the aspect ratio of the walls also influence the modes of failure. The various types of confinement reinforcement investigated in masonry piers were also tested in shear walls subjected to in-plane loading. An increase in compressive strain capacity was reported in the walls, resulting in improvements in ductility.

1.2 SCOPE AND OBJECTIVES

This study evaluated the effectiveness of various confinement reinforcement methods on the compressive performance of masonry piers as well as in shear walls. Tests were conducted on masonry piers whose cores contained polymer fibers mixed into the grout in order to determine their stress-strain behavior in compression. The results, as well as those of previous studies using steel plates or seismic combs as confinement reinforcement in masonry piers, were used to characterize the stress-strain behavior for modeling shear walls. An evaluation of the load-displacement capacity was conducted and compared to experimental results of previous studies. Increased amounts of confinement reinforcement were also studied analytically in order to evaluate the improvement in load-displacement capacity of shear walls.

This thesis first reviews the previous studies conducted on masonry piers and shear walls. It then describes the experiments conducted on fiber reinforced masonry piers and the results that were obtained. Modeling of the stress-strain behavior of the masonry piers is discussed, and a description of the shear wall models is provided. A comparison between results from previous studies and the analytical results of this study is also included. Finally, an investigation of the effects of increased confinement reinforcement amounts on the load-displacement capacity of the modeled shear walls is given. Conclusions based on experimental and analytical results were reached on the overall effectiveness of the confinement reinforcement on the masonry compressive behavior. Improvements in wall performance from each confinement technique were compared.

CHAPTER TWO: LITERATURE REVIEW

2.1 INTRODUCTION

The past thirty years have seen many studies conducted on the behavior of masonry piers and shear walls subjected to compressive loading and in-plane lateral loading. These studies have led to the development of various confinement reinforcement methods for improving the behavior of masonry structures during seismic events. This chapter provides a review of this previous research.

2.2 2005 MASONRY STANDARDS JOINT COMMITTEE (MSJC) BUILDING CODE

According to the 2003 International Building Code, "masonry structures and components shall comply with the requirements in Section 1.13.2.2.2 of ACI 530/ASCE 5/TMS 402 and Section 1.13.1, 1.13.2, 1.13.3, 1.13.4, 1.13.5, 1.131.6 and 1.13.7 of ACI 530/ASCE 5/TMS 402 depending on the structure's seismic design category as determined in Section 1616.3". The 2005 Masonry Standards Joint Committee Building Code, in order to ensure a minimum ductility capacity in masonry structures, establishes provisions that limit the amount of flexural reinforcement, ρ_{max}, that can be placed in masonry shear walls. Two limit values for fully grouted masonry structures were established and are described in the commentaries of Section 3.3.3.5 of the 2005 MSJC. The goal of the limits is to avoid the ultimate masonry compressive strain being exceeded, which would result in crushing of the compressive zone of the member, prior to a certain ductility level being reached.

Assuming the strain distribution presented in Figure 2.1 for a fully-grouted shear wall subjected to in-plane loading, the forces in the masonry, C_m, in the tensile steel, T_s, and in the

compressive steel, C_s, can be calculated using Equations 2.1, 2.2 and 2.3, respectively. Depending on the amount of curvature ductility desired, the tensile strain factor, α, used in these equations varies from 1.5 to 4.

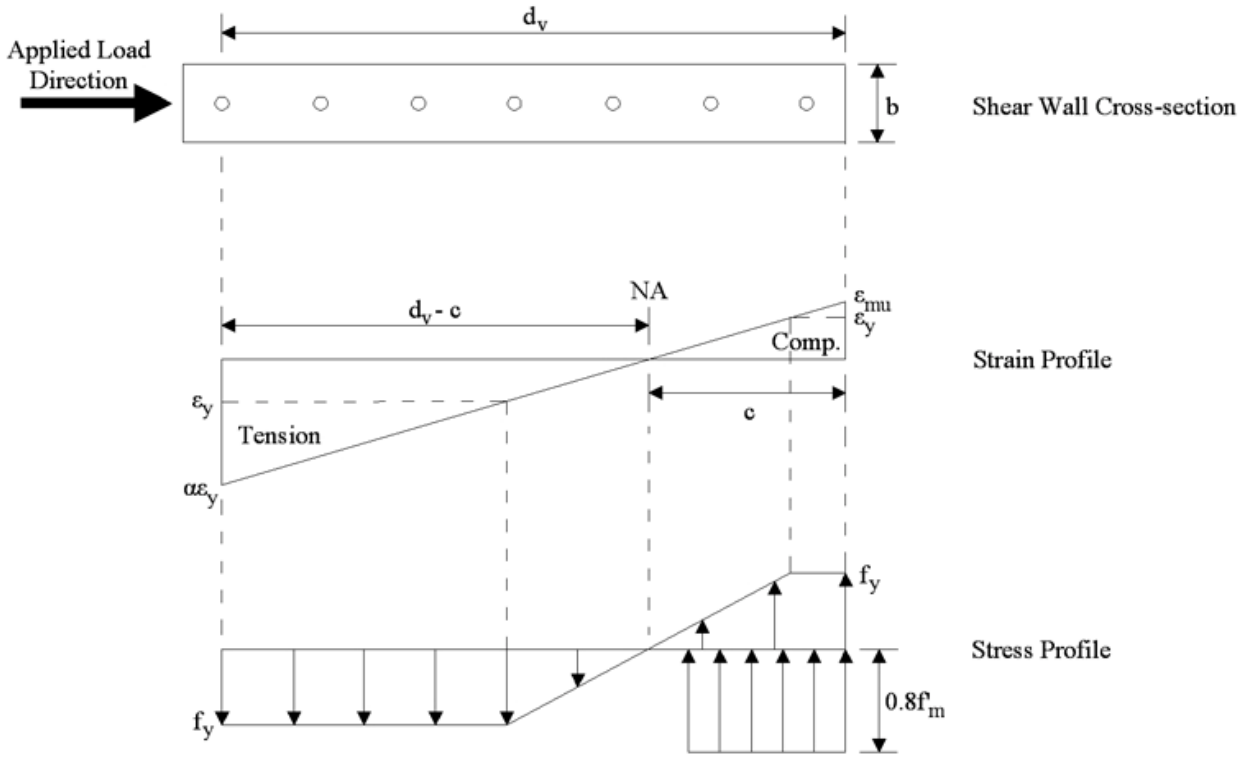

Figure 2.1: Strain and stress profiles

$$C_m = 0.8f'_m\left[0.8\frac{\varepsilon_{mu}}{\varepsilon_{mu}+\alpha\varepsilon_y}d_v\right]b \qquad \textit{Equation 2.1}$$

$$T_s = f_y A_s\left(\frac{\alpha\varepsilon_y}{\varepsilon_{mu}+\alpha\varepsilon_y}\right)\left[\frac{\alpha\varepsilon_y-\varepsilon_y}{\alpha\varepsilon_y}+\left(\frac{1}{2}\right)\frac{\varepsilon_y}{\alpha\varepsilon_y}\right] \qquad \textit{Equation 2.2}$$

$$C_s = f_y A_s \left(\frac{\varepsilon_{mu}}{\varepsilon_{mu} + \alpha\varepsilon_y} \right) \left[\frac{\varepsilon_{mu} - \varepsilon_y}{\varepsilon_{mu}} + \left(\frac{1}{2} \right) \frac{\varepsilon_y}{\varepsilon_{mu}} \right] \qquad \textit{Equation 2.3}$$

Where:

- C_m is the masonry force, lb;
- f'_m is the specified compressive strength of masonry, psi;
- ε_{mu} is the maximum usable compressive strength of masonry, in./in.;
- α is the tension reinforcement strain factor;
- ε_y is the tensile reinforcement yield strain, in./in.;
- d_v is the actual depth of masonry in direction of shear considered, in.;
- b is the width of the section, in.;
- T_s is the steel tension force, lb;
- f_y is the specified yield strength of steel for reinforcement, psi;
- A_s is the effective cross-sectional area of steel reinforcement, in²; and
- C_s is the steel compression force, lb.

Two formulas are provided in the 2005 MSJC to calculate the maximum flexural reinforcement ratio, ρ_{max}, and they depend on the tensile and compressive steel present in the walls. If the shear walls only include tension steel, ρ_{max} can be calculated using Equation 2.4. If there is compression steel with an area equal to the tension steel, A_s, ρ_{max} can be evaluated using Equation 2.5.

$$\rho_{\max} = \frac{A_s}{bd} = \frac{0.64 f'_m \left(\frac{\varepsilon_{mu}}{\varepsilon_{mu} + \alpha \varepsilon_y} \right) - \frac{P}{bd}}{f_y} \qquad \textit{Equation 2.4}$$

$$\rho_{\max} = \frac{A_s}{bd} = \frac{0.64 f'_m \left(\frac{\varepsilon_{mu}}{\varepsilon_{mu} + \alpha \varepsilon_y} \right) - \frac{P}{bd}}{f_y - \min\left\{ \varepsilon_{mu} - \frac{d'}{d}\left(\varepsilon_{mu} + \alpha \varepsilon_y\right), \varepsilon_y \right\} E_s} \qquad \textit{Equation 2.5}$$

Where:

- ρ_{max} is the maximum flexural reinforcement ratio;
- P is the total factored axial load, lb

  $= C_m - T_s + C_s$ (by statics);
- d' is the distance from the extreme compression fiber to the centroid of the compression reinforcement, in.; and
- E_s is the specified modulus of elasticity of steel, psi.

According to 2005 MSJC, no confinement reinforcement is required for the case of structures that will respond elastically because the ultimate masonry compressive strain will not be exceeded. In the case of structures responding inelastically, Section 3.3.3.5 described previously can not be applied, and therefore Section 3.3.6.7 has to be considered. In this section, it is stated that the need for special boundary elements (see Figure 2.2) at the edges of shear walls shall be evaluated in accordance with Sections 3.3.6.8, 3.3.6.9 and 3.3.6.10. Boundary elements are basically confined areas that will develop larger strain capacities than elsewhere in the wall and that will improve the behavior of the entire wall. For walls bent in single curvature

designed by Section 3.3.6.8, boundary elements shall be provided over portions of compression zones and be extended vertically until reaching the larger of l_w or $M_u/4V_u$, where l_w is the length of the entire wall or of the segment considered in the direction of shear force in in., M_u is the factored moment in in.-lb, and V_u is the factored shear force in lb. For walls bent in double curvature, Section 3.3.6.9 states that special boundary elements shall be provided "at boundaries and edges around openings…..where the maximum extreme fiber compressive stress, corresponding to factored forces including earthquake effect, exceeds 0.2 f'_m. The special boundary element shall be permitted to be discontinued where the calculated compressive stress is less than 0.15 f'_m." Note that the behavior of the boundary elements is directly linked to their strain capacities and influences the overall behavior of the masonry wall.

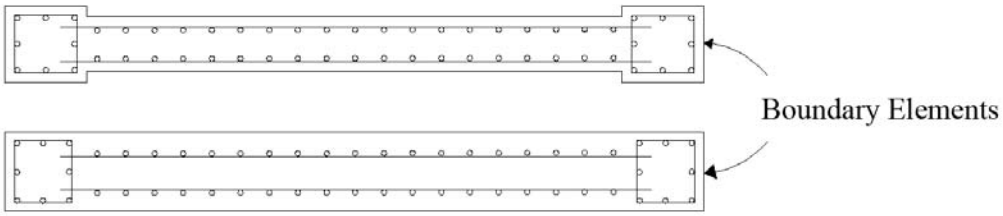

Figure 2.2: Boundary elements

2.3 COMPRESSIVE BEHAVIOR OF CONFINED MASONRY PIERS

2.3.1 Priestley and Elder

Priestley and Elder (1983) investigated the stress-strain behavior of fully-grouted reinforced concrete masonry piers loaded in compression. They conducted tests on piers where thin type 304 stainless steel plates (0.122 in. (0.3 cm) thickness) were placed in the mortar beds in order to increase the peak stress and the strain capacity of the piers (see Figure 2.3). These plates were first proposed by Priestley and Bridgeman in 1974. Tests were run at two different

strain rates (5×10^{-6}/sec and 5×10^{-3} to 6×10^{-3}/sec) to compare the results between low traditional testing rates and high rates that may be experienced during seismic events. Parameters investigated were block width (5.5 in. (14 cm) or 7.5 in. (19 cm)), longitudinal reinforcement within the grout cells (two D20 grade 275 bars), and the presence of the steel plates. A volumetric confinement ratio of 0.007 was used, corresponding to the volume of a steel plate divided by the volume of material that it confines.

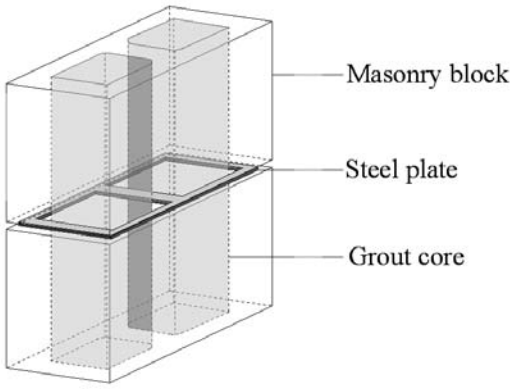

Figure 2.3: Detail of the placement of steel plates in the mortar beds used by Priestley and Elder (1983)

Tests were conducted using a servo-hydraulically-controlled universal testing machine operated under controlled rates of ram travel. The five-course piers consisted of alternate courses of one full block and two half blocks. Two adjustments were applied to the test results. The first adjustment accounted for the machine stiffness within both the ascending and descending branches of the load-displacement curves. The second adjustment resulted from observations made during testing. The piers, after reaching the peak stress values, developed cracks in the central region but typically not over the entire height, leaving the top and bottom courses intact.

If linear elastic behavior is assumed, the displacement due to the relaxation of the two intact courses increases deformations of the cracked courses. Recovered displacements of the end courses were calculated and added to the displacement measurements in order to calculate strains in the damaged region. This adjustment was applied only for the declining branches of the stress-strain curves. The damaged region was defined after each test based on physical observations.

Results showed that the addition of confining plates dramatically changed the mode of failure of the piers. Vertical splitting present in the unconfined piers almost disappeared when steel plates were used, and only one or two blocks were damaged due to compression forces, even when the D20 bars buckled. Confined piers showed higher strains at peak stress, and the slope of the declining branches of the stress-strain diagrams was flatter, resulting in an increase in the strain capacity of the piers (see Figure 2.4 and Figure 2.5).

An increase of the strain rate from 0.05%/sec to 0.5%/sec resulted in an average increase of about 17% in the strength value and steepened the descending part of the stress-strain curve. Priestley and Elder recommended designing for a 0.0025 ultimate compressive strain for unconfined masonry and 0.008 for confined masonry. Block width and vertical reinforcement did not show significant effects on pier performance.

The second goal of the project was to develop a behavioral model of the experimental results. Priestley and Elder (1983), after consideration of several approaches, determined that a modified Kent-Park model provided the best fit to their experimental stress-strain curves (see Figure 2.4 and Figure 2.5). This model is discussed later in this chapter.

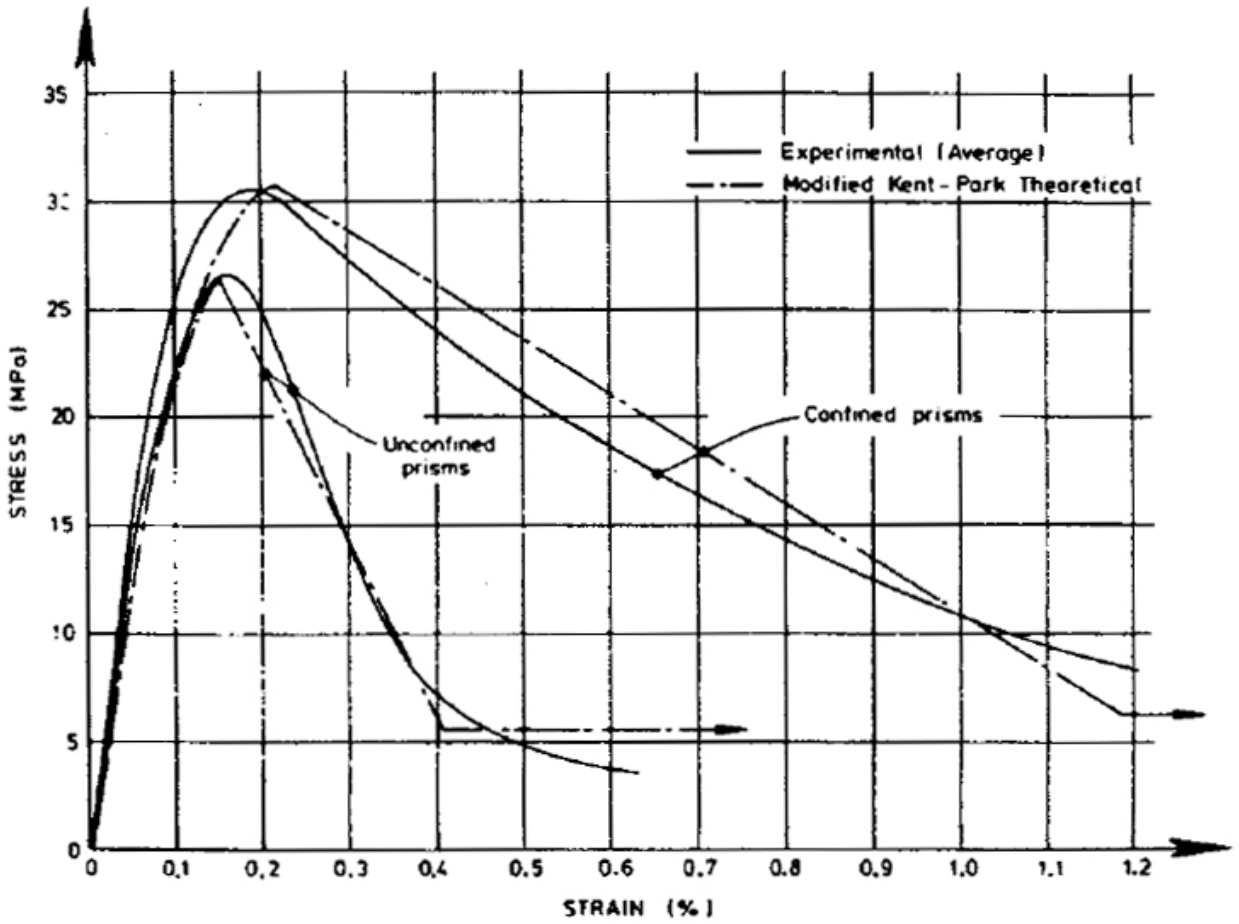

Figure 2.4: Stress-strain curves from experimental and theoretical tests at low strain rates from Priestley and Elder (1983) (1 MPa = 145 psi)

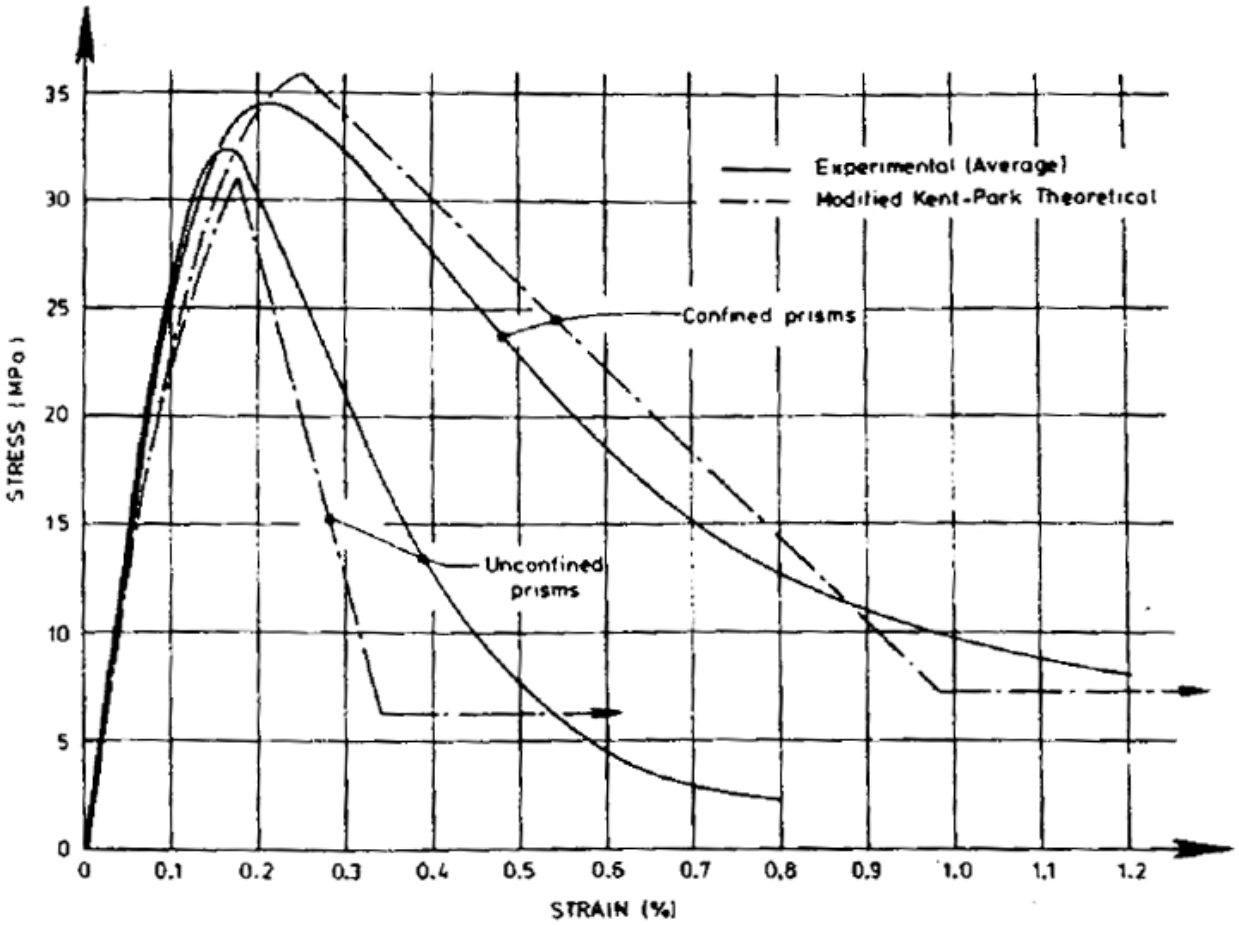

Figure 2.5: Stress-strain curves from experimental and theoretical tests at high strain rates from Priestley and Elder (1983) (1 MPa = 145 psi)

2.3.2 Hart et al

Hart et al (1988) investigated the effects of several types of confinement on the stress-strain behavior of fully grouted reinforced concrete masonry piers in compression. The types of confinement studied included horizontal steel rebar (No. 3 bars at 8 in. or 4 in. spacing), Priestley's stainless steel plates, open or closed wire meshes, cages, hoops and spiral reinforcement. Piers tested were four courses high and made of full blocks. The seventy-one piers tested all had an 8-in. (20.3 cm) nominal thickness. Clearance requirements of the 1988

UBC Section 2409(e)-2 were provided by choosing appropriate dimensions of the reinforcement. Two types of vertical reinforcement were considered. Type 1 corresponded to the minimum UBC requirement, while type 2 doubled this value. Volumetric confinement reinforcement ratios for piers with plates were 0.005 and 0.01 for type 1 and 2, respectively. With comb confinement, these ratios were equal to 0.001 and 0.002, respectively. Tests were conducted using a compression test machine operated under displacement control.

Results showed that unreinforced and vertically reinforced unconfined piers behaved the same way, failing in a very brittle manner. The ascending branches of the stress-strain curves were not affected by the different types of confinement, while the descending branches presented larger areas under the curves and greater ultimate strain values (see Figure 2.6 and Figure 2.7). Priestley's steel plates provided the best results in regard to increasing peak stress values, areas under the curves and ultimate strain values. The open wire mesh performed very well and produced results very close to those obtained using Priestley's plates. Hoops made of No. 3 bars also had a positive effect on the maximum stress value and the area under the curve. A 4 in. (10.1 cm) spacing on center of the ties presented even better results than an 8 in. (20.3 cm) spacing and increased noticeably the area under the curve.

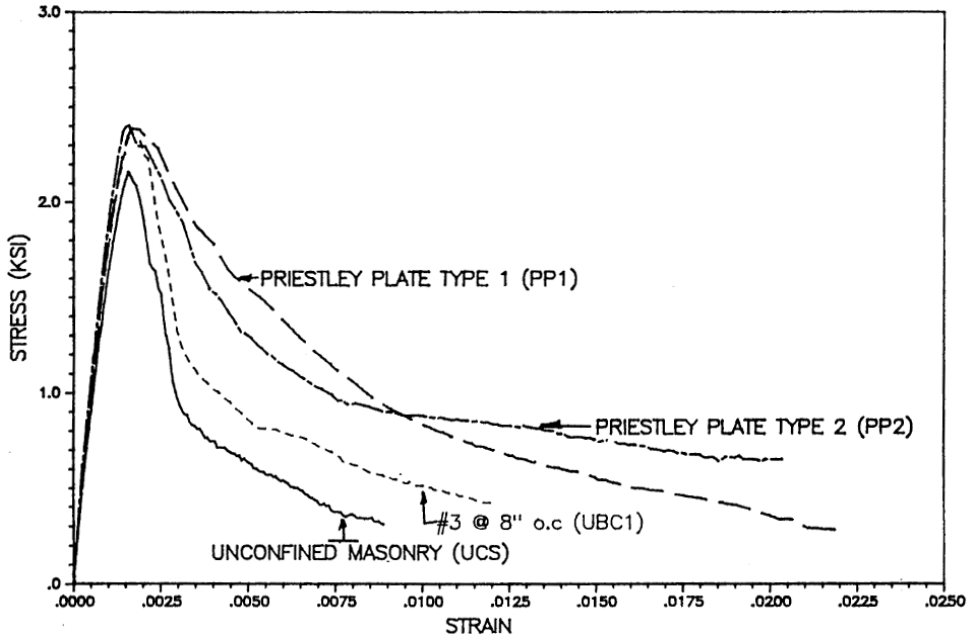

Figure 2.6: Stress-strain curves for unconfined masonry, confined masonry with hoops and two volumetric confinement ratios for steel plates from Hart et al (1988) (1 MPa = 145 psi)

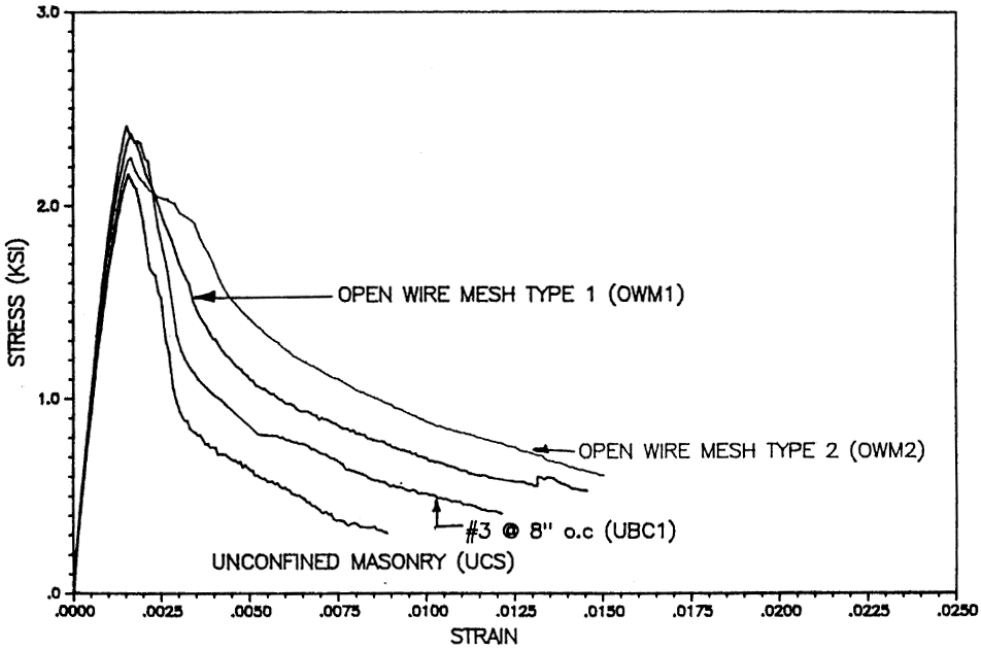

Figure 2.7: Stress-strain curves for unconfined masonry, confined masonry with hoops and open wire meshes from Hart et al (1988) (1 MPa = 145 psi)

2.3.3 Ewing and Kowalsky

Ewing and Kowalsky (2004) investigated the compressive behavior of unconfined and confined clay brick masonry piers. The type of confinement used in this project was Priestley's steel plates with and without holes in the flanges. The holes are intended to improve the bond between the plates and the mortar. Fifteen piers were tested using a compression testing machine operated under displacement control.

Tests results showed that the ultimate masonry strength for confined piers was increased by nearly 40% compared to that for unconfined piers. The strain capacity was also increased by the use of confining plates. Ewing and Kowalsky (2004) reported that the results obtained with solid plates were as good as or better than those obtained with plates with holes. They assumed that the lack of difference in behavior came from two factors: the cross-sectional area of the plate flanges was greater with the solid plates, and there may have been stress concentrations occurring in the plates with the holes. This observation is important because plates with holes cost more than using solid plates.

The modified Kent-Park model described by Priestley and Elder (1983) was used to model the stress-strain behavior of the piers and was found to appropriately model the test results, regardless of the volumetric ratio of confining steel.

2.3.4 Malmquist

Malmquist (2004) investigated the effects of confinement reinforcement on the compressive stress-strain behavior of 32-in. (81.3 cm) high piers made of unreinforced concrete, concrete blocks or clay bricks. Piers made of blocks or bricks were fully grouted and had thicknesses of 5 1/2 in. (14 cm) and 5 5/8 in. (14.3 cm), respectively. The goal of this project was

to evaluate the compressive strength and the ductility of the piers. These two characteristics are important variables that affect the behavior of structures during seismic events.

In all, forty-five piers were constructed. Two different types of confinement were used: Priestley's steel plates, and the combs previously used by Hart et al (1988) and Shing et al (1989) in reinforced masonry shear walls (see Figure 2.8).

Tests were conducted using an Universal Testing Machine (UTM) operated under displacement control at a rate of 0.05 in./min (0.13 cm/min). Stress-strain curves were obtained, and an analysis of variance (ANOVA) was conducted to determine if the confinement had a statistically significant effect on the results.

Results showed that the confinement reinforcement significantly increased the strain capacity by flattening the descending branch of the stress-strain curve and also increased the ultimate strain values for all materials investigated (see Figure 2.9 and Figure 2.10).

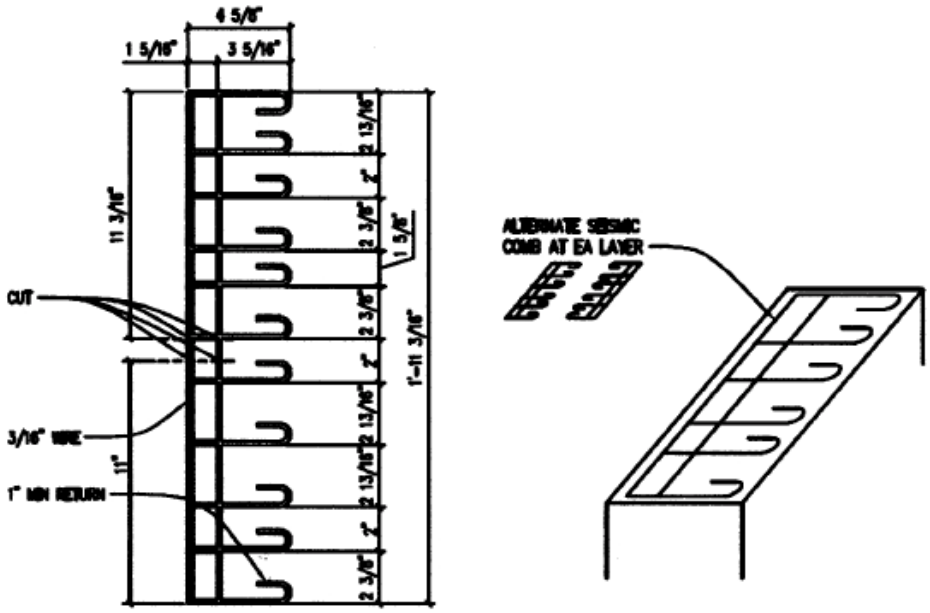

Figure 2.8: Seismic comb from Malmquist (2004) (1 in. = 2.54 cm)

Strains at 50% of the peak stress value were 0.004, 0.0055 and 0.006 for unconfined concrete block masonry piers, piers with plates, and piers with combs, respectively, corresponding to an increase in peak strain of approximately 50% as a result of providing confinement reinforcement. For clay, in the same order of type of confinement, strains of 0.0047, 0.0061, 0.0057 were obtained, corresponding to an increase of approximately 30%. The ANOVA with a 90% confidence level showed that comparable ductility improvements were obtained for the confinement reinforcement methods for each of the materials.

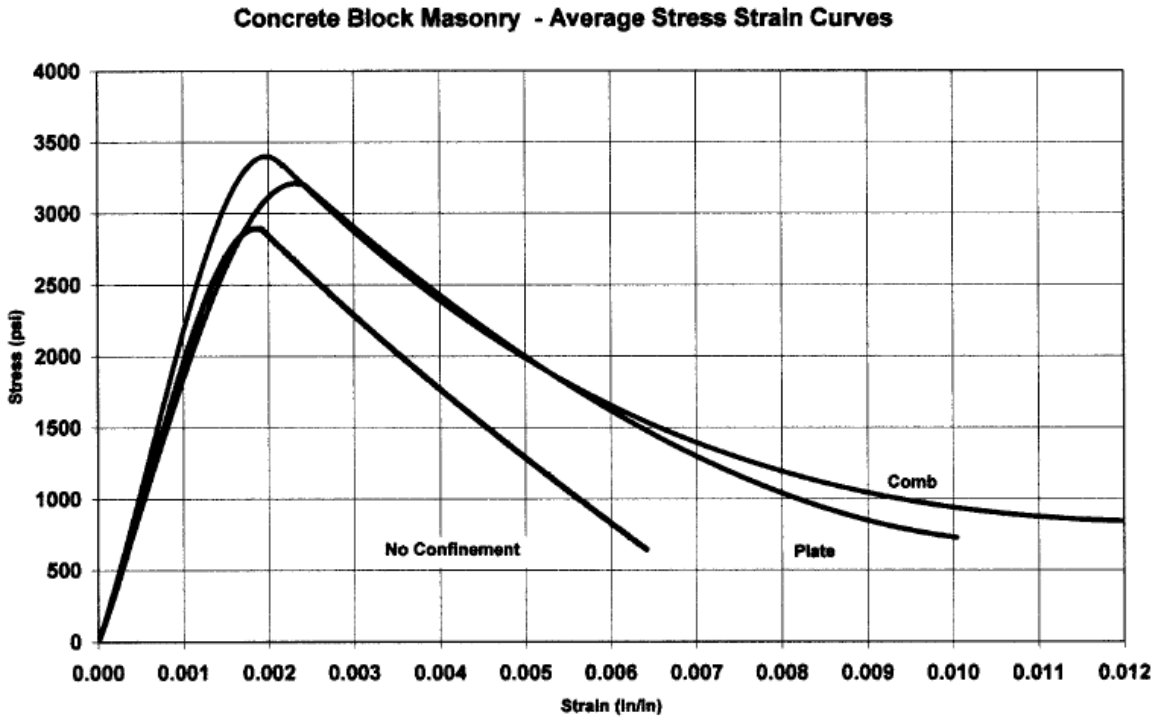

Figure 2.9: Stress-strain curves for concrete block masonry piers with no confinement, plates and combs from Malmquist (2004) (1 MPa = 145 psi)

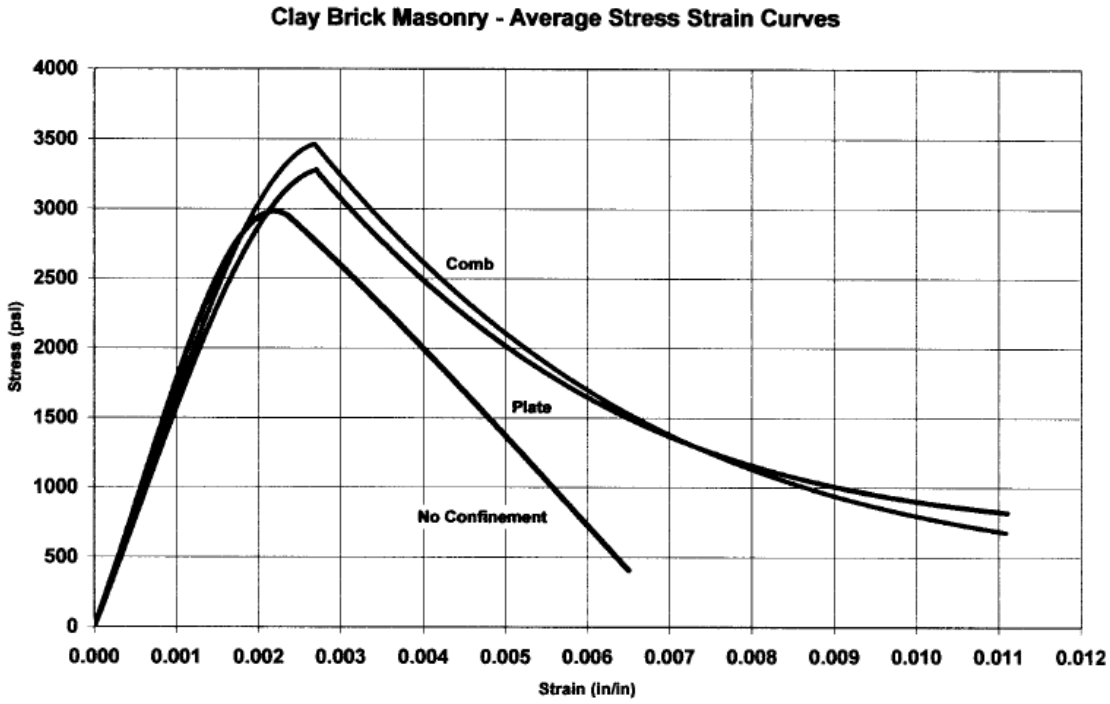

Figure 2.10: Stress-strain curves for clay brick masonry piers with no confinement, plates and combs from Malmquist (2004) (1 MPa = 145 psi)

2.4 BEHAVIOR OF MASONRY SHEAR WALLS

2.4.1 Shing, Noland, Klamerus and Spaeh

Shing et al (1989) investigated the inelastic behavior of concrete masonry shear walls. Sixteen of twenty-two fully grouted walls were built of concrete masonry blocks and tested to determine the effects of various load conditions and design parameters. Variables included the applied axial load and the amounts of vertical and horizontal reinforcement. Walls were 72 in. (183 cm) high, 72 in. (183 cm) wide, and were fixed at both ends, resulting in an aspect ratio of 0.5. The nominal block thickness was 6 in. (15.2 cm). A spacing of 16 in. (40.6 cm) was used for both vertical and horizontal reinforcement. A constant axial load and an in-plane cyclic load were applied.

The researchers performed moment-curvature analysis and found good correlation between analytical and experimental results for a vertical reinforcement ratio of 0.0038. When the latter value reached 0.0054 and 0.0074, the correlations were poorer. The moment-curvature analyses were based on flexural behavior assumptions. These assumptions become invalid with larger amounts of steel reinforcement due to the larger shear deformations and plane sections not remaining plane after bending. These results showed that analytical moment-curvature analysis is not appropriate for walls experiencing large shear deformations. "Specimens containing relatively low amounts of vertical reinforcement reached ultimate resistance immediately following the first major diagonal crack, whereas those specimens containing higher amounts of vertical reinforcement could resist an additional 15-20% in load following the first major diagonal crack" (Shing et al., 1989). Horizontal reinforcement did not show a large influence on the results but may change the inelastic behavior from shear-dominated to flexure-dominated.

An increase of the axial load increased the likelihood of having a failure due to shear, and the authors concluded that the flexural strength must be increased more than the shear strength when axial load increases.

2.4.2 Tallon

Tallon (2001) performed analytical studies in order to investigate flexural reinforcement limits for masonry shear walls. He also evaluated provisions in the 2000 International Building Code (IBC) with regard to flexural reinforcement limits for shear walls. Moment-curvature analyses were conducted on walls with five different flexural reinforcement ratios and for six different axial loads ranging from 0 to 350 psi (2.41 MPa). Various masonry compressive strengths and reinforcement yield strengths were evaluated.

Results showed that the 2000 IBC underestimated predicted curvature capacities and used simplified assumptions that made predictions for shear wall performance and behavior inaccurate. This study also showed that curvature is a function of the aspect ratio of the wall, a criterion not taken into account by the IBC, resulting in underestimations of the curvature for squat shear walls. Tallon (2001) also studied the effects of the plastic hinge length on his results by investigating the two relationships for plastic hinge lengths proposed by Paulay et al (1992). According to both Tallon and Paulay et al (1992), Equation 2.6 is more appropriate for squat shear walls because the influence of plasticity spread due to diagonal cracking is accounted for by integrating the length of the wall, l_w. Equation 2.7 is more dependent on the height of the wall because it was originally developed for columns and therefore is more appropriate for walls with high aspect ratios.

$$L_p = 0.2l_w + 0.044h_w \qquad \textit{Equation 2.6}$$

$$L_p = 0.08h_w + 0.15f_y d_{bl} \qquad \textit{Equation 2.7}$$

Where:

- L_p is the plastic hinge length, in.;
- l_w is the wall plan length, in.;
- h_w is the wall height from base to point of load application, in.;
- f_y is the yielding strength of the steel, ksi; and
- d_{bl} is the diameter of the flexural reinforcement, in.

Defining failure when the ultimate masonry strain is reached was found to be inaccurate. Indeed, if failure at 10% load degradation is considered, Tallon showed increases in the ultimate curvatures of 30 to 200%. The analytical results showed that masonry shear walls were able to experience greater curvatures than predicted by the IBC (2000). If this was considered, larger amounts of steel reinforcement could be used, which would enable greater use of masonry is seismic areas.

2.4.3 Eikanas

Eikanas (2003) investigated the effects of varying wall aspect ratio and flexural reinforcement on concrete masonry shear wall behavior. He compared measured drifts to the International Building Code's (IBC 2000) 1% drift requirement. Seven fully-grouted cantilever concrete masonry shear walls were tested. In-plane loading was applied cyclically at the free end of the wall. A constant axial stress of 27 psi (0.19 MPa) was applied at the free end simulating upper floors. Aspects ratios included 0.72, 0.93, 1.50 and 2.10. Flexural reinforcement ratios were approximately equal to either the maximum IBC (2000) reinforcement ratio ρ_{max} or twice ρ_{max}. Hysteretic load-displacement diagrams were obtained from experiments. Displacement ductilities were computed and curvature along the height of the wall was determined. Eikanas (2003) also conducted compression tests, following ASTM C1314, on fully-grouted two-course masonry prisms. An average compressive strength f'_m of 1630 psi (11.24 MPa) was measured. The yield strength of the vertical reinforcement was measured as 66.1 ksi (455 MPa).

Details about the tested walls are provided in Table 2.1. H_{tot} refers to the total height of the wall, H_{la} is the height from the bottom to the point of load application, L_w is the width of the wall, H_{la}/L_w is the wall aspect ratio.

	Wall	H_{tot} (in.)	H_{la} (in.)	L_w (in.)	H_{la}/L_w	Vert. Reinf.
Eikanas	1	72	52	55.63	0.93	4#5@16
	2	104	84	55.63	1.51	4#5@16
	3	104	84	39.63	2.12	3#5@16
	4	72	52	55.63	0.93	7#5@8
	5	104	84	55.63	1.51	7#5@8
	6	104	84	39.63	2.12	5#5@8
	7	72	52	71.63	0.73	5#5@16

Table 2.1: Eikanas' walls properties

Toe crushing was observed at strains significantly exceeding 0.0025. According to Eikanas (2003), toe crushing occurred always at or near the maximum load and was accompanied by significant drifts. Concerning the aspect ratio of the walls, squat shear walls experienced greater shear deformations, while slender walls experienced more flexural deformations. Regarding the effects of the ratio of reinforcement provided, ρ, the larger the amount of steel, the smaller the drift capacity. However, Eikanas (2003) noticed that drift values were always greater than 1.5% drift before reaching 20% load degradation.

Observed plastic hinge lengths were determined to be between Paulay and Priestley's (1992) recommendations (see Equation 2.6) and those given in ACI 318 (2002) (see Equation 2.8).

Eikanas concluded that the IBC provisions were overly restrictive and do not appropriately take into account the aspect ratio of the wall. Furthermore, considering flexural deformations is not a good representation of the response for squat shear walls which will mainly experience large shear deformations. Shear should be taken into account for low aspect ratios.

$$L_p = \frac{l_w}{2} \qquad \textit{Equation 2.8}$$

Where: L_p = plastic hinge length, in.;

l_w = wall plan length, in.; and

h_w = wall height from base to point of load application, in.

2.4.4 Priestley

Priestley (1986) investigated the seismic design of shear walls and presented arguments for using a capacity design method. Two questionable premises were exposed. First, many design codes used elastic design methods that assume a structure's behavior is more predictable at service loads than at ultimate. Second, elastic design is supposed to prevent structures from inelastic actions, but during earthquake events, it becomes highly doubtful.

At service loads, parameters such as shrinkage, creep, temperature and settlement influence the stresses experienced by the structures so that elastic design predictions do not show good results. At ultimate loads, stresses are less sensitive to these parameters, and predictions of performance will be improved. Priestley observed that squat shear walls could achieve very ductile flexural response even for aspect ratios as low as 0.5, but the energy absorption is limited by the base slip.

Tests were conducted on 19.7 ft (600 cm) high cantilever shear walls with an aspect ratio of 2.5. The goal was to study the behavior of slender fully-grouted concrete masonry shear walls to examine if the ductility capacities would decrease as the aspect ratio increases. Concrete units used in this study were 5 ½ in. (14 cm) thick. An investigation of the plastic hinge length in the base region and of the potential lateral buckling of the compression end was conducted. Confinement with steel plates was provided in the plastic hinge region to several walls, but only at each end and only in the bottom seven mortar beds. Walls were loaded cyclically in plane at

the free end. Load-displacement curves for unconfined and confined concrete masonry shear walls are presented by Figure 2.11 and Figure 2.12.

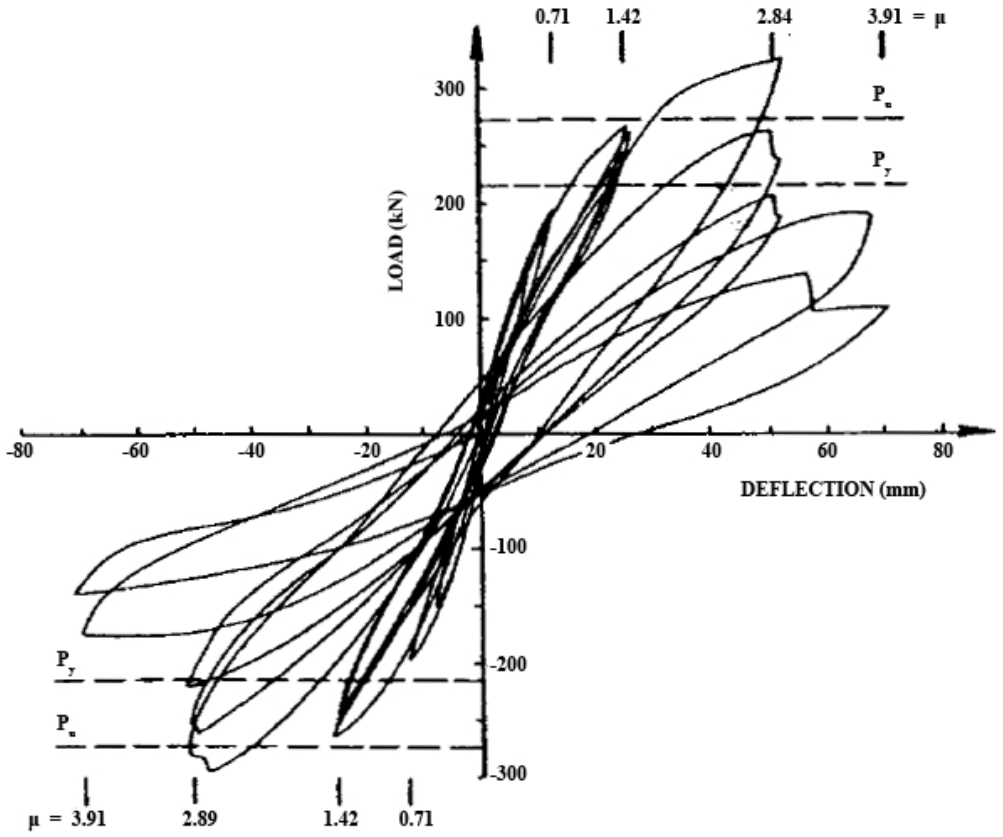

Figure 2.11: Load-deflection behavior of unconfined concrete masonry walls of high aspect ratio from Priestley (1986) (1 kN = 225 lbs, 1 mm = 0.03937 in.)

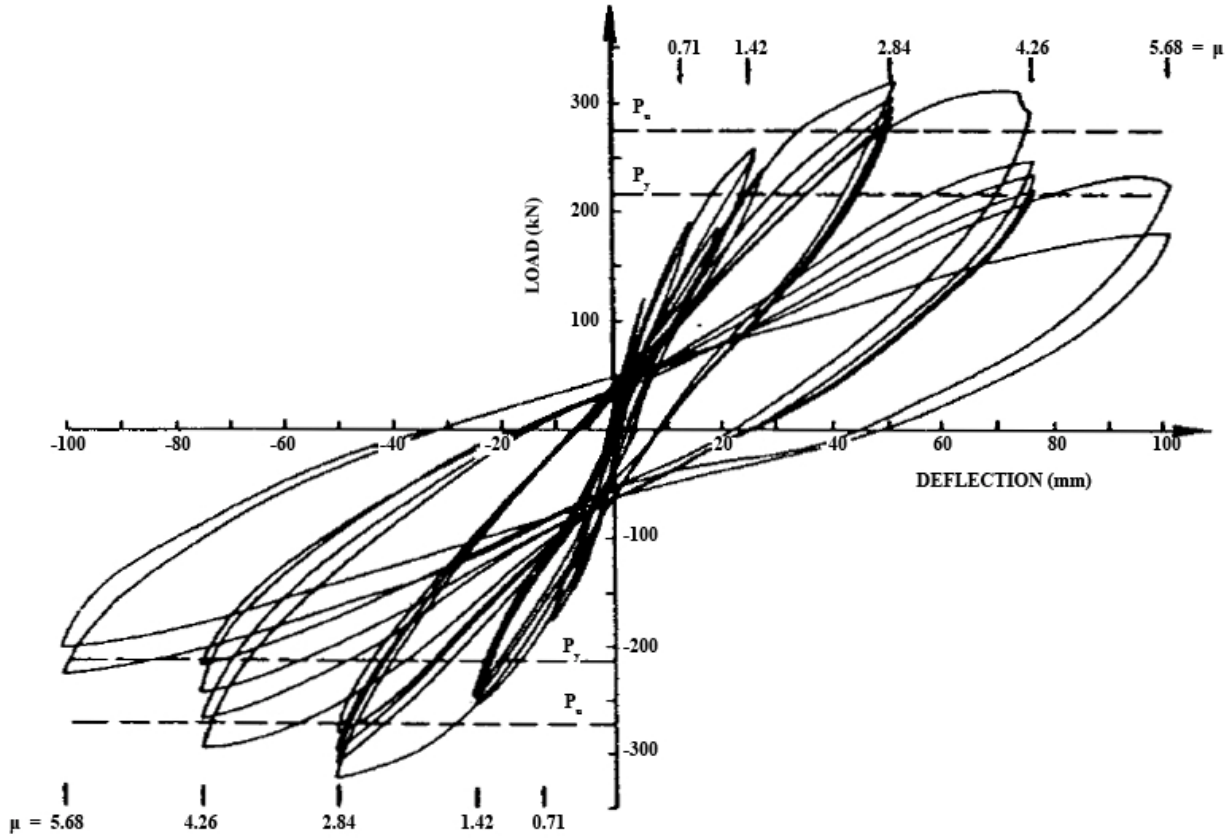

Figure 2.12: Load-deflection behavior of confined concrete masonry walls of high aspect ratio from Priestley (1986) (1 kN = 225 lbs, 1 mm = 0.03937 in.)

Results showed that cantilever shear walls with a flexible floor slab will behave better than coupled shear walls or walls with openings. The confinement in the plastic hinge region provided very good results by improving the ultimate strength and the ductility capacity. Furthermore, less visible damage occurred in the wall at the end of testing when compared to walls without confinement. Another conclusion was that the lapping of flexural reinforcement should be avoided in the plastic hinge region. No lateral buckling of the reinforcement was observed. Ductility decreased as the aspect ratio of the wall increased.

Priestley provided several design recommendations that were later incorporated into the New Zealand Masonry Design Code (1985). It was concluded that flexural design of masonry shear walls should be based on the ultimate strength theory. A capacity design approach should be used for the required shear strength. Distributing flexural and shear reinforcement along the entire length of the wall instead of concentrating it will improve performance. Walls with high aspect ratios should contain a type of confinement (preferably steel plates) in the end regions in order to provide adequate ductility.

2.4.5 Shing, Carter and Noland

Research was conducted by Shing et al (1993) on the influence of confining steel on flexural response of reinforced masonry shear walls. Tests on four-course piers were followed by tests on shear walls. Three confinement schemes were investigated: ring, comb and spiral-cage (see Figure 2.13). Specimens were made of 6, 8 or 12 in. (15.2, 20.3 or 30.5 cm) thick hollow concrete blocks. Vertical and horizontal steel reinforcement was provided in all specimens in order to comply with the minimum requirements of the UBC (1988). Vertical and horizontal reinforcement was equally spaced at a 16 in. (40.6 cm) center-to-center spacing. Confinement was provided along the entire height of the wall with only the center region around the central vertical bar not confined. All walls were subjected to a 100 psi (0.7 MPa) compressive stress and loaded cyclically in plane. Loading was applied at the top of the cantilever wall.

Results showed that flexure governed for all walls even if shear had an effect on the mode of failure and the maximum strength values. Visual observations showed that the combs provided the best results, usually confining the toe crushing to only one course compared to damage in at least two courses with the other types of confinement.

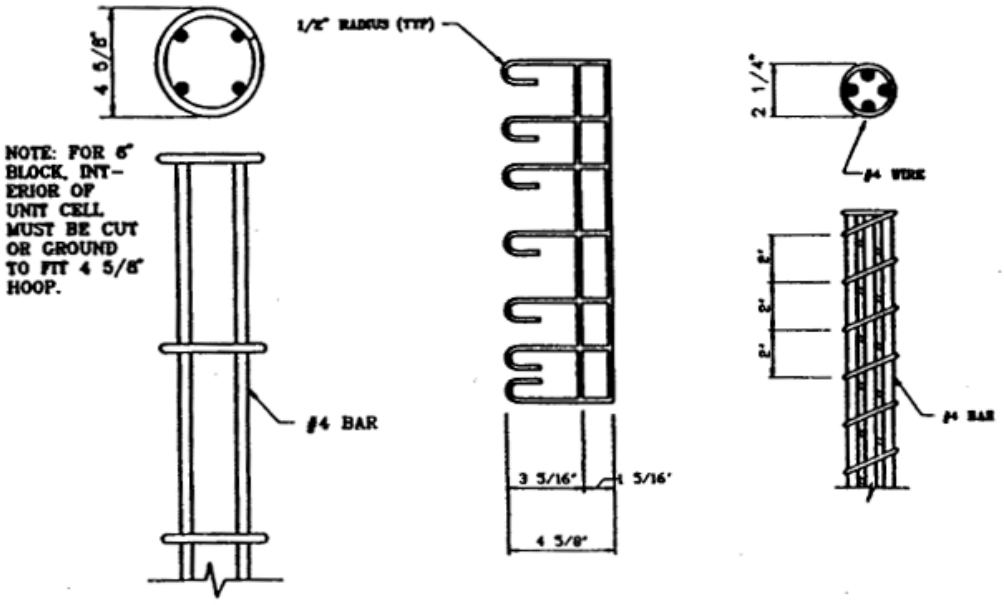

Figure 2.13: Three confinement schemes investigated by Shing et al (1993). From left to right, the rings, combs and spiral cage

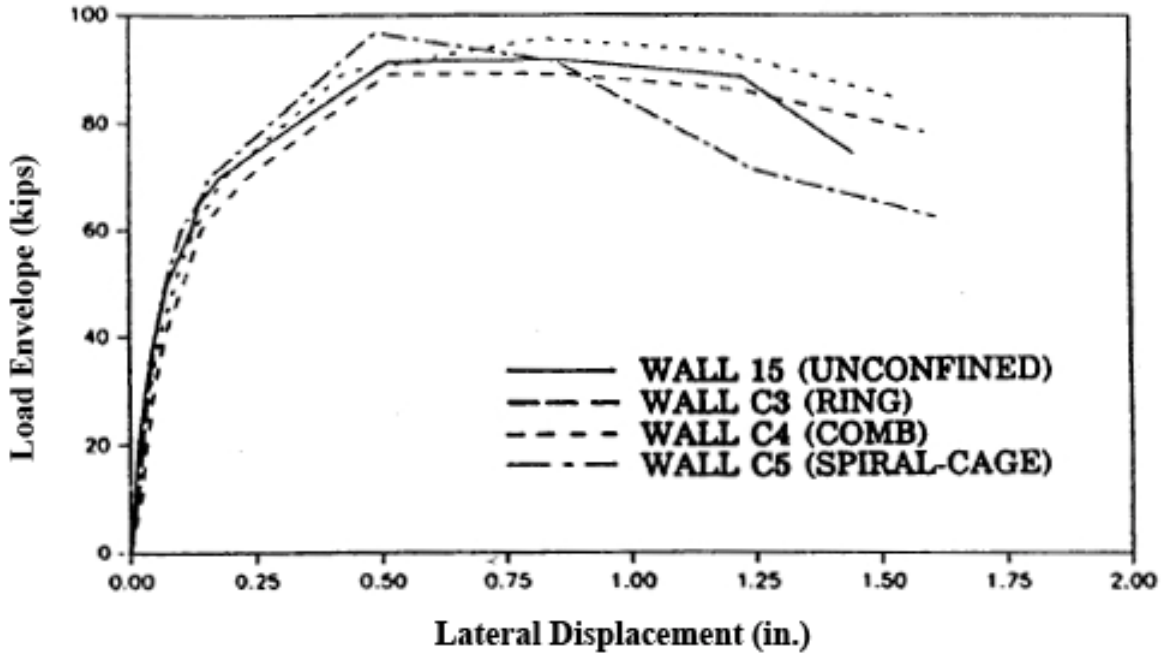

Figure 2.14: Load-lateral displacement envelope curves for the different confinement reinforcements (1 kips = 4.448 kN, 1 in. = 2.54 cm)

Flexural ductility results exhibited either small improvements or no improvements between unconfined walls and walls containing one of the confinement schemes (see Figure 2.14). Overall, the comb reinforcement provided the best results from the experimental and numerical studies. Shing et al (1993) concluded that the volumetric ratio of confining steel and the ratio of the least dimension of the confined area to the spacing of confining space influenced the compressive strain behavior of confined masonry shear walls.

2.4.6 Laursen and Ingham

Laursen and Ingham (2004) performed structural tests on two unbonded posttensioned concrete masonry (PCM) cantilever walls. Both walls were subjected to cyclic in-plane loading in order to reproduce seismic excitations. The walls were 67% of full scale and modeled typical 4 to 5 story high cantilever walls usually encountered in apartment buildings. They were 5,250 mm (206.7 in.) (height) × 2,400 mm (94.5 in.) (width) × 140 mm (5.51 in.) (thickness) and represented two RC floor slabs distributed along the entire length of the walls. Three-millimeter thick steel plates, similar to the Priestley plates described previously, were incorporated in mortar beds in the wall's toe regions over 1,000 mm (39.4 in.) in height and were extended to 600 to 800 mm (23.6 to 31.5 in.) from the wall corners. Three 15.2-mm (0.6 in.) high-strength post-tensioning strands were placed at -400 mm (-15.7 in.), 0 mm (0 in.) and 400 mm (15.7 in.) from the centerline of the walls, respectively, and were prestressed to an initial force of 133 kN based on the assumption that the walls would rock around their lowers corners and a required drift of 2% before tendons yield. Horizontal shear reinforcement was provided at 400 mm (15.7 in.) spacing.

Two previous studies by Laursen and Ingham (2001) and Laursen and Ingham (unpublished, 2003) evaluated the effects of confinement on PCM walls. “It was found for unconfined walls that the maximum in-plane displacement (drift) capacity developed prior to significant strength degradation attributable to masonry crushing was 1%” (Laursen and Ingham, 2004). When confined masonry was used, the authors found that the displacement ductility could reach 1% to 1.5%.

Results showed that tendons reached maximum forces of 209 kN, smaller than the nominal yield force of 213 kN. Sliding represented less than 3% of the total lateral displacement. Only the bottom three courses experienced face shell spalling and grout core crushing; the upper courses only presented either small cracks or no damage. It was concluded that the PCM walls can sustain severe in-plane cyclic loading accounted during seismic events. Reliable drift capacities were obtained and reached up to 1.5%. Only small regions of the wall were damaged, allowing the structure to be repaired. At ultimate displacement, strains accounted were between 0.019 and 0.024, indicating that the load was no longer carried by the masonry as face shell spalling had occurred.

2.4.7 Snook

Snook (2005) investigated the effects of confinement reinforcement on the performance of fully-grouted concrete masonry shear walls. Nine cantilever walls were tested. Two wall aspect ratios (0.93 and 1.5) and three types of confinement reinforcement were investigated, namely stainless steel plates, open wire mesh and polymer fibers. The walls had an 8-in. (20.3 cm) nominal thickness and a length of 55.625 in. (141.3 cm). Wall heights were either 72 or 104 in. (183 or 264 cm). Cyclic lateral load was applied at a height of either 52 or 84 in. (132 or 213

cm) from the base while a constant axial stress of 34 psi (0.24 Mpa) was maintained at the free end. Vertical reinforcement consisted of seven Grade 60 No.5 bars equally spaced at 8 in. (20.3 cm) corresponding to a vertical reinforcement ratio of 0.0055. Bar yield strength was measured as 63.3 ksi (436 MPa). Lap splices were avoided in the plastic hinge length region. Horizontal reinforcement consisted in either five No. 5 bars at 16 in. (40.6 cm) spacing, or seven No. 4 bars at the same spacing.

Confining plates measured 15.1 in. (38.4 cm) in length by 7.1 in. (18.1 cm) in width by 3/16 in. (0.46 cm) in thickness and were placed in the bottom four or six mortar beds of the 72 or 104 in. (182.8 or 264.2 cm) high walls, respectively. Plate confinement was provided only in the end regions over a length of one full block. The open wire mesh was made of 3/16-in. (0.46-cm) diameter steel wire and was provided in the same regions as that described for the steel plates. Details are provided in Figure 2.15.

Fibers used in the study were fabricated from a polypropylene and polyethylene mixture. They were directly mixed with the grout and placed in the walls cells. Two different concentrations of fibers were used: "Fiber 1" refers to 5 lbs/yd^3 (2.97 kg/m^3) and "Fiber 2" to 8 lbs/yd^3 (4.76 kg/m^3). Walls were cyclically loaded in-plane under displacement control while supporting an axial stress of 34 psi (0.23 MPa).

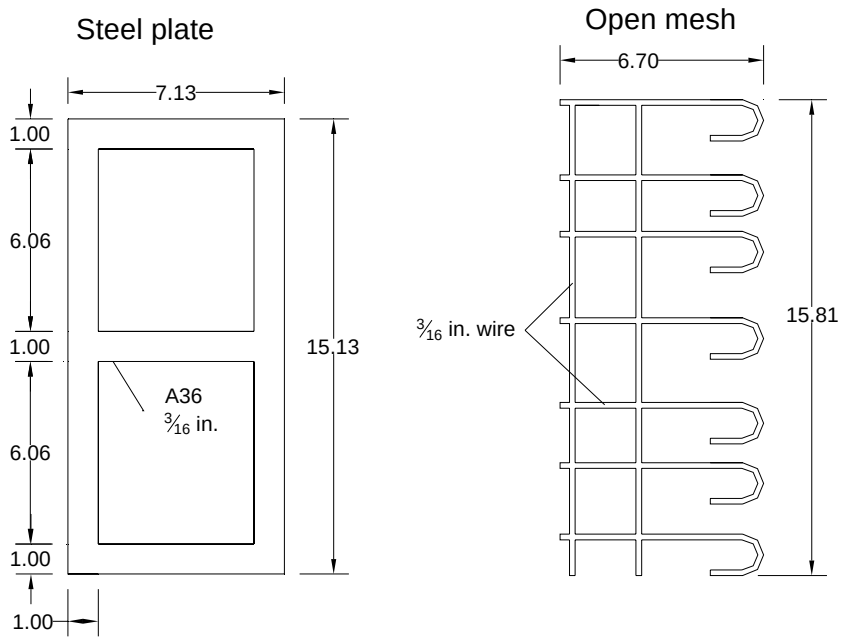

Figure 2.15: Steel plates and open mesh comb from Snook. Dimensions are in inches (1 in. = 2.54 cm)

Details about the tested walls are provided in Table 2.2. H_{tot} refers to the total height of the wall, H_{la} is the height from the bottom to the point of load application, L_w is the width of the wall, H_{la}/L_w is the wall aspect ratio.

Snook also conducted compression tests, following ASTM C1314, on grouted two-course masonry prisms. An average compressive strength f'_m of 1730 psi (11.93 MPa) was obtained.

Wall failure mechanisms, drifts, load-displacement curves and displacement ductilities were evaluated. All four walls with an aspect ratio of 0.93 experienced damage due to shear and flexure. Wall 1, 2 and 3, not confined, confined with steel plates and confined with seismic combs, respectively, experienced spalling over the bottom two or three courses. Wall 4, confined with "Fiber 1", experienced large shear cracks but no spalling of the face shell. The five walls with an aspect ratio of 1.5 all experienced a failure pattern mainly due to flexure, characterized

by toe crushing of side regions. Usually, three or more courses were damaged at failure, however, the major cracks for fiber reinforced walls were only situated in the bottom two courses. Buckling of the vertical reinforcement occurred in each wall. The shear wall confined with fibers experienced the least amount of shear damage among the squat shear walls that were tested.

	Wall	H_{tot} (in.)	H_{la} (in.)	L_w (in.)	H_{la}/L_w	Vert. Reinf.	Conf.
Snook	1	72	52	55.63	0.93	7#5@8	No
	2	72	52	55.63	0.93	7#5@8	Plates
	3	72	52	55.63	0.93	7#5@8	Combs
	4	72	52	55.63	0.93	7#5@8	Fiber 1
	5	104	84	55.63	1.51	7#5@8	No
	6	104	84	55.63	1.51	7#5@8	Plates
	7	104	84	55.63	1.51	7#5@8	Combs
	8	104	84	55.63	1.51	7#5@8	Fiber 1
	9	104	84	55.63	1.51	7#5@8	Fiber 2

Table 2.2: Snook's walls properties

Overall, the wall confined with "Fiber 2" achieved the highest drift. However, the wall with "Fiber 1" achieved a drift similar to that for the unconfined wall, showing that the larger amount of fibers may be required to increase the drift capacity. Walls with plates and with combs behaved similarly. Regarding the load-displacement curves for the 0.93 aspect ratio, Wall 4 (Fiber 1) presented the best performance, achieving higher peak load and larger displacements than in the other walls. For the 1.5 aspect ratio, Wall 9 (Fiber 2) had the best results, achieving slightly larger displacements than other walls. The largest displacement ductilities were obtained with the fiber reinforced walls.

2.5 STRESS-STRAIN MODELS

2.5.1 Kent and Park

Kent and Park (1971) used existing experimental stress-strain curves to create a mathematical model to describe the behavior of confined concrete with steel hoops or spirals. Their proposed model is illustrated in Figure 2.16. The goal was to represent each portion of the curves by mathematical equations based on the material properties.

The ascending portion of the curve (between points A and B) was approximated using a second degree parabola. Assuming that the steel did not have any effect on the shape of the curve, that the maximum flexural stress was the same for unconfined and confined masonry, and that it was equal to the cylinder strength f'_c, they produced Equation 2.9 which gives the concrete stress values for each value of strain lower than 0.002.

$$f_c = f'_c \left[\frac{2\varepsilon_c}{\varepsilon_0} - \left(\frac{\varepsilon_c}{\varepsilon_0} \right)^2 \right] \qquad \textit{Equation 2.9}$$

Where:

- f_c is the concrete stress, psi;
- f'_c is the compressive strength of a 6 in. diameter × 12 in. concrete cylinder, psi;
- ε_c is the concrete strain, in./in.; and
- ε_0 is the strain in concrete at peak strain, in./in.
  = 0.002.

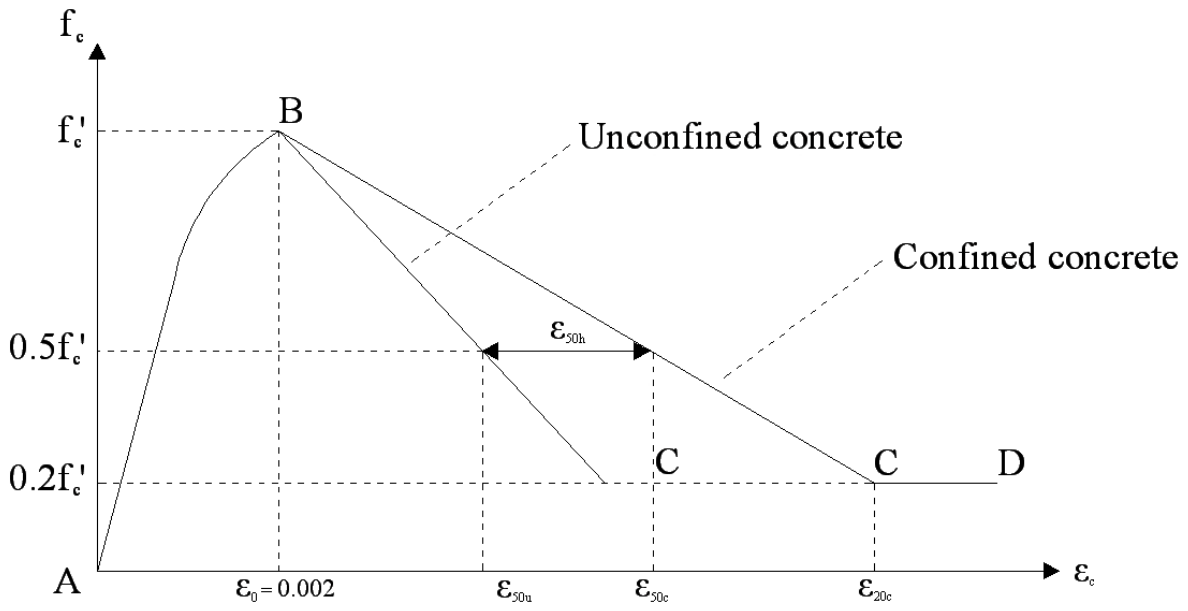

Figure 2.16: Proposed Stress-strain relationship for unconfined and confined concrete by Kent and Park (1971)

Kent and Park (1971) assumed that the falling branch could be represented by a linear curve and developed Equations 2.10, 2.11, 2.12 and 2.13.

$$\varepsilon_{50h} = \frac{3}{4} p'' \sqrt{\frac{b''}{s}} \qquad \textit{Equation 2.10}$$

$$\varepsilon_{50u} = \frac{3 + 0.002 f'_c}{f'_c - 1{,}000} \qquad \textit{Equation 2.11}$$

$$Z = \frac{0.5}{\varepsilon_{50h} + \varepsilon_{50u} - \varepsilon_0} \qquad \textit{Equation 2.12}$$

$$f_c = f'_c \left[1 - Z(\varepsilon_c - \varepsilon_0)\right] \qquad \textit{Equation 2.13}$$

Where:

- ε_{50h} is the difference between the strains at 50% of the peak stresses of confined and unconfined concretes, in./in.;
- p" is the ratio of volumetric hoops to volume of concrete core measured to outside of hoops;
- b" is the width of confined core measured to outside of hoops, in.
- s is the spacing between hoops, in.;
- ε_{50u} is the strain at 50% peak stress on falling branch of stress-strain curve, in./in.; and
- Z is a constant.

For confined concrete in the CD region, the authors assumed a constant stress value of $0.2f'_c$ can be supported from ε_{20c} to infinity. The model presented a good correlation between analytical and experimental results.

2.5.2 Priestley and Elder

Priestley and Elder (1983) presented a modified Kent-Park model developed initially by Park and Priestley in 1982. The original model had been modified in order to fit experimental data on confined square concrete columns. Equations derived were very close to those of the original model developed by Kent and Park described previously. The modified model is presented by Equations 2.14 and 2.15.

For the ascending portion of the curve for strains lower or equal to 0.002K:

$$f_c = Kf'_c\left[\frac{2\varepsilon_c}{0.002K} - \left(\frac{\varepsilon_c}{0.002K}\right)^2\right] \qquad \textit{Equation 2.14}$$

Where:

- f_c is the concrete stress, MPa;
- f'_c is the compressive strength of a concrete cylinder, MPa;
- ε_c is the concrete strain, mm/mm;
- K is a strength enhancement coefficient

  $= 1 + \rho_s \frac{f_{yh}}{f'_c}$;

- ρ_s is the volumetric ratio of confining steel equal to the volume of confining steel divided by the volume of confined concrete; and
- f_{yh} is the confining steel yield strength, MPa.

For the descending portion of the curve for strains greater than 0.002K:

$$f_c = Kf'_c\left[1 - Z_m\left(\varepsilon_c - 0.002K\right)\right] \qquad \textit{Equation 2.15}$$

Where:

- Z_m is a constant

  $= \frac{0.5}{\left[\frac{3 + 0.29f'_c}{145f'_c - 1{,}000}\right] + \frac{3}{4}\rho_s\sqrt{\frac{h''}{s_h}} - 0.002K}$;

- h" is the lateral dimension of confined core, mm; and

- s_h is the longitudinal spacing of confining steel, mm.

Priestley and Elder (1983) made additional modifications to the model to account for low values of strain at peak stress (0.0015) of the masonry piers obtained in their tests. These equations won't be described here because, after testing them, it appeared that the first modified Kent-Park model fitted experimental results better. Strain at peak stress was closer to 0.002 than 0.0015.

CHAPTER THREE: MASONRY PIER TESTS

3.1 INTRODUCTION

The 2005 Masonry Standards Joint Committee (MSJC) Building Code provides the option to utilize confined boundary elements in order to improve the performance of masonry walls. In this study, the effects of fiber reinforcement on compressive stress-strain curves of fully-grouted masonry piers were investigated. Two variables were considered. The first one was the masonry material. Either concrete blocks or clay bricks were used to build the piers. The second variable investigated was the amount of fibers mixed with the grout poured inside the pier cells (two different amounts and a control).

Thirty piers were built. All possible combinations of test parameters were applied on groups of five piers (different material or amount of fibers in the grout). After 28 days curing, the piers were tested in compression in order to obtain a stress-strain curve for each specimen. An analysis of variance was performed to determine if the amount of fibers had a significant effect on the performance of the piers. This chapter presents details of the experimental program and the results of the tests.

3.2 MATERIAL PROPERTIES

The piers measured approximately 32 in. (81 cm) high (see Figure 3.1). They were made of either four concrete block units or eight clay brick units. The dimensions of a single concrete block were 5 ⅝ ×11 ⅝ ×7 ⅝ in. (14.3×29.5×19.4 cm) and those of a clay brick were 5 ½ ×11 ½ ×3 ½ in. (14.0×29.2×8.9 cm). The hollow concrete block masonry units were made from medium density concrete according to ASTM C 90 and had nominal 6W×12L×8D in.

(15W×30L×20D cm) dimensions with a net-area-to-gross-area ratio of 0.56. The hollow clay brick units met ASTM C 652 specifications and had nominal 6W×12L×4D in. (15.24W×30.48L×10.16D cm) dimensions. Their net-area-to-gross-area ratio was 0.63 (see Figure 3.1). The grout used in this study was a bagged coarse grout confirming to ASTM C 476. Bagged Type S mortar was used.

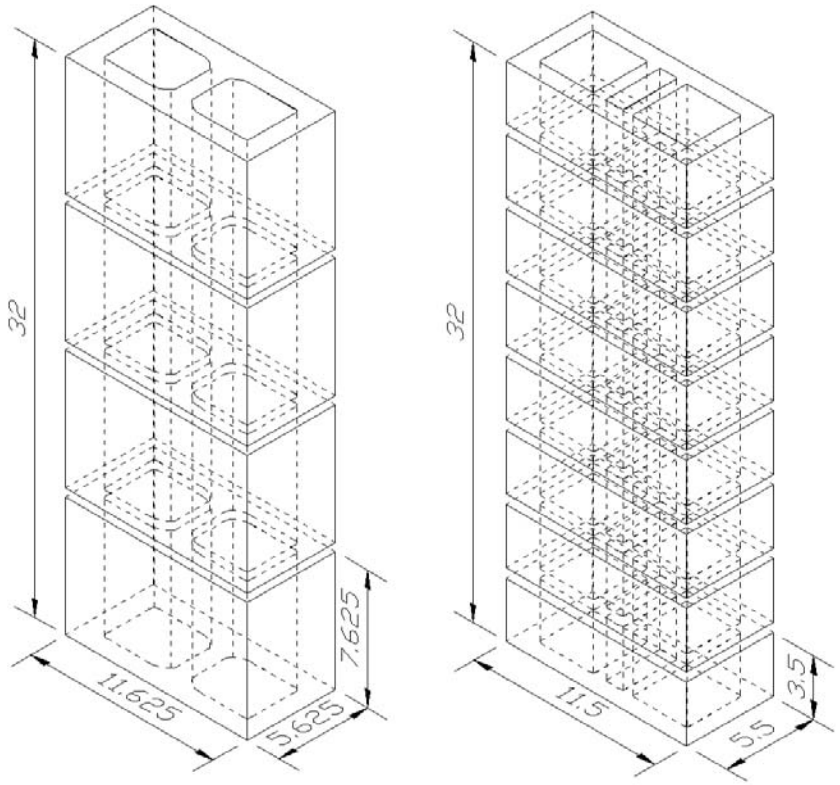

Figure 3.1: Piers made of 4 concrete blocks or 8 clay bricks (1 in. = 2.54 cm)

Tests were conducted to determine the average compressive strength for the blocks, the bricks, the grout (following ASTM C1019 requirements), and the mortar (following ASTM C 270 and UBC Std. 24-22). Results are summarized in Table 3.1. Note that the average compressive strength obtained for the grout samples was higher than the traditional values.

	Compressive strength (psi)
Concrete block	**2500**
Clay brick	**4690**
Grout	**8120**
Mortar	**4340**

(1 ksi = 6.89 MPa)

Table 3.1: Strengths of the different materials

3.3 FIBER PROPERTIES

Fiber reinforcement is gaining more use in concrete construction because of its ability to provide effective crack control for plastic shrinkage and for drying shrinkage, absence of corrosion, reduction of injury risks with the installation of traditional steel rebar, and ease of use.

The fibers used in this investigation were synthetic macro fibers made of a blend of two types of polymers: polypropylene and polyethylene. Engineered to enhance the ductility of concrete, these fibers also provide post-crack control, a characteristic which is not traditionally achieved by micro fibers. The modulus of elasticity of the fibers was matched to the elastic modulus of concrete paste, while the geometry of the fibers was optimized to obtain a good bond between the fibers and the concrete matrix. The fibers do not increase the tensile strength of the concrete. The fibers measured 1.55 in (40 mm) long and possessed an aspect ratio of 90 (see Figure 3.2). Fibers were added to the already mixed grout. The grout with fibers was placed and vibrated inside the pier cells using conventional techniques. Table 3.2 provides properties of the fibers.

Specific gravity	**0,92**
Absorption	**None**
Modulus of Elasticity	**9.5 GPa (1,378 ksi)**
Tensile strength	**620 MPa (90 ksi)**
Melting point	**160°C (320°F)**
Ignition point	**590°C (1,094°F)**
Alkali, Acid and Salt resistance	**High**

Table 3.2: Fiber properties

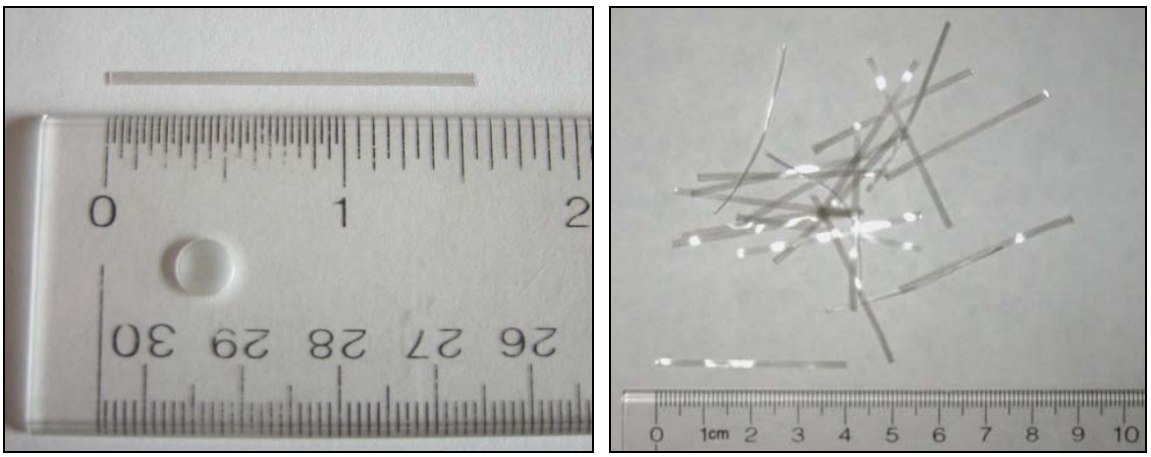

Figure 3.2: Polymer fiber (1 in. = 2.54 cm)

3.4 PIER CONSTRUCTION

Thirty piers were constructed by qualified masons: fifteen made of 4 concrete blocks, and the other fifteen made of 8 clay bricks (see Figure 3.3). The piers were constructed on leveled plywood boards inside plastic bags. After 24 hours, they were separated into 6 groups of 5 piers and then fully grouted with one of the three amounts of fibers selected for this study (see Table 3.3). 0.12% by weight refers to a dosage of fibers of 5 lbs/yd^3 (2.97 kg/m^3), while 0.20% by weight refers to a dosage of 8 lbs/yd^3 (4.76 kg/m^3). The piers without fibers served as a control for the study.

The grout was poured in two lifts and vibrated twice with a 1-in. (25-mm) diameter vibrator for 1 min. After the vibration of the grout, the plastic bags were sealed to retain moisture and provide for curing of the grout for 28 days (see Figure 3.3).

% of Fibers by weight / Materials	0%	0.12%	0.20%
Concrete Prisms	5	5	5
Clay Prisms	5	5	5

Table 3.3: Test matrix

Figure 3.3: Both kinds of piers before being grouted and sealed in the plastic bags

Both concrete blocks and clay bricks were obtained from commercial suppliers. A number of the bricks possessed cracks in the central region, probably associated with the manufacturing process (see Figure 3.4).

Figure 3.4: Cracked bricks

3.5 PIER PREPARATION FOR TESTING

The piers were capped on both sides using a commercially-available white gypsum plaster called Hydrocal. Leveled glass plates were secured with plaster to the building floor. Wet plaster was spread on these plates and the piers were set in the plaster. The top cap was created by pressing and leveling a glass plate into wet plaster spread over the tops of the piers (see Figure 3.5).

Figure 3.5: Capping with gypsum cement

3.6 TEST SETUP

The piers were tested in compression using a 400-kip (1780-kN) Universal Testing Machine (UTM) at Washington State University. The machine consisted of a two-screw load frame and a single hydraulic ram at the bottom which compressed the pier against the top platen (see Figure 3.6 - left).

Displacements of the bottom loading platen were controlled to produce a constant rate of displacement of 0.05 in./min (0.13 cm/min) during testing. Because of the elastic deformation of the two screws supporting the top crosshead, an instantaneous adjustment of the bottom platen speed was necessary. Ram stroke was recorded by a linear variable differential transformer (LVDT) mounted centrally on the back edge of the lower platen. Displacement measurements recorded by the UTM LVDT included the testing flame flexibility.

A spherical bearing plate was used as the upper platen in order to accommodate slight differences in alignment of the upper and lower surfaces of the piers (see Figure 3.6 - right).

The load and the displacement of the lower platen were directly recorded from the UTM machine. Five additional 2-in. (5-cm) range potentiometers were added, one to control the speed of the bottom table and four on the bearing plate to record the displacements of each corner of the specimen (see Figure 3.6 - right). All test information measured by either the testing machine or potentiometers was processed with commercial data acquisition software and collected at a rate of 5 Hz.

ASTM C 1314 procedures were generally followed throughout the testing process. Each specimen was loaded at a convenient rate up to 20 kips (90 N) and then unloaded until the load reached values less than 0.5 kips (2 N). The experiment was then started and data was recorded until the specimen failed or the load fell below 30 kips (130 N).

Figure 3.6: 400-kip Tinius Olsen Universal Testing Machine (left) and details of the bearing plate and potentiometers (right)

Each specimen was labeled. The first three letters refer to the material from which it was made (CON for concrete blocks or CLA for clay bricks) followed by "N" for No fibers, "F1" for fibers at 0.12% by weight (1st percentage of fiber), or "F2" for 0.20% by weight (2nd percentage of fibers). The last part of the label is the number of the specimen (1 to 5). For example: CON-N-4 for the fourth specimen made of concrete blocks with no fibers in the grout, or CLA-F1-5 for the fifth specimen made of clay bricks and with a grout mixed with the first percentage of fibers.

3.7 TESTING

Each specimen was tested in less than 3 minutes. In general, piers made of concrete blocks experienced a more gradual mode of failure when compared to failures in the brick

specimens. This behavior is likely due to clay bricks being inherently more brittle than concrete blocks.

Figure 3.7: Unreinforced clay masonry pier (left) and reinforced concrete masonry pier (right) after testing

Another observation was that piers without fibers typically developed vertical splitting and face shell spalling during testing. Damaged regions developed over a large portion of the specimen length and typically included damage penetrating into the grout cores (see Figure 3.7 - left). Pieces of masonry were often ejected from the piers in an explosive manner. Failure in the piers with fibers tended to extend over a smaller portion of the specimen length. In most cases, the fiber-reinforced grout cores remained intact even after the masonry spalled away (see Figure

3.7 - left). Some of the concrete specimens did not even break apart; only a long crack indicated that it had failed. All clay brick piers lost pieces of material even when fibers were incorporated in the grout. Before collapsing, a heavy crunching sound was audible for most of the piers.

3.8 RESULTS AND ANALYSES

3.8.1 Results processing and adjustments

Stress-strain curves could be obtained using two different methods. The first method was to use the displacements recorded by the UTM LVDT to calculate the strain, and the second was to use the average displacements of the four potentiometers placed around the pier. However, during the first several tests, wires of these potentiometers were not protected from the impact of ejected pieces of materials, resulting in compromised data for some of these tests. Two wood panels were later added to minimize this problem.

When the UTM LVDT displacements were used to calculate the strain, an adjustment of the results was necessary to take into account the machine stiffness. The UTM LVDT displacement readings reflected the specimen stiffness as well as the stiffness of the two-screw load frame. Thus, strain values calculated in this way do not represent the pier behavior itself, but rather a composite behavior. The adjustment described by Priestley and Elder in 1983 permitted a correction. It consisted of determining the stiffness of the pier and that of the composite (pier and UTM frame acting in series) from the load data record and the two displacement data sets available (see Equations 3.1 and 3.2).

$$P = K_{prism} \times U_{pots} \qquad \textit{Equation 3.1}$$

$$P = K_{comp} \times U_{UTM} \qquad \textit{Equation 3.2}$$

Where:

- P is the load;
- K_{pier} is the stiffness of the pier;
- K_{comp} is the composite stiffness;
- U_{pots} is the displacement based on the average of the four potentiometers; and
- U_{UTM} is the displacement of the bottom table.

The stiffness of the UTM is calculated as described by Equation 3.3:

$$K_{UTM} = \frac{1}{\frac{1}{K_{comp}} + \frac{1}{K_{prism}}} \qquad \textit{Equation 3.3}$$

During the pier loading, the machine stiffness was subtracted from the stress-strain curves and added during pier unloading.

Figure 3.8 presents the stress-strain curves obtained by the two methods. The first curve (1) is based on the average displacement of the four potentiometers, the second one (2) is based on the UTM LVDT displacement (composite), and the third one (3) is the stress-strain curve based on the UTM LVDT but after the adjustment described previously. It can be seen that the third curve (3) closely reproduces that obtained from the four-potentiometer strains. This correction technique was not necessary for all the piers, but only for those that possessed

compromised data due to specimen pieces touching the wires. When no problem was recorded, the average displacement of the four potentiometers was used. In this case, only the pier stiffness was taken into account and therefore no adjustment was required.

Another adjustment in the stress-strain curves from the tests was necessary. In most cases, the piers experienced damage in the central region. Not all the blocks or bricks were cracked. If a linear elastic behavior is assumed, the displacement due to the relaxation of the undamaged blocks or bricks increases even more the deformation of the cracked courses. Recovered displacements of the end courses were calculated and added to the displacement measurements in order to calculate strains in the damaged region. This adjustment was applied only for the declining slope of the stress-strain curves after reaching the peak stress values. The damaged region was defined after each test based on physical observations. This adjustment is the same as that described by Priestley and Elder (1983).

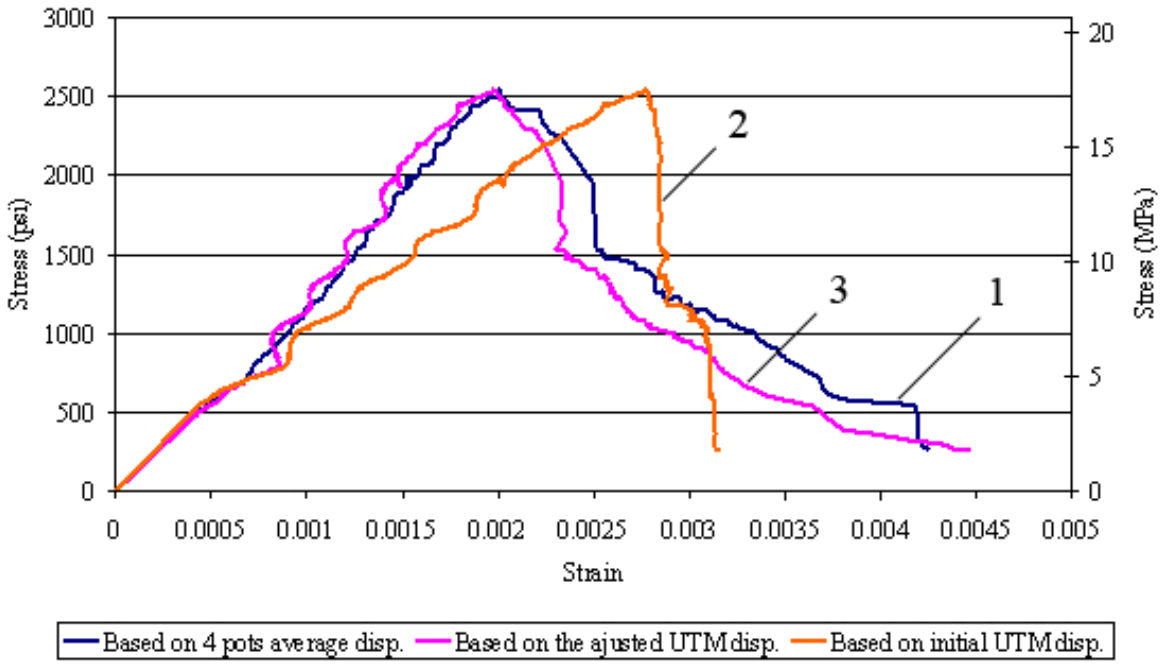

Figure 3.8: Stress-strain curves before and after adjustment

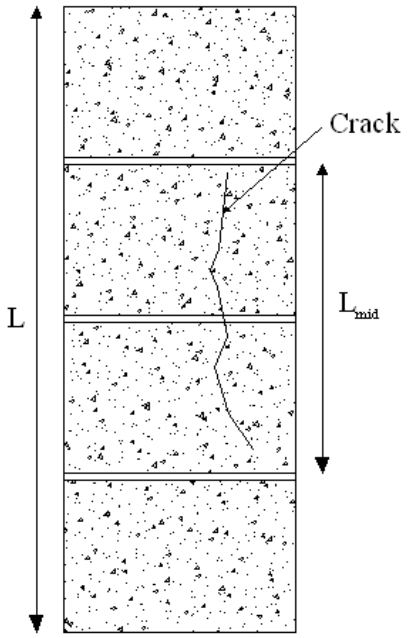

Figure 3.9: Damaged pier

L_{mid} is the total length of the damaged area. L_{ends} is equal to the total length of the specimen, L, minus L_{mid} (see Equation 3.4 and Figure 3.9). The strains for each length are described by Equations 3.5 and 3.6. The total strain is given by Equation 3.7.

$$L_{ends} = L - L_{mid} \qquad \textit{Equation 3.4}$$

$$\varepsilon_{mid} = \frac{\Delta_{mid}}{L_{mid}} \qquad \textit{Equation 3.5}$$

$$\varepsilon_{ends} = \frac{\Delta_{ends}}{L_{ends}} \qquad \textit{Equation 3.6}$$

$$\varepsilon_{tot} = \frac{\Delta_{tot}}{L} \qquad \textit{Equation 3.7}$$

Where:

- L is the total length of the pier;
- L_{ends} is the length of the non-damaged area;
- L_{mid} is the length of the damaged area;
- ε's are the strains of the corresponding part of the pier; and
- Δ's are the changes in lengths.

For the loading portion of the stress-strain curve, $\varepsilon_{tot} = \varepsilon_{mid} = \varepsilon_{ends}$, and no adjustments is needed. For the unloading part of the same curve, $\varepsilon_{mid} > \varepsilon_{tot} > \varepsilon_{ends}$ and therefore the adjustment becomes necessary.

Considering two consecutive points of the unloading part of the stress-strain curve, the adjusted strain is therefore described by Equation 3.8.

$$\varepsilon_{mid_2} = \varepsilon_{mid_1} + \frac{\left[(\Delta_2 - \Delta_1) + \frac{|\sigma_2 - \sigma_1| \times L_{ends}}{E_{el}}\right]}{L_{mid}} \qquad \textit{Equation 3.8}$$

Where:

- ε_{mid} is the strain of the damaged area at the considered point;
- Δ is the displacement at the considered point;
- σ is the stress at the considered point; and
- E_{el} is the modulus of elasticity of the pier calculated from the loading part of the stress-strain curve.

An example of the adjustment is shown in Figure 3.10. The first curve (1) represents the initial stress-strain curve, whereas the second curve (2) is the adjusted one.

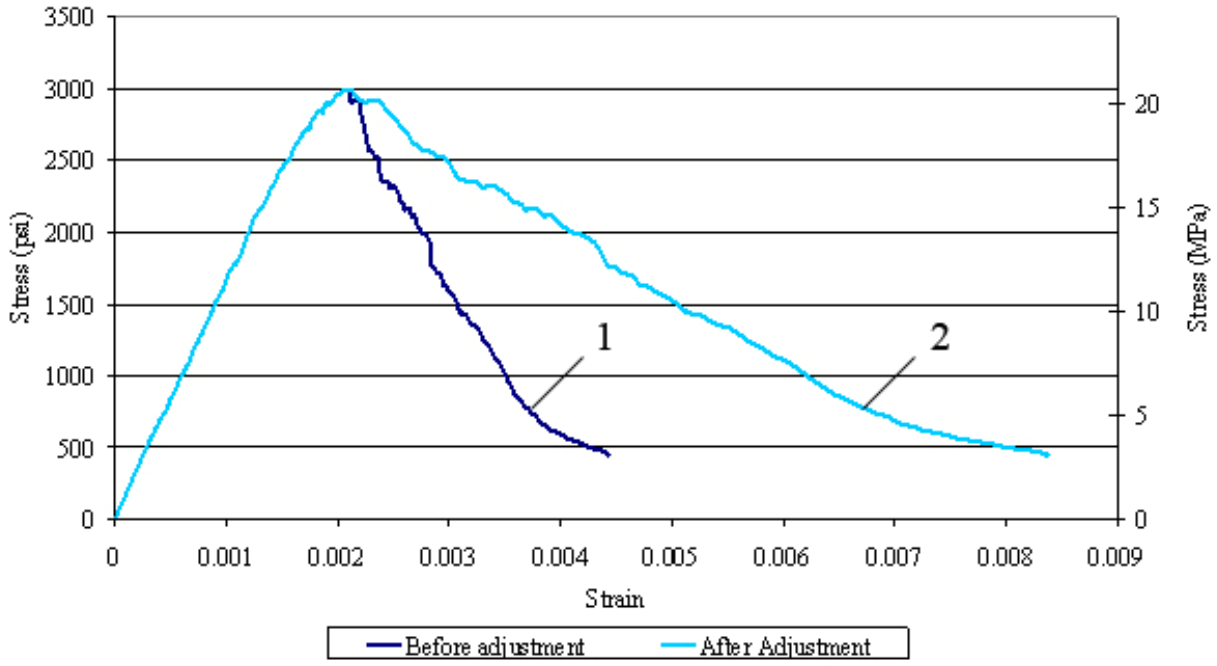

Figure 3.10: Stress vs. strain curves before and after adjustment for unloading of the ends

3.8.2 Influence of the amount of fiber

In order to obtain the average stress-strain curves for the two materials and the two amounts of fibers, individual curves had to be determined. When data was collected during testing, it was at equal time intervals. To be able to calculate an average, a stress value was needed at identical strain values for each of the curves (0.00001 in./in. intervals). An Excel function was developed with Visual Basic editor (see Appendix A for the code). The function processed the experimental data from the beginning to the end. For each strain value, two adjacent points were found from the experimental results (one before the desired strain value – Point 1, and one after – Point 2, see Figure 3.11). The linear equation of the line between points

1 and 2 was calculated, and therefore it became quite simple to obtain the stress value corresponding to the desired strain value (here 0.001375). An example is presented in Figure 3.12.

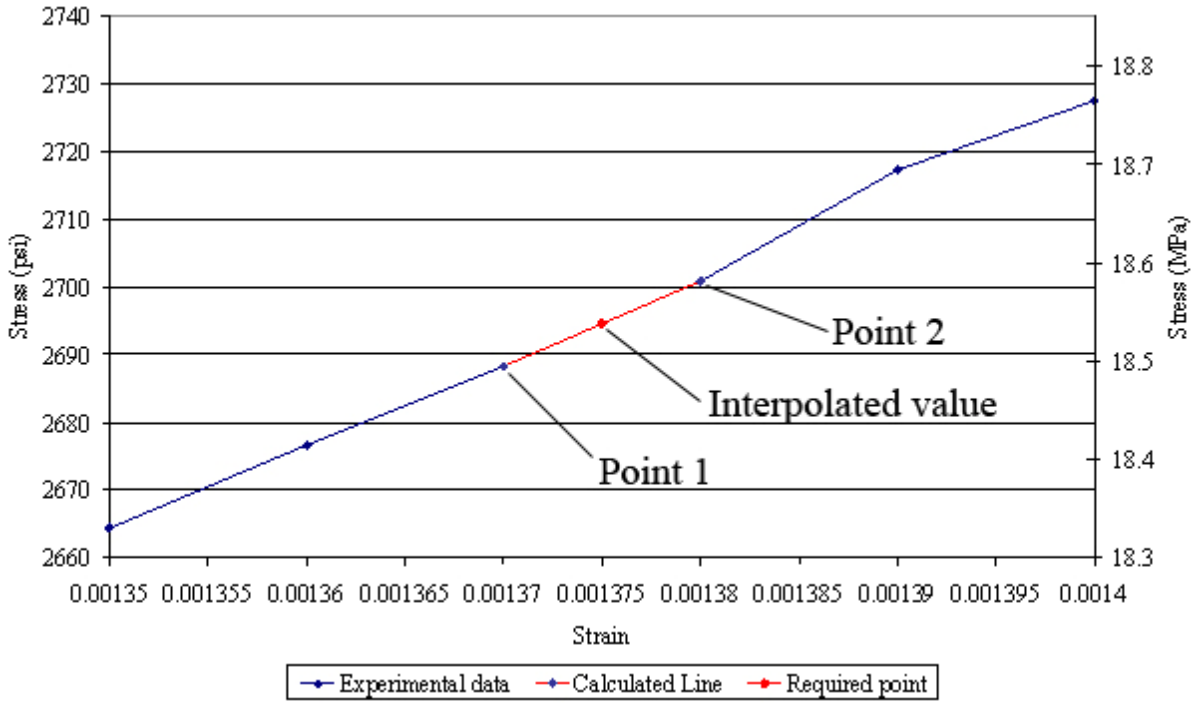

Figure 3.11: Discretization of the experimental curves

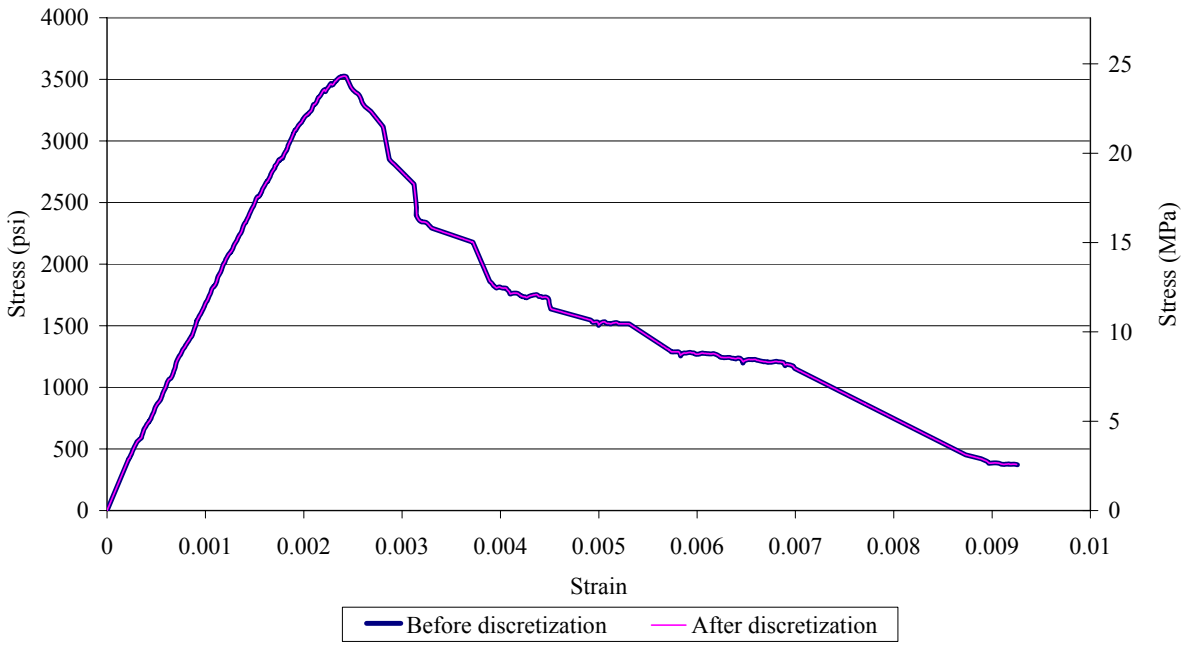

Figure 3.12: Example of discretized stress vs. Strain curve

Figure 3.13 and Figure 3.14 present the average curves for each material and amount of fibers. The average curves were determined by summing the stresses of each specimen at a given strain value and dividing it by the number of specimens having available data. Note that the curve presented discontinuities at strains corresponding to the end of a specimen data. The adopted solution was to fit a polynomial using a Matlab script presented in Appendix B. Appendix C presents results from each tested prism and its corresponding stress-strain curve. The average peak stresses values for the different materials and amount of fibers are given in Table 3.4 along with strain at peak stress and strain at 50% of the peak stress.

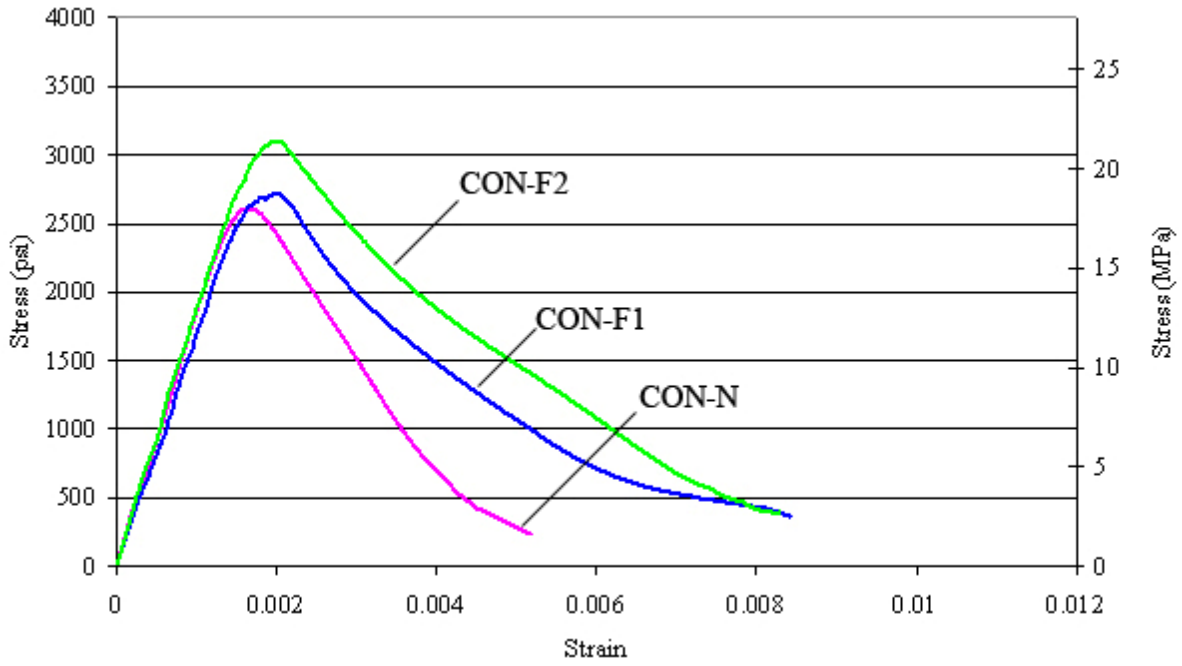

Figure 3.13: Average Stress-Strain curves for concrete masonry piers

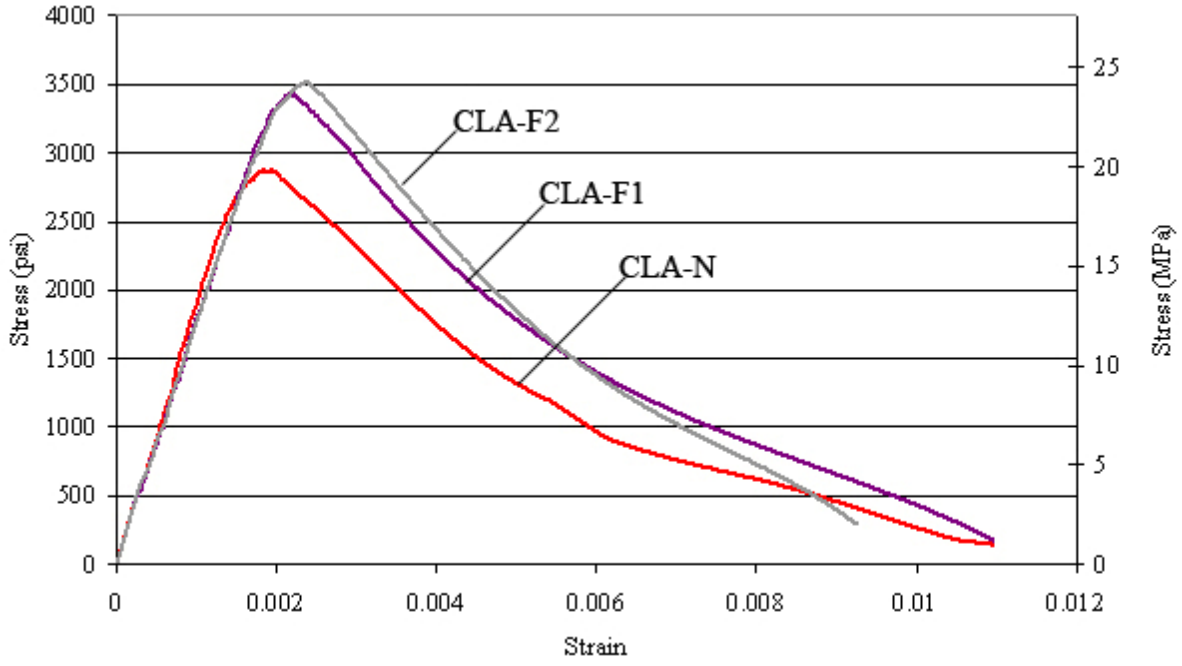

Figure 3.14: Average Stress vs. Strain curves for clay masonry piers

	Peak stress (psi)	Strain at peak stress	Strain at 50% of the peak stress
CON-N	**2680**	**0.00163**	**0.00323**
CON-F1	**2900**	**0.00185**	**0.00389**
CON-F2	**3140**	**0.00193**	**0.00472**
CLA-N	**3015**	**0.00176**	**0.00447**
CLA-F1	**3480**	**0.00217**	**0.00526**
CLA-F2	**3545**	**0.00224**	**0.00499**

Table 3.4: Average peak stress, strain at peak stress and strain at 50% of the peak stress for every group of 5 piers (1 ksi = 6.89 MPa)

One concrete specimen without fiber (CON-N-2) was accidentally broken without collecting data; this specimen was not included in the values of the previous table. Nevertheless, it was considered during the analysis of variance by having different sample sizes. Also, a problem with the potentiometer controlling the table speed resulted in two pier failures after only a few seconds of testing (CON-F1-3 and CLA-N-4). The load-displacement curves were recorded, but the strain rates were a lot higher than for all other tests.

Observations were made of the specimens after testing. In several piers, when the grout core was visible, a hole of approximately the size of the grout vibrator was visible, showing that the grout wasn't fluid enough or that the fibers made the grout too thick to fill the holes correctly (see Figure 3.15). This phenomenon was observed in piers constructed of both types of materials.

For the concrete masonry specimens, the average peak stress was improved when fibers were added. The larger amount of fibers gave the best results. The ductility capacity was also increased compared to the specimens without fibers. Strains at 50% of the peak stress were 28% to 47% greater when fibers were added in the grout.

For clay brick specimens, the larger the amount of fiber, the higher the peak stress. The ductility capacity was also increased. Note that the ductilities for piers with fibers were very close. Strains at 50% of the peak stress were only 11% to 18% greater when fibers were added in the grout.

Figure 3.15: Holes in the grout due to the vibrator

Figure 3.16 and Figure 3.17 compare the slopes of the descending branches of the stress-strain curves for both materials. It can be observed that the greater the amount of fibers added to the grout, the larger the increase in strain capacity for concrete masonry, regardless of the increase in peak stress values. For the clay brick piers, even when specimens with Fiber 2 presented a slightly superior capacity than the others, the specimens did not show noticeable differences in slopes of the descending branches of the curves. Therefore, the fibers increased the

strain capacity because the peak stress values were increased, but they did not change the behavior of the falling part of the stress-strain diagrams. Note that focus is on the descending part of the stress-strain curve prior to reaching strains at 50% of the peak stresses.

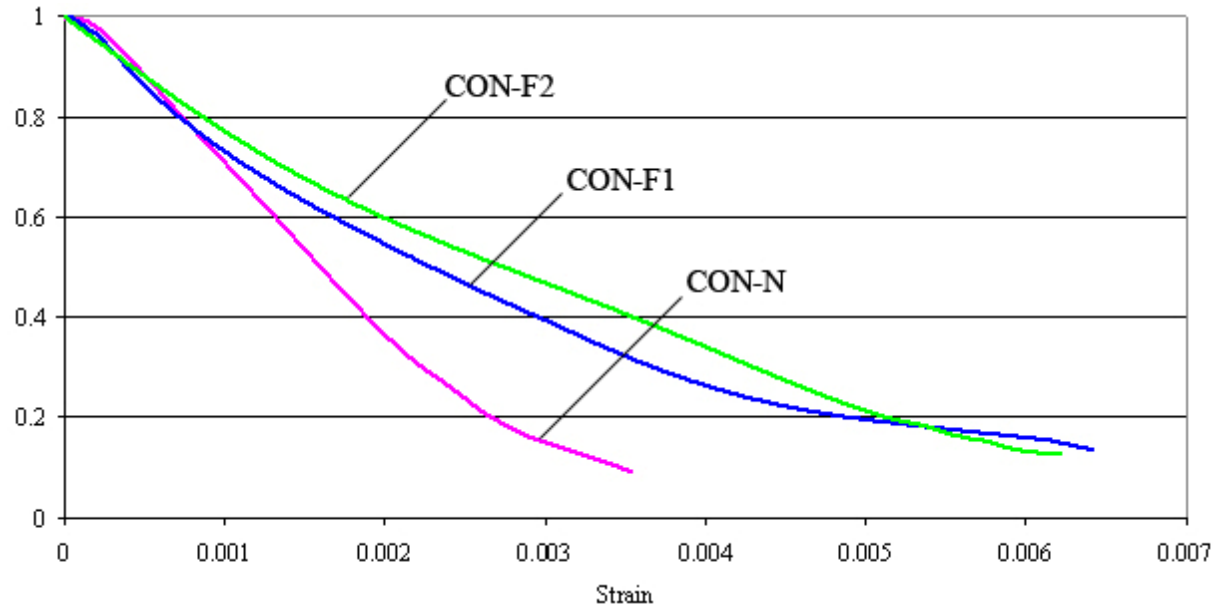

Figure 3.16: Comparison of the slopes of the falling branches of the Stress vs. Strain curves for concrete masonry

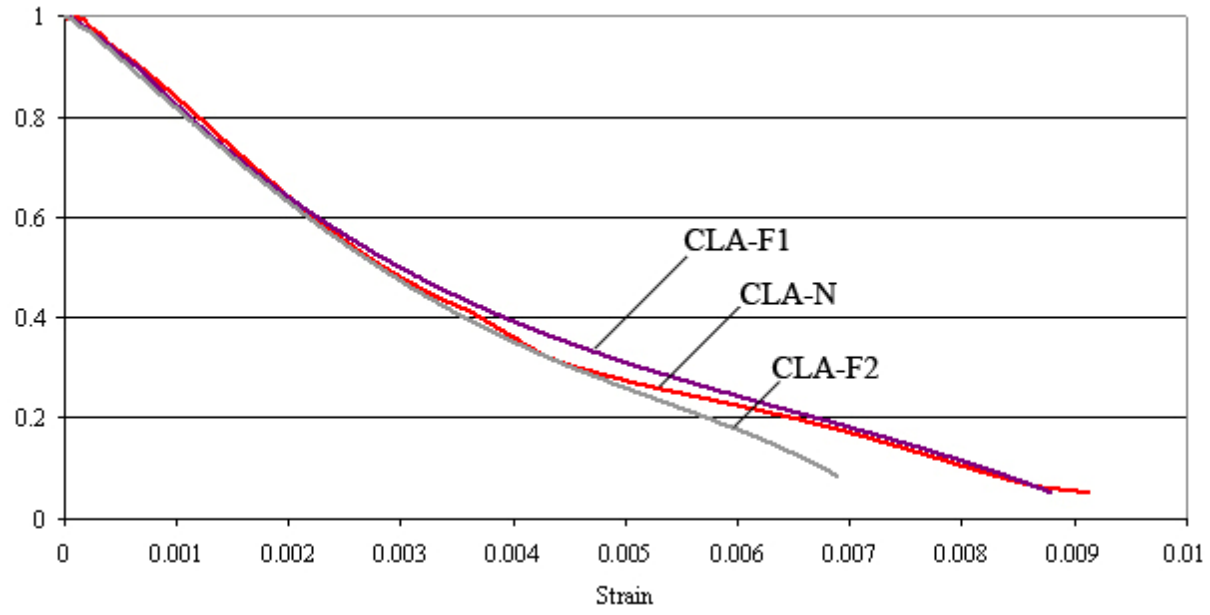

Figure 3.17: Comparison of the slopes of the falling branches of the Stress vs. Strain curves for clay masonry

3.8.3 Analysis of variance (ANOVA)

An analysis of variance (ANOVA) was conducted using SAS in order to determine if the amount of fibers had a statistically significant effect on peak stress values as well as on the strains at peak stress and at 50% of the peak stress for both materials. In both analyses, a 90% confidence level was used. The coding for the ANOVA function and the imported values for both materials are presented in Appendix D.

For the clay piers, the ANOVA showed that the amount of fibers had a significant effect on the values of peak stresses and on the corresponding strains, but not on the values of strain at 50% of the peak stress (see Table 3.5). A Duncan's grouping compared the results two by two, considering every combination, and is presented in Table 3.6. Two identical letters indicate no statistical difference. Two different letters indicate statistical difference.

Clay	Peak stress	Strain at peak stress	Strain at 50% of the peak stress
Significance	**YES**	**YES**	**NO**

Table 3.5: Significance of the amount of fibers on the different parameters investigated for the clay piers

Clay	Peak stress	Strain at peak stress	Strain at 50% of the peak stress
F2	**A**	**A**	**-**
F1	**A**	**A**	**-**
No Fibers	**B**	**B**	**-**

Table 3.6: Duncan's grouping for the clay bricks

Column 1 of Table 3.6 shows that the results for peak stresses are not statistically different for the two percentages of fibers evaluated (group A), but results from specimens with fibers are statistically different from the results obtained for specimens with no fibers (group B). The conclusion is the same for column 2 concerning the strains at peak stresses. Duncan's grouping for column 3 is not relevant because no significance of the amount of fibers was observed for the strains at 50% of the peaks stresses.

For the concrete masonry piers, the ANOVA showed that there is a significant effect of the amount of fibers on the peak stresses (see Table 3.7). Results are inverted for the strains at peak stresses and strains at 50% of the peak stresses. The amount of fibers showed no significance on the values of the strains at peak stresses, while the results for strains at 50% of the peak stresses do show a significant difference.

Concrete	Peak stress	Strain at peak stress	Strain at 50% of the peak stress
Significance	**YES**	**NO**	**YES**

Table 3.7: Significance of the amount of fibers on the different parameters investigated for the concrete piers

Concrete	Peak stress	Strain at peak stress	Strain at 50% of the peak stress
F2	**A**	**-**	**A**
F1	**A B**	**-**	**A B**
No Fibers	**B**	**-**	**B**

Table 3.8: Duncan's grouping for the concrete blocks

Duncan's grouping is the same for the three columns (see Table 3.8), but only columns 1 and 3 are relevant. The grouping shows that when you compare two values together, "F2" and "F1" are not statistically different (group A), and "F1" and "No fibers" are also not statistically different (group B). However, if we consider the results of "F2" and "No fibers", they are statistically different (groups A and B, respectively).

3.8.4 Comparison with previous results

Results from the studies conducted by Priestley and Elder (1983), Hart et al (1988) and Malmquist et al (2004) on the influence of confinement reinforcement on the compressive behavior of concrete blocks and clay brick masonry piers are summarized in Table 3.9. They used two types of confinement: a seismic comb made of 3/16 in. (4.7 mm) diameter galvanized wires, and 3/16 in. (4.7 mm) thick steel plates.

	Confinement	Authors	Strain at peak stress (in/in)	Strain at 50% of the peak stress
Concrete masonry	Steel plates	Priestley	0.0020	0.0074
	Steel plates	Hart et al	0.0019	0.0065
	Steel plates	Malmquist	0.0023	0.0055
	Combs	Hart et al	0.0016	0.0055
	Combs	Malmquist	0.0019	0.0060
	Fibers (5 lbs/yd^3)	Hervillard	0.0019	0.0039
	Fibers (8 lbs/yd^3)	Hervillard	0.0019	0.0047
Clay masonry	Steel plates	Malmquist	0.0026	0.0061
	Combs	Malmquist	0.0026	0.0057
	Fibers (5 lbs/yd^3)	Hervillard	0.0022	0.0053
	Fibers (8 lbs/yd^3)	Hervillard	0.0022	0.0050

Table 3.9: Previous and current results

For the strain at peak stress for concrete masonry piers, it can be seen that fibers produce increases that are similar to or better than those for the steel plates used by Hart or the combs used by Hart or Malmquist. However, when strain at 50% of the peak stress is considered, the two dosages of fibers did not show as large an increase when compared to that obtained with the other types of confinement. Priestley and Malmquist, with the steel plates, showed better results for both strain at peak stress and strain at 50% of the peak stress than with the fibers.

For the clay piers, the fibers showed a smaller increase in the strain at peak stress and strain at 50% of the peak stress values when compared to those obtained by Malmquist with the steel plates or the combs.

3.9 CONCLUSIONS

The following conclusions are reached based on the pier tests of this study:

1. A statistical analysis conducted with a 90% confidence level showed that the use of fibers in the grout as a reinforcement for clay masonry is effective for increasing the peak stresses and the corresponding strains, but it appears to not have a significant influence on the strains at 50% of the peak stresses.
2. A statistical analysis conducted with a 90% confidence level showed that for concrete masonry fibers increase significantly the peak stresses and the strain at 50% of the peak stresses but have no significant influence on the strains at peak stresses.
3. Clay masonry developed larger peak stresses and larger strain capacities than did concrete masonry. The best results for concrete masonry were obtained with 8 lbs/yd^3 of fibers mixed with the grout, and these results were very close to those of clay masonry piers without fibers. Results obtained with both dosages of fibers for clay masonry were similar and resulted in the largest peak stresses and strain capacities.
4. When compared to results from previous research, where other types of confinement reinforcement were used, the fibers did not produce similar improvements in performance. While the addition of the fibers improved important properties such as peak stress values, strains at peak stresses and strains at 50% of the peak stresses, the increases were less than those reported for steel plates and seismic combs.
5. The fibers had a positive effect on the grout core protection. Indeed, even when the masonry units were damaged during testing, grout cores almost always remained intact. Fibers provided an efficient post-crack control to the grout. However, as no fibers were incorporated in the mortar joints, and bonding with the masonry units was not improved by the addition of

the fibers, the masonry face shells were not restrained from spalling, diminishing considerably the strain that the piers could attain. Incorporation of fibers in the mortar joints may have the effect of confining the masonry units and therefore could show better results. Another possibility is to incorporate fibers in the masonry units. This may be a very good way to provide an efficient post crack control to the units themselves. Research should be conducted on piers containing larger amounts of fibers in the grout in order to see if higher values can be achieved for peak stresses and strain capacities. However, a modification of the grout slump may be necessary in order to achieve proper grout consolidation with larger amounts of fibers.

CHAPTER FOUR: MODELING OF SHEAR WALLS

4.1 INTRODUCTION

After completion of the tests on the piers confined with polymer fibers, the Modified Kent-Park model was used to characterize the stress-strain behavior of the concrete masonry and clay brick masonry confined with fibers. The study by Malmquist (2004) provided results that enabled the same model to be utilized to characterize the stress-strain behavior of masonry piers confined with steel plates or seismic combs. The resulting stress-strain models were imported into commercial software to obtain moment-curvature predictions that were used to analyze the shear walls tested by Eikanas (2003) and Snook (2005). Analytical results were compared to the experimental results obtained in the two previous studies. The relationship between the confinement reinforcement ratio and the load-displacement behavior was also investigated.

4.2 MODELING THE STRESS-STRAIN CURVES OF THE DIFFERENT MATERIALS

Various mathematical models, such as the Kent-Park model created by Kent and Park in 1971, the Modified Kent-Park model proposed by Park and Priestley in 1982, and the Mander model in 1988, were created to fit the compressive stress-strain behavior of concrete. Priestley and Elder (1983) adjusted the Modified Kent-Park model to fit unconfined and confined masonry results, reducing the value of the strain at peak stress to obtain a better fit for masonry. After testing the models to fit the experimental data collected in the current study and by Malmquist in 2004, the Modified Kent-Park model was determined to provide the best fit. The model is described by Equations 2.13 and 2.14 in Chapter 2.

The Modified Kent-Park model directly depends on the compressive strength of the material; therefore, it was possible to adjust the model to account for Eikanas (2003) and Snook (2005) prism compressive strengths.

Figure 4.1 presents the experimental data, the Modified Kent-Park model and the Modified Kent-Park model adjusted for Eikanas' f'_m for unreinforced concrete masonry. Figures 4.2 to 4.6 present the same diagrams for unconfined and confined concretes adjusted for Snook's f'_m. The stress-strain behavior of clay brick masonry piers was also modeled, and the curves are presented in Appendix E. Good correlation between experimental data and the model was obtained for unconfined and confined clay masonry with seismic combs and both dosages of fibers but not for the steel plates because the model overestimated the strain capacity in this specific case. However, as no shear walls made of this material were tested, it was not possible to compare experimental and analytical results and, therefore, no further investigations on the clay brick masonry piers were conducted. Note that the model also seems to overestimate results for the case of confined concrete masonry with steel plates. However, the results obtained with the Modified Kent-Park model were considered acceptable and were used in the modeling of the walls. Good correlation between the model and the experimental results for the masonry contained with fibers in the grout was obtained. Notice that in the following figures, the Modified Kent-Park curves and Modified Kent-Park adjusted for f'_m curves stop at the same strain as that obtained for the experimental results. When the adjusted Modified Kent-Park model was used to model the shear walls, the slope of each curve was continued until reaching zero stress. No plateau at 0.2 f'_m was included.

A modification of the Modified Kent-Park model was necessary to account for fiber reinforcement. Only the strength enhancement coefficient, K, used in Equations 2.13 and 2.14, and the constant, Z_m, were modified in order to take into account the amount of fibers mixed with the grout. Flexural tests on grout beams containing fibers provided tensile strengths, f_{flex}, of 100 psi (0.69 MPa) and 160 psi (1.10 MPa) for the two dosages of fibers investigated in this study. It is possible to relate these values to the action of the traditional steel confinement reinforcement as $2f_{flex} = \rho_s f_{yh}$. Therefore, the new formula for calculating the enhancement coefficient K is given by Equation 4.1:

$$K = 1 + 2\frac{f_{flex}}{f'_c} \qquad \textit{Equation 4.1}$$

Where:

- f_{flex} is the flexural tensile strength of the grout beams, MPa; and
- f'_c is the compressive strength of a concrete cylinder, MPa.
- ρ_s is the volumetric ratio of confining steel equal to the volume of confining steel divided by the volume of confined concrete; and
- f_{yh} is the confining steel yield strength, MPa.

The constant Z_m becomes:

$$Z_m = \frac{0.5}{\left[\frac{3 + 0.29f'_c}{145f'_c - 1{,}000}\right] + \frac{\rho_f}{8{,}000} - 0.002K} \qquad \textit{Equation 4.2}$$

Where:

- ρ_f is the volumetric ratio of confining fibers equal to the weight of fibers in kg divided by the volume of grout in m^3.

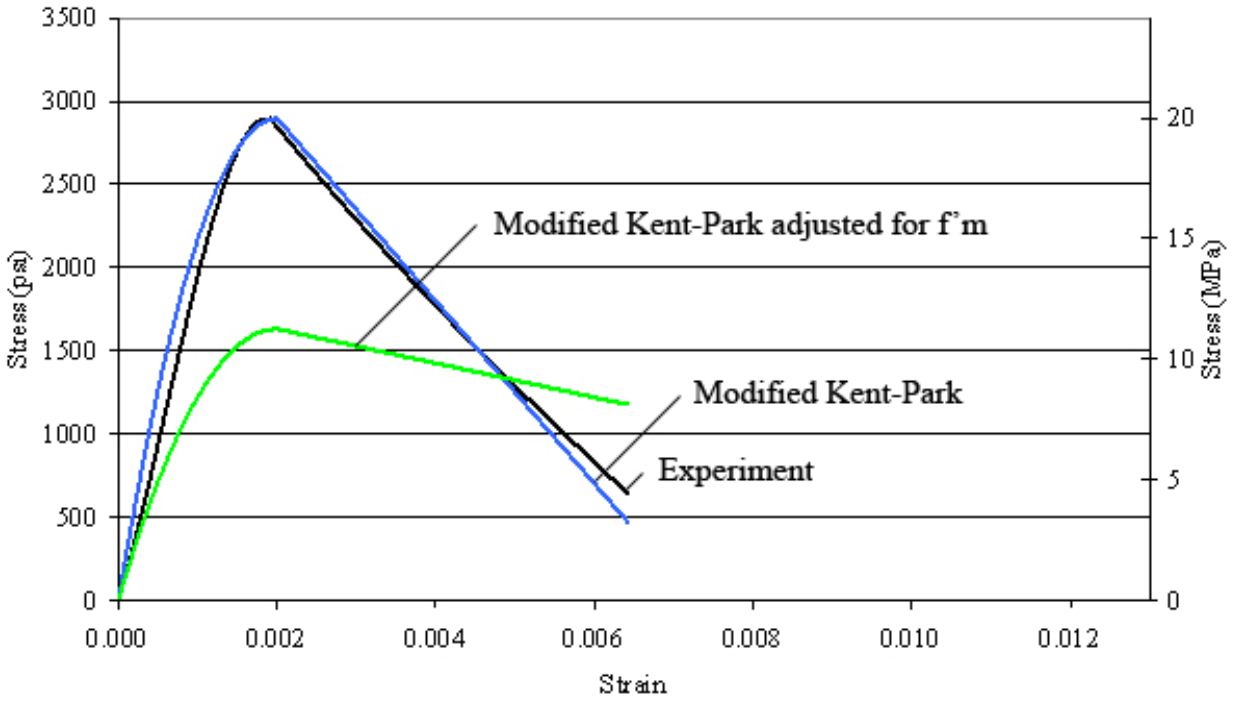

Figure 4.1: Stress vs. Strain curves for CON-N adjusted for Eikanas's f'_m

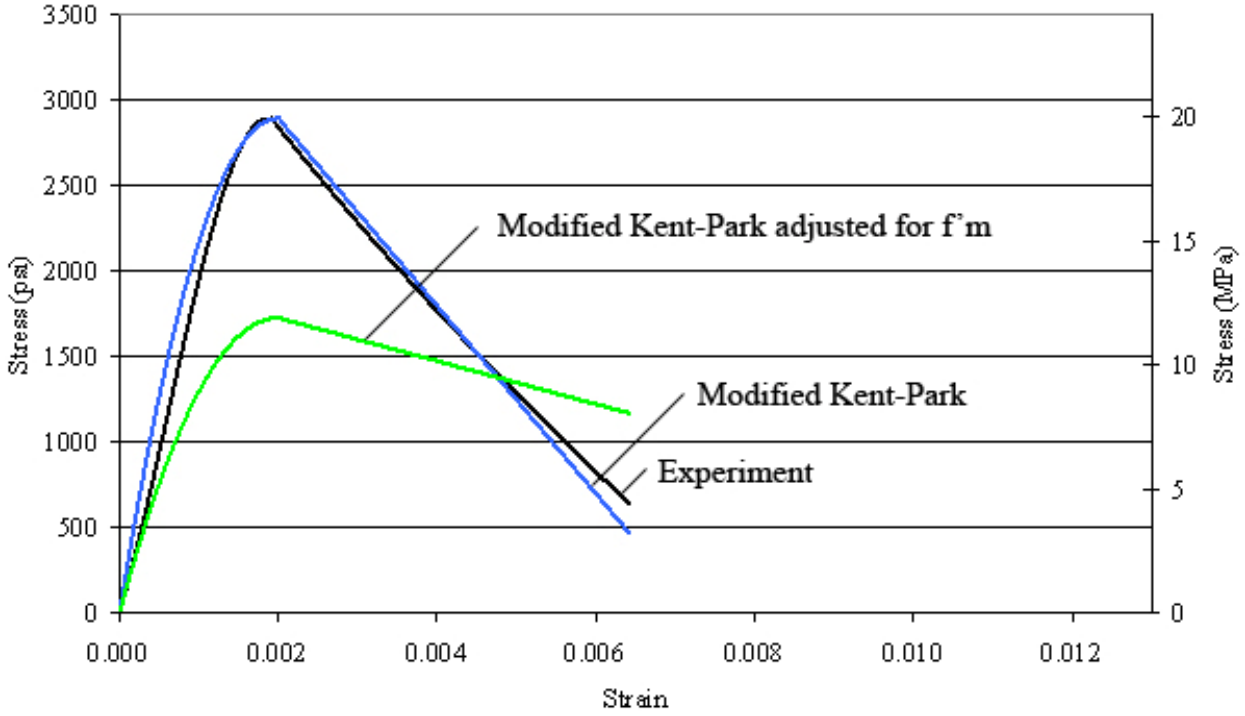

Figure 4.2: Stress vs. Strain curves for CON-N adjusted for Snook's f'_m

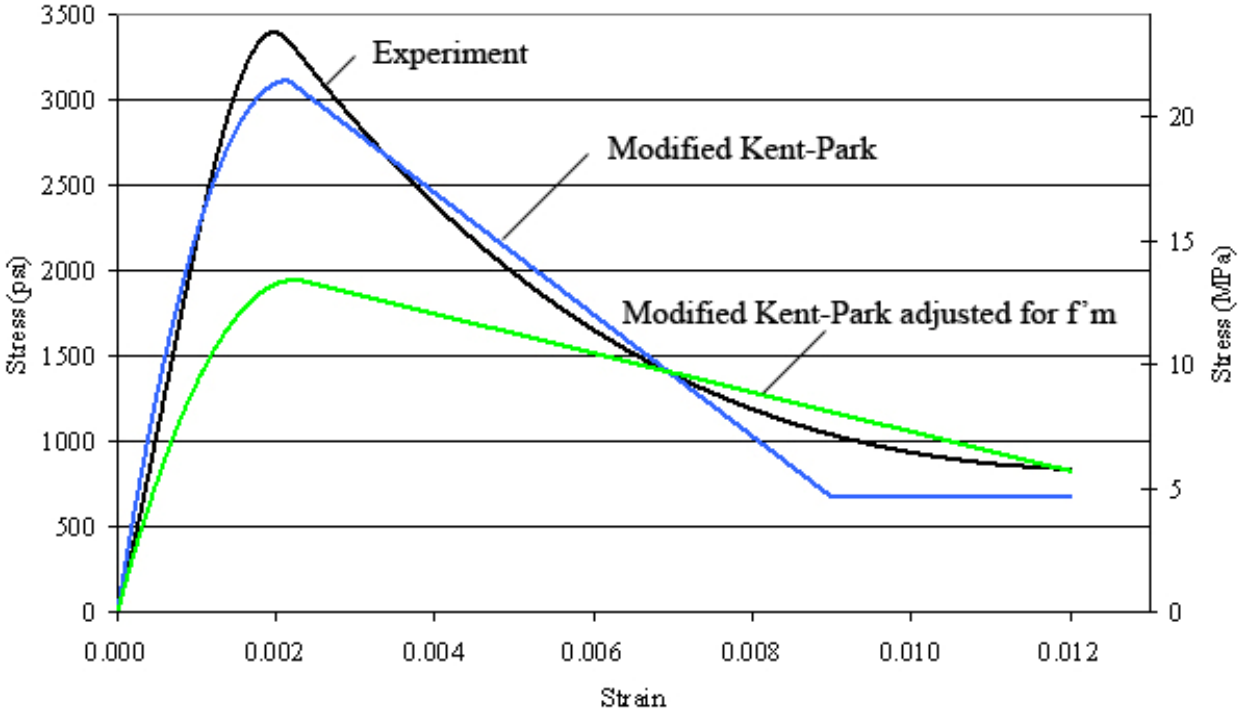

Figure 4.3: Stress vs. Strain curves for CON-C adjusted for Snook's f'_m

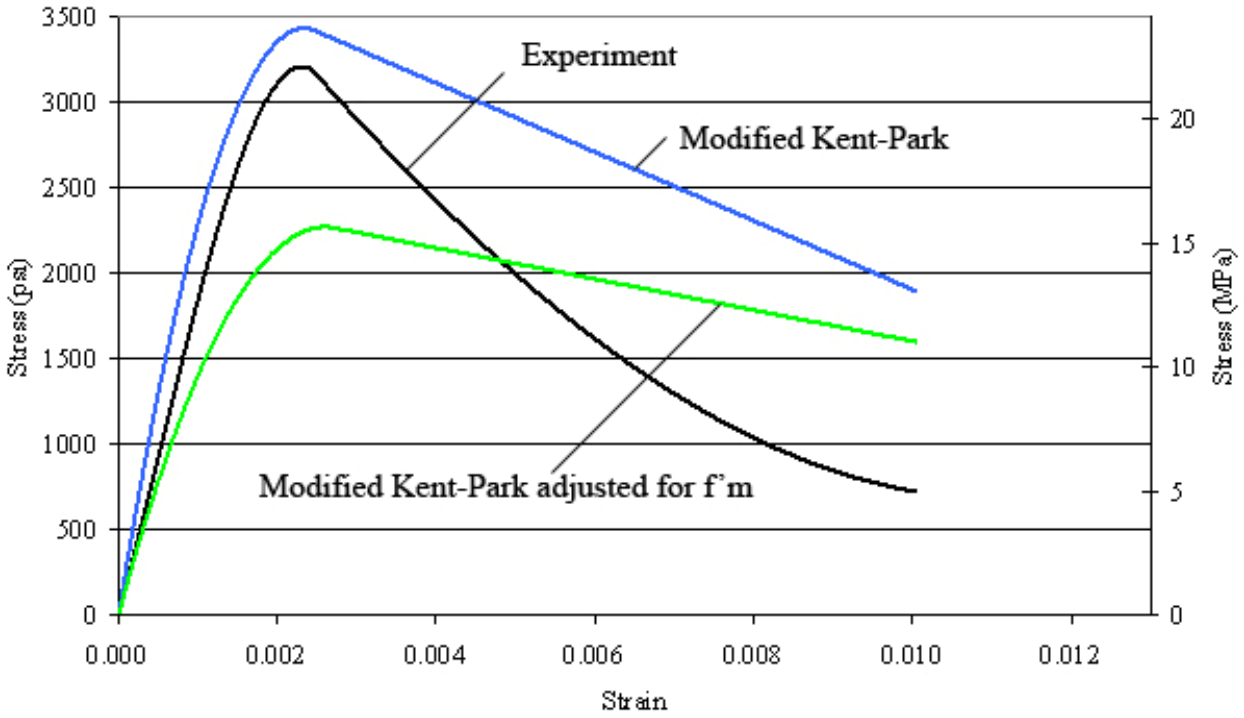

Figure 4.4: Stress vs. Strain curves for CON-P adjusted for Snook's f'_m

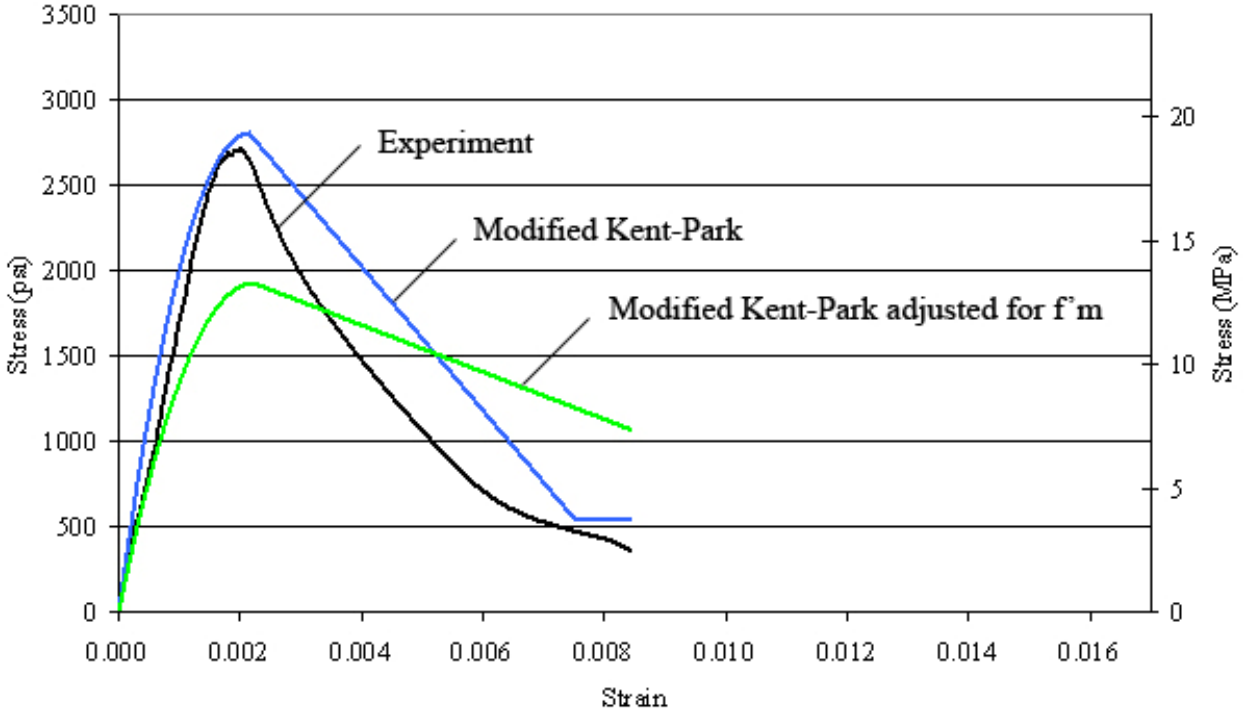

Figure 4.5: Stress vs. Strain curves for CON-F1 adjusted for Snook's f'_m

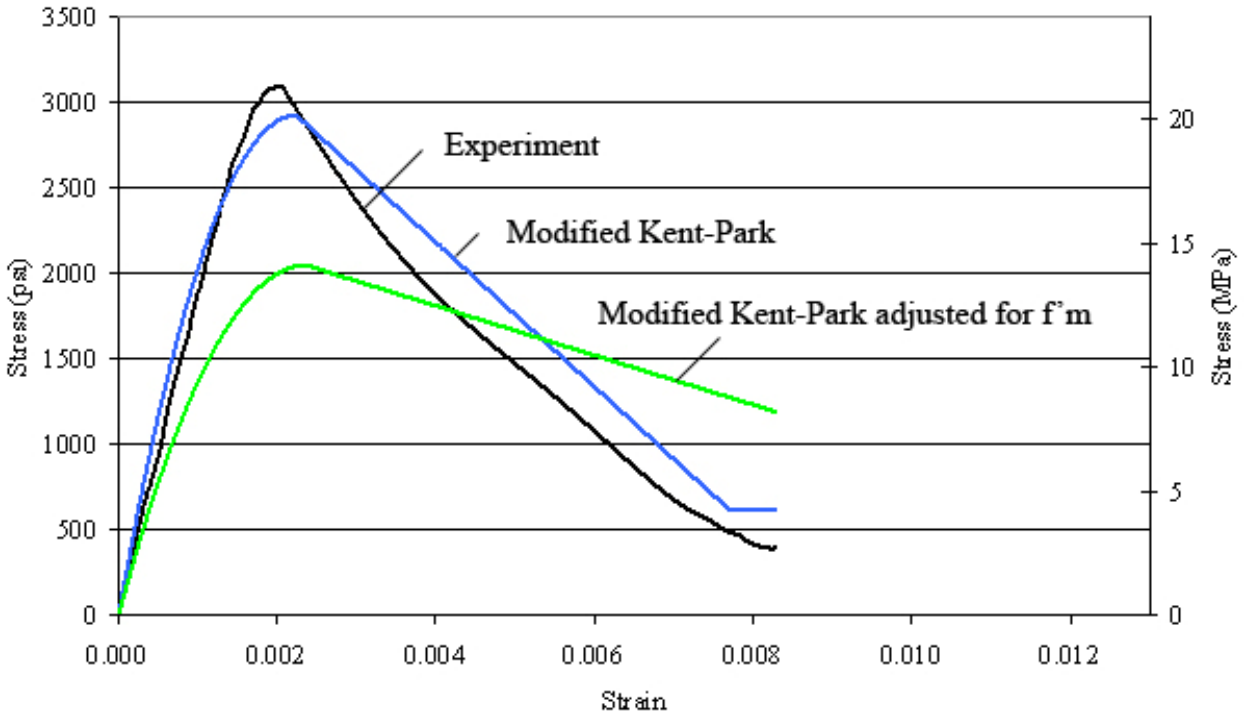

Figure 4.6: Stress vs. Strain curves for CON-F2 adjusted for Snook's f'_m

4.3 MODELING OF THE SHEAR WALLS

The commercial software XTRACT v.3.0.4 was used to model the shear wall cross-section flexural response. This software allows the user to import stress-strain curves to describe the behavior of user-defined materials. This option along with the ability to run moment-curvature analyses are the main reasons that XTRACT was selected for use in this study. Load-displacement diagrams can be derived from the moment-curvature results and can therefore be compared to experimental load-displacement results of the walls.

Each wall cross-section was represented with the appropriate dimensions and amount of vertical steel reinforcement (see Figure 4.7). The software provided a pre-defined bilinear steel model with strain hardening that was used for this study. The only modification made was to adjust for the yield strengths measured by Eikanas (2003) and Snook (2005). Then, if the wall

was confined by steel plates or seismic combs, it was divided into three parts representing the two confined areas on each side of the wall and the unconfined area in the center. Each part of the wall was assigned a material defined by its stress-strain behavior (based on the Modified Kent-Park model). In the case of walls confined with polymer fibers, the entire cross-section was confined and only one stress-strain model was used. An axial load was applied to the cross-section to represent the applied axial stresses of 27 psi (0.19 MPa) for Eikanas and 34 psi (0.24 MPa) for Snook. Note that the horizontal reinforcement used in both studies was not modeled in the walls. Results from XTRACT only reflect the flexural behavior of the walls.

A typical results file produced by XTRACT is presented by Figure 4.8. Moment-curvature results for each wall are given in Appendix F. XTRACT output includes the axial load applied at the free end, the material which failed (steel or concrete), the effective yield curvature, the effective yield moment, and the ultimate curvature. These last three values define a bilinear curve, based on equal areas over and under the calculated curve (see bottom diagram of Figure 4.8). The top diagram on Figure 4.8 represents the state of the cross-section at failure. The different states of the cross-section (from left to right) are: masonry cracked in tension, uncracked masonry in tension, uncracked masonry in compression, and masonry in compression experiencing strains larger than the strain at peak stress.

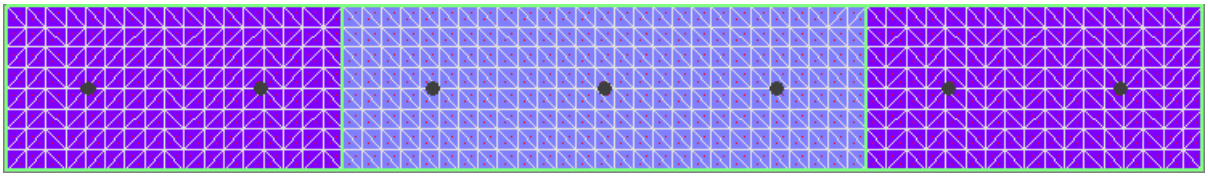

Figure 4.7: Example of cross-section of a confined wall produced by XTRACT

Eikanas (2003) and Snook (2005) defined failure at 20% load degradation, and the moment-curvature analyses were run until a 20% moment drop was obtained. However, the program occasionally did not go until that point, but rather stopped when a material failed. Failure occurs when the ultimate strain of a material is reached. Analysis beyond that point was forced by continuing the analysis beyond when failure of a material occurred. This is why the moment-curvature diagrams are not always smooth in the ultimate curvature zone.

XTRACT Analysis Report - Educational

Thomas Hervillard
Washington State University
9/17/2005

Section Name: Section2
Loading Name: Loading
Analysis Type: Moment Curvature

Ian - Wall 1 - Con-N-Kirk

Section Details:

X Centroid:	27.81 in
Y Centroid:	3.812 in
Section Area:	424.1 in^2

Loading Details:

Constant Load - P:	11.45E+3 lbs
Incrementing Loads:	Myy Only
Number of Points:	80
Analysis Strategy:	Displacement Control

Analysis Results:

Failing Material:	Con-N-Kirk
Failure Strain:	26.00E-3 Compression
Curvature at Initial Load:	-.2818E-19 1/in
Curvature at First Yield:	57.48E-6 1/in
Ultimate Curvature:	1.845E-3 1/in
Moment at First Yield:	1.682E+6 lb-in
Ultimate Moment:	2.288E+6 lb-in
Centroid Strain at Yield:	.9000E-3 Ten
Centroid Strain at Ultimate:	25.45E-3 Ten
N.A. at First Yield:	15.66 in
N.A. at Ultimate:	13.80 in
Energy per Length:	4569 lbs
Effective Yield Curvature:	86.70E-6 1/in
Effective Yield Moment:	2.537E+6 lb-in
Over Strength Factor:	.9022
Plastic Rotation Capacity:	23.58E-3 rad
EI Effective:	2.93E+7 kip-in^2
Yield EI Effective:	0 kip-in^2
Bilinear Harding Slope:	0 %
Curvature Ductility:	21.28

Comments:

User Comments

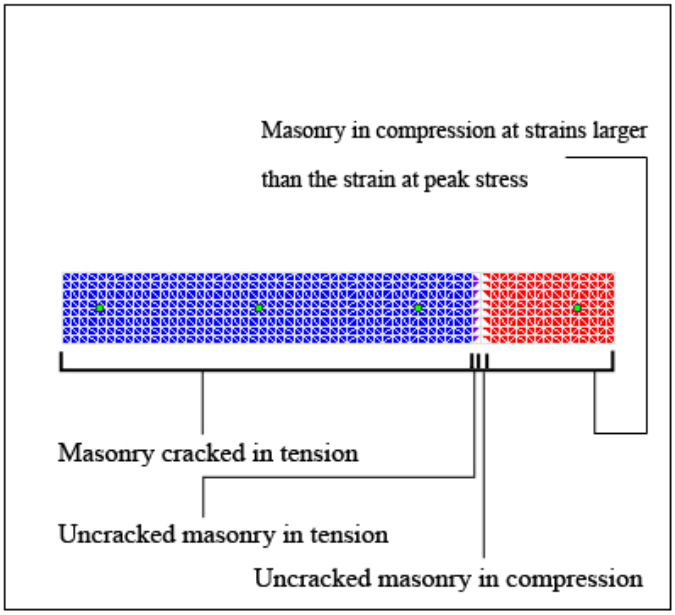

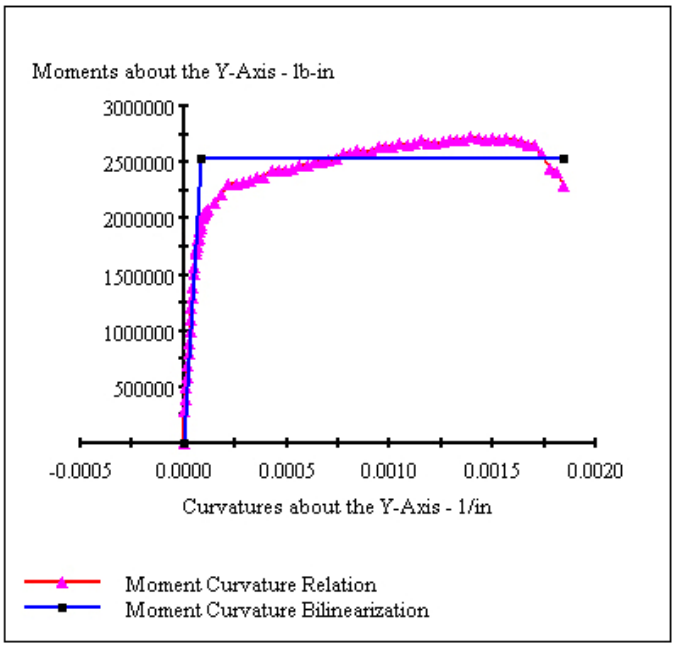

Figure 4.8: Typical result file produced by XTRACT

4.4 RESULTS

4.4.1 Results from XTRACT

XTRACT calculates the effective yield curvature, ϕ_y, the effective yield moment, M_y, and the ultimate curvature, ϕ_u, based on equal areas over and under the bilinearized moment-curvature curve. Knowing these three values allows for plotting of the load-displacement diagram by applying Equations 4.3 to 4.5.

The ultimate load, P_u, is assumed to be equal to the yielding load, P_y:

$$P_u = \frac{M_y}{h_w} \qquad \textit{Equation 4.3}$$

Where :

- M_y is the effective yield moment, in.-lb

  = M_u the ultimate moment, in.-lb; and
- h_w is the height of the wall, in.

The yield displacement, Δ_y, is given by Equation 4.4:

$$\Delta_y = \frac{\phi_y h_w^{\,2}}{3} \qquad \textit{Equation 4.4}$$

Where:

- ϕ_y is the effective yield curvature, 1/in.

The ultimate displacement, Δ_u, of a cantilever shear wall considering only flexural deformation can be calculated by Equation 4.5:

$$\Delta_u = \frac{\phi_y h_w^{\,2}}{3} + (\phi_u - \phi_y) L_p \left(h_w - \frac{L_p}{2} \right) \qquad \textit{Equation 4.5}$$

Where:

- ϕ_u is the ultimate curvature, 1/in.; and
- L_p is the plastic hinge length, in. (see Equations 2.6 and 2.7).

4.4.2 Results from experiments

Eikanas (2003) and Snook (2005) measured the total displacement corresponding to 20% load degradation, $\Delta_{20\%}$, (see Table 4.1). In order to be able to compare the ultimate displacements recorded during tests with those calculated by XTRACT, the displacements due to flexure should be determined. Both researchers provided a percentage of the total drift due to flexure (see Table 4.1), allowing the calculation of the ultimate displacement due to flexure, $\Delta_{u,flex}$, (see Equation 4.6 and Table 4.1).

$$\Delta_{u,flex} = \Delta_{20\%} \times (\%\ of\ Flexure) \qquad \textit{Equation 4.6}$$

	Wall	Aspect ratio	Total disp. at 20% load deg (in.)	% of total drift due to flexure	Disp. at 20% due to flexure (in.)	Load at 20% load degradation (kip)
Eikanas	**1**	0.93	1.12	50%	0.56	45.78
	2	1.51	1.99	81%	1.61	25.46
	3	-	-	-	-	-
	4	0.93	0.69	65%	0.45	48.76
	5	1.51	1.38	87%	1.20	34.49
	6	2.12	2.24	92%	2.06	22.54
	7	0.73	0.70	50%	0.35	62.69
Snook	**1**	0.93	1.10	42%	0.46	57.24
	2	0.93	1.07	42%	0.45	56.46
	3	0.93	1.18	37%	0.44	63.84
	4	0.93	1.60	43%	0.69	65.18
	5	1.51	2.31	84%	1.94	43.16
	6	1.51	2.62	83%	2.17	42.44
	7	1.51	2.35	81%	1.90	44.97
	8	1.51	2.25	74%	1.67	45.32
	9	1.51	2.60	76%	1.98	45.61

Table 4.1: Results from previous studies

XTRACT provided an effective yield moment based on the equal area method leading to an "average" ultimate load. Therefore, it was necessary to calculate the ultimate experimental load by the same method. A Matlab script (see Appendix G) calculated the ultimate load, P_u, by the equal area method based on the load-displacement envelopes reported by Eikanas (2003) and Snook (2005). An example is presented in Figure 4.9. Results are given in Table 4.1. Eikanas's Wall 3 was not studied because a problem with the hydraulic system caused a sudden displacement in the wall and damaged it prior to applying cyclic loading.

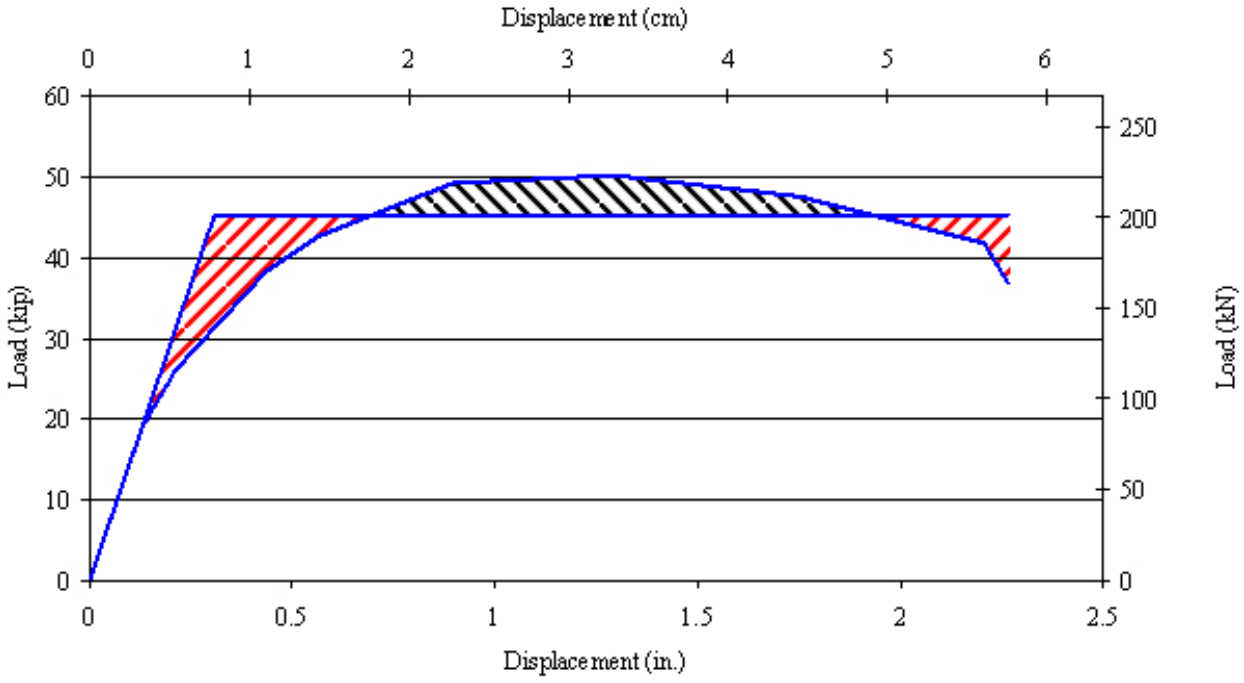

Figure 4.9: Example of 20% load degradation calculation based on experiment (1 in. = 2.54 cm, 1 kip = 4.448 kN)

From experimental data, the slope of the first loading cycle can be determined. The yielding displacement, Δ_y, can therefore be calculated by Equation 4.7.

$$\Delta_y = \frac{P_u}{Slope} \qquad \textit{Equation 4.7}$$

Where:

- P_u is the ultimate load, kip; and
- *Slope* is the slope of the first loading cycle.

The yield curvature, ϕ_y, can be calculated by Equation 4.8:

$$\phi_y = \frac{3\Delta_y}{h_w^{\,2}} \qquad \textit{Equation 4.8}$$

Where:

- Δ_y is the yield displacement, in.; and
- h_w is the height of the wall, in.

The ultimate moment, M_u, can be calculated by Equation 4.9:

$$M_u = P_u h_w \qquad \textit{Equation 4.9}$$

And the ultimate curvature, ϕ_u, can be calculated by Equation 4.10:

$$\phi_u = \phi_y + \frac{\Delta_{u,flex} - \Delta_y}{L_p\left(h_w - \frac{L_p}{2}\right)} \qquad \textit{Equation 4.10}$$

4.4.3 Comparison of analytical and experimental results

It is possible to compare the experimental and analytical results in terms of moment-curvature or load-displacement. The second method was used in this study. Note that the conclusions obtained will be the same if the results were compared in terms of moment-curvature.

In the calculations, the ultimate displacement and curvature depend on the plastic hinge length. Paulay and Priestley (1992) proposed two equations to calculate the plastic hinge length depending on the wall aspect ratio (see Equation 2.6 and Equation 2.7). All of the tested walls had aspect ratios less than or equal to 2.1. Equation 2.6 was selected because it is more applicable to squat shear walls. Eikanas estimated the plastic hinge lengths of the walls he tested and found that Equation 2.6 slightly underestimated his measurements; therefore, the displacements calculated with Equation 4.5 are likely to be slightly smaller than in actuality. In Table 4.2, L_p refers to the plastic hinge lengths calculated with equation 2.6 for the different walls.

	Wall	Lp (in.)	Lp (cm)
Eikanas	1	13.4	34.1
	2	14.8	37.6
	3	11.6	29.5
	4	13.4	34.1
	5	14.8	37.6
	6	11.6	29.5
	7	16.6	42.2
Snook	1	13.4	34.1
	2	13.4	34.1
	3	13.4	34.1
	4	13.4	34.1
	5	14.8	37.6
	6	14.8	37.6
	7	14.8	37.6
	8	14.8	37.6
	9	14.8	37.6

Table 4.2: Plastic hinge lengths calculated with Paulay and Priestley's equation

XTRACT's predictions of the moment-curvature and load-displacement capacities were closer to the experimental results for the walls with higher aspect ratios (see Figure 4.10 and Figure 4.11) than for squat shear walls (see Figure 4.12 and Figure 4.13*Figure 4.13*). XTRACT predictions do not model shear deformations; therefore, the calculated displacements are only those due to flexure. Results would be expected to be more accurately predicted when large flexural displacements were recorded, and large flexural displacements are traditionally associated with high aspect ratios. Eikanas (2003) and Snook (2005) estimated the percentage of total drift due to flexure (see Table 4.1) and obtained larger results in the case of higher aspect ratios; however, these results were only estimations, and part of these displacements could be due to shear or even sliding. All load-displacement curves obtained with XTRACT are given in Appendix H.

The predictions of the load-displacement curves by the model were not perfect and could be improved if further research was conducted in order to better approximate the stress-strain behavior of the masonry piers. A more precise estimation of the plastic hinge length would also increase the accuracy of the model. Another source of error may come from the estimations of the percentage of the total drift due to flexure during experiments.

Overall, four predictions provided by the model were considered poor, four were considered fair, and seven were considered good. Of course, some differences in load and displacement capacities between experiments and the model are expected.

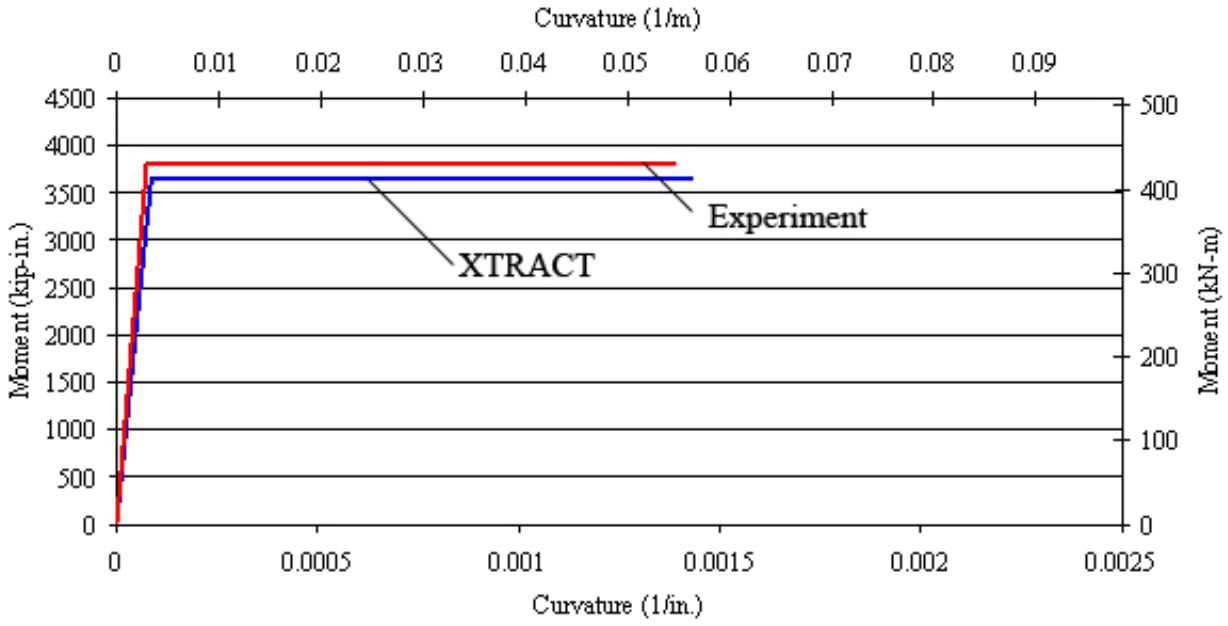

Figure 4.10: Moment-Curvature curves based on experiment and XTRACT for a slender wall

(Wall 8: Aspect ratio: 1.51 – Fiber 1)

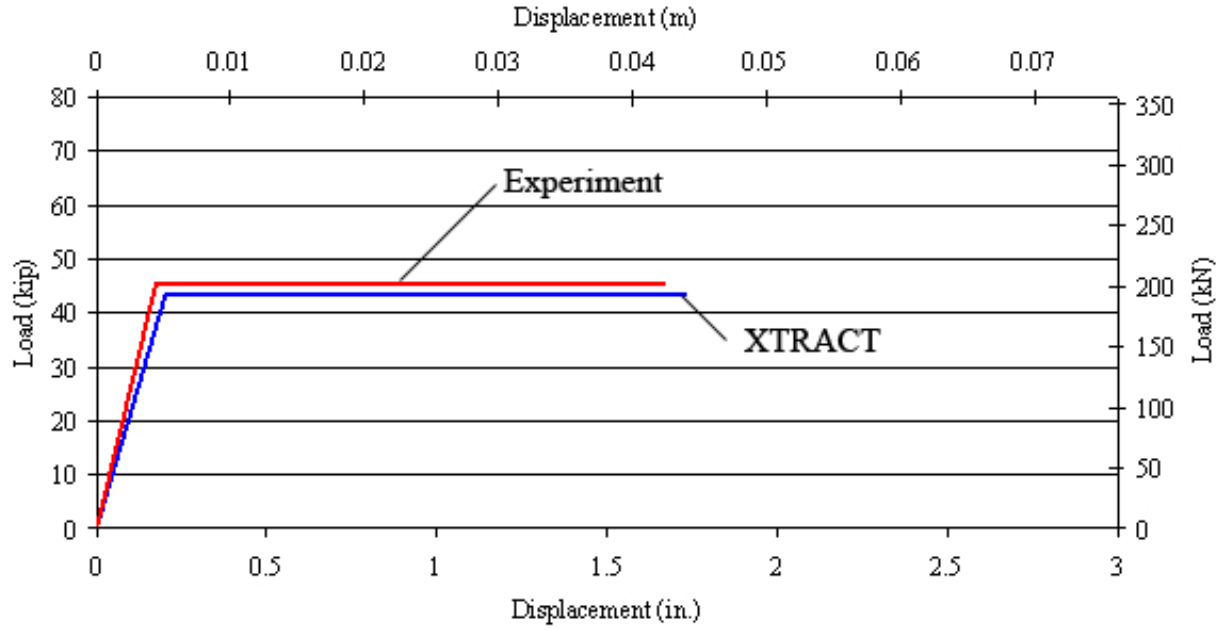

Figure 4.11: Load-Displacement curves based on experiment and XTRACT for a slender wall

(Wall 8: Aspect ratio: 1.51 – Fiber 1)

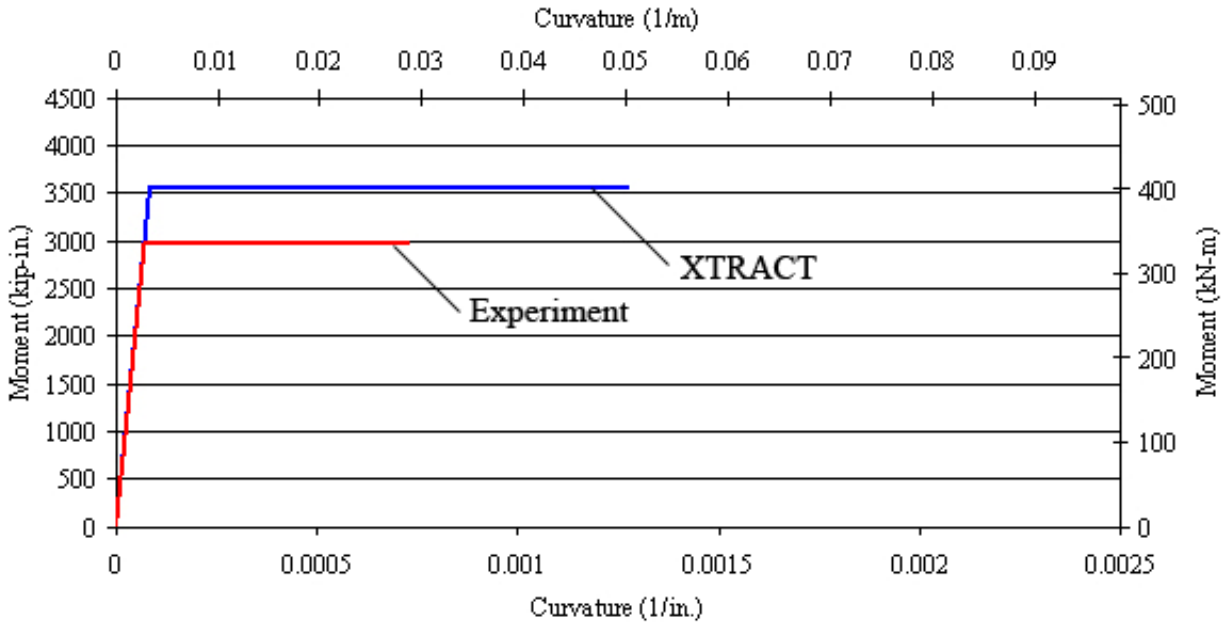

Figure 4.12: Moment-Curvature curves based on experiment and XTRACT for a squat wall

(Wall 1: Aspect ratio: 0.93 – Unconfined)

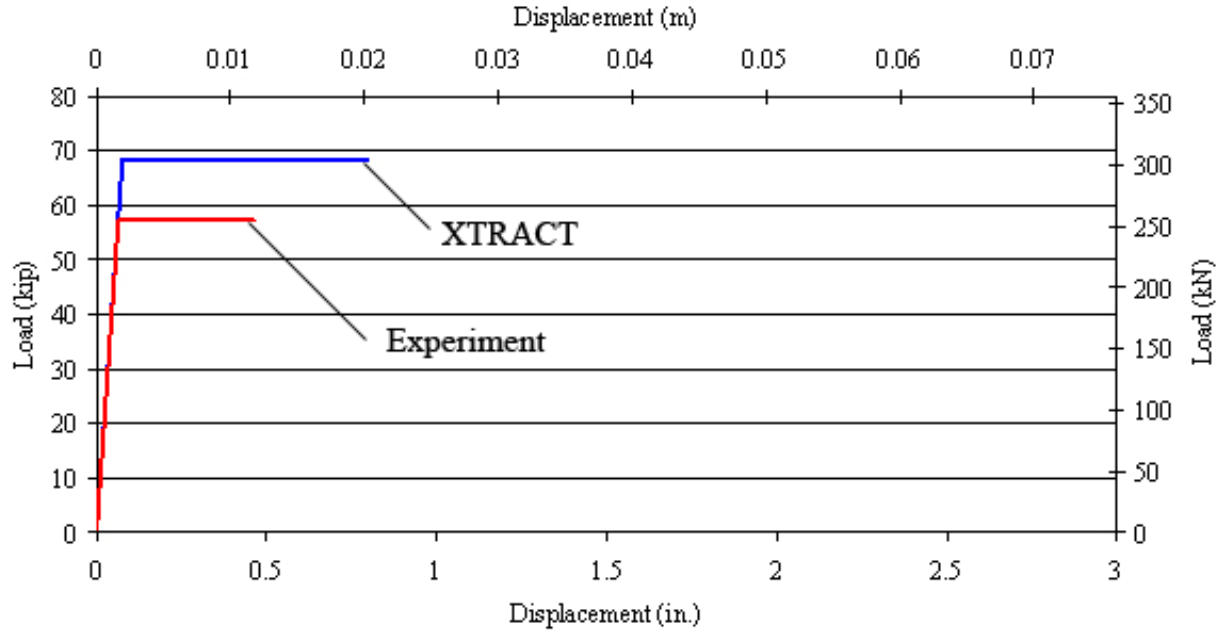

Figure 4.13: Load-Displacement curves based on experiment and XTRACT for a squat wall

(Wall 1: Aspect ratio: 0.93 – Unconfined)

An evaluation of the increase in displacement capacity due to confinement was made on Snook's walls for both experimental and XTRACT results in order to see if the model predicted the same increase obtained in the experimental results. The evaluation is summarized in Table 4.3. The increase in displacement in the experiments is based on the total improvement due to the confinement. It includes the displacements due to shear, flexure and sliding. The increase in displacement from XTRACT is only based on flexural displacements. Note that often the percentages of the total drifts due to flexure (see Table 4.1) for confined walls are smaller than for their unconfined replicas. If the increases in flexural displacements from experiments were calculated, it would therefore provide negative numbers. This would indicate a decrease in displacement, while the overall effect of the confinement would be expected to provide increases. As a result of this observation, it was decided to compare the total experimental displacement increase to the flexural displacement increase calculated by XTRACT. Also note that walls 2 and 8 presented smaller ultimate displacements than their unconfined replicas, walls 1 and 5, respectively.

It can be seen that the model did not predict the same increases in displacement obtained from the experiments. Note that the percentages of increase from XTRACT are directly related to the improvements observed during pier tests between unconfined and confined masonry. In fact, the addition of any type of confinement in the masonry piers always increased the strain capacity. However, during tests conducted on walls, this was not the case. Therefore, differences between experimental results and the model are to be expected.

Walls	Tot. disp. at 20% load deg. (in.)	Increase in disp. (Exp.)	Flex. disp. at 20% load deg. From XTRACT	Increase in disp. (XTRACT)
1	1.102	-	0.798	-
2	1.065	-3.36%	1.468	84.11%
3	1.181	7.17%	1.033	29.56%
4	1.600	45.19%	0.895	12.25%
5	2.308	-	1.547	-
6	2.619	13.48%	3.097	100.13%
7	2.368	2.60%	1.988	28.49%
8	2.252	-2.43%	1.729	11.75%
9	2.606	12.91%	1.851	19.60%

Table 4.3: Increases in displacement from experiments and XTRACT

Figures 4.14 to 4.17 present the load vs. displacement diagrams from experiments and from XTRACT for confined and unconfined walls with different aspect ratios. As a reminder, Fiber 1 refers to walls with a dosage of fibers of 5 lbs/yd^3 (2.97 kg/m^3), and Fiber 2 to walls with a dosage of fibers of 8 lbs/yd^3 (4.76 kg/m^3). Comparison of the load-displacement curves for an aspect ratio of 0.93 showed that the best results from experiments were obtained with 5 lbs/yd^3 of fibers, followed by the walls confined by seismic combs. Squat unconfined walls and confined by steel plates presented very similar results in terms of ultimate displacement but Snook reported that Wall 2 had some problems during testing, possibly explaining the poor performance observed in the test and the differences in peak displacement in the experiment and that obtained from XTRACT. It was also noticed that the Modified Kent-Park model overestimated the experimental results leading to larger ultimate displacements than expected. Considering Figure 4.16, it is noticeable that the steel plates and 8 lbs/yd^3 of fibers provided the best results and were very similar to each other, while the seismic combs provided intermediate results with respect to the unconfined case. Finally the walls with 5 lbs/yd^3 of fibers presented the worst results for walls with high aspect ratios. These results did not coincide with those obtained during tests on masonry piers. This might be due to the variability and the differences in strengths of the

materials. It could also be due to the differences in stresses experienced by the toe regions of the walls compared to those in compressive piers.

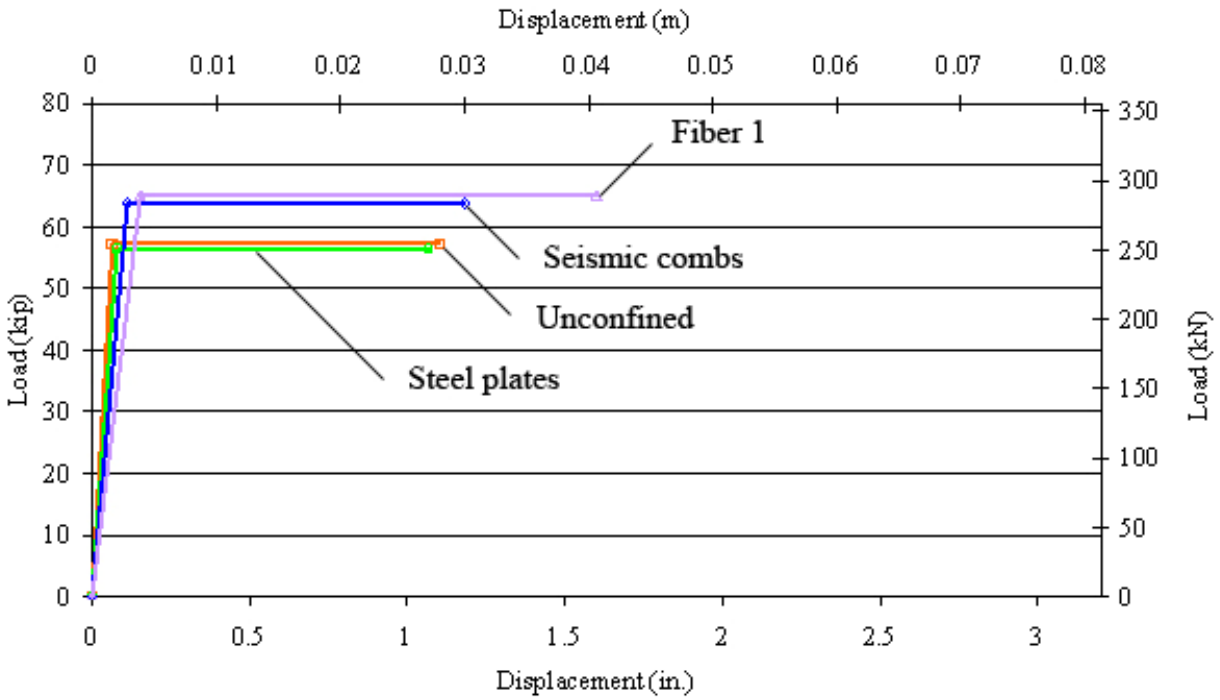

Figure 4.14: Load vs. Total Displacement from experiments – Aspect ratio: 0.93

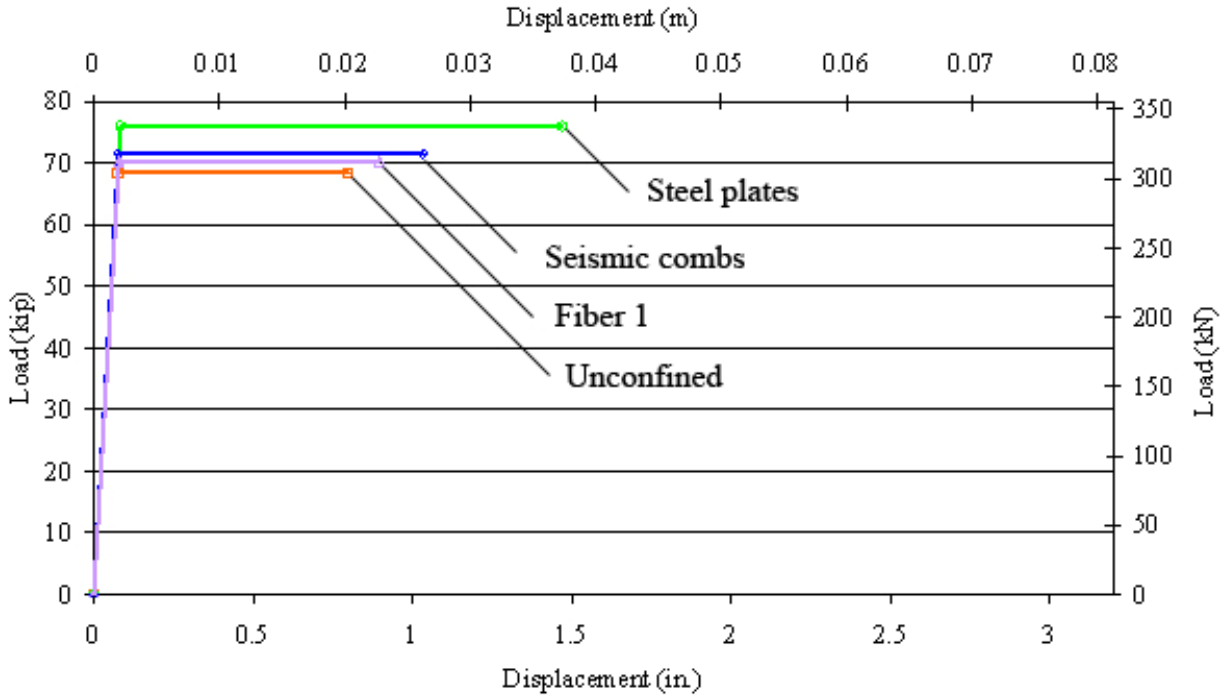

Figure 4.15: Load vs. Flexural Displacement from XTRACT – Aspect ratio: 0.93

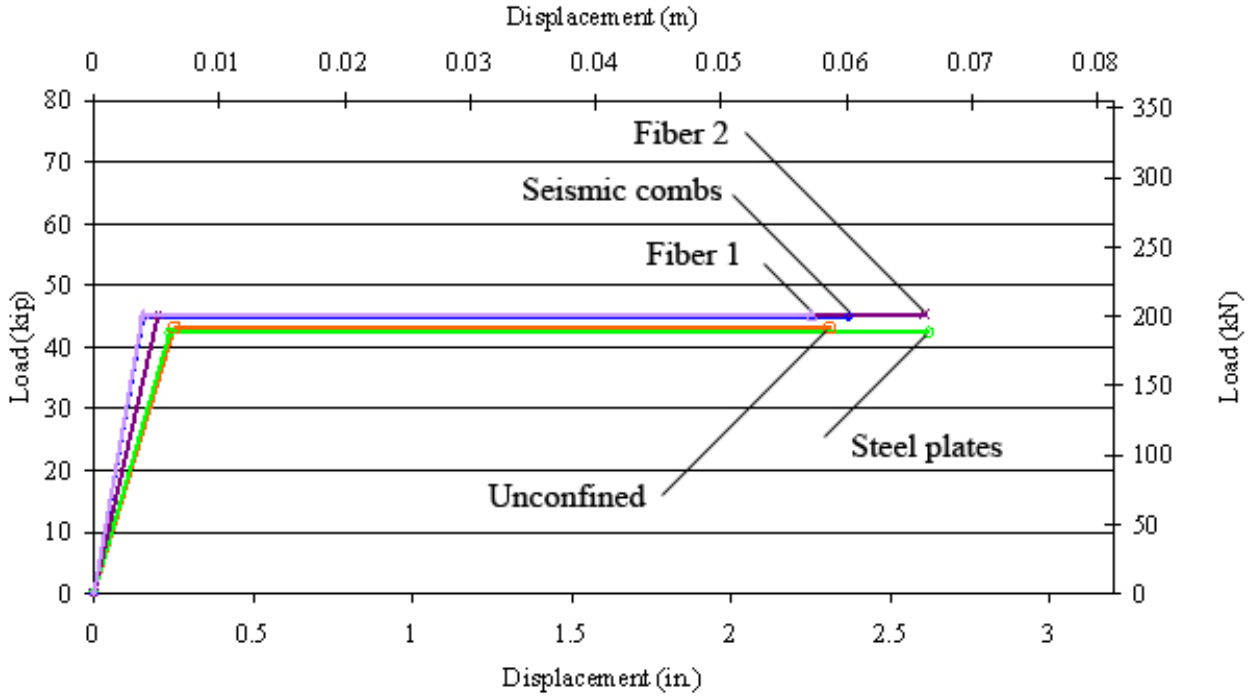

Figure 4.16: Load vs. Total Displacement from experiments – Aspect ratio: 1.51

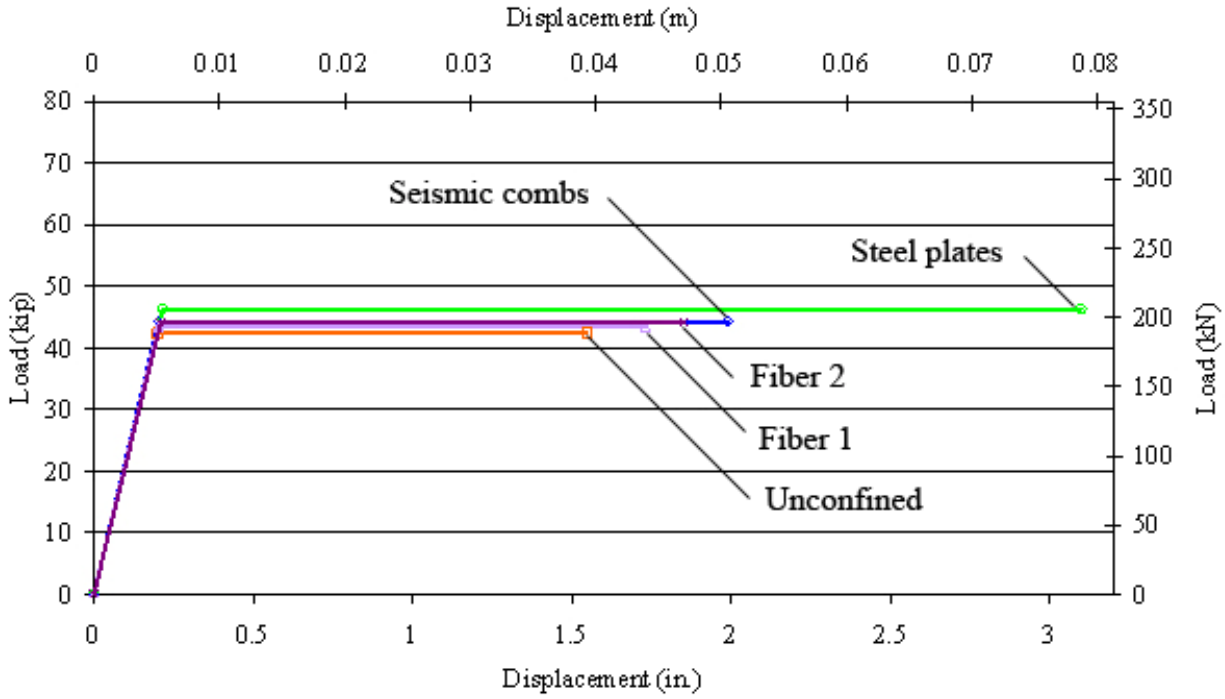

Figure 4.17: Load vs. Flexural Displacement from XTRACT – Aspect ratio: 1.51

4.5 EFFECTS OF THE VOLUMETRIC RATIO OF CONFINEMENT ON THE LOAD-DISPLACEMENT CAPACITY

The effects of the volumetric ratio of confinement reinforcement or dosage of fibers on the stress-strain behavior of compressive masonry piers and on the load-displacement curves of masonry shear walls are evident in the previous figures. The Modified Kent-Park model can be utilized to obtain new stress-strain curves in order to account for a larger volumetric ratio of confining steel in the mortar joints or for a larger dosage of fibers in the grout. Doubling the amounts of reinforcement or dosages of fibers was investigated and produced the stress-strain curves presented in Appendix I. As no flexural tests were conducted on grout beams with twice the initial amount of fibers, the flexural tensile stresses were assumed to double as well.

Note that curves given in Appendix I for fiber reinforced piers present small increases in ultimate strains between the initial dosages and twice these amounts. This is due to the modifications applied to the Modified Kent-Park model in order to account for the fibers. As the differences in ultimate strains are less than in the cases of concrete masonry confined with seismic combs or steel plates, it is predictable that the ultimate displacements will not change as significantly for walls with fibers than for walls confined with combs or plates. A modification of the Modified Kent-Park model to account for that would have been desirable, but the development of a model for fiber reinforced masonry was beyond the scope of this study.

Analyses using XTRACT were run on Snook's (2005) confined walls (see Appendix J). In the case of walls confined by steel plates, doubling the amount of confining steel resulted in the failure of the flexural reinforcement before crushing the masonry. A value of 1.5 times the volumetric ratio of steel was selected instead of twice in order to see if crushing of the masonry could be reached. However, again, the flexural reinforcement failed first. Note that the ultimate strain of the steel model used in the analyses was equal to 0.012.

A comparison between the load-displacement curves from XTRACT with ρ and 2ρ (2ρ refers either to twice the amount of confinement reinforcement or to twice the dosage of fibers) showed a slight increase in load capacities and larger increase in displacement capacities (see Figure 4.18 and Appendix K). Fiber reinforced walls presented smaller increases as expected. This last observation was mainly due to the problem with the model of the stress-strain curves described previously. Also, note that the Modified Kent-Park model with steel plates overestimated the strain capacity leading to larger displacements than actually occurred.

Producing the benefits obtained in terms of displacement capacity may be worthwhile depending on the price of the materials. Doubling the amount of reinforcement showed fair

increases with this model; it would be interesting to adjust the different factors that limited the results to predict the increases with more accuracy.

All results presented in this chapter were based on the Modified Kent-Park model used to represent the stress-strain behavior of the various materials. This model gave acceptable results and provided a reasonable basis for comparison with results from other studies. However, it would be beneficial to conduct further studies on the model to improve the predictions of the stress-strain behavior of masonry piers. A model to account for the fibers in the grout core should also be developed to better evaluate the falling branch of the stress-strain curves.

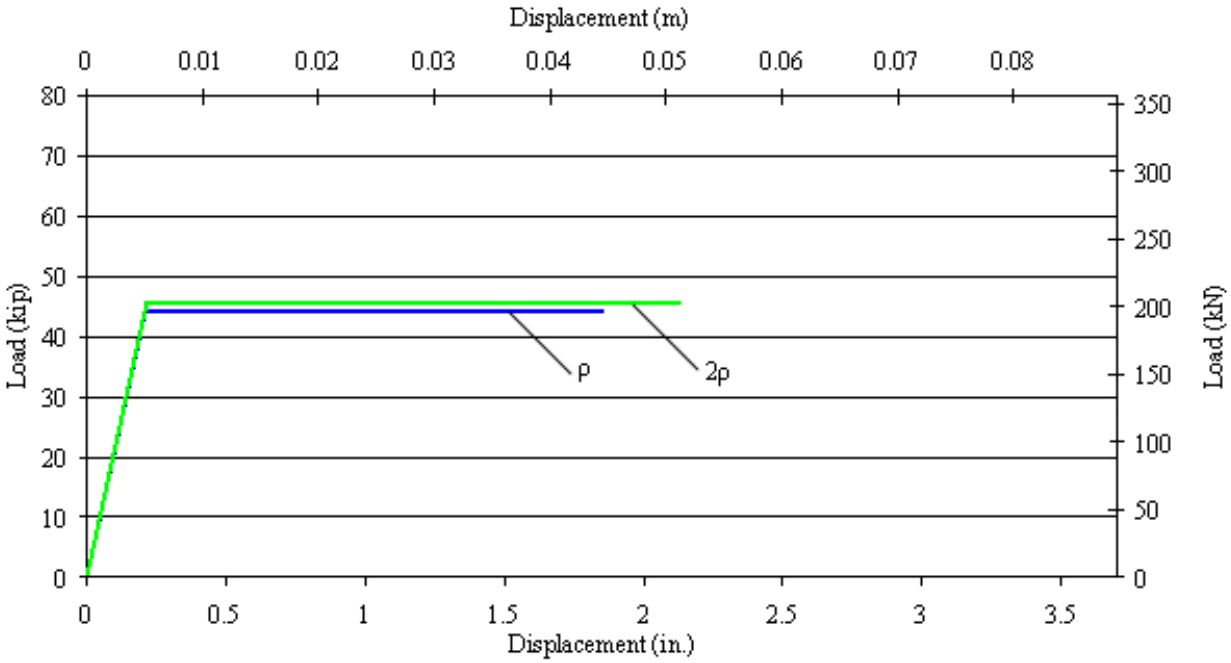

Figure 4.18: Example of load-displacement curves with ρ and 2ρ based on XTRACT

4.6 CONCLUSIONS

The following conclusions were reached based on the modeling of the shear walls:

1. The Modified Kent-Park model provided a reasonable representation of the stress-strain behavior of compressive masonry piers confined by steel plates and seismic combs. An empirical modification was made to model the concrete masonry with fiber reinforcement, and it reasonably described the stress-strain behavior of fiber reinforced masonry piers.
2. The XTRACT model provided reasonable predictions of the load and displacement capacities of the shear walls. Predictions were closer to the experimental results in the case of walls with higher aspect ratios. Results from XTRACT generally followed the trend of improvements in strain capacity observed during tests on unconfined and confined masonry piers. The results for shear did not follow the same trend because of the variability of the materials and testing procedures, and therefore there were differences between the experimental results and XTRACT predictions.
3. Increases in confinement reinforcement resulted in modest increases in load capacities and increases in displacement capacities for all confinement schemes. Larger improvements were observed for walls confined with steel plates and seismic combs than for fiber reinforced walls. This observation was expected considering the small increases in strain capacity of the stress-strain models for fiber reinforced piers. Modifications may be needed for the fiber stress-strain model, but this was beyond the scope of this study.

CHAPTER 5: SUMMARY AND CONCLUSIONS

5.1 SUMMARY

This study evaluated the effects of confinement reinforcement on the load and displacement capacities of masonry piers and shear walls. Compression tests were conducted on fully-grouted fiber-reinforced masonry piers. Two materials were used in the pier tests: concrete blocks and clay bricks. Two dosages of polymer fibers were mixed with the grout, and the effects of the addition of the fibers on the stress-strain behavior of the compressive piers were evaluated. Results were compared to previous studies on reinforced masonry piers using other types of confinement reinforcement, including steel plates and seismic combs. Conclusions on the effectiveness of confinement reinforcement for improving the ductility of masonry were derived. A Modified Kent-Park model was used to analytically represent the stress-strain behaviors of the tested piers. Shear walls were modeled with XTRACT, and moment-curvature results were utilized to predict the load-displacement behavior of the walls. Comparisons between analytical results obtained with XTRACT and experimental results from previous studies were made.

5.2 CONCLUSIONS

General effects of polymer fibers on the stress-strain behavior of the piers: Results showed that the fibers improved the performance of compressive piers for both concrete masonry and clay masonry. Considering the strains at 50% of the peak stresses, increases of 47% and 18% were measured for concrete masonry and for clay masonry, respectively. A statistical analysis, with a 90% confidence level, showed that the fibers had a significant effect on the peak stress and the corresponding strain values for clay masonry piers. No statistical effect of the fibers was

determined for the strain at 50% of the peak stress values. In the case of concrete masonry, the statistical evaluation showed that the fibers had a significant effect on the peak stress values and the strain at 50% of the peak stress values but not on the strain at peak stress.

Effects of the fibers on the grout core: The fibers had a positive effect on protecting the grout core. Even if the masonry units were damaged during testing, grout cores almost always remained intact. Fibers provided an efficient post-crack control to the grout. However, since no fibers were incorporated in the mortar joints, and bonding with masonry units was not improved with the addition of the fibers, no restraint was provided for the masonry face shells, diminishing considerably the stress that the piers could attain. The incorporation of fibers in the mortar joints may have the effect of confining the masonry units. Another possibility is to incorporate fibers in the masonry units in order to improve bonding with the grout.

Comparison with results from previous studies: The two amounts of fibers used in this study resulted in similar improvements in strain capacity and peak stress values when compared to each other. When compared to results from previous research, where other types of confinement reinforcement were evaluated, the fibers showed lower improvements in strain capacity, even though some increases were obtained for peak stress values, strains at peak stresses and strains at 50% of the peak stresses. Future research should be conducted to investigate if an increase in the amount of fibers results in greater levels of improvements. A modification of the grout slump may be necessary in order to achieve proper grout consolidation.

Modeling the stress-strain curves of the piers: Several mathematical models developed for concrete were used to represent the stress-strain behavior of the reinforced masonry piers tested in compression. Four types of confinement reinforcement were investigated: steel plates and seismic combs placed in the mortar joints and two different dosages of polymer fibers mixed

with the grout. Satisfactory results were obtained with the Modified Kent-Park model proposed by Park and Priestley in 1982 for confined concrete masonry and clay masonry, both confined with steel plates and seismic combs. An empirical modification of the model was made to account for the fibers in the grout and it produced reasonable results.

Modeling the shear walls: Shear walls were modeled and load-displacement curves were obtained from moment-curvature analyses. Comparison of the experimental and analytical results showed that the predictions of the load and displacement capacities were good for the case of shear walls with higher aspect ratios. For squat shear walls, the predictions were less accurate.

Effects of the confinement reinforcement ratio on the load-displacement curves: By doubling the amount of confinement reinforcement or dosage of fibers, a slight increase in load capacity was observed while larger displacement capacities were attained. The moment-curvature analyses predicted significant improvements for walls confined by steel plates or seismic combs, and moderate increases for walls confined by polymer fibers because of the stress-strain models which did not present large increases in strain capacities. Development of a model for fiber confined masonry piers is necessary in order to improve the evaluation of the behavior of fiber reinforced shear walls.

REFERENCES

"2005 MSJC (Masonry Standards Joint Committee) Building Code Requirements and Specification for Masonry Structures" (ACI 530/ASCE 5/TMS 402 and ACI 530.1/ASCE 6/TMS 602)

2000 International Building Code (IBC)

American Society for Testing and Materials (ASTM). (2003) *Annual book of ASTM Standards,* West Conshohocken, PA:

C90-03 Standard Specification for Loadbearing Concrete Masonry Units, Vol. 04.05
C270-03b Standard Specification for Mortar for Unit Masonry, Vol. 04.05
C476-02 Standard Specification for Grout for Masonry, Vol. 04.05
C652-04 Standard Specification for Hollow Brick (Hollow Masonry Units Made from Clay or Shale), Vol. 04.05
C1019-03 Standard Test Method for Sampling and Testing Grout, Vol. 04.04
C1314-03b Standard Test Method for Compressive Strength of Masonry Prisms, Vol.04.05

Building Code Requirements for Structural Concrete and Commentary. ACI 318-02 (2002). American Concrete Institute, Detroit, Michigan.

"Code of Practice for Masonry Design," (NZS 4203P), Standards Association of New Zealand, Wellington, 1985, 130 pp.

Eikanas, I.K., (2003). "Behavior of Concrete Masonry Shear Walls with Varying Aspect Ratio and Flexural Reinforcement." *M.S Thesis*, Department of Civil and Environmental Engineering, Washington State University, August 2003.

Ewing, B.D., and Kowalsky, M.J., (2004). "Compressive Behavior of Unconfined and Confined Clay Brick Masonry." *Journal of Structural Engineering,* ASCE, April 2004, pp 650-661.

Hart, G., Noland, J., Kingsley, G., Englekirk, R., and Sajjad, N. A. (1988). "The Use of Confinement Steel to Increase the Ductility in Reinforced Concrete Masonry Shear Walls." *Masonry Society Journal*., Vol. 7, No.2, T19-42.

Kent, D.C, and Park, R., (1971). "Flexural Members with Confined Concrete." *Journal of the Structural Division,* ASCE., Vol.97, No. ST7 Proc. Paper 8243, July 1971, pp 1969-1990.

Laursen, P.T., and Ingham J.M., (2001). "Structural Testing of Single-Story Posttensioned Concrete Masonry Walls." *Masonry Society Journal,* Vol.19, No. 1, pp 69-82.

Laursen, P.T., and Ingham J.M., (2004). "Structural Testing of Large-Scale Posttensioned Concrete Masonry Walls." *Journal of Structural Engineering,* ASCE, October 2004, pp 1497-1505.

Malmquist, K.J., (2004). "Influence of Confinement Reinforcement on the Compressive Behavior of Concrete Block Masonry and Clay Brick Masonry Prisms", *M.S Thesis*, Department of Civil and Environmental Engineering, Washington State University, June 2004.

Park, R., Priestley, M.J.N., and Gill, W.D., (1982). "Ductility of Square-Confined Concrete Columns." *Proceedings,* ASCE, Vol. 108, ST4, April 1982, pp 929,-950.

Paulay T., and Priestley, M. J. N. (1992). "*Seismic Design of Reinforced Concrete and Masonry Buildings*.", John Wiley & Sons, Inc., New York.

Priestley, M.J.N. (1986). "Seismic Design of Concrete Masonry Shear Walls." ACI Journal., Vol. 83, No. 8, pp 58-68.

Priestley, M.J.N., and Bridgeman, D.O. (1974). "Seismic resistance of brick masonry walls." Bull. of the New Zealand National Society for Earthquake Engineering, Vol. 7, No. 4, pp167-187.

Priestley, M.J.N., and Elder, D.M. (1983). "Stress-Strain Curves for Unconfined and Confines Concrete Masonry." ACI Journal., Vol. 80, No. 3, pp 192-201.

Shing, P.B., Carter, E.W., and Noland J.L. (1993). "Influence of Confine Steel on Flexural Response of Reinforced Masonry Shear Walls." *Masonry Society Journal*, Vol. 11, No.2, pp 72-85.

Shing, P.B., Noland, J.L., Klamerus, E., and Spaeh, H. (1989). "Inelastic Behavior of Concrete Masonry Shear Walls," *Journal of Structural Engineering*, ASCE, Vol. 115, No. 9, pp. 2204-2225.

Snook, M.K., (2005). "Effects of Confinement Reinforcement on the Performance of Masonry Shear Walls." *M.S Thesis*, Department of Civil and Environmental Engineering, Washington State University, August 2005.

Tallon, C.L. (2001). "Investigation of Flexural Reinforcement Limits for Masonry Shear Walls," *M.S. Thesis*, Department of Civil and Environmental Engineering, Washington State University, 2001.

Uniform Building Code (UBC), *International Conference of Building Officials*, Whittier, CA, 1988.

XTRACT (Imbsen Software Systems 2005) Version 3.0.4, *Imbsen & Associated Inc. Engineering Consultants. www.imbsen.com*

APPENDICIES

APPENDIX A

This appendix contains the code of the Excel function to discretize stress-strain curves from experiments.

```
'*********************************************************************'
'                                                                     '
'   Goal : Function that discretize test curves for doing an average of all curves   '
'                                                                     '
'*********************************************************************'

Function Test(Cellx As Range, NbValues As Double, FirstStress As Range)

' Cellx is the x (strain value) value where we want to calculate the stress
' NbValues is the total number of values from the diagram (from the test, not the number of x-values that we want)
' FirstStress has to be fixed with $$ (e.g : $A$1) and is the first non-zero value for the stress
' Note: - Don't include the 0-stress, 0-strain into the number of values NbValues
'       - You need to have the columns in this order: Stress - Strain - X - Result of this function

Dim i As Double

x = Cellx.Value
Row1 = FirstStress.Row
Row2 = Cellx.Row
Beg = Row1 - Row2
foundbefore = 0 ' 0 if we only have one stress-value for a given x
Test = 0
MaxStrain = 0
MaxStress = 0

  For i = 1 To (NbValues - 1)

    Stress1 = Cellx.Offset((i - 1 + Beg), -2)
    Stress2 = Cellx.Offset(i + Beg, -2)
    Strain1 = Cellx.Offset((i - 1 + Beg), -1)
    Strain2 = Cellx.Offset(i + Beg, -1)

    If (MaxStress < Stress2) Then
      MaxStress = Stress2
      MaxStrain = Strain2
    End If

      If ((Strain1 <= x) And (Strain2 > x)) Or ((Strain1 >= x) And (Strain2 < x)) Then

        a = (Stress2 - Stress1) / (Strain2 - Strain1)
        b = Stress1 - a * Strain1

        If foundbefore = 0 Then
          foundbefore = 1
          Test = a * x + b
```

```
            Else
                Test = (a * x + b + Test) / 2
            End If
        End If
        If ((Strain2 > (x + 0.0001)) And (Strain2 <= MaxStrain)) Then
            Exit For
        End If

    Next i

End Function
```

APPENDIX B

This appendix contains a Matlab script for fitting a polynomial to a stress-strain average curve.

```
clc;
format short g
A = load('Cla-f2-desc.txt');
NumX=size(A,1);
X=A(1:NumX,1);
Y=A(1:NumX,2);
P=polyfit(X,Y,7); %7 is the degree of the fitted polynomial, different degrees were used in order to fit the experimental results better.
Result=polyval(P,X);
plot(X,Y,X,Result)
d=[X,Result];
xlswrite('Cla-f2-2',d);
```

APPENDIX C

This appendix presents pictures and corresponding stress-strain curves of each masonry pier tested.

CON-N-1

Con-N-1 Stress vs. Strain

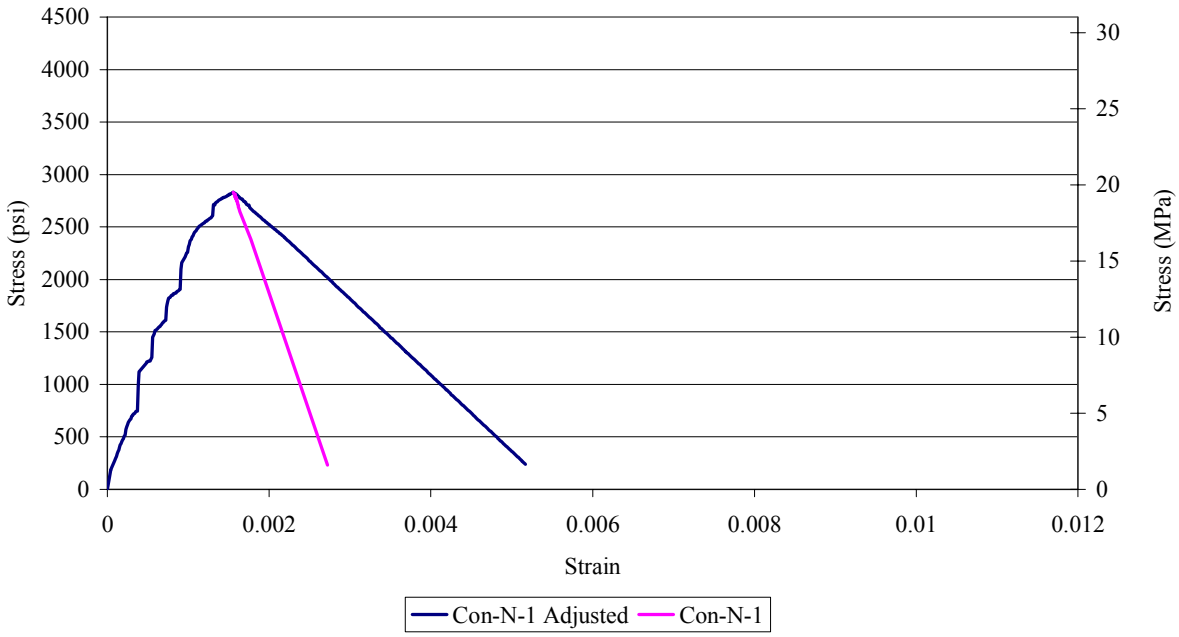

CON-N-3

Con-N-3 Stress vs. Strain

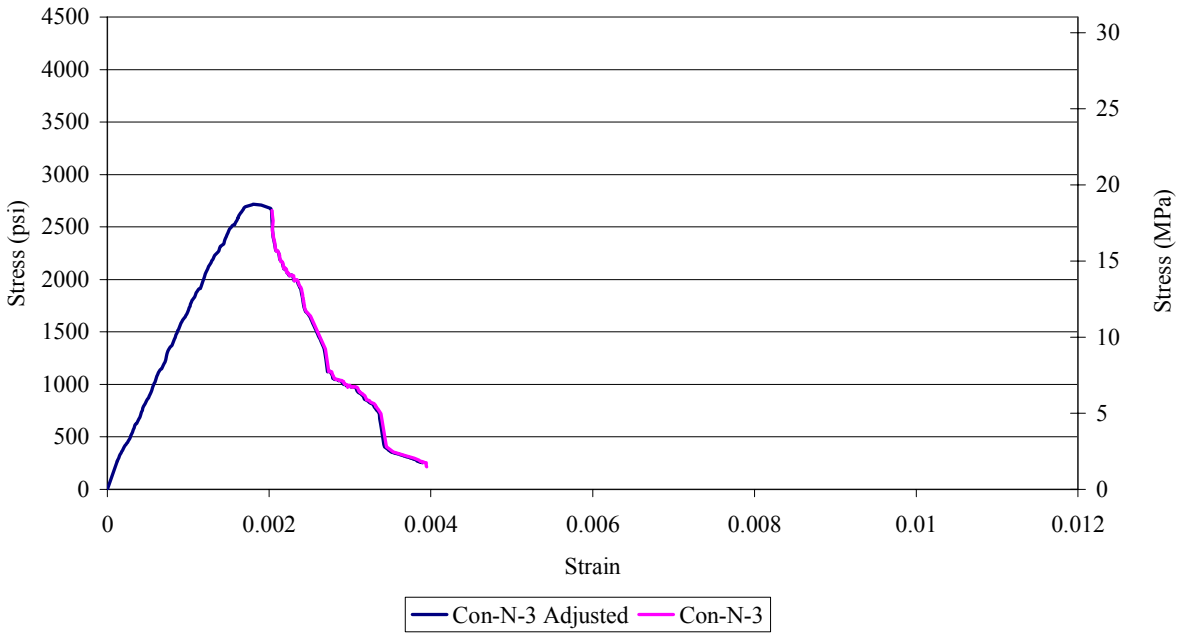

CON-N-4

Con-N-4 Stress vs. Strain

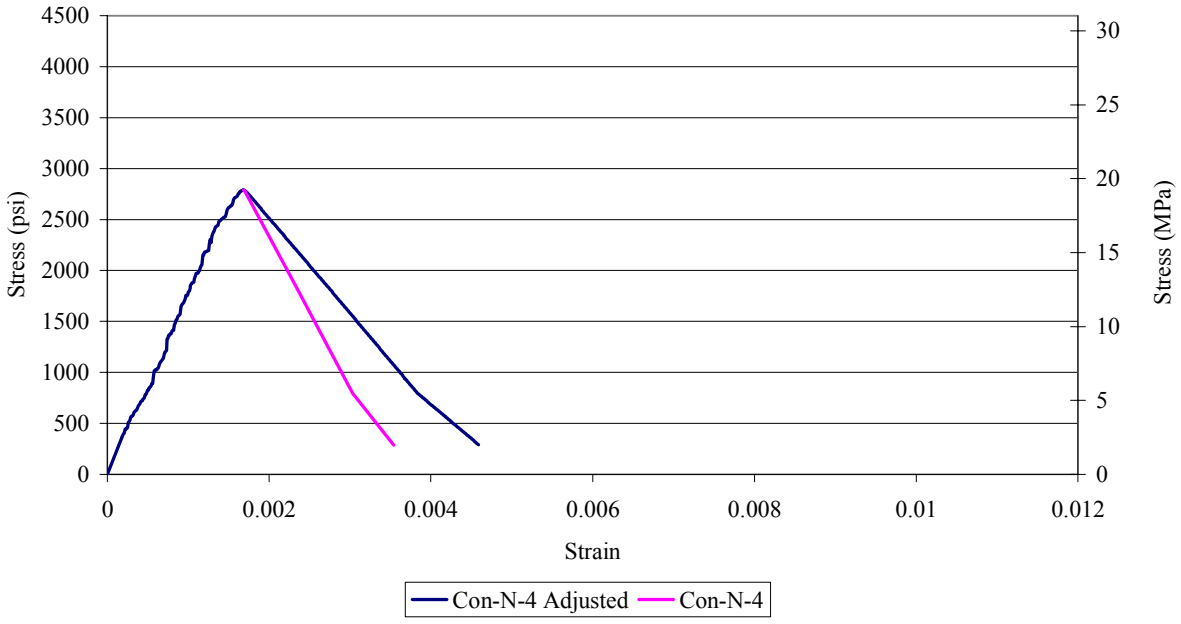

CON-N-5

Con-N-5 Stress vs. Strain

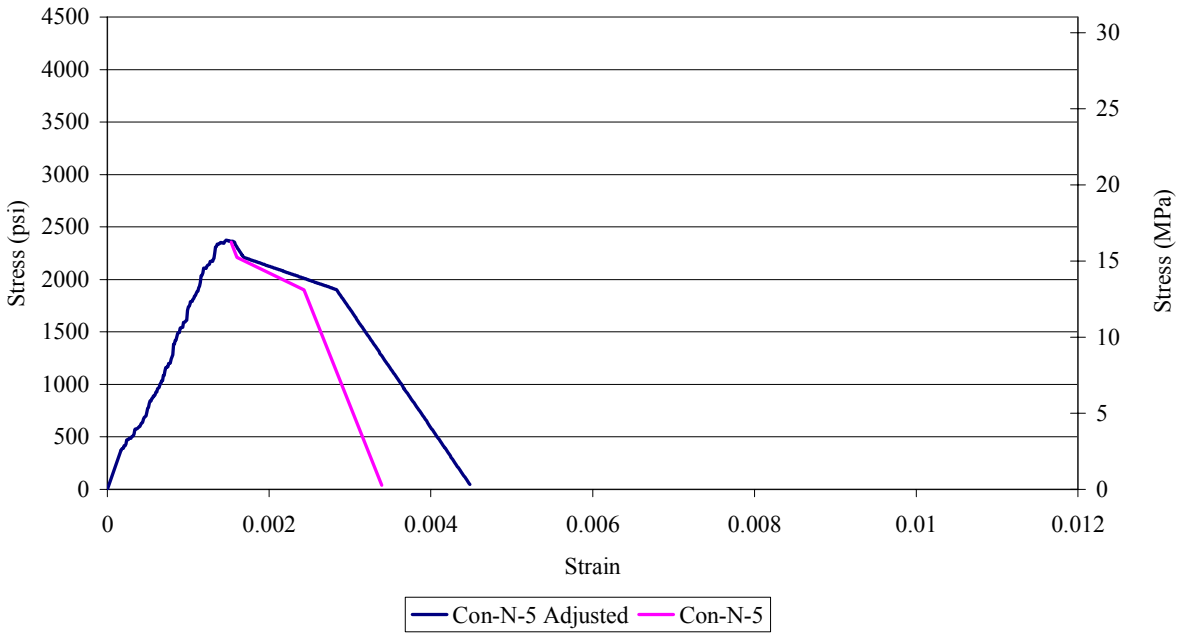

CON-F1-1

Con-F1-1 Stress vs. Strain

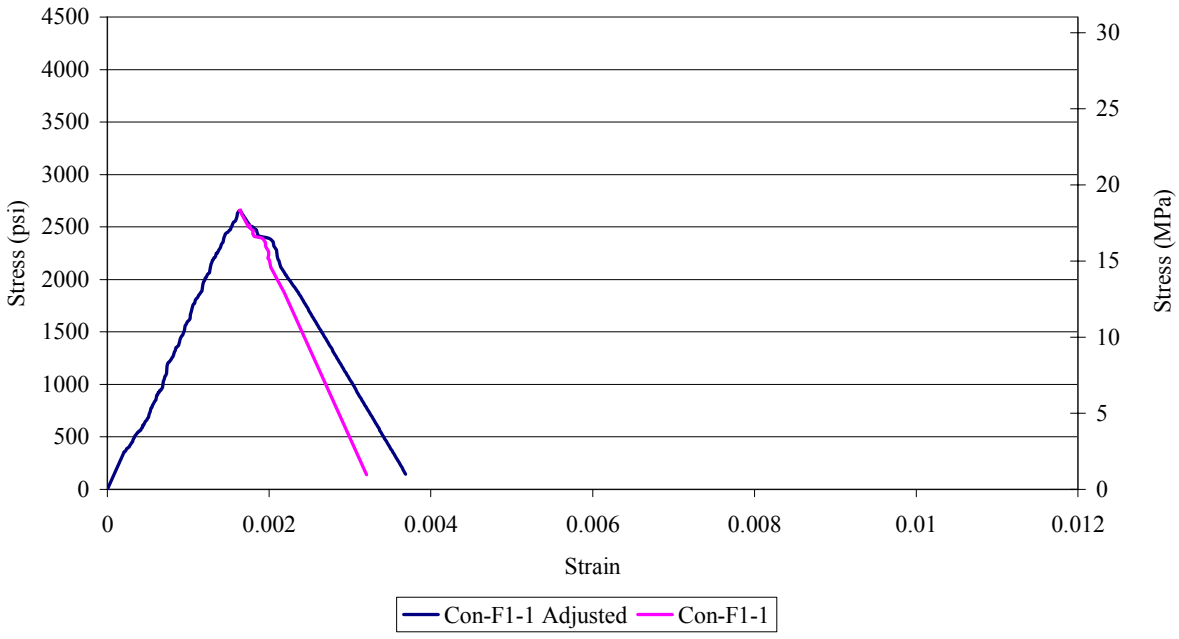

CON-F1-2

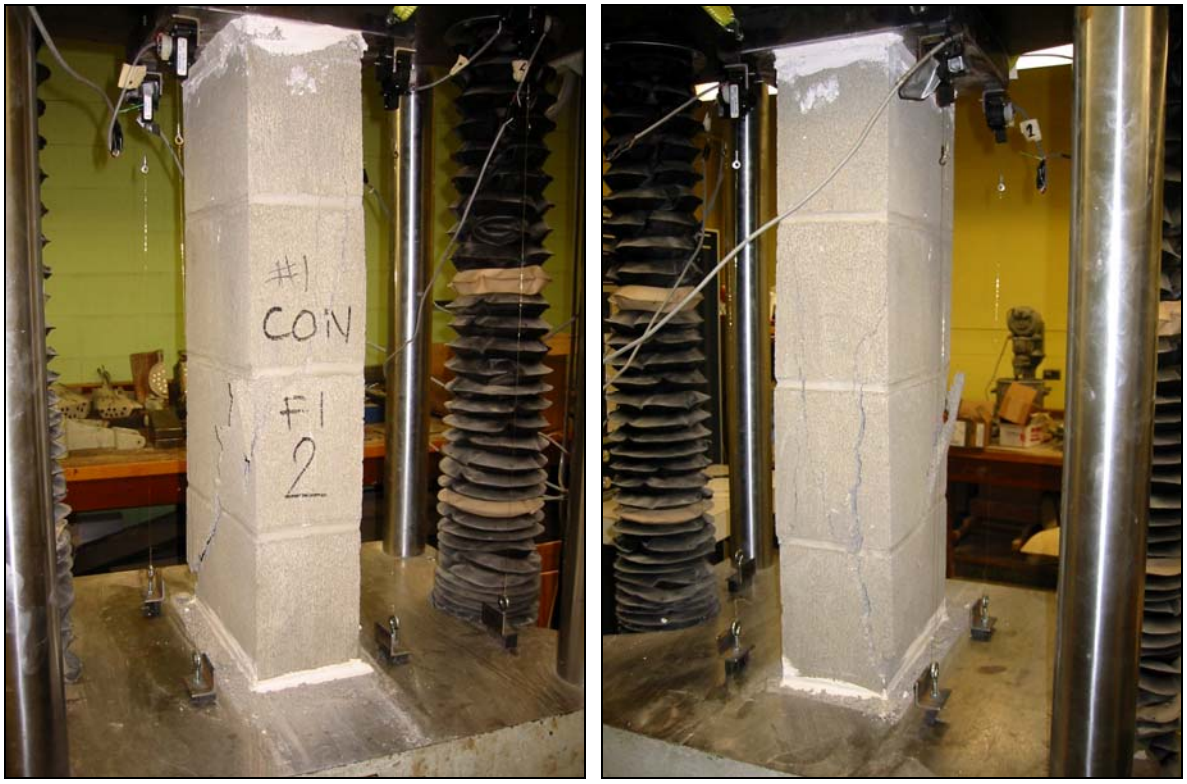

Con-F1-2 Stress vs. Strain

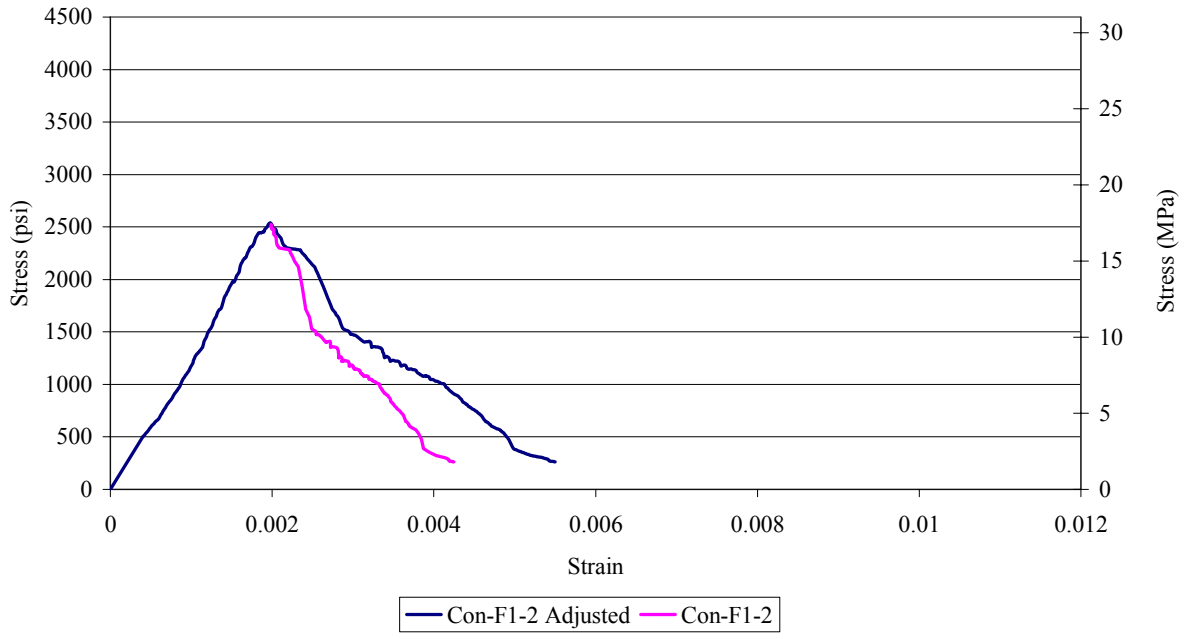

CON-F1-3

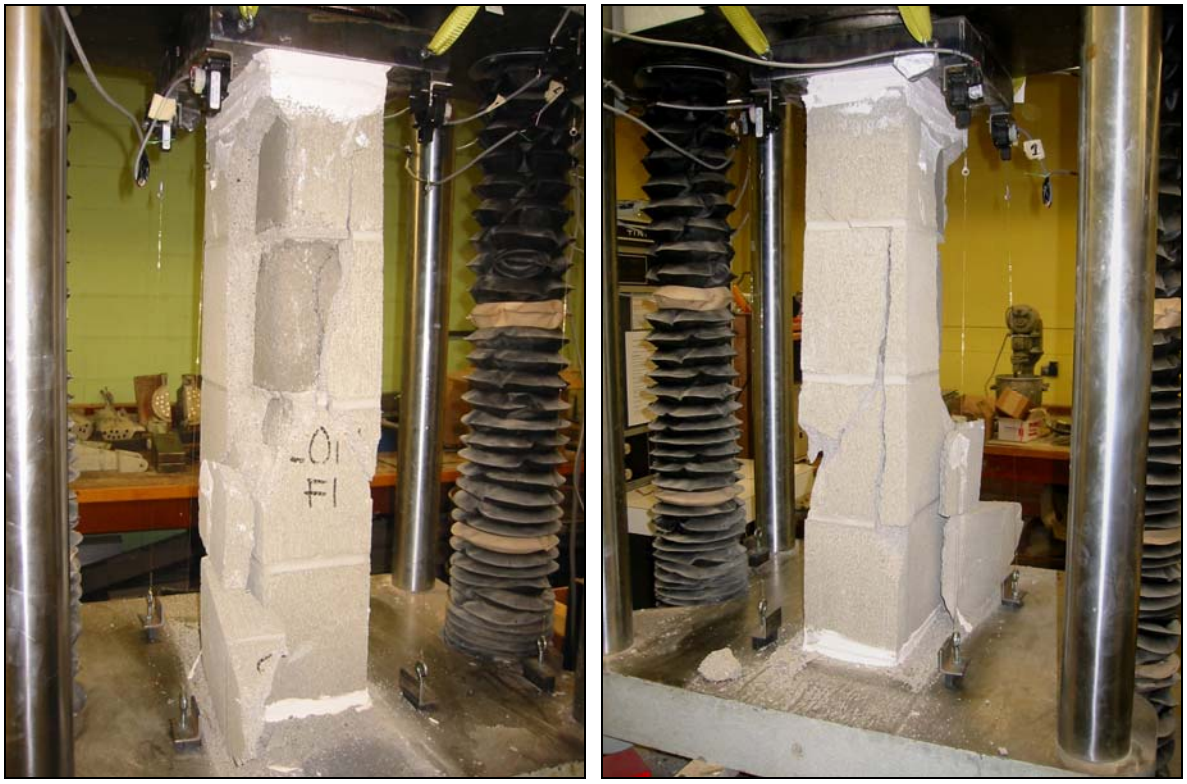

Con-F1-3 Stress vs. Strain

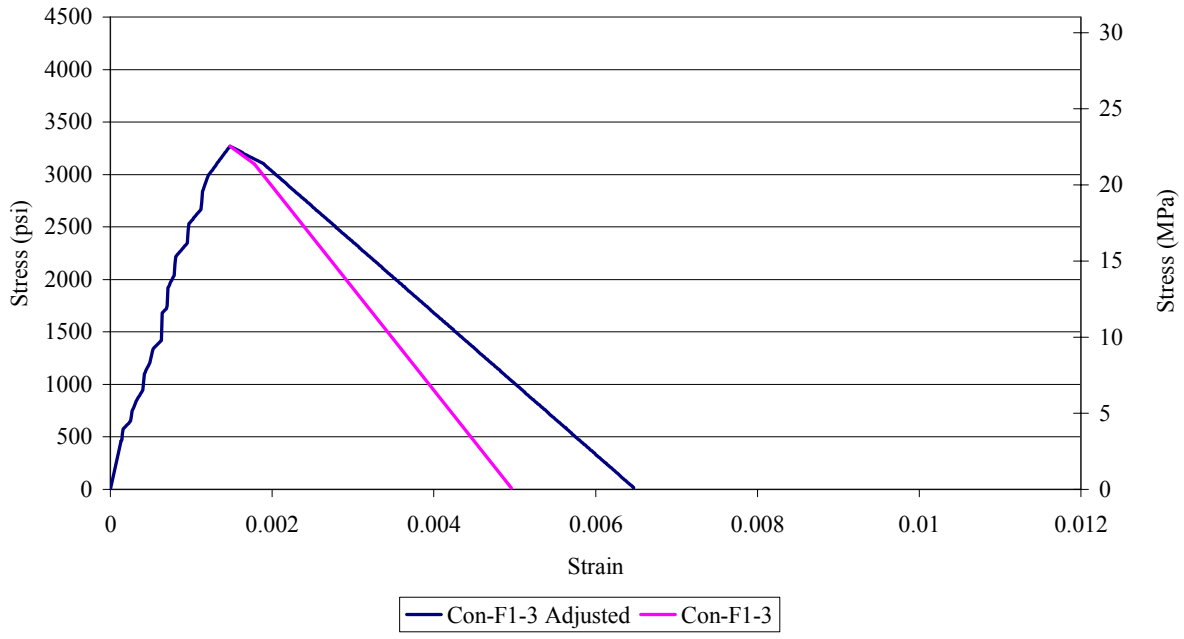

CON-F1-4

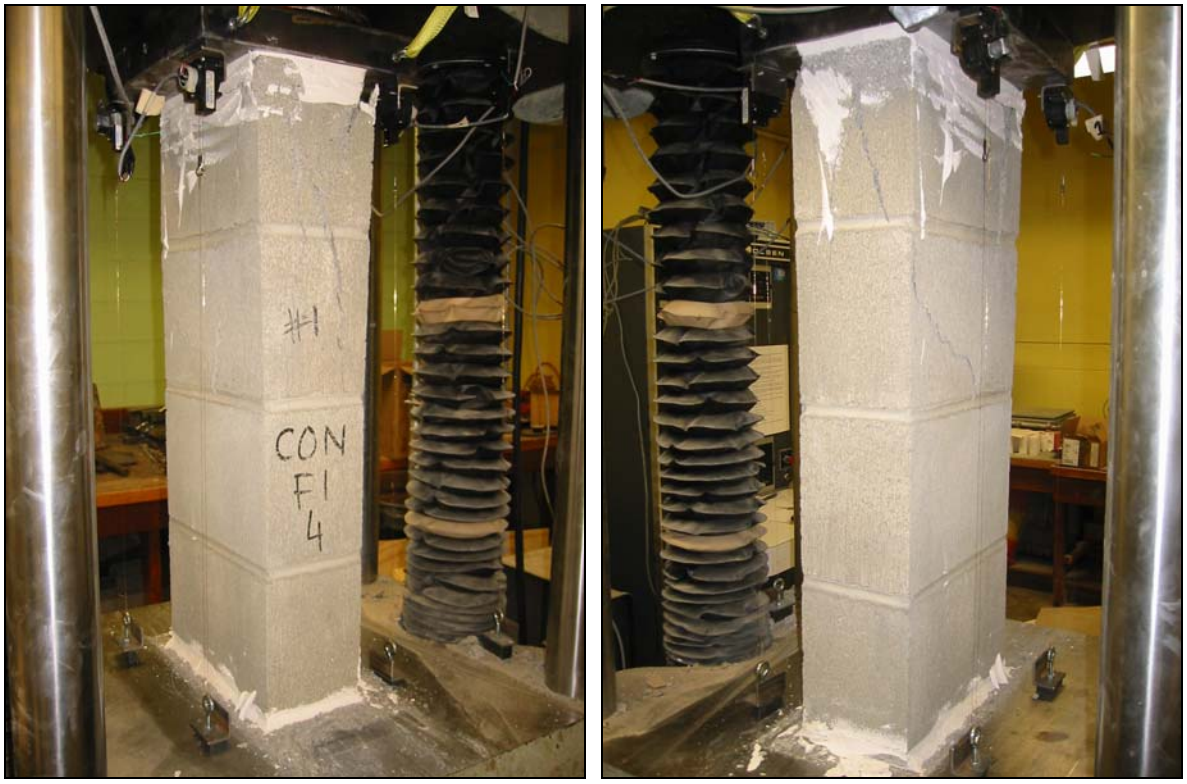

Con-F1-4 Stress vs. Strain

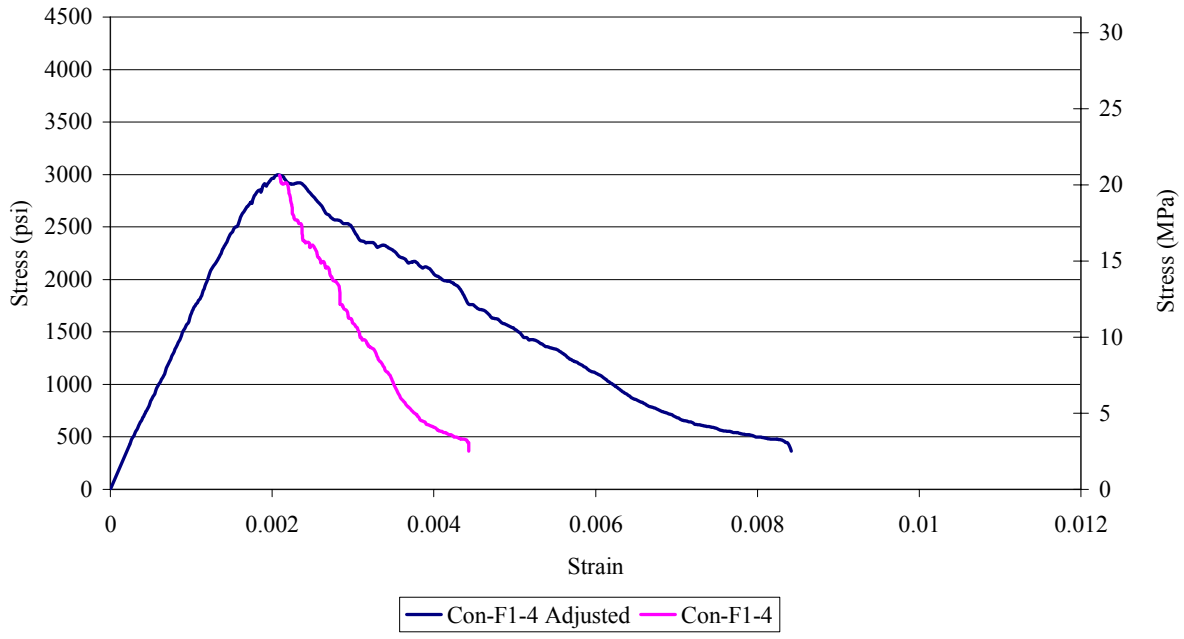

CON-F1-5

Con-F1-5 Stress vs. Strain

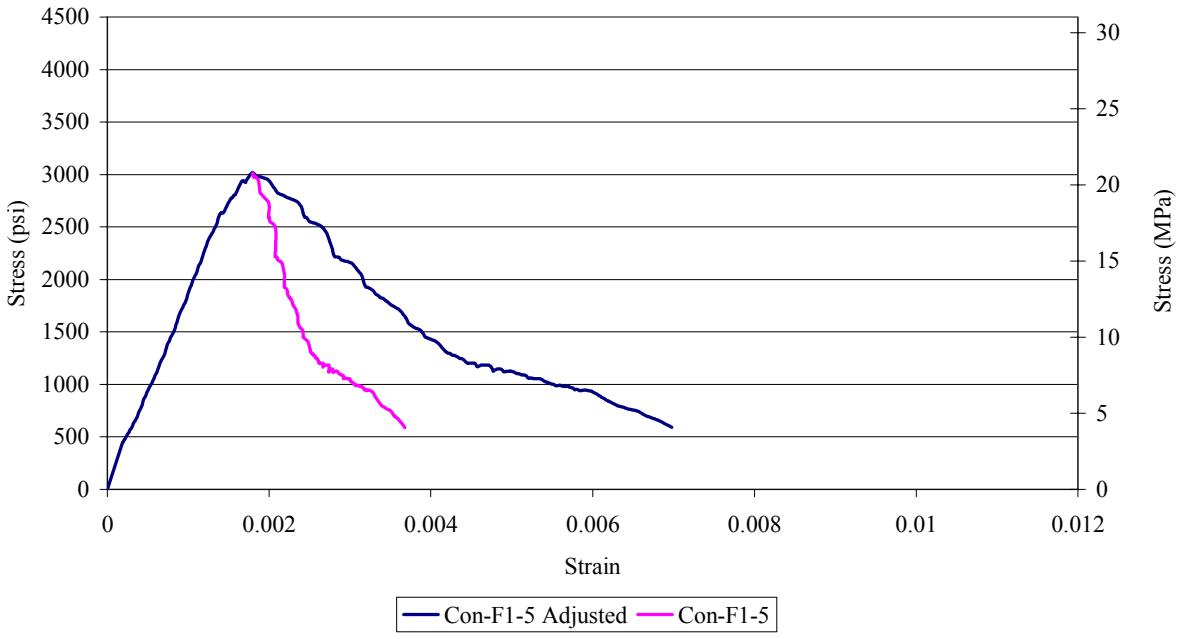

CON-F2-1

Con-F2-1 Stress vs. Strain

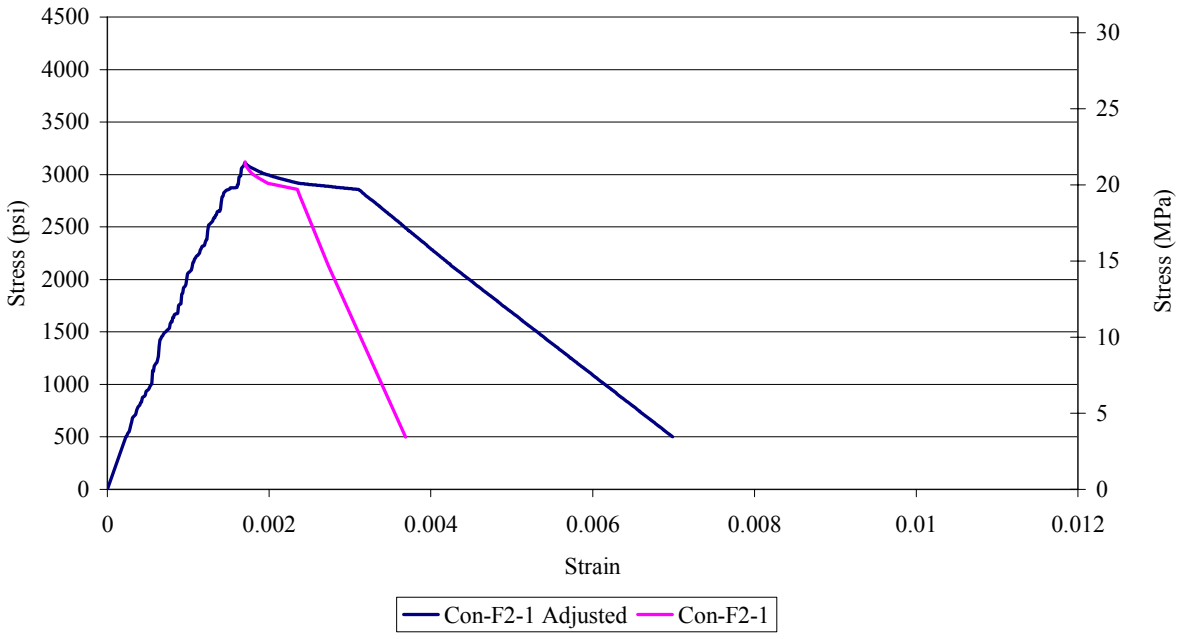

CON-F2-2

Con-F2-2 Stress vs. Strain

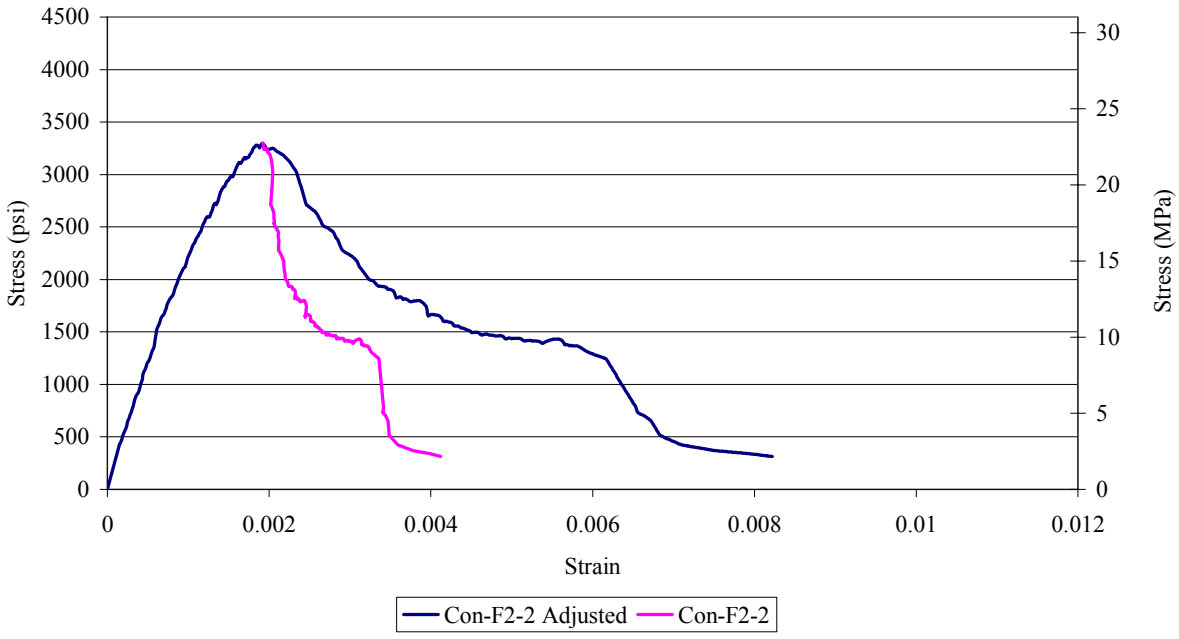

CON-F2-3

Con-F2-3 Stress vs. Strain

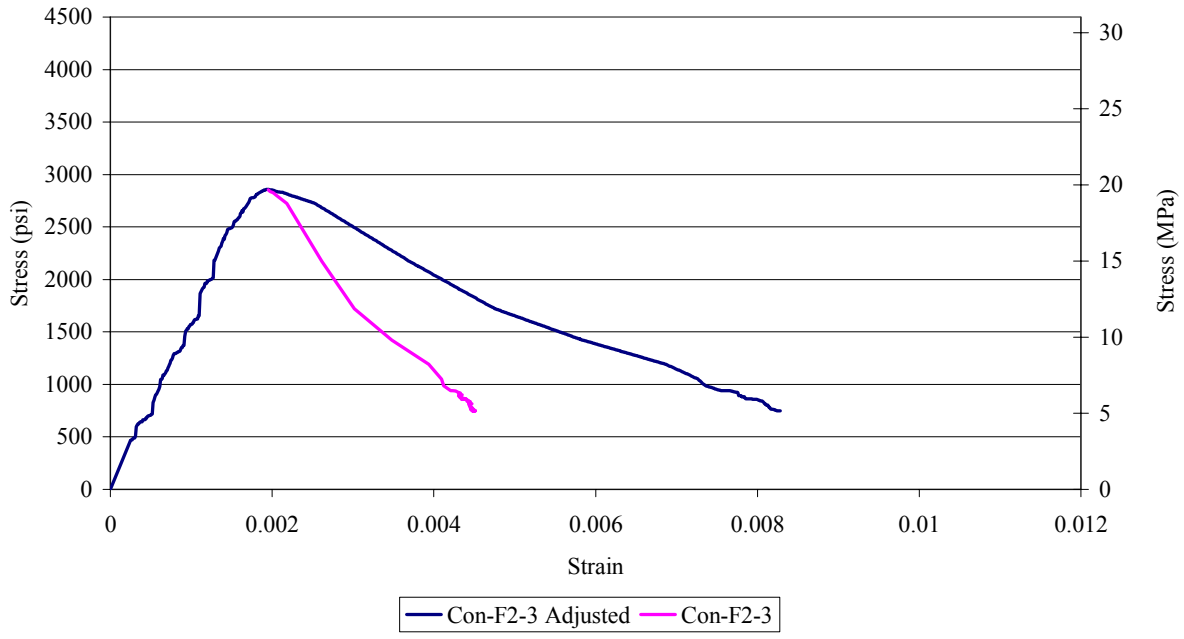

CON-F2-4

Con-F2-4 Stress vs. Strain

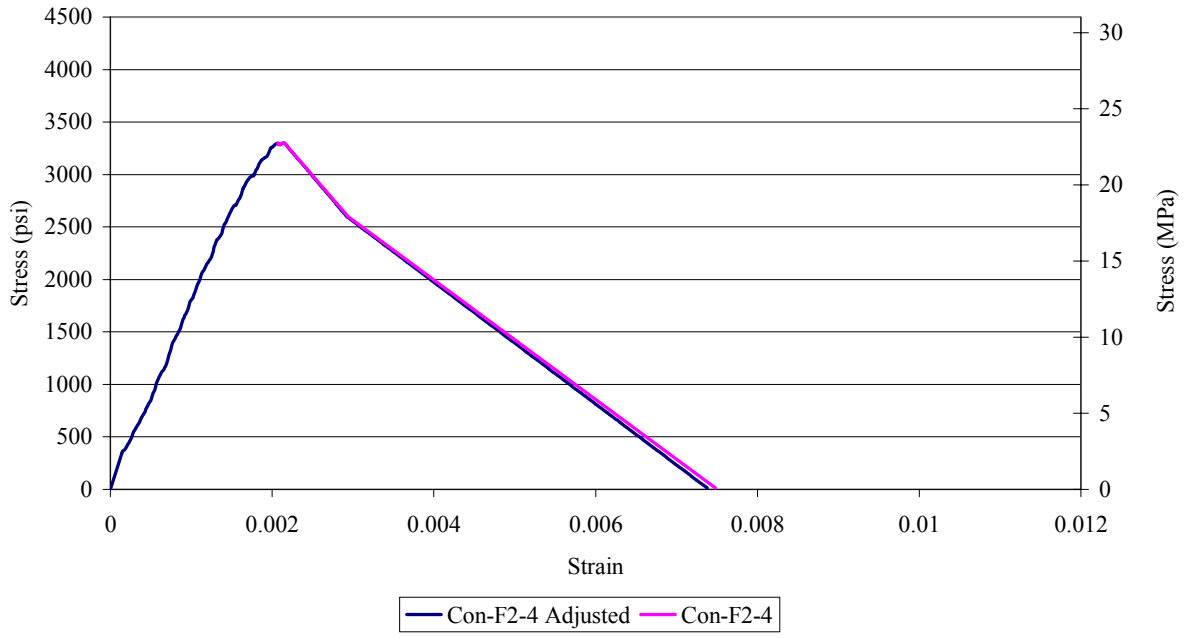

CON-F2-5

Con-F2-5 Stress vs. Strain

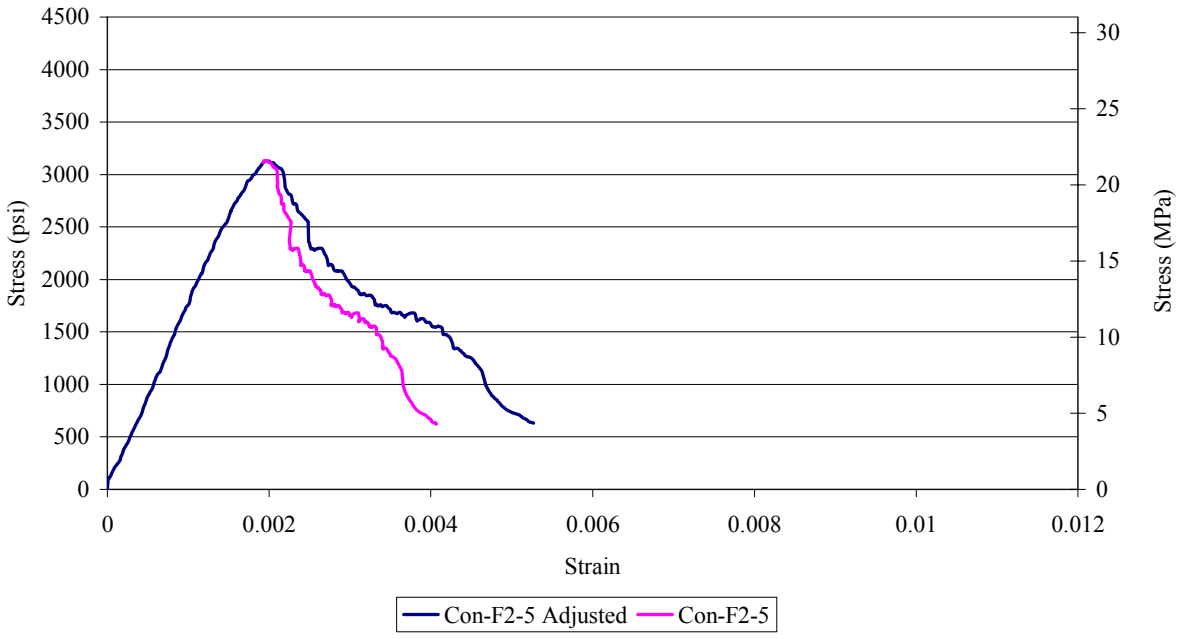

CLA-N-1

Cla-N-1 Stress vs. Strain

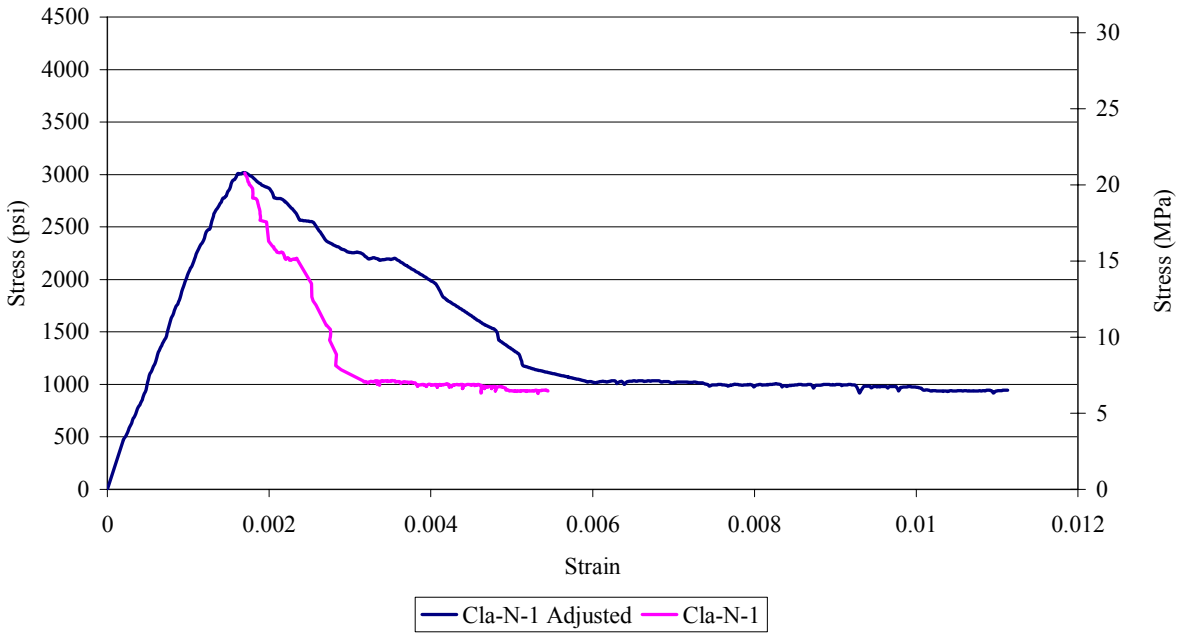

CLA-N-2

Cla-N-2 Stress vs. Strain

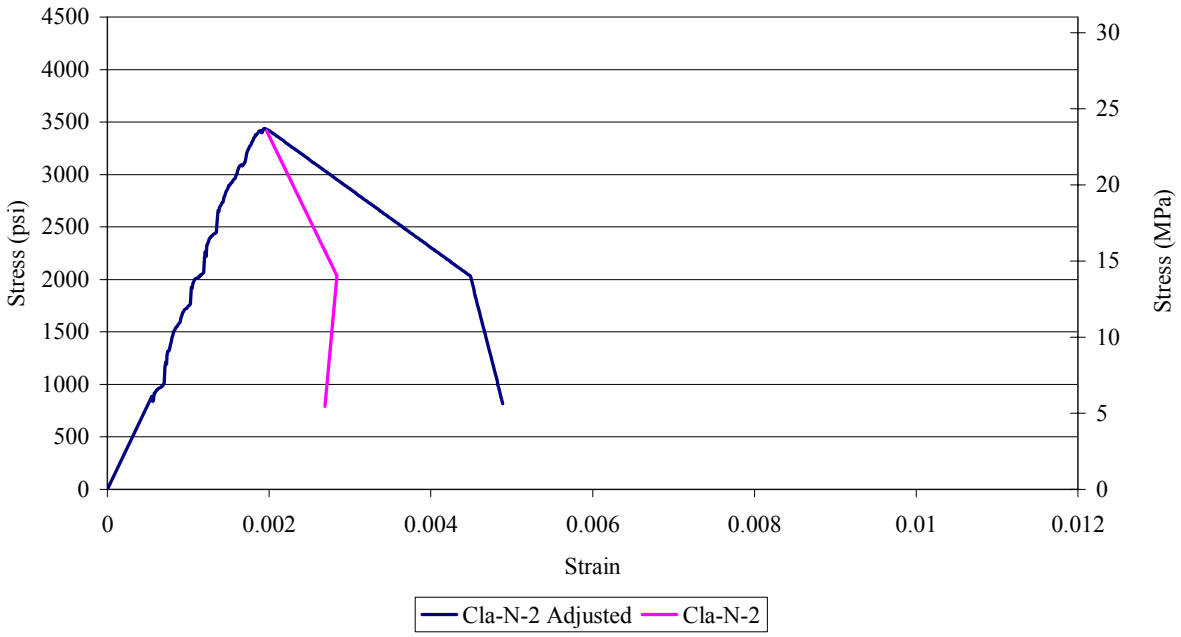

CLA-N-3

Cla-N-3 Stress vs. Strain

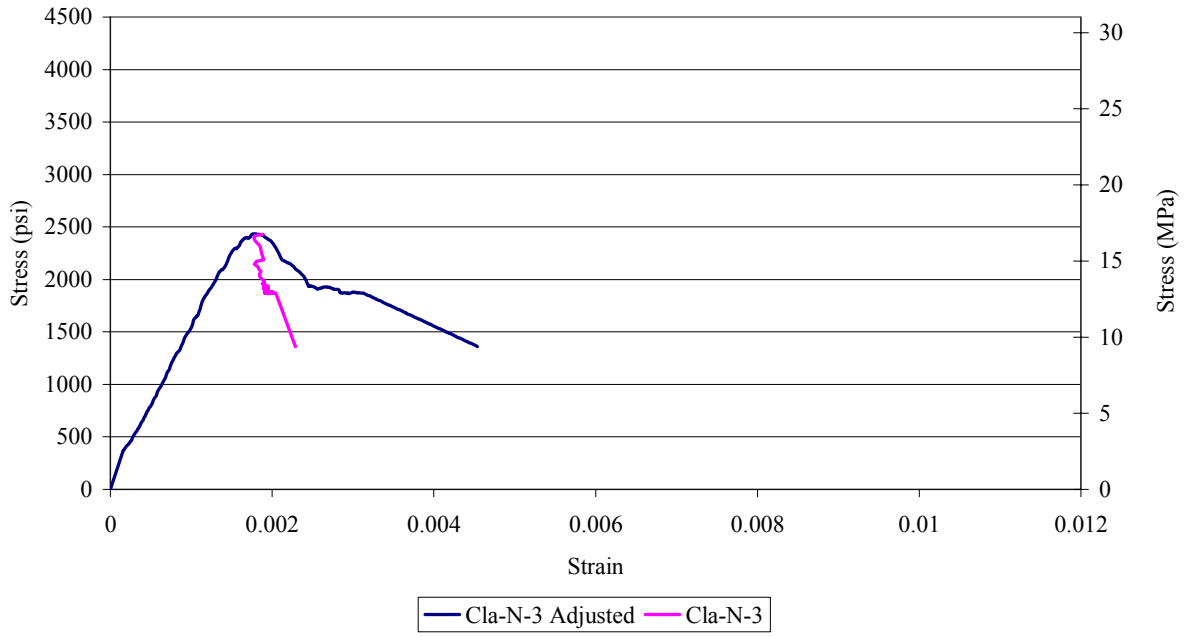

CLA-N-4

Cla-N-4 Stress vs. Strain

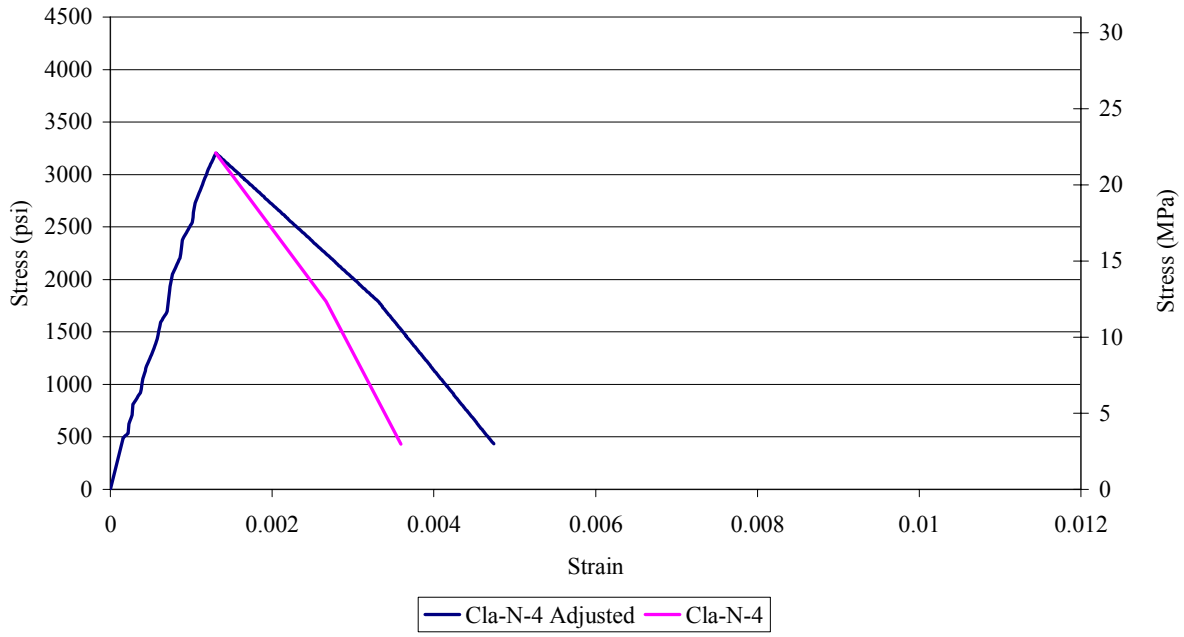

CLA-N-5

Cla-N-5 Stress vs. Strain

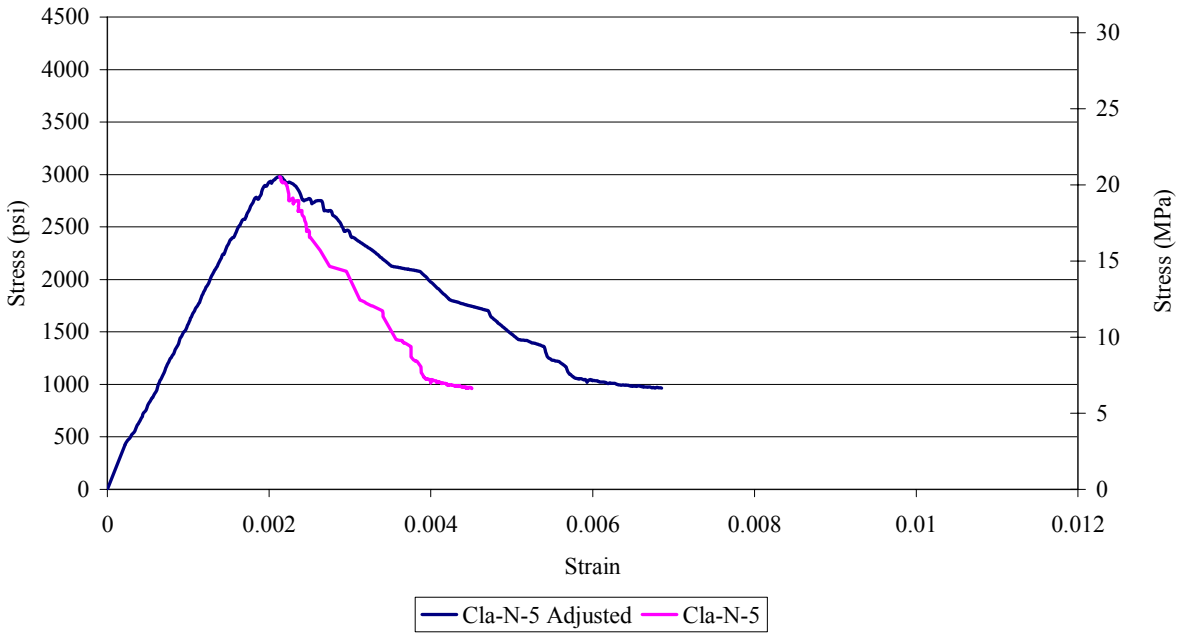

CLA-F1-1

Cla-F1-1 Stress vs. Strain

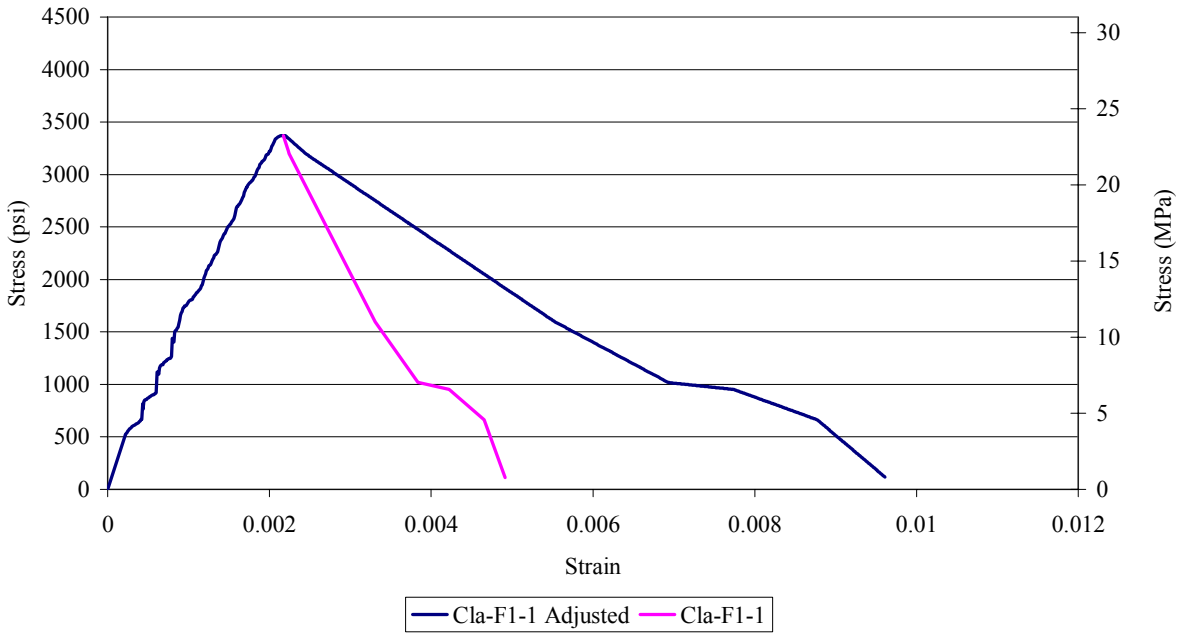

CLA-F1-2

Cla-F1-2 Stress vs. Strain

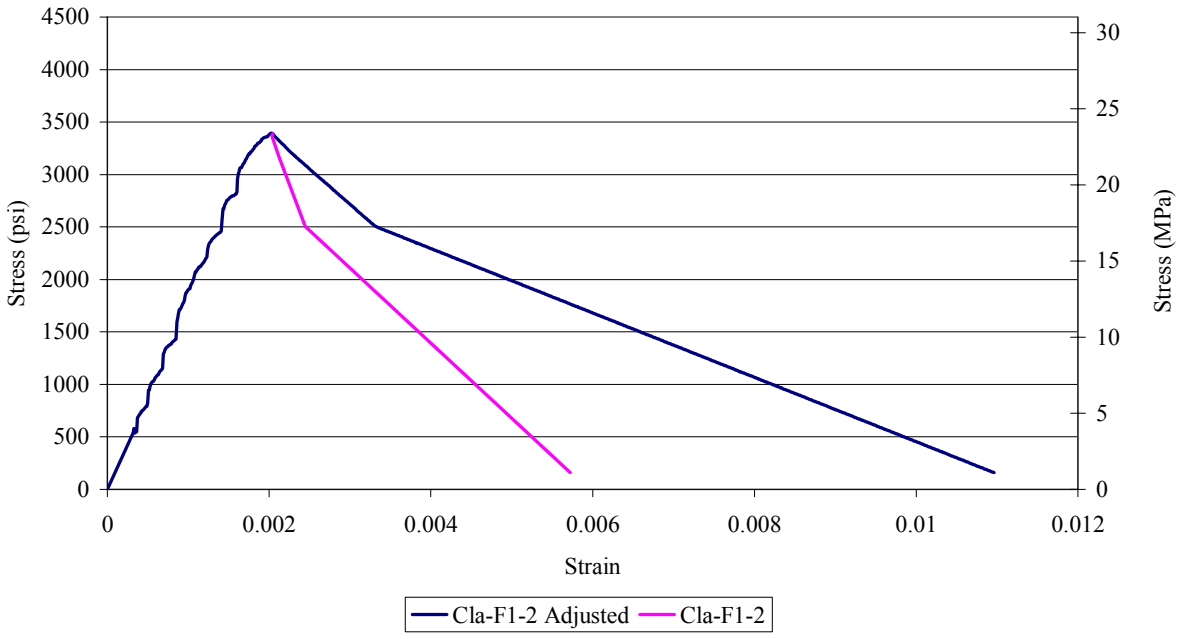

CLA-F1-3

Cla-F1-3 Stress vs. Strain

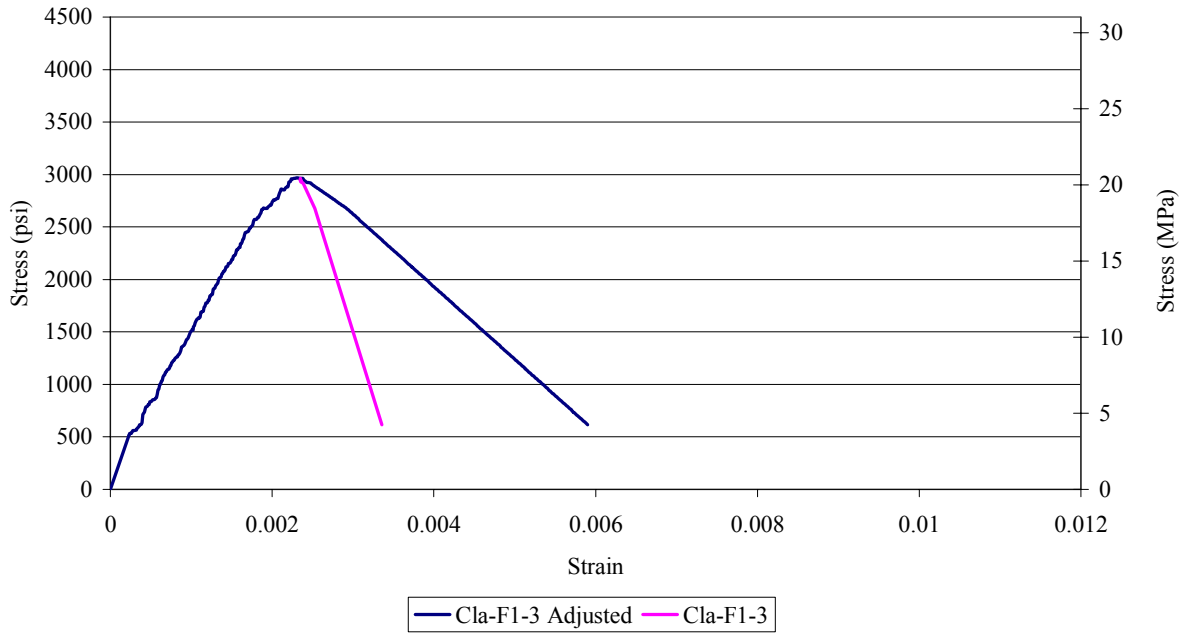

CLA-F1-4

Cla-F1-4 Stress vs. Strain

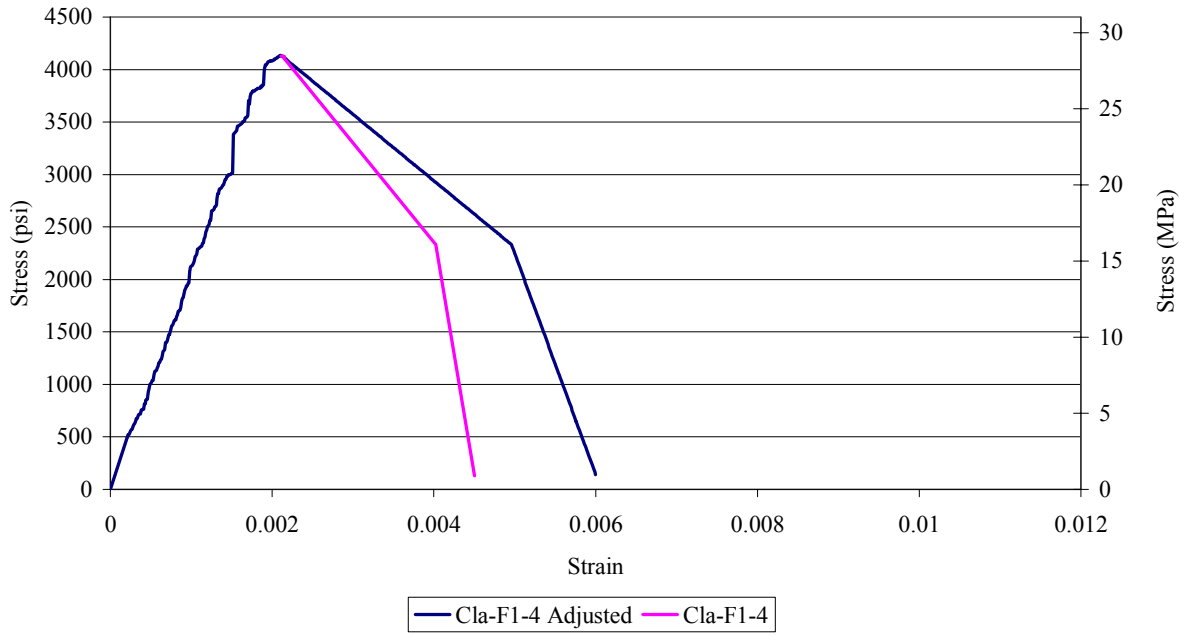

CLA-F1-5

Cla-F1-5 Stress vs. Strain

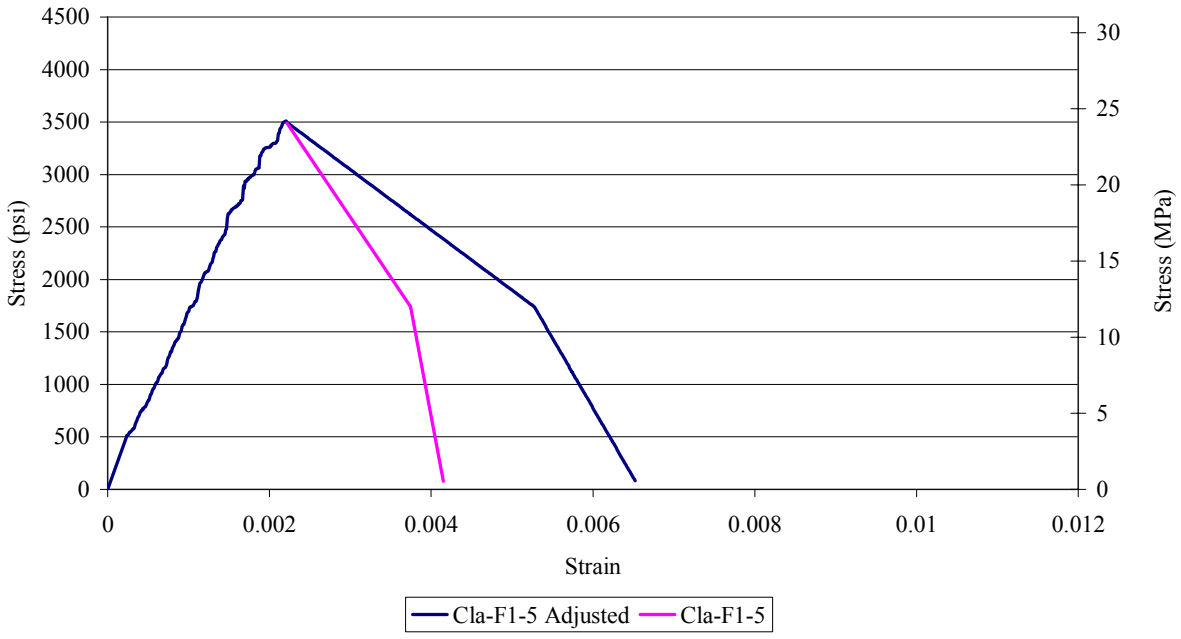

CLA-F2-1

Cla-F2-1 Stress vs. Strain

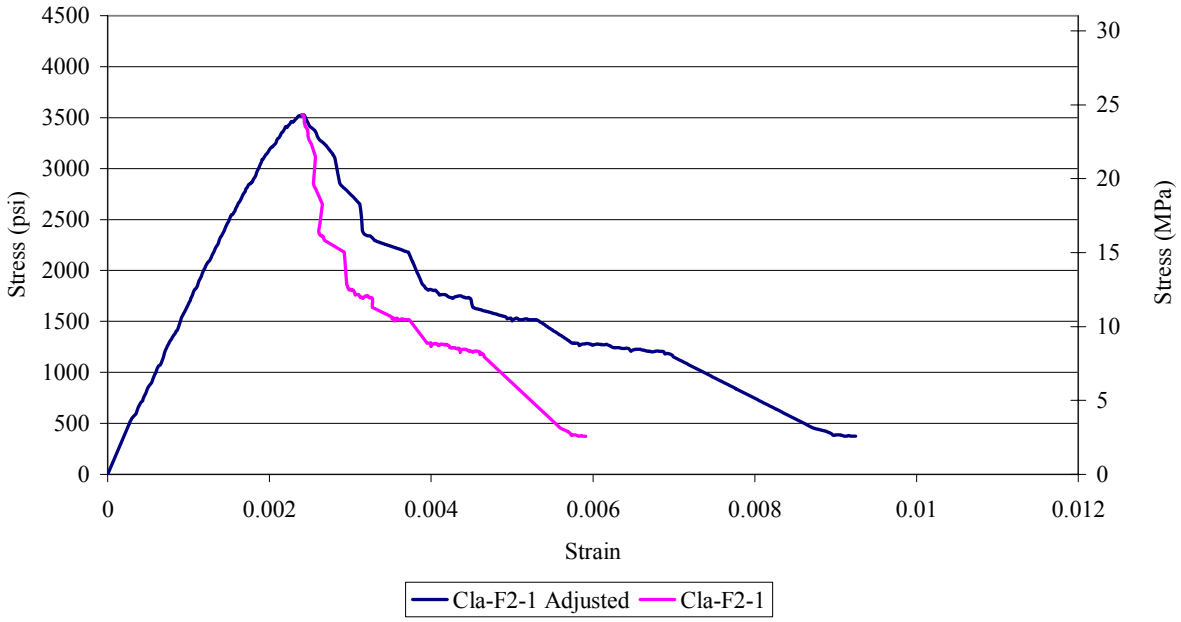

CLA-F2-2

Cla-F2-2 Stress vs. Strain

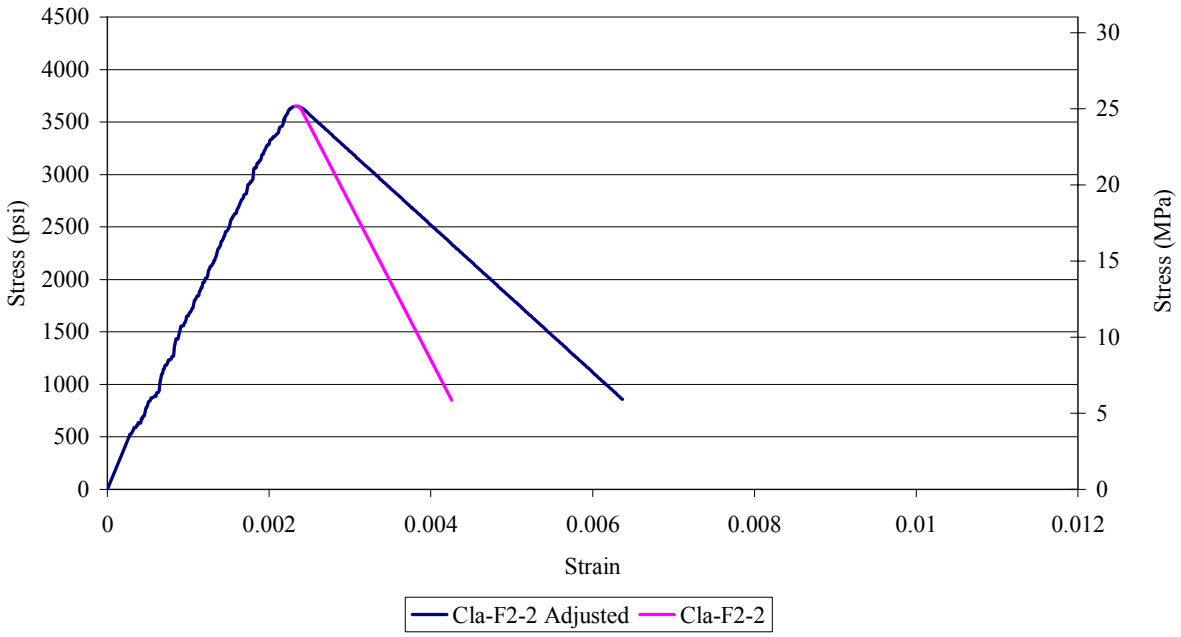

CLA-F2-3

Cla-F2-3 Stress vs. Strain

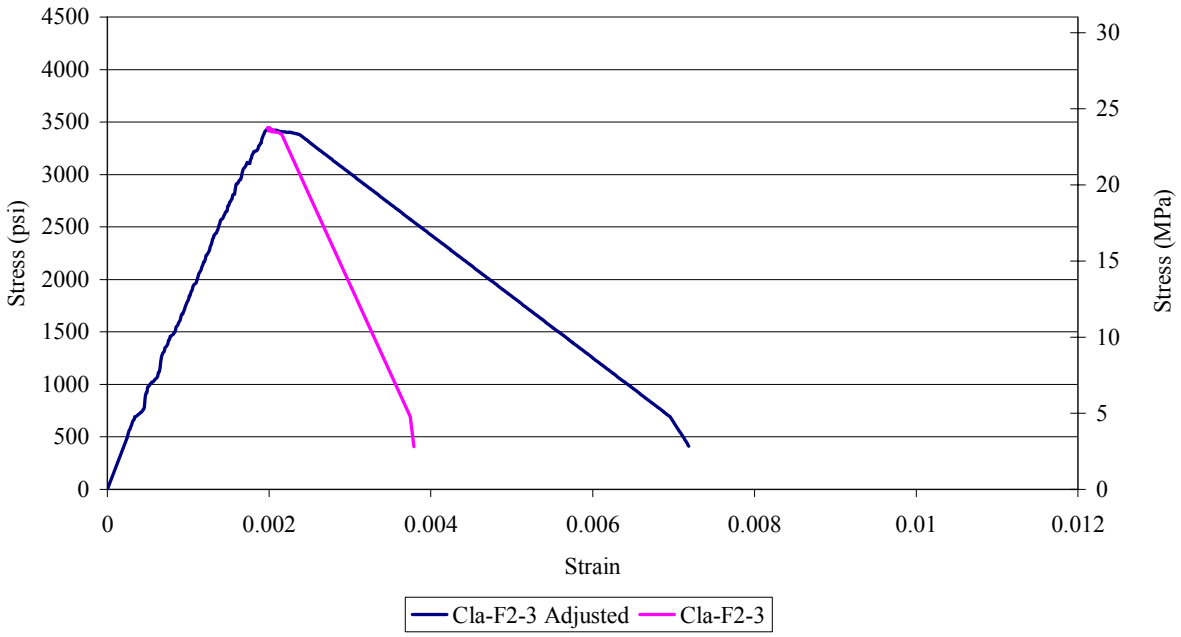

CLA-F2-4

Cla-F2-4 Stress vs. Strain

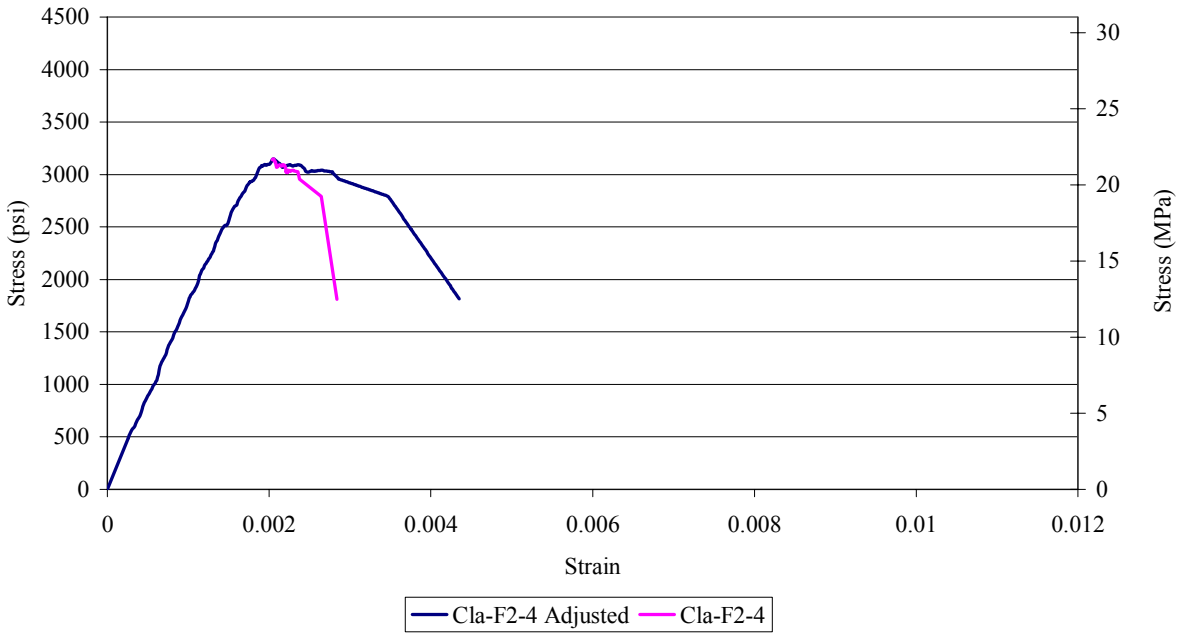

CLA-F2-5

Cla-F2-5 Stress vs. Strain

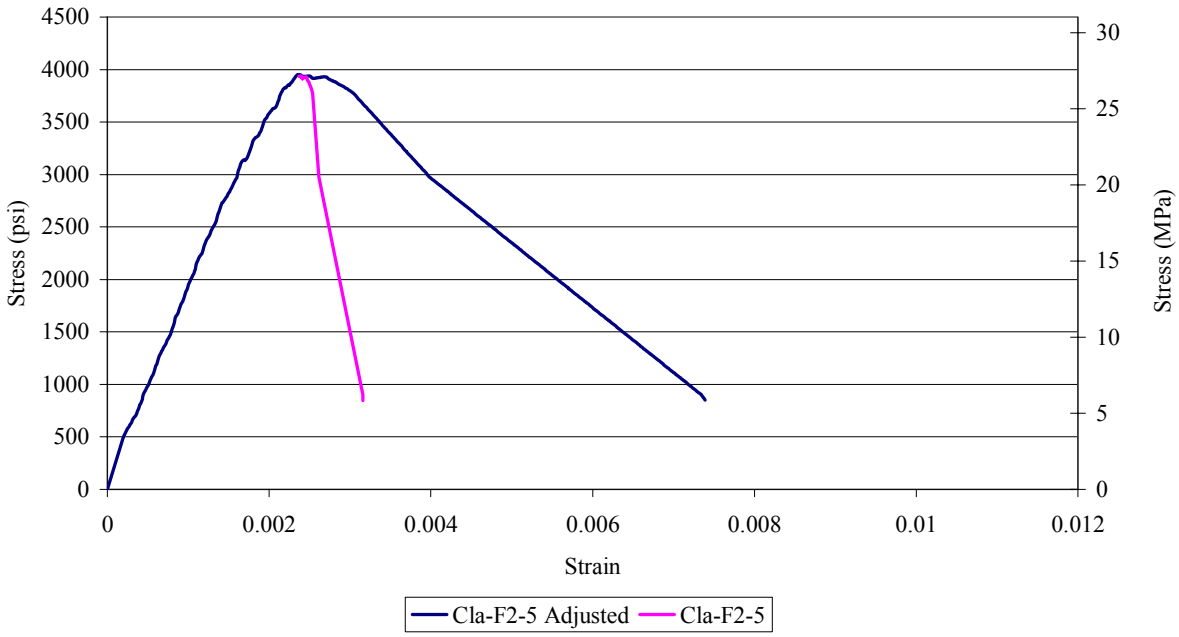

CON-N

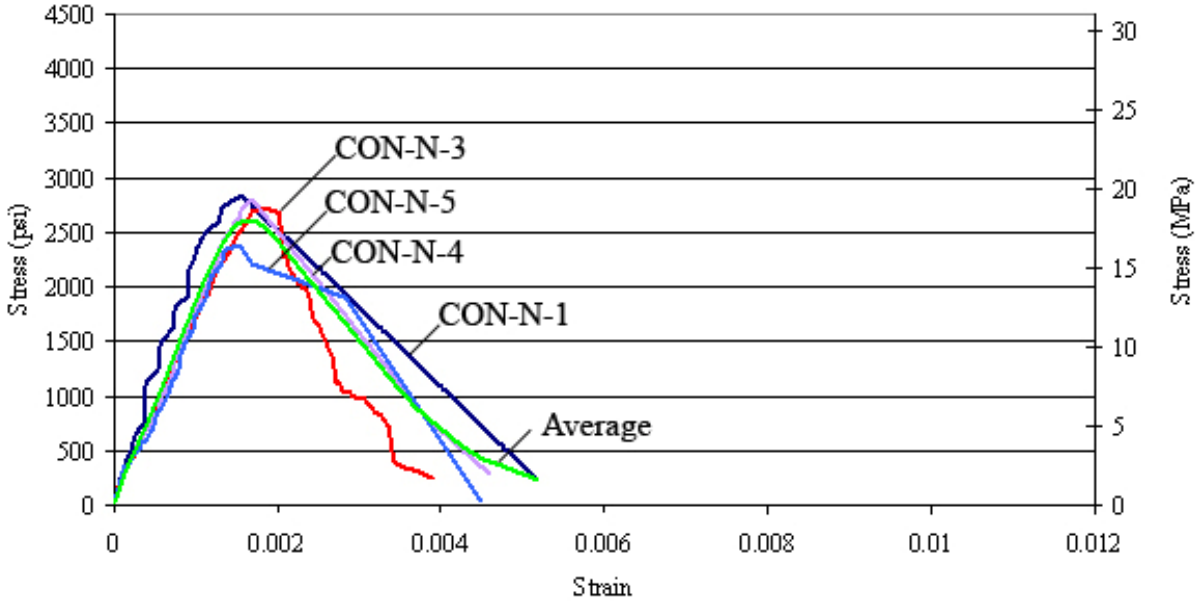
4500
4000
3500
3000
2500
2000
1500
1000
500
0
Stress (psi)
30
25
20
15
10
5
0
Stress (MPa)
0
0.002
0.004
0.006
0.008
0.01
0.012
Strain
CON-N-3
CON-N-5
CON-N-4
CON-N-1
Average

CON-F1

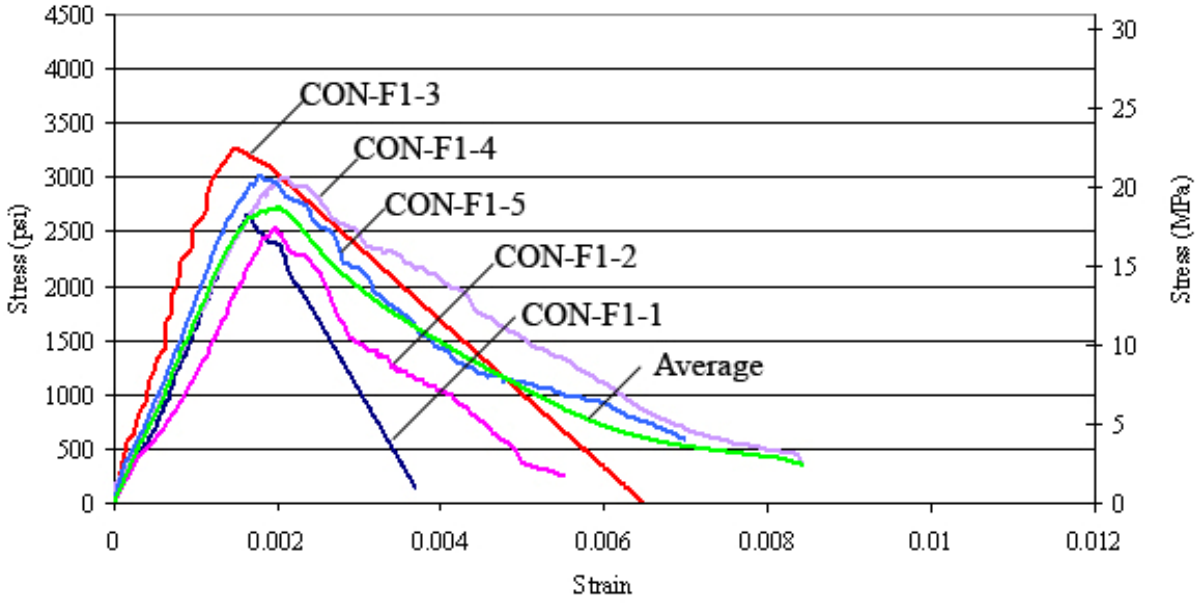
4500
4000
3500
3000
2500
2000
1500
1000
500
0
Stress (psi)
30
25
20
15
10
5
0
Stress (MPa)
0
0.002
0.004
0.006
0.008
0.01
0.012
Strain
CON-F1-3
CON-F1-4
CON-F1-5
CON-F1-2
CON-F1-1
Average

CON-F2

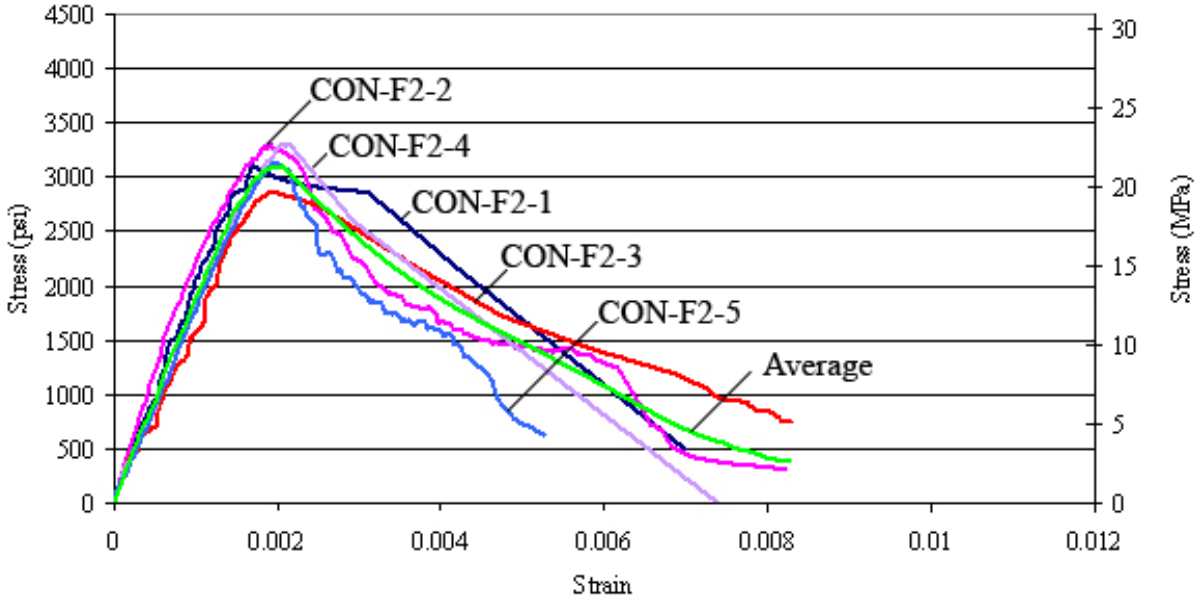
CON-F2-2
CON-F2-4
CON-F2-1
CON-F2-3
CON-F2-5
Average
Stress (psi)
Stress (MPa)
Strain
4500
4000
3500
3000
2500
2000
1500
1000
500
0
30
25
20
15
10
5
0
0
0.002
0.004
0.006
0.008
0.01
0.012

CLA-N

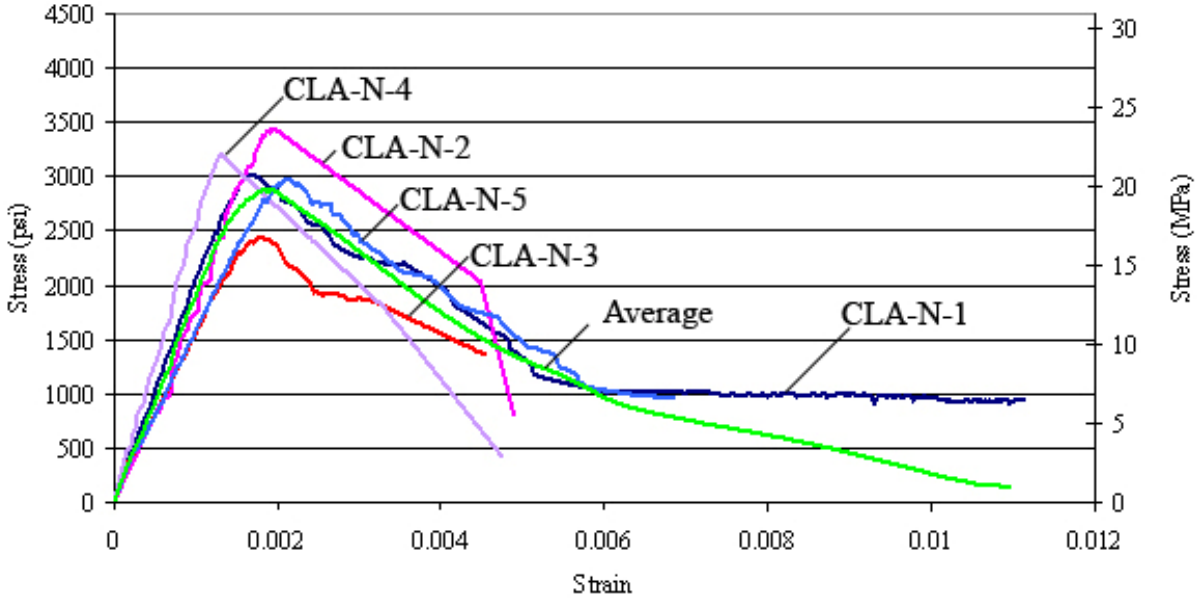
CLA-N-4
CLA-N-2
CLA-N-5
CLA-N-3
Average
CLA-N-1
Stress (psi)
Stress (MPa)
Strain
4500
4000
3500
3000
2500
2000
1500
1000
500
0
30
25
20
15
10
5
0
0
0.002
0.004
0.006
0.008
0.01
0.012

CLA-F1

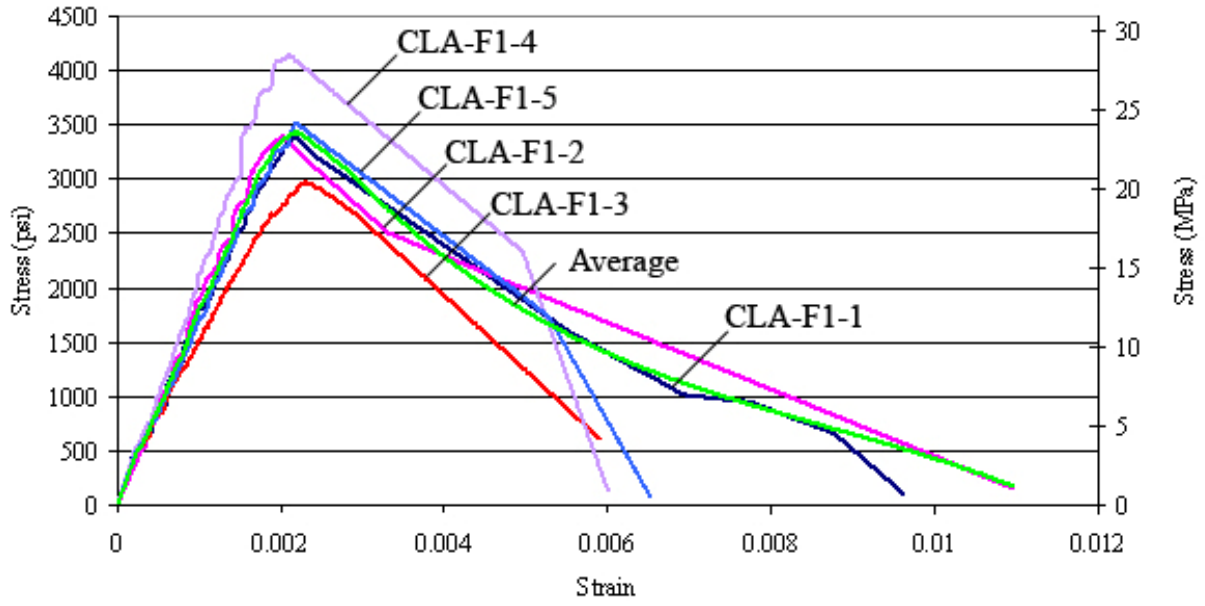
CLA-F1-4
CLA-F1-5
CLA-F1-2
CLA-F1-3
Average
CLA-F1-1
Stress (psi)
Stress (MPa)
Strain
4500
4000
3500
3000
2500
2000
1500
1000
500
0
30
25
20
15
10
5
0
0
0.002
0.004
0.006
0.008
0.01
0.012

CLA-F2

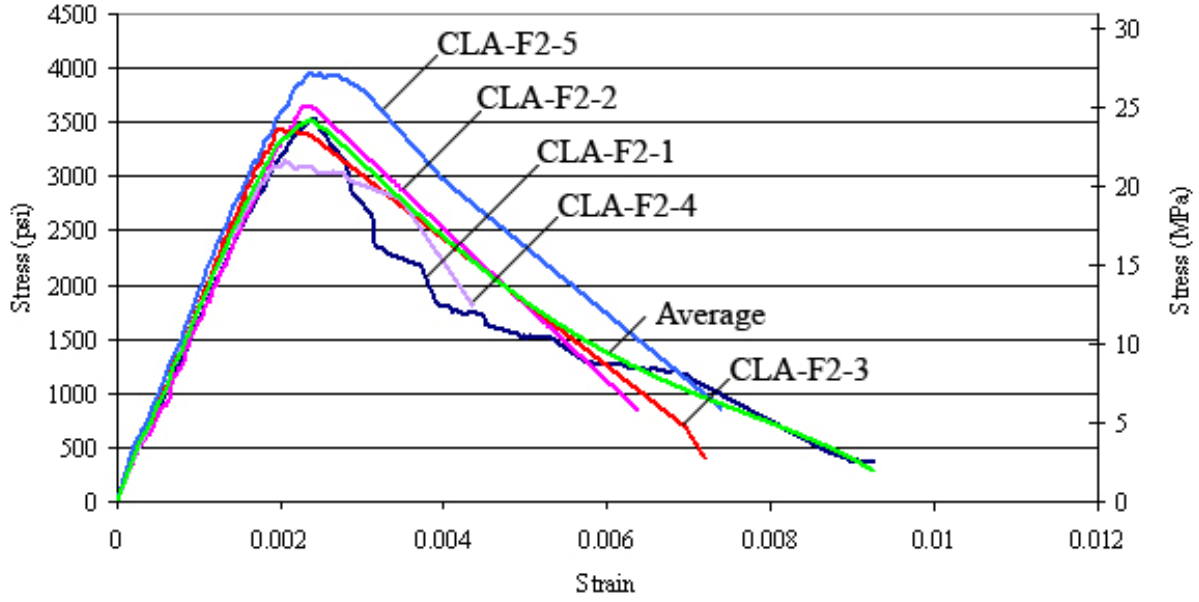
CLA-F2-5
CLA-F2-2
CLA-F2-1
CLA-F2-4
Average
CLA-F2-3
Stress (psi)
Stress (MPa)
Strain
4500
4000
3500
3000
2500
2000
1500
1000
500
0
30
25
20
15
10
5
0
0
0.002
0.004
0.006
0.008
0.01
0.012

APPENDIX D

This appendix presents the SAS code for the analysis of variance (ANOVA) conducted on the peak stresses, strains at peak stresses and strains at 50% of the peak stresses values. It also presents the Excel files imported into SAS to run the ANOVA.

```
Title GLM for Fiber reinforced masonry prisms;

proc glm data=sasuser.thomas;
    class Fiber;
    model StressP StrainP Strain50 = Fiber;
      means Fiber /duncan alpha=0.1;
      lsmeans Fiber;
      run;
proc means data=sasuser.thomas vardef=DF MEAN  CV;
     var StressP StrainP Strain50;
     class Fiber ;
quit;
```

Excel file imported into SAS for concrete masonry piers

Fiber	StressP	StrainP	Strain50
NoF	2833,312586	0,001557671	0,003550000
NoF	2717,647958	0,001809036	0,002683606
NoF	2787,730081	0,001659807	0,003200000
NoF	2374,918642	0,001510203	0,003470000
F1	2660,034256	0,001646097	0,002780000
F1	2541,306163	0,002281352	0,003685969
F1	3269,913442	0,001478260	0,004070000
F1	2997,835755	0,002073781	0,005058817
F1	3020,266249	0,001791639	0,003867576
F2	3119,930876	0,001703283	0,005210000
F2	3299,068665	0,001925365	0,003965341
F2	2857,024774	0,001901535	0,005833039
F2	3300,094816	0,002152803	0,004560000
F2	3130,855177	0,001945125	0,004006973

Excel file imported into SAS for clay masonry piers

Fiber	StressP	StrainP	Strain50
NoF	3020,980237	0,001681899	0,004787464
NoF	3441,326324	0,001943310	0,004590000
NoF	2433,954466	0,001755820	NA
NoF	3206,139289	0,001304196	0,003510000
NoF	2979,462451	0,002113810	0,004990000
F1	3372,269723	0,002146936	0,005360000
F1	3393,937233	0,002026610	0,005950000
F1	2971,242055	0,002320972	0,004640000
F1	4136,006640	0,002130922	0,005080000
F1	3518,081265	0,002218882	0,005274561
F2	3526,712095	0,002417633	0,004175887
F2	3650,691700	0,002354767	0,004990000
F2	3443,787668	0,001981271	0,005200000
F2	3148,372016	0,002059520	NA
F2	3953,482213	0,002362191	0,005600000

APPENDIX E

This appendix presents the stress-strain diagrams for clay masonry from experiment, from the Modified Kent-Park model and from the Modified Kent-Park model adjusted for the compressive strength of Snook (2005).

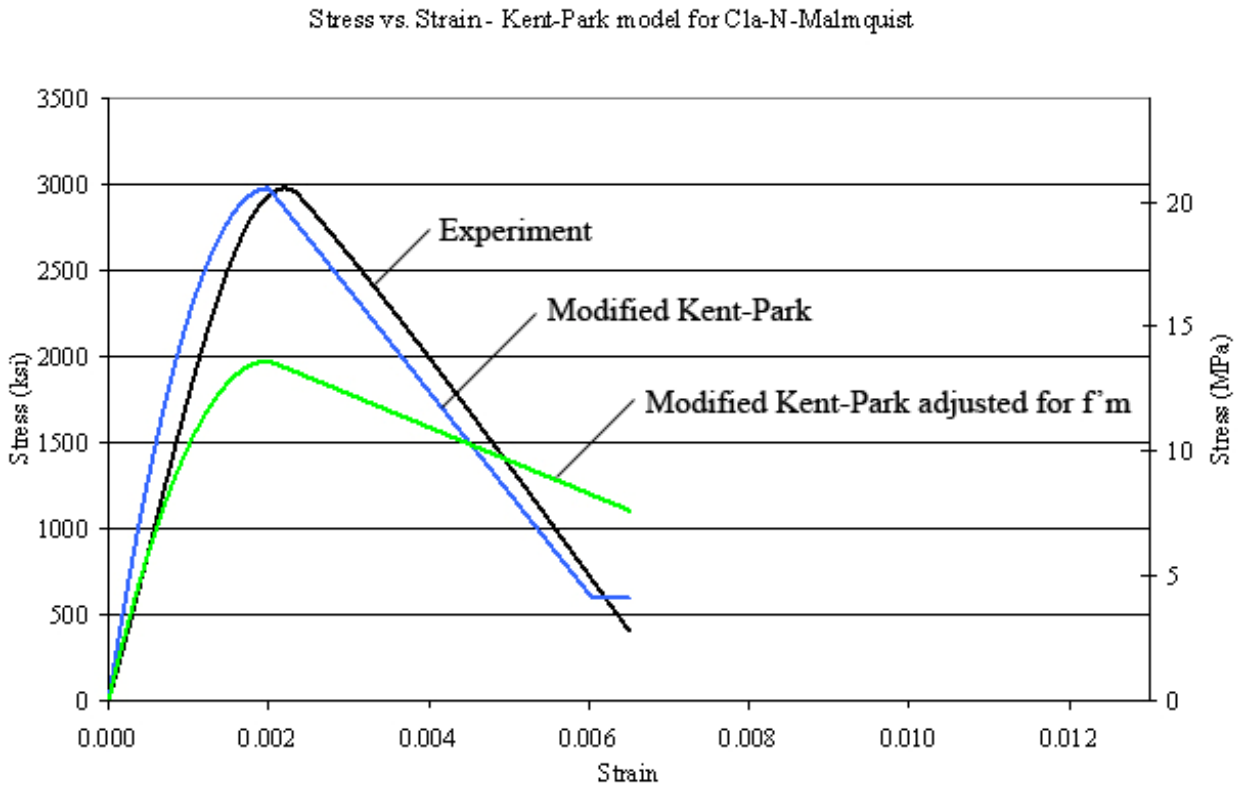
Stress vs. Strain - Kent-Park model for C1a-N-Malmquist
Stress (ksi)
Stress (MPa)
Strain
Experiment
Modified Kent-Park
Modified Kent-Park adjusted for f'm
3500
3000
2500
2000
1500
1000
500
0
20
15
10
5
0
0.000
0.002
0.004
0.006
0.008
0.010
0.012

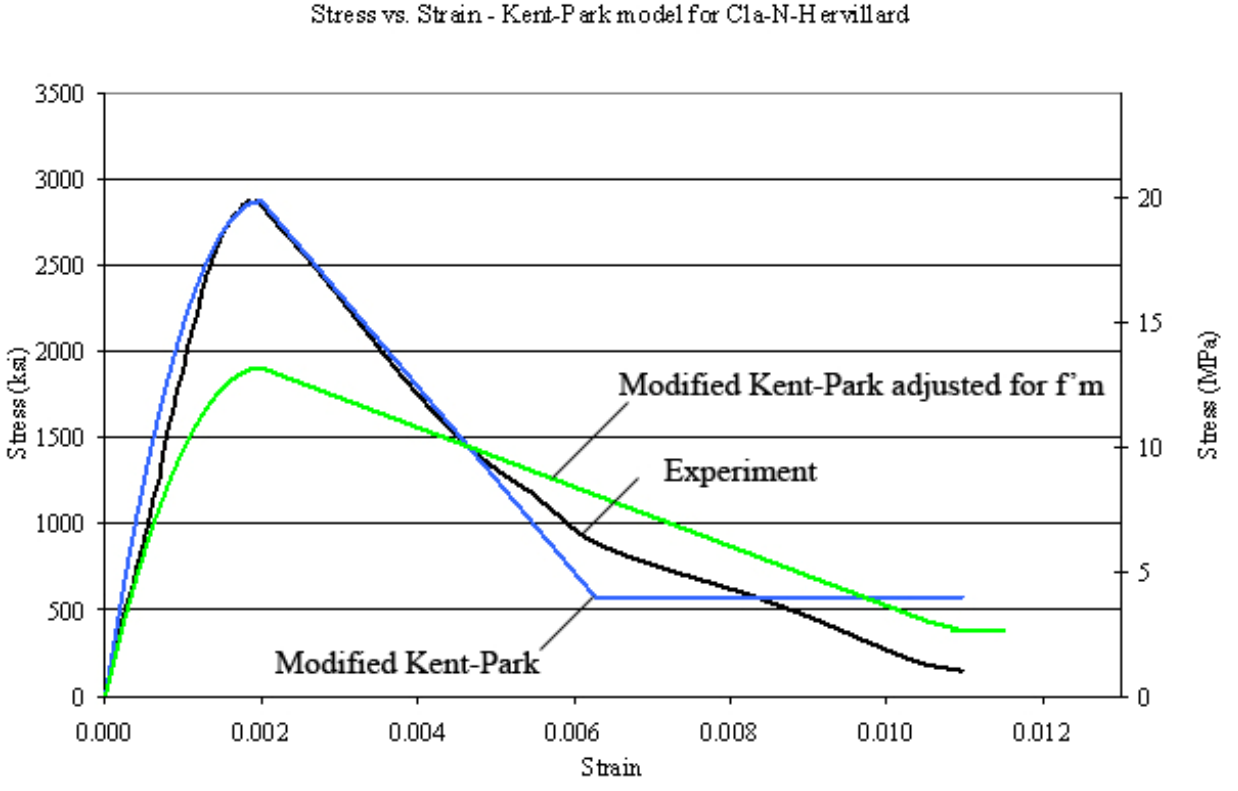
Stress vs. Strain - Kent-Park model for C1a-N-Hervillard
Stress (ksi)
Stress (MPa)
Strain
Modified Kent-Park adjusted for f'm
Experiment
Modified Kent-Park
3500
3000
2500
2000
1500
1000
500
0
20
15
10
5
0
0.000
0.002
0.004
0.006
0.008
0.010
0.012

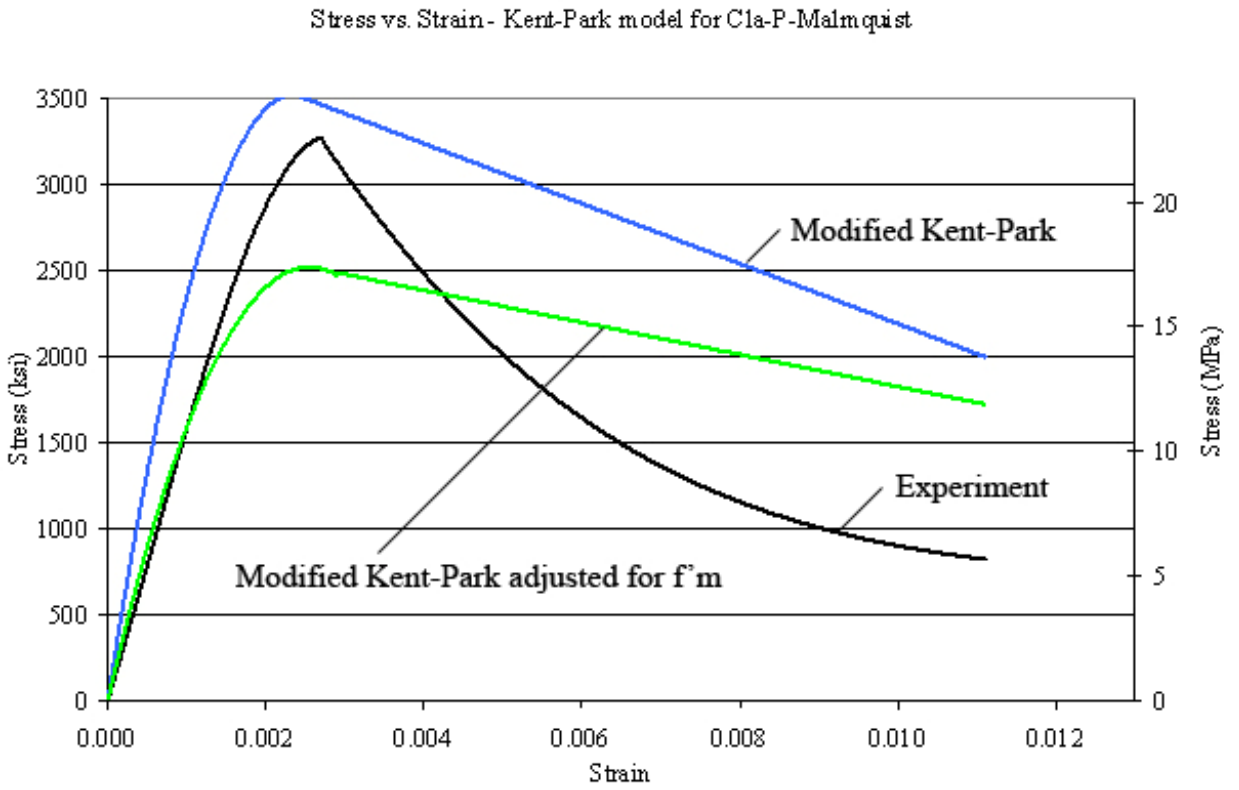
Stress vs. Strain - Kent-Park model for C1a-P-Malmquist
Stress (ksi)
Stress (MPa)
Strain
Modified Kent-Park
Experiment
Modified Kent-Park adjusted for f'm
0
500
1000
1500
2000
2500
3000
3500
0
5
10
15
20
0.000
0.002
0.004
0.006
0.008
0.010
0.012

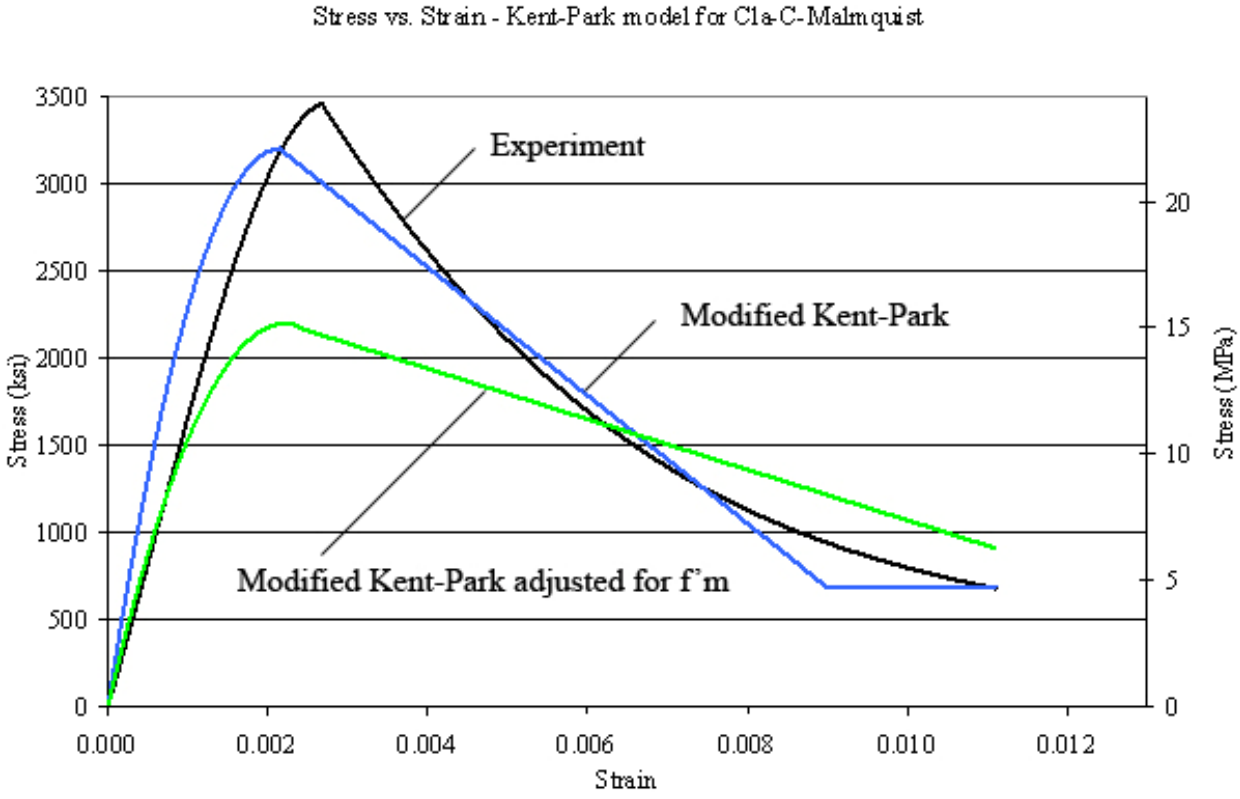
Stress vs. Strain - Kent-Park model for C1a-C-Malmquist
Stress (ksi)
Stress (MPa)
Strain
Experiment
Modified Kent-Park
Modified Kent-Park adjusted for f'm
0
500
1000
1500
2000
2500
3000
3500
0
5
10
15
20
0.000
0.002
0.004
0.006
0.008
0.010
0.012

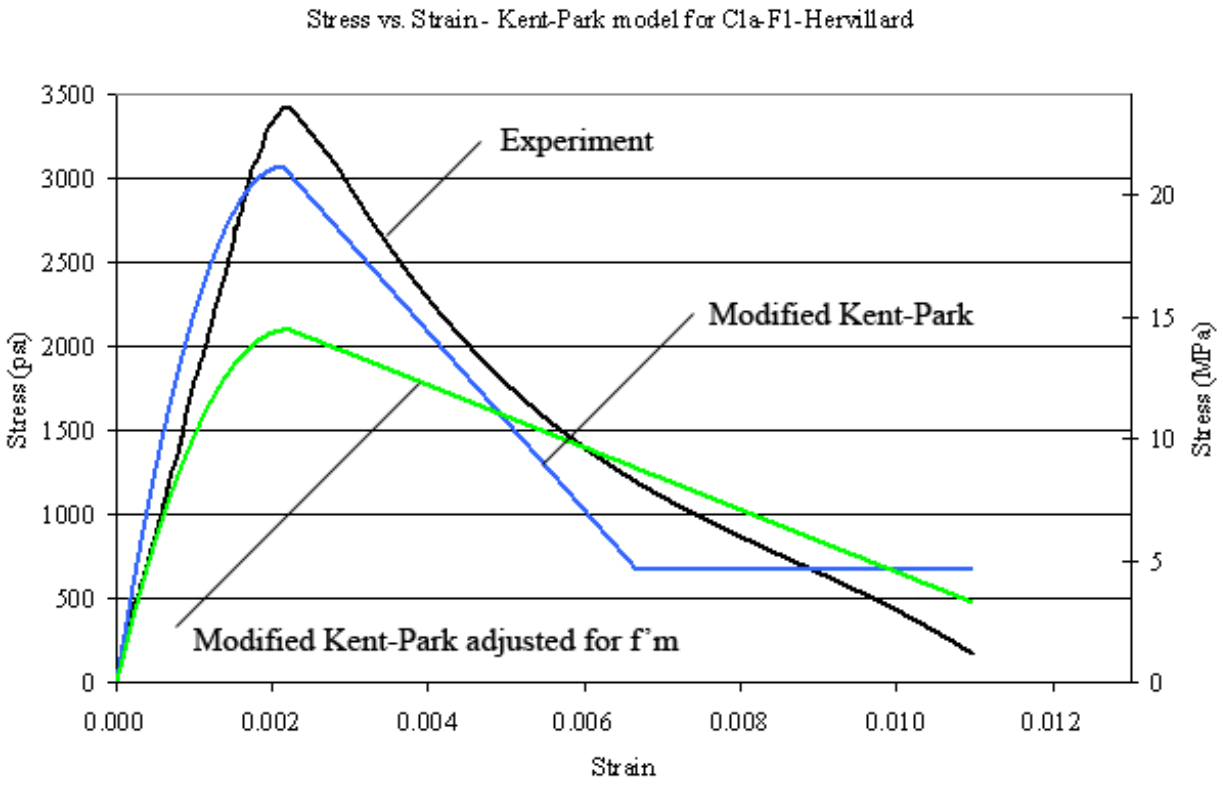
Stress vs. Strain - Kent-Park model for C1a-F1-Hervillard
Experiment
Modified Kent-Park
Modified Kent-Park adjusted for f'm
Stress (psi)
Stress (MPa)
Strain
3500
3000
2500
2000
1500
1000
500
0
20
15
10
5
0
0.000
0.002
0.004
0.006
0.008
0.010
0.012

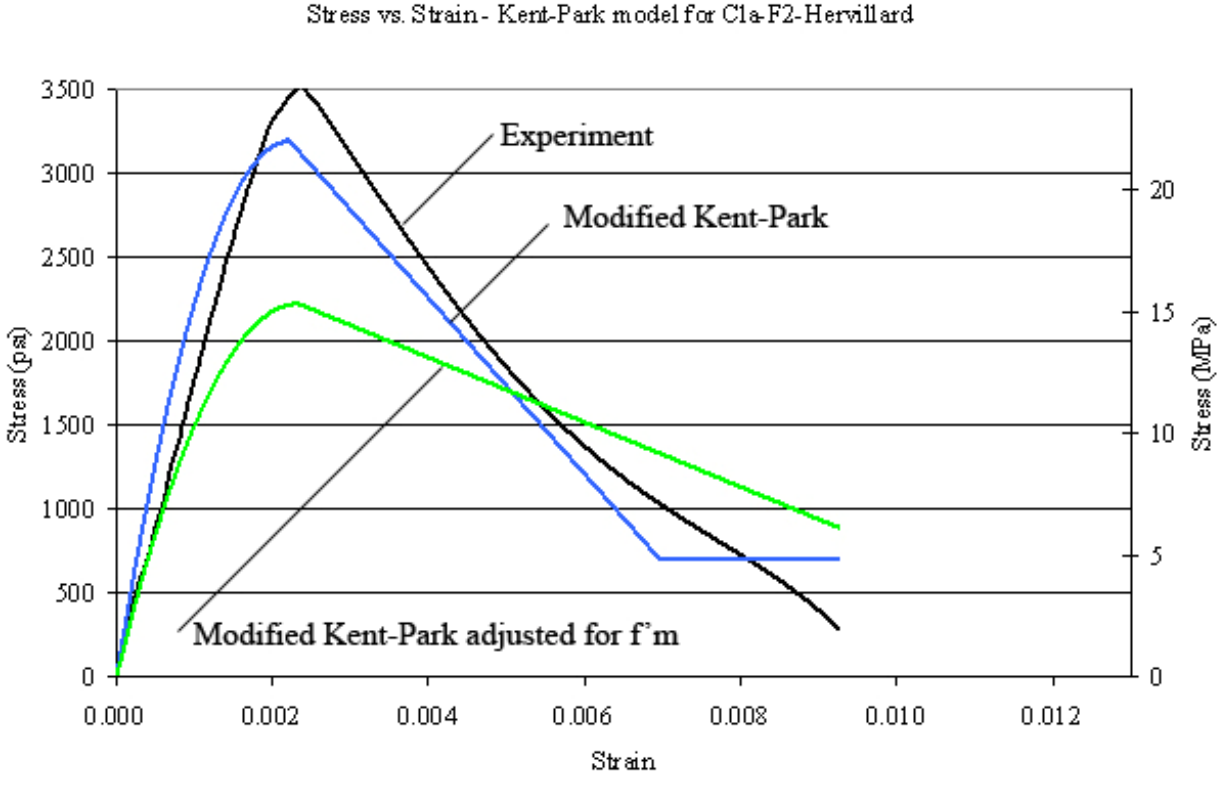
Stress vs. Strain - Kent-Park model for C1a-F2-Hervillard
Experiment
Modified Kent-Park
Modified Kent-Park adjusted for f'm
Stress (psi)
Stress (MPa)
Strain
3500
3000
2500
2000
1500
1000
500
0
20
15
10
5
0
0.000
0.002
0.004
0.006
0.008
0.010
0.012

APPENDIX F

This appendix presents Xtract result files. It presents the state of the cross-section of each wall at failure and the moment-curvature analysis results.

XTRACT Analysis Report - Educational

Thomas Hervillard
Washington State University
9/17/2005

Section Name: Section2
Loading Name: Loading
Analysis Type: Moment Curvature

Section Details:

X Centroid:	27.81 in
Y Centroid:	3.812 in
Section Area:	424.1 in^2

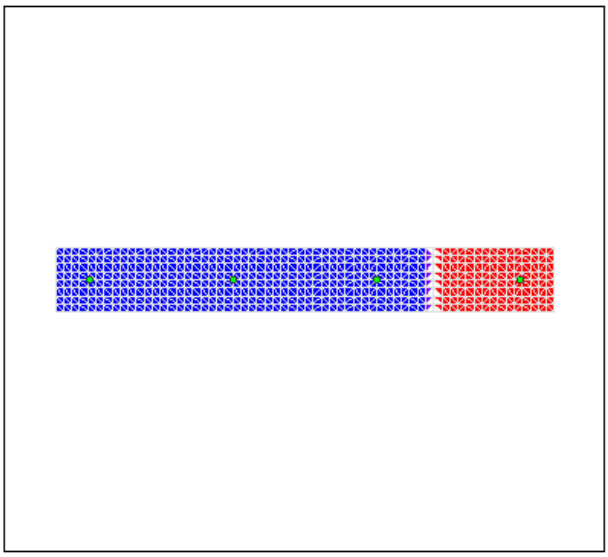

Loading Details:

Constant Load - P:	11.45E+3 lbs
Incrementing Loads:	Myy Only
Number of Points:	80
Analysis Strategy:	Displacement Control

Analysis Results:

Failing Material:	Con-N-Kirk
Failure Strain:	26.00E-3 Compression
Curvature at Initial Load:	-.2818E-19 1/in
Curvature at First Yield:	57.48E-6 1/in
Ultimate Curvature:	1.845E-3 1/in
Moment at First Yield:	1.682E+6 lb-in
Ultimate Moment:	2.288E+6 lb-in
Centroid Strain at Yield:	.9000E-3 Ten
Centroid Strain at Ultimate:	25.45E-3 Ten
N.A. at First Yield:	15.66 in
N.A. at Ultimate:	13.80 in
Energy per Length:	4569 lbs
Effective Yield Curvature:	86.70E-6 1/in
Effective Yield Moment:	2.537E+6 lb-in
Over Strength Factor:	.9022
Plastic Rotation Capacity:	23.58E-3 rad
EI Effective:	2.93E+7 kip-in^2
Yield EI Effective:	0 kip-in^2
Bilinear Harding Slope:	0 %
Curvature Ductility:	21.28

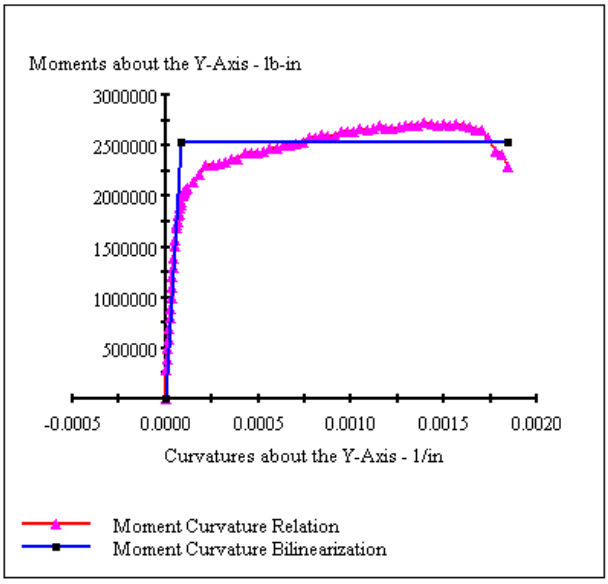

Comments:

User Comments

XTRACT Analysis Report - Educational

Thomas Hervillard
Washington State University
9/18/2005

Section Name: Section1
Loading Name: Loading
Analysis Type: Moment Curvature

Ian - Wall 2 - Con-N-Kirk

Section Details:

X Centroid:	27.81 in
Y Centroid:	3.812 in
Section Area:	424.2 in^2

Loading Details:

Constant Load - P:	11.45E+3 lbs
Incrementing Loads:	Myy Only
Number of Points:	80
Analysis Strategy:	Displacement Control

Analysis Results:

Failing Material:	Con-N-Kirk
Failure Strain:	23.00E-3 Compression
Curvature at Initial Load:	-.1393E-19 1/in
Curvature at First Yield:	57.46E-6 1/in
Ultimate Curvature:	1.797E-3 1/in
Moment at First Yield:	1.680E+6 lb-in
Ultimate Moment:	2.414E+6 lb-in
Centroid Strain at Yield:	.9003E-3 Ten
Centroid Strain at Ultimate:	27.48E-3 Ten
N.A. at First Yield:	15.67 in
N.A. at Ultimate:	15.30 in
Energy per Length:	4461 lbs
Effective Yield Curvature:	87.04E-6 1/in
Effective Yield Moment:	2.545E+6 lb-in
Over Strength Factor:	.9485
Plastic Rotation Capacity:	25.34E-3 rad
EI Effective:	2.92E+7 kip-in^2
Yield EI Effective:	0 kip-in^2
Bilinear Harding Slope:	0 %
Curvature Ductility:	20.64

Comments:

User Comments

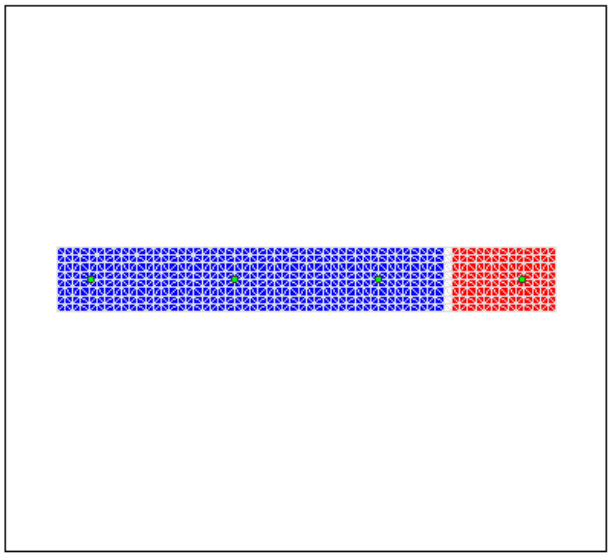

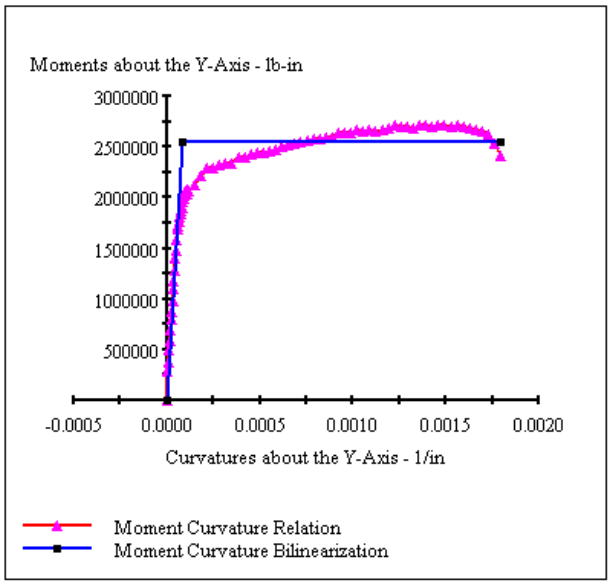

XTRACT Analysis Report - Educational

Thomas Hervillard
Washington State University
9/18/2005

Section Name: Section1
Loading Name: Loading
Analysis Type: Moment Curvature

Ian - Wall 3 - Con-N-Kirk

Section Details:

X Centroid:	19.81 in
Y Centroid:	3.813 in
Section Area:	302.2 in^2

Loading Details:

Constant Load - P:	8159 lbs
Incrementing Loads:	Myy Only
Number of Points:	80
Analysis Strategy:	Displacement Control

Analysis Results:

Failing Material:	Con-N-Kirk
Failure Strain:	23.00E-3 Compression
Curvature at Initial Load:	.2775E-19 1/in
Curvature at First Yield:	84.09E-6 1/in
Ultimate Curvature:	2.986E-3 1/in
Moment at First Yield:	931.8E+3 lb-in
Ultimate Moment:	1.237E+6 lb-in
Centroid Strain at Yield:	.9338E-3 Ten
Centroid Strain at Ultimate:	28.50E-3 Ten
N.A. at First Yield:	11.11 in
N.A. at Ultimate:	9.545 in
Energy per Length:	3941 lbs
Effective Yield Curvature:	.1216E-3 1/in
Effective Yield Moment:	1.348E+6 lb-in
Over Strength Factor:	.9178
Plastic Rotation Capacity:	33.29E-3 rad
EI Effective:	1.11E+7 kip-in^2
Yield EI Effective:	0 kip-in^2
Bilinear Harding Slope:	0 %
Curvature Ductility:	24.55

Comments:

User Comments

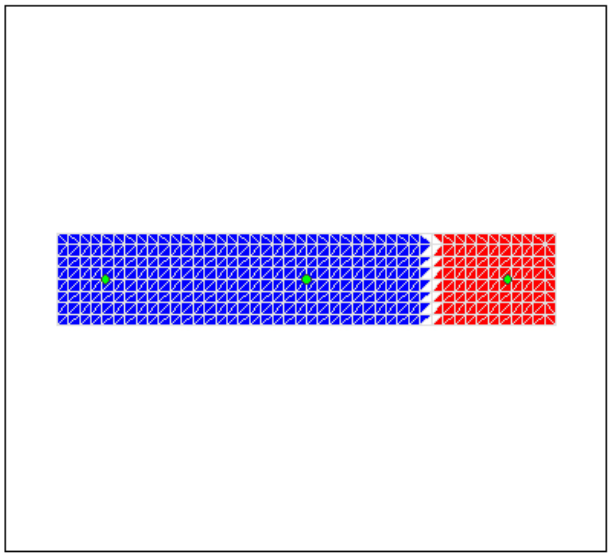

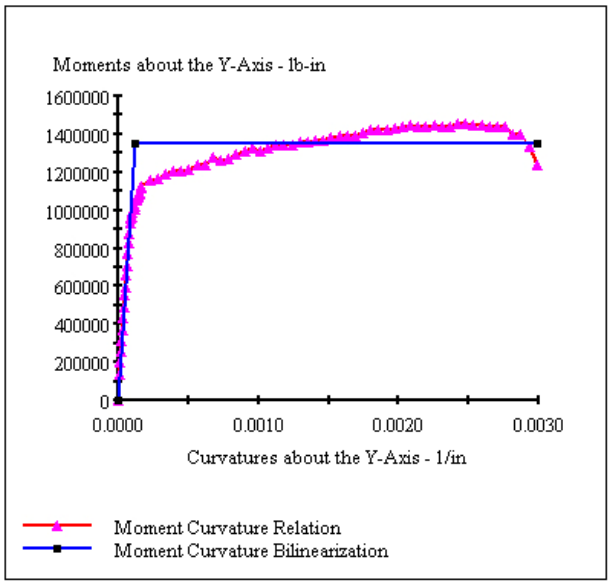

XTRACT Analysis Report - Educational

Thomas Hervillard
Washington State University
9/18/2005

Section Name: Section2
Loading Name: Loading
Analysis Type: Moment Curvature

Ian - Wall 4 - Con-N-Kirk

Section Details:

X Centroid:	27.81 in
Y Centroid:	3.813 in
Section Area:	424.2 in^2

Loading Details:

Constant Load - P:	11.45E+3 lbs
Incrementing Loads:	Myy Only
Number of Points:	80
Analysis Strategy:	Displacement Control

Analysis Results:

Failing Material:	Con-N-Kirk
Failure Strain:	23.00E-3 Compression
Curvature at Initial Load:	-.1302E-19 1/in
Curvature at First Yield:	57.48E-6 1/in
Ultimate Curvature:	1.348E-3 1/in
Moment at First Yield:	1.682E+6 lb-in
Ultimate Moment:	3.172E+6 lb-in
Centroid Strain at Yield:	.9000E-3 Ten
Centroid Strain at Ultimate:	14.14E-3 Ten
N.A. at First Yield:	15.66 in
N.A. at Ultimate:	10.49 in
Energy per Length:	4682 lbs
Effective Yield Curvature:	.1245E-3 1/in
Effective Yield Moment:	3.643E+6 lb-in
Over Strength Factor:	.8706
Plastic Rotation Capacity:	16.41E-3 rad
EI Effective:	2.93E+7 kip-in^2
Yield EI Effective:	0 kip-in^2
Bilinear Harding Slope:	0 %
Curvature Ductility:	10.82

Comments:

User Comments

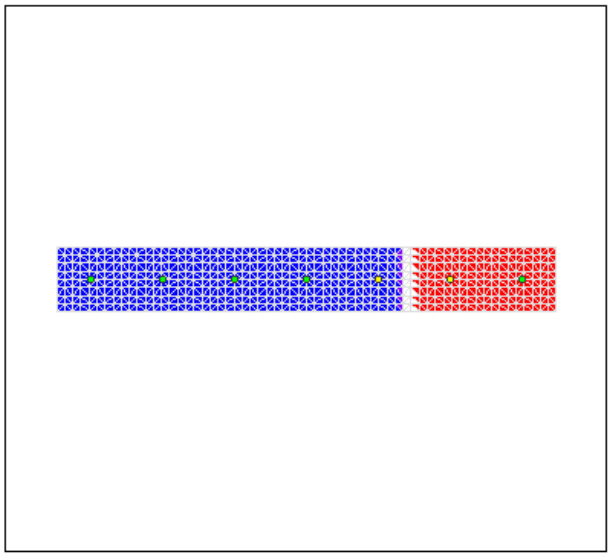

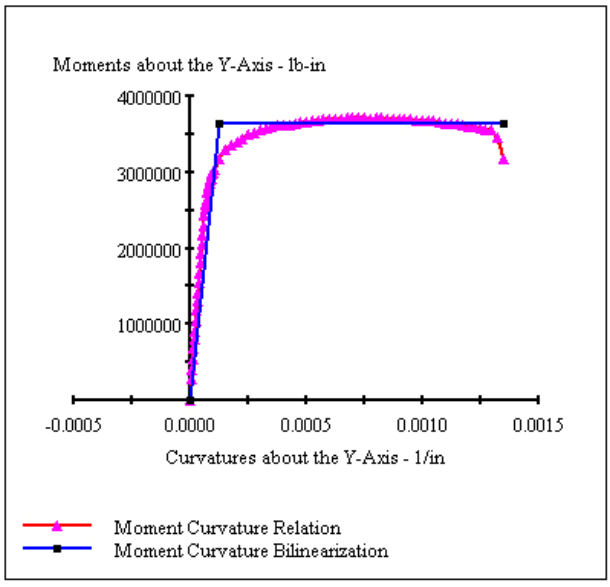

XTRACT Analysis Report - Educational

Thomas Hervillard
Washington State University
9/18/2005

Section Name: Section1
Loading Name: Loading
Analysis Type: Moment Curvature

Section Details:

X Centroid:	27.81 in
Y Centroid:	3.812 in
Section Area:	424.2 in^2

Loading Details:

Constant Load - P:	11.45E+3 lbs
Incrementing Loads:	Myy Only
Number of Points:	80
Analysis Strategy:	Displacement Control

Analysis Results:

Failing Material:	Con-N-Kirk
Failure Strain:	23.00E-3 Compression
Curvature at Initial Load:	-.1320E-19 1/in
Curvature at First Yield:	57.46E-6 1/in
Ultimate Curvature:	1.348E-3 1/in
Moment at First Yield:	1.680E+6 lb-in
Ultimate Moment:	3.172E+6 lb-in
Centroid Strain at Yield:	.9003E-3 Ten
Centroid Strain at Ultimate:	14.14E-3 Ten
N.A. at First Yield:	15.67 in
N.A. at Ultimate:	10.49 in
Energy per Length:	4682 lbs
Effective Yield Curvature:	.1246E-3 1/in
Effective Yield Moment:	3.643E+6 lb-in
Over Strength Factor:	.8706
Plastic Rotation Capacity:	18.13E-3 rad
EI Effective:	2.92E+7 kip-in^2
Yield EI Effective:	0 kip-in^2
Bilinear Harding Slope:	0 %
Curvature Ductility:	10.81

Comments:

User Comments

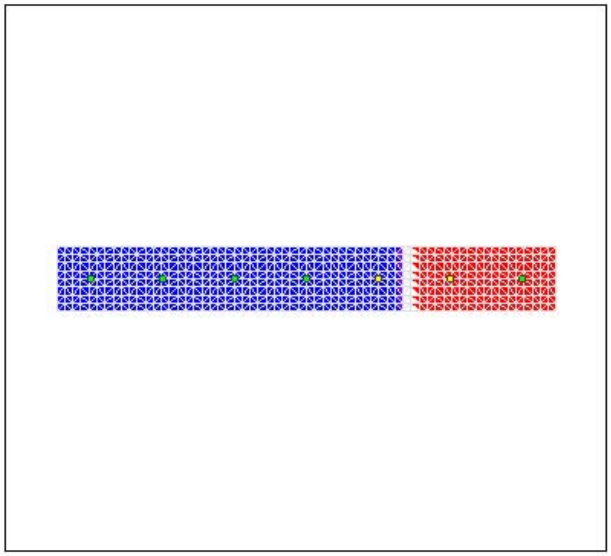

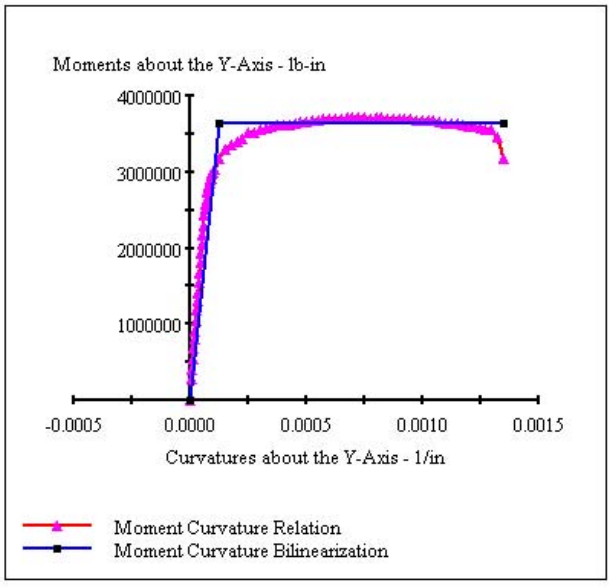

XTRACT Analysis Report - Educational

Thomas Hervillard
Washington State University
9/18/2005

Section Name: Section1
Loading Name: Loading
Analysis Type: Moment Curvature

Section Details:

X Centroid:	19.81 in
Y Centroid:	3.813 in
Section Area:	302.2 in^2

Loading Details:

Constant Load - P:	8159 lbs
Incrementing Loads:	Myy Only
Number of Points:	80
Analysis Strategy:	Displacement Control

Analysis Results:

Failing Material:	Con-N-Kirk
Failure Strain:	23.00E-3 Compression
Curvature at Initial Load:	.2790E-19 1/in
Curvature at First Yield:	84.09E-6 1/in
Ultimate Curvature:	1.990E-3 1/in
Moment at First Yield:	931.8E+3 lb-in
Ultimate Moment:	1.598E+6 lb-in
Centroid Strain at Yield:	.9338E-3 Ten
Centroid Strain at Ultimate:	15.97E-3 Ten
N.A. at First Yield:	11.11 in
N.A. at Ultimate:	8.024 in
Energy per Length:	3452 lbs
Effective Yield Curvature:	.1632E-3 1/in
Effective Yield Moment:	1.809E+6 lb-in
Over Strength Factor:	.8837
Plastic Rotation Capacity:	21.24E-3 rad
EI Effective:	1.11E+7 kip-in^2
Yield EI Effective:	0 kip-in^2
Bilinear Harding Slope:	0 %
Curvature Ductility:	12.20

Comments:

User Comments

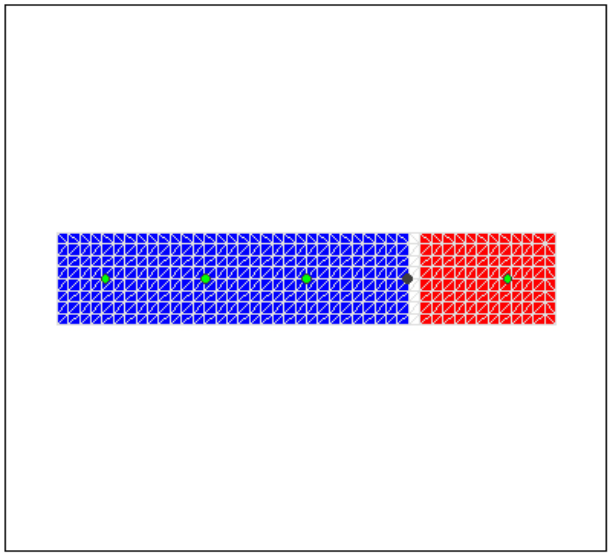

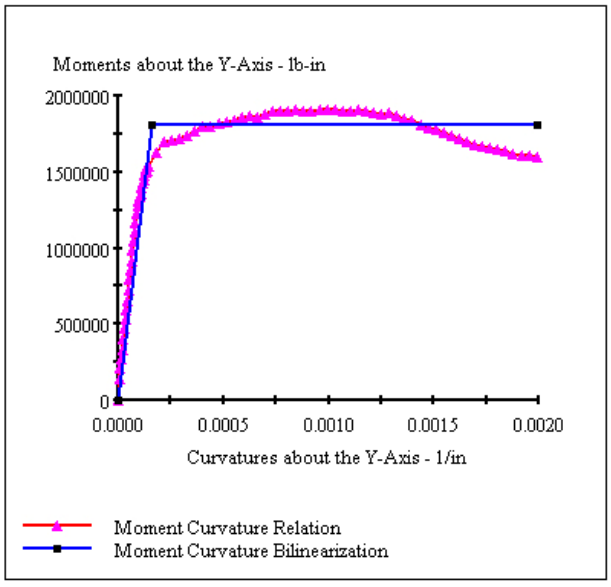

XTRACT Analysis Report - Educational

Thomas Hervillard
Washington State University
9/18/2005

Section Name: Section1
Loading Name: Loading
Analysis Type: Moment Curvature

Ian - Wall 7 - Con-N-Kirk

Section Details:

X Centroid:	35.82 in
Y Centroid:	3.812 in
Section Area:	546.2 in^2

Loading Details:

Constant Load - P:	14.75E+3 lbs
Incrementing Loads:	Myy Only
Number of Points:	80
Analysis Strategy:	Displacement Control

Analysis Results:

Failing Material:	Con-N-Kirk
Failure Strain:	23.00E-3 Compression
Curvature at Initial Load:	.2435E-20 1/in
Curvature at First Yield:	43.58E-6 1/in
Ultimate Curvature:	1.317E-3 1/in
Moment at First Yield:	2.632E+6 lb-in
Ultimate Moment:	3.636E+6 lb-in
Centroid Strain at Yield:	.8848E-3 Ten
Centroid Strain at Ultimate:	23.14E-3 Ten
N.A. at First Yield:	20.30 in
N.A. at Ultimate:	17.57 in
Energy per Length:	5227 lbs
Effective Yield Curvature:	67.43E-6 1/in
Effective Yield Moment:	4.072E+6 lb-in
Over Strength Factor:	.8928
Plastic Rotation Capacity:	20.77E-3 rad
EI Effective:	6.04E+7 kip-in^2
Yield EI Effective:	0 kip-in^2
Bilinear Harding Slope:	0 %
Curvature Ductility:	19.54

Comments:

User Comments

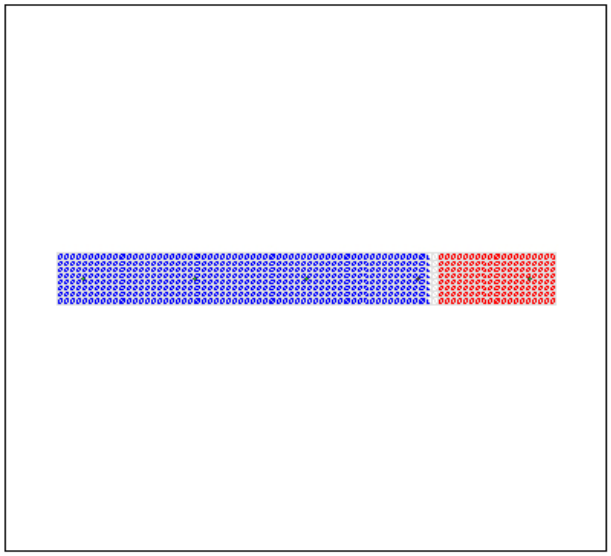

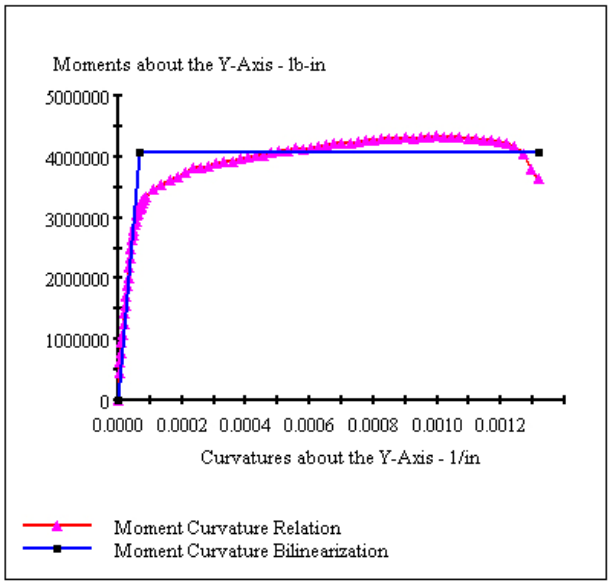

XTRACT Analysis Report - Educational

Thomas Hervillard
Washington State University
9/11/2005

Section Name: Section1
Loading Name: Loading
Analysis Type: Moment Curvature

Matt - Wall 1 - Con-N-Kirk

Section Details:

X Centroid:	27.81 in
Y Centroid:	3.813 in
Section Area:	424.2 in^2

Loading Details:

Constant Load - P:	14.42E+3 lbs
Incrementing Loads:	Myy Only
Number of Points:	80
Analysis Strategy:	Displacement Control

Analysis Results:

Failing Material:	Con-N-Kirk
Failure Strain:	22.00E-3 Compression
Curvature at Initial Load:	.1791E-19 1/in
Curvature at First Yield:	57.37E-6 1/in
Ultimate Curvature:	1.272E-3 1/in
Moment at First Yield:	2.424E+6 lb-in
Ultimate Moment:	3.032E+6 lb-in
Centroid Strain at Yield:	.8059E-3 Ten
Centroid Strain at Ultimate:	12.58E-3 Ten
N.A. at First Yield:	14.05 in
N.A. at Ultimate:	9.888 in
Energy per Length:	4378 lbs
Effective Yield Curvature:	84.23E-6 1/in
Effective Yield Moment:	3.559E+6 lb-in
Over Strength Factor:	.8520
Plastic Rotation Capacity:	15.94E-3 rad
EI Effective:	4.23E+7 kip-in^2
Yield EI Effective:	0 kip-in^2
Bilinear Harding Slope:	0 %
Curvature Ductility:	15.10

Comments:

User Comments

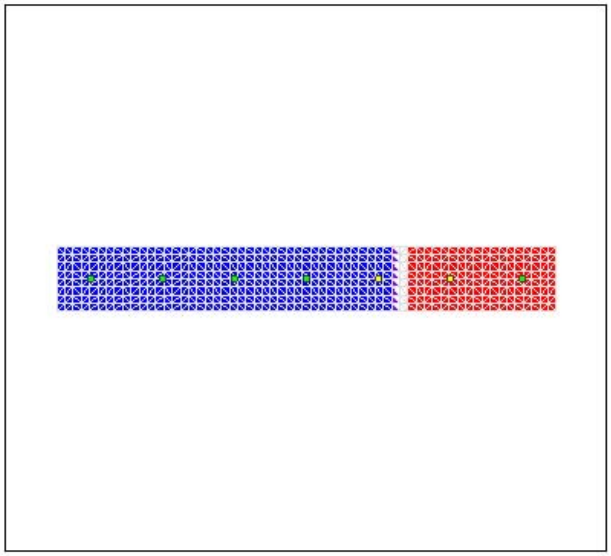

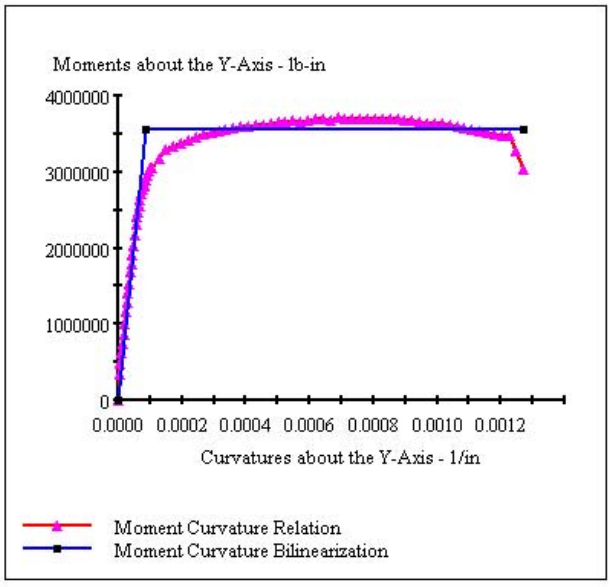

XTRACT Analysis Report - Educational

Thomas Hervillard
Washington State University
10/30/2005

Section Name: Section1
Loading Name: Loading
Analysis Type: Moment Curvature

Section Details:

X Centroid:	27.81 in
Y Centroid:	3.813 in
Section Area:	424.2 in^2

Loading Details:

Constant Load - P:	14.42E+3 lbs
Incrementing Loads:	Myy Only
Number of Points:	80
Analysis Strategy:	Displacement Control

Analysis Results:

Failing Material:	Steel-Matt
Failure Strain:	90.00E-3 Tension
Curvature at Initial Load:	-.1351E-19 1/in
Curvature at First Yield:	57.61E-6 1/in
Ultimate Curvature:	2.611E-3 1/in
Moment at First Yield:	2.394E+6 lb-in
Ultimate Moment:	3.504E+6 lb-in
Centroid Strain at Yield:	.8000E-3 Ten
Centroid Strain at Ultimate:	33.10E-3 Ten
N.A. at First Yield:	13.89 in
N.A. at Ultimate:	12.68 in
Energy per Length:	9992 lbs
Effective Yield Curvature:	93.78E-6 1/in
Effective Yield Moment:	3.897E+6 lb-in
Over Strength Factor:	.8991
Plastic Rotation Capacity:	33.76E-3 rad
EI Effective:	4.16E+7 kip-in^2
Yield EI Effective:	0 kip-in^2
Bilinear Harding Slope:	0 %
Curvature Ductility:	27.84

Comments:

User Comments

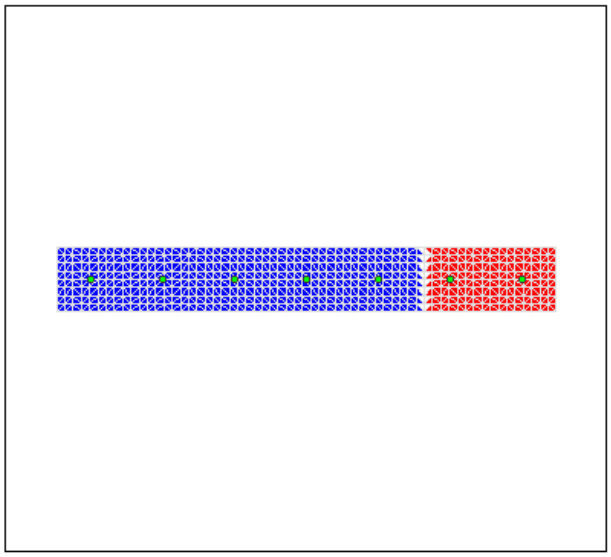

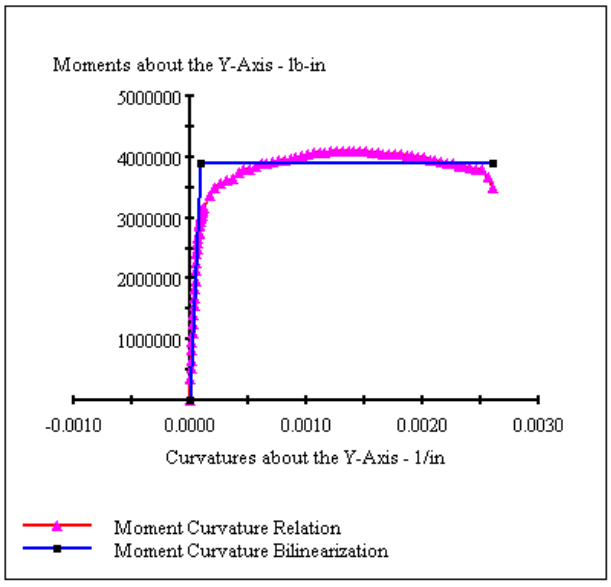

XTRACT Analysis Report - Educational

Thomas Hervillard
Washington State University
10/30/2005

Section Name: Section1
Loading Name: Loading
Analysis Type: Moment Curvature

Matt - Wall 3 - Con-C

Section Details:

X Centroid:	27.81 in
Y Centroid:	3.813 in
Section Area:	424.2 in^2

Loading Details:

Constant Load - P:	14.42E+3 lbs
Incrementing Loads:	Myy Only
Number of Points:	80
Analysis Strategy:	Displacement Control

Analysis Results:

Failing Material:	Con-C
Failure Strain:	30.00E-3 Compression
Curvature at Initial Load:	.1300E-19 1/in
Curvature at First Yield:	43.45E-6 1/in
Ultimate Curvature:	1.659E-3 1/in
Moment at First Yield:	1.871E+6 lb-in
Ultimate Moment:	3.161E+6 lb-in
Centroid Strain at Yield:	.5952E-3 Ten
Centroid Strain at Ultimate:	16.87E-3 Ten
N.A. at First Yield:	13.70 in
N.A. at Ultimate:	10.17 in
Energy per Length:	6005 lbs
Effective Yield Curvature:	86.34E-6 1/in
Effective Yield Moment:	3.718E+6 lb-in
Over Strength Factor:	.8502
Plastic Rotation Capacity:	21.09E-3 rad
EI Effective:	4.31E+7 kip-in^2
Yield EI Effective:	0 kip-in^2
Bilinear Harding Slope:	0 %
Curvature Ductility:	19.21

Comments:

User Comments

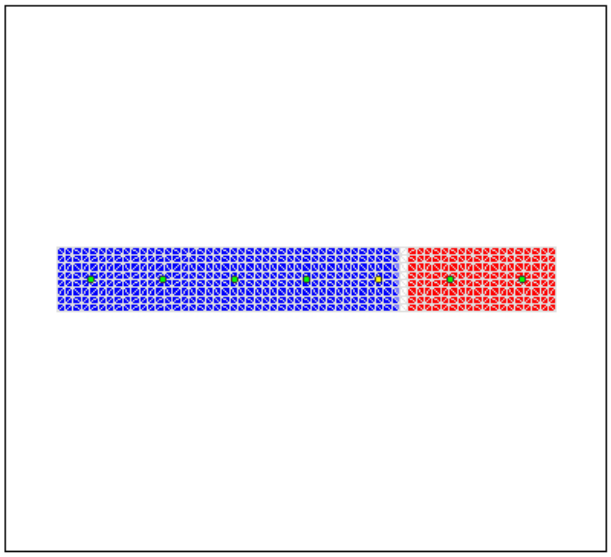

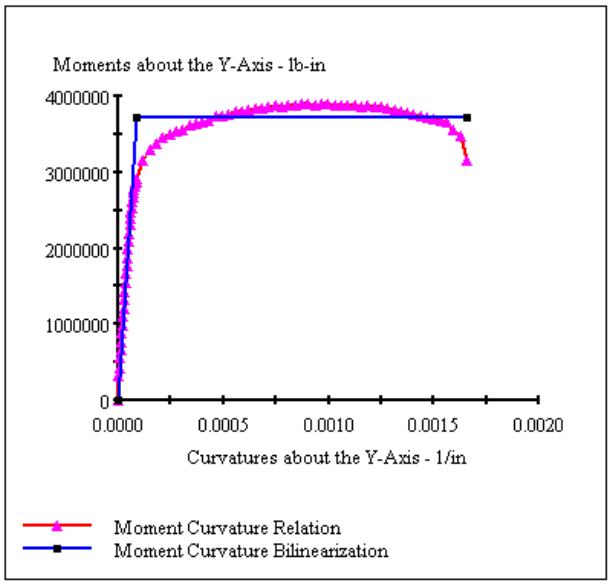

XTRACT Analysis Report - Educational

Thomas Hervillard
Washington State University
10/30/2005

Section Name: Section1
Loading Name: Loading
Analysis Type: Moment Curvature

Matt - Wall 4 - Con-F1

Section Details:

X Centroid:	27.81 in
Y Centroid:	3.813 in
Section Area:	424.2 in^2

Loading Details:

Constant Load - P:	14.42E+3 lbs
Incrementing Loads:	Myy Only
Number of Points:	80
Analysis Strategy:	Displacement Control

Analysis Results:

Failing Material:	Con-F1
Failure Strain:	22.00E-3 Compression
Curvature at Initial Load:	-.9745E-20 1/in
Curvature at First Yield:	57.59E-6 1/in
Ultimate Curvature:	1.431E-3 1/in
Moment at First Yield:	2.393E+6 lb-in
Ultimate Moment:	3.086E+6 lb-in
Centroid Strain at Yield:	.8006E-3 Ten
Centroid Strain at Ultimate:	14.38E-3 Ten
N.A. at First Yield:	13.90 in
N.A. at Ultimate:	10.04 in
Energy per Length:	5072 lbs
Effective Yield Curvature:	87.99E-6 1/in
Effective Yield Moment:	3.655E+6 lb-in
Over Strength Factor:	.8441
Plastic Rotation Capacity:	18.02E-3 rad
EI Effective:	4.15E+7 kip-in^2
Yield EI Effective:	0 kip-in^2
Bilinear Harding Slope:	0 %
Curvature Ductility:	16.27

Comments:

User Comments

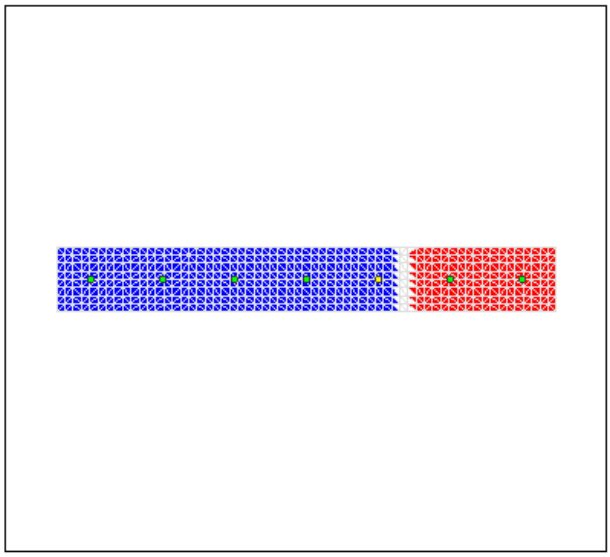

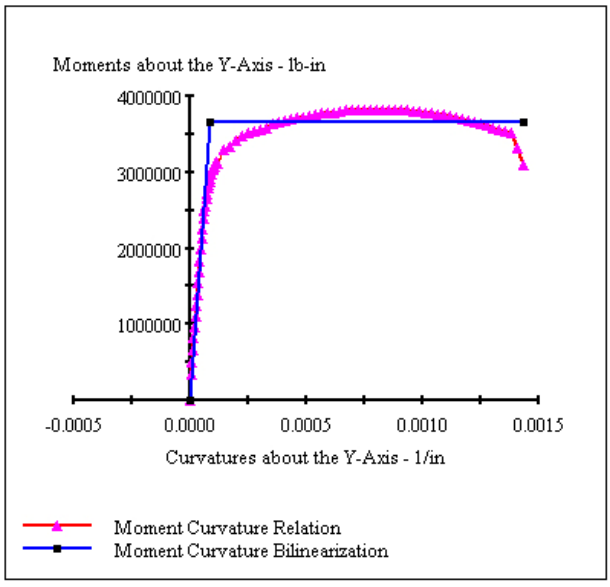

XTRACT Analysis Report - Educational

Thomas Hervillard
Washington State University
9/17/2005

Section Name: Section1
Loading Name: Loading
Analysis Type: Moment Curvature

Section Details:

X Centroid:	27.81 in
Y Centroid:	3.813 in
Section Area:	424.2 in^2

Loading Details:

Constant Load - P:	14.42E+3 lbs
Incrementing Loads:	Myy Only
Number of Points:	80
Analysis Strategy:	Displacement Control

Analysis Results:

Failing Material:	Con-N-Kirk
Failure Strain:	22.00E-3 Compression
Curvature at Initial Load:	.1791E-19 1/in
Curvature at First Yield:	52.14E-6 1/in
Ultimate Curvature:	1.272E-3 1/in
Moment at First Yield:	2.182E+6 lb-in
Ultimate Moment:	3.032E+6 lb-in
Centroid Strain at Yield:	.7142E-3 Ten
Centroid Strain at Ultimate:	12.58E-3 Ten
N.A. at First Yield:	13.70 in
N.A. at Ultimate:	9.888 in
Energy per Length:	4378 lbs
Effective Yield Curvature:	85.07E-6 1/in
Effective Yield Moment:	3.560E+6 lb-in
Over Strength Factor:	.8517
Plastic Rotation Capacity:	17.60E-3 rad
EI Effective:	4.19E+7 kip-in^2
Yield EI Effective:	0 kip-in^2
Bilinear Harding Slope:	0 %
Curvature Ductility:	14.96

Comments:

User Comments

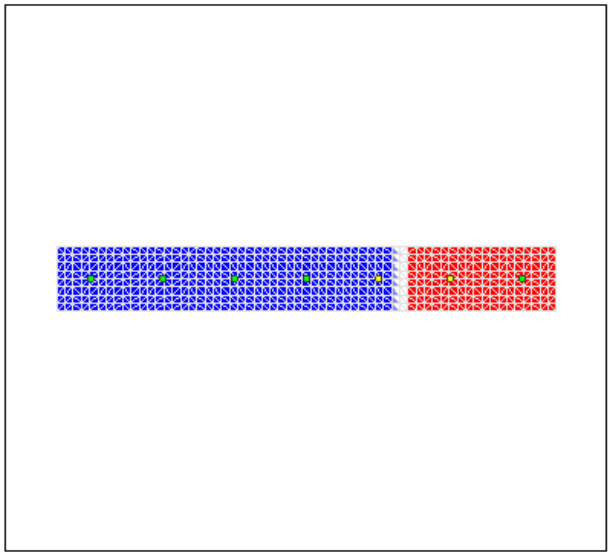

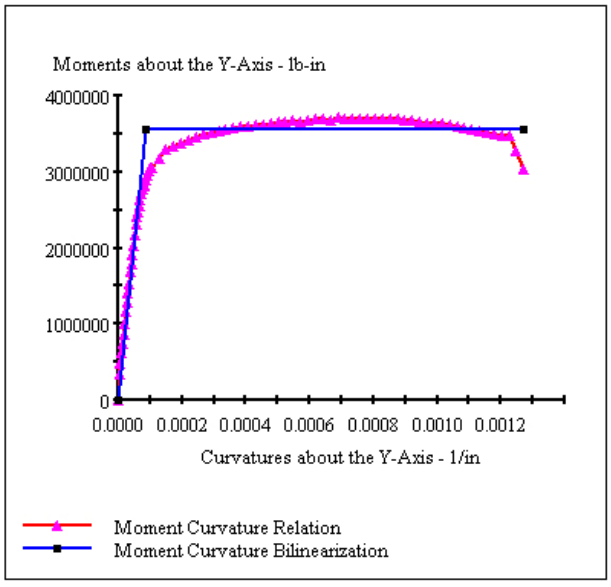

XTRACT Analysis Report - Educational

Thomas Hervillard
Washington State University
10/30/2005

Section Name: Section1
Loading Name: Loading
Analysis Type: Moment Curvature

Matt - Wall 6 - Con-P

Section Details:

X Centroid:	27.81 in
Y Centroid:	3.813 in
Section Area:	424.2 in^2

Loading Details:

Constant Load - P:	14.42E+3 lbs
Incrementing Loads:	Myy Only
Number of Points:	80
Analysis Strategy:	Displacement Control

Analysis Results:

Failing Material:	Con-P
Failure Strain:	40.00E-3 Compression
Curvature at Initial Load:	-.1351E-19 1/in
Curvature at First Yield:	49.40E-6 1/in
Ultimate Curvature:	2.630E-3 1/in
Moment at First Yield:	2.100E+6 lb-in
Ultimate Moment:	3.313E+6 lb-in
Centroid Strain at Yield:	.6788E-3 Ten
Centroid Strain at Ultimate:	28.86E-3 Ten
N.A. at First Yield:	13.74 in
N.A. at Ultimate:	10.97 in
Energy per Length:	10.06E+3 lbs
Effective Yield Curvature:	91.60E-6 1/in
Effective Yield Moment:	3.893E+6 lb-in
Over Strength Factor:	.8509
Plastic Rotation Capacity:	37.63E-3 rad
EI Effective:	4.25E+7 kip-in^2
Yield EI Effective:	0 kip-in^2
Bilinear Harding Slope:	0 %
Curvature Ductility:	28.72

Comments:

User Comments

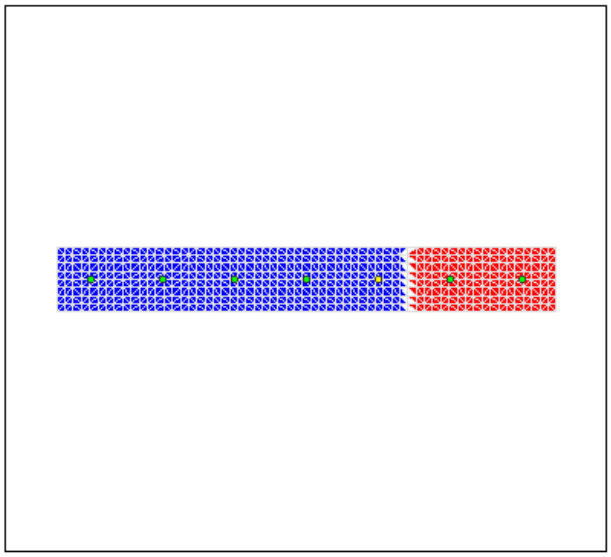

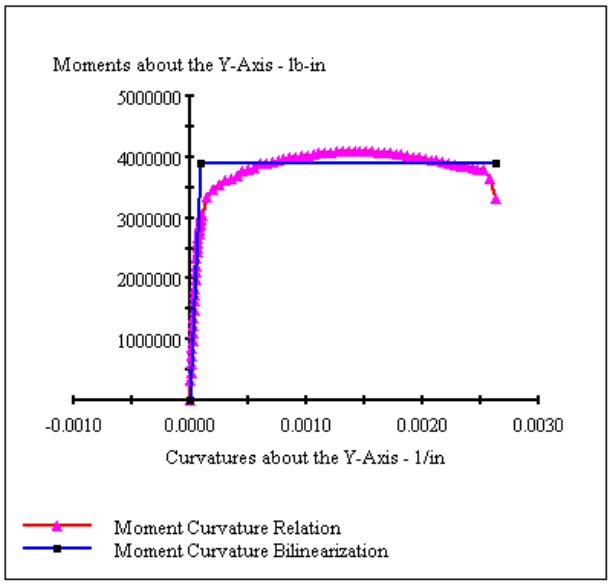

XTRACT Analysis Report - Educational

Thomas Hervillard
Washington State University
10/30/2005

Section Name: Section1
Loading Name: Loading
Analysis Type: Moment Curvature

Matt - Wall 7 - Con-C

Section Details:

X Centroid:	27.81 in
Y Centroid:	3.813 in
Section Area:	424.2 in^2

Loading Details:

Constant Load - P:	14.42E+3 lbs
Incrementing Loads:	Myy Only
Number of Points:	80
Analysis Strategy:	Displacement Control

Analysis Results:

Failing Material:	Con-C
Failure Strain:	30.00E-3 Compression
Curvature at Initial Load:	.1300E-19 1/in
Curvature at First Yield:	43.45E-6 1/in
Ultimate Curvature:	1.659E-3 1/in
Moment at First Yield:	1.871E+6 lb-in
Ultimate Moment:	3.161E+6 lb-in
Centroid Strain at Yield:	.5952E-3 Ten
Centroid Strain at Ultimate:	16.87E-3 Ten
N.A. at First Yield:	13.70 in
N.A. at Ultimate:	10.17 in
Energy per Length:	6005 lbs
Effective Yield Curvature:	86.34E-6 1/in
Effective Yield Moment:	3.718E+6 lb-in
Over Strength Factor:	.8502
Plastic Rotation Capacity:	23.30E-3 rad
EI Effective:	4.31E+7 kip-in^2
Yield EI Effective:	0 kip-in^2
Bilinear Harding Slope:	0 %
Curvature Ductility:	19.21

Comments:

User Comments

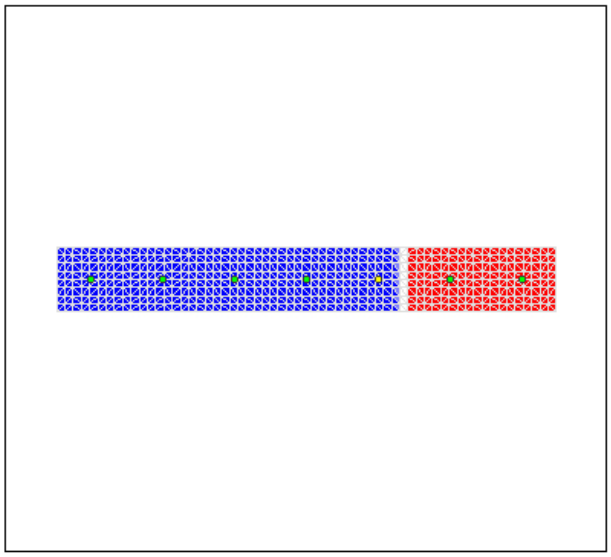

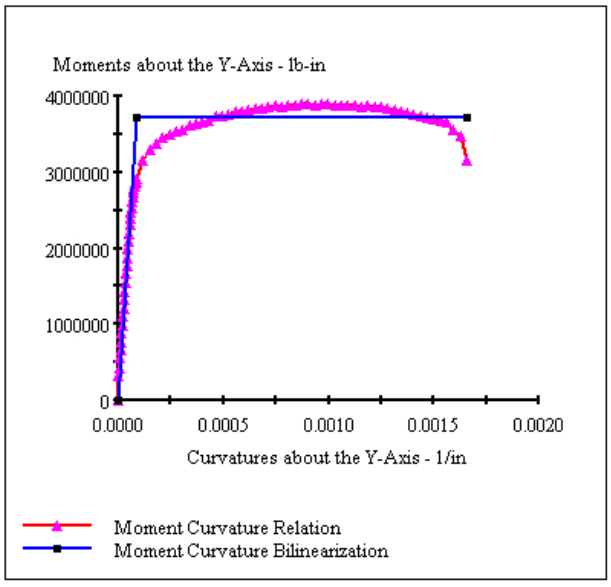

XTRACT Analysis Report - Educational

Thomas Hervillard
Washington State University
10/30/2005

Section Name: Section1
Loading Name: Loading
Analysis Type: Moment Curvature

Section Details:

X Centroid:	27.81 in
Y Centroid:	3.813 in
Section Area:	424.2 in^2

Loading Details:

Constant Load - P:	14.42E+3 lbs
Incrementing Loads:	Myy Only
Number of Points:	80
Analysis Strategy:	Displacement Control

Analysis Results:

Failing Material:	Con-F1
Failure Strain:	22.00E-3 Compression
Curvature at Initial Load:	-.9745E-20 1/in
Curvature at First Yield:	50.28E-6 1/in
Ultimate Curvature:	1.431E-3 1/in
Moment at First Yield:	2.130E+6 lb-in
Ultimate Moment:	3.087E+6 lb-in
Centroid Strain at Yield:	.6932E-3 Ten
Centroid Strain at Ultimate:	14.40E-3 Ten
N.A. at First Yield:	13.79 in
N.A. at Ultimate:	10.06 in
Energy per Length:	5070 lbs
Effective Yield Curvature:	86.19E-6 1/in
Effective Yield Moment:	3.652E+6 lb-in
Over Strength Factor:	.8452
Plastic Rotation Capacity:	18.04E-3 rad
EI Effective:	4.24E+7 kip-in^2
Yield EI Effective:	0 kip-in^2
Bilinear Harding Slope:	0 %
Curvature Ductility:	16.61

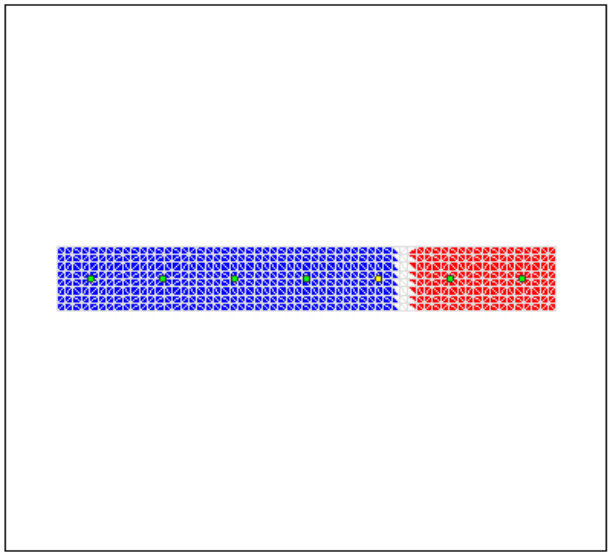

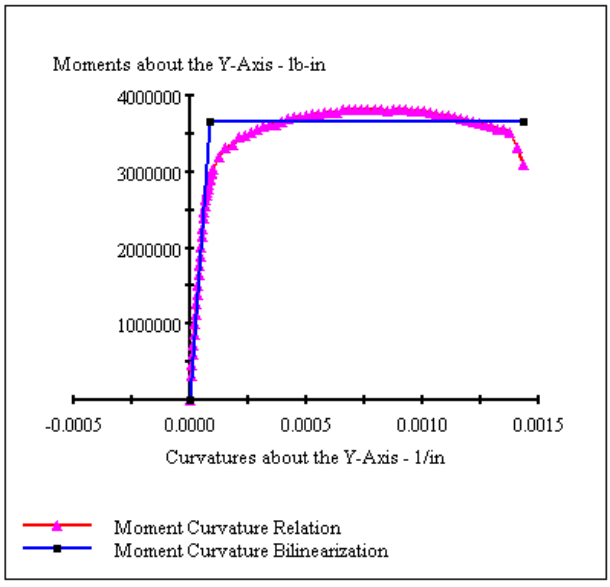

Comments:

User Comments

XTRACT Analysis Report - Educational

Thomas Hervillard
Washington State University
10/30/2005

Section Name: Section1
Loading Name: Loading
Analysis Type: Moment Curvature

Matt - Wall 9 - Con-F2

Section Details:

X Centroid:	27.81 in
Y Centroid:	3.813 in
Section Area:	424.2 in^2

Loading Details:

Constant Load - P:	14.42E+3 lbs
Incrementing Loads:	Myy Only
Number of Points:	80
Analysis Strategy:	Displacement Control

Analysis Results:

Failing Material:	Con-F2
Failure Strain:	25.00E-3 Compression
Curvature at Initial Load:	.5135E-20 1/in
Curvature at First Yield:	57.53E-6 1/in
Ultimate Curvature:	1.535E-3 1/in
Moment at First Yield:	2.397E+6 lb-in
Ultimate Moment:	3.175E+6 lb-in
Centroid Strain at Yield:	.8021E-3 Ten
Centroid Strain at Ultimate:	16.65E-3 Ten
N.A. at First Yield:	13.94 in
N.A. at Ultimate:	10.85 in
Energy per Length:	5522 lbs
Effective Yield Curvature:	88.92E-6 1/in
Effective Yield Moment:	3.705E+6 lb-in
Over Strength Factor:	.8570
Plastic Rotation Capacity:	21.43E-3 rad
EI Effective:	4.17E+7 kip-in^2
Yield EI Effective:	0 kip-in^2
Bilinear Harding Slope:	0 %
Curvature Ductility:	17.26

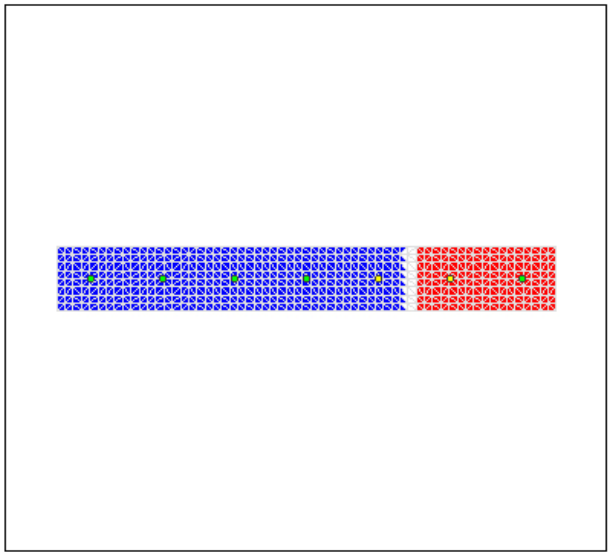

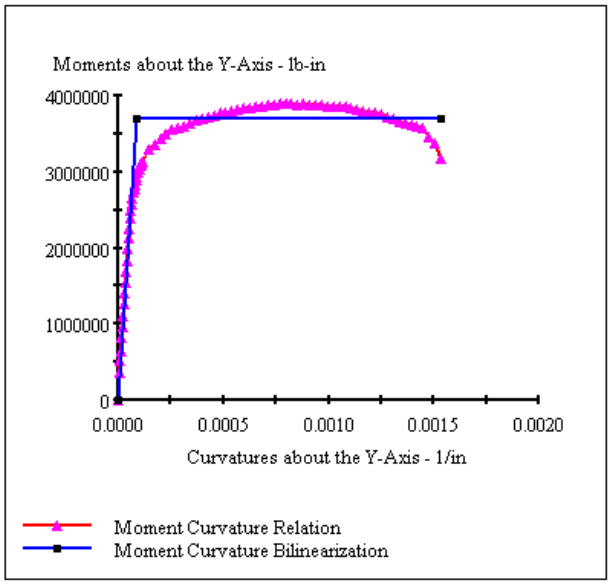

Comments:

User Comments

APPENDIX G

This appendix presents the Matlab code of a script which calculates the ultimate load from load-displacement envelops based on the equal area method.

```
clc;
format short g
clear AreaEnv
clear TotArea
clear TotArea2
clear Slope
clear b
clear xInit
clear slopeInit
clear MaxLoad
clear MaxDisp
clear Triangle
clear X
clear Y
Envelop=load('Wall1-envelop.txt');  % loading of the coord. of the points
Num=size(Envelop,1);                 % number of points of the envelop
Disp=Envelop(1:Num,1);               % Displacement values
Load=Envelop(1:Num,2);               % Load values

TotArea=zeros([Num,1]);
TotArea2=zeros([Num,1]);
Triangles=zeros([Num,1]);
SumAreas=0;
AreaCurve=zeros([Num,1]);
for i=1:(Num-1)
    clear Disp1
    clear Disp2
    clear Load1
    clear Load2
    Disp1=Disp(i,1);
    Disp2=Disp(i+1,1);
    Load1=Load(i,1);
    Load2=Load(i+1,1);

    if Load2>=Load1
        MaxLoad=Load2;
        MaxDisp=Disp2;
    end

    Slope(i,1)=(Load2-Load1)/(Disp2-Disp1);

    if i==1
        SlopeInit=Slope;
        xInit=Disp2;
    end

    b(i,1)=Load1-Slope(i,1)*Disp1;

    if Load2 >= Load1
        AreaEnv(i,1)=(Disp2-Disp1)*Load1+((Disp2-Disp1)*(Load2-Load1))/2;
        SumAreas=SumAreas + AreaEnv(i,1);
    else
        AreaEnv(i,1)=(Disp2-Disp1)*Load2+((Disp2-Disp1)*(Load1-Load2))/2;
        SumAreas=SumAreas + AreaEnv(i,1);
    end

end
```

```
TotArea(1,1)=0;
for i=2:(Num)
    TotArea(i,1)=TotArea(i-1,1)+AreaEnv(i-1,1);
end

TotArea2(Num,1)=0;
for i=(Num-1):-1:1
    TotArea2(i,1)=TotArea2(i+1,1)+AreaEnv(i,1);
end

for i=1:(Num-1)
   if (Disp(i,1) < MaxDisp)
       Triangles(i,1)=0;
   else
       if (Load(i,1) == MaxLoad)
           Triangles(i,1)=((Disp(i+1,1)-Disp(i,1))*(Load(i,1)-Load(i+1,1)))/2;
       end
       if (Load(i,1) ~= MaxLoad)
           Triangles(i,1)=((Disp(i+1,1)-Disp(i,1))*(Load(i,1)-Load(i+1,1)))/2
+ (Disp(i+1,1)-Disp(i,1))*(Load(i-1,1)-Load(i,1));
       end
    end
end

x=xInit;
while (x*SlopeInit < MaxLoad)
    LoadCheck=x*SlopeInit;
    Cross1Disp=0;
    Cross2Disp=0;
    Cross1Load=0;
    Cross2Load=0;
    Cross1Disp2=0;
    Cross2Disp2=0;
    Cross1Load2=0;
    Cross2Load2=0;
    j=0;
    k=0;
    CrossDisp=0;
    TotalArea=0;
    TopArea=0;
    PrevArea=0;
    BotArea=0;
    UnderArea1=0;
    OverArea=0;
    CrossDisp2=0;
    UnderArea2=0;
    UnderArea=0;



    for i=1:(Num-1)
        if ((LoadCheck > Load(i,1)) & (LoadCheck < Load(i+1,1)))
            Cross1Disp=Disp(i,1);
            Cross2Disp=Disp(i+1,1);
            Cross1Load=Load(i,1);
            Cross2Load=Load(i+1,1);
```

```
            j=i;
        end
        if ((LoadCheck < Load(i,1)) & (LoadCheck > Load(i+1,1)))
            Cross1Disp2=Disp(i,1);
            Cross2Disp2=Disp(i+1,1);
            Cross1Load2=Load(i,1);
            Cross2Load2=Load(i+1,1);
            k=i;
        end
    end



    if ((j~=0) & (k==0)) %It cuts only the ascending part
        CrossDisp=(x*SlopeInit - b(j,1))/Slope(j,1);
        TotalArea=(CrossDisp*CrossDisp*SlopeInit)/2;
        TopArea=((CrossDisp-x)*(CrossDisp*SlopeInit-LoadCheck))/2;
        PrevArea=TotArea(j);
        BotArea=(CrossDisp-Cross1Disp)*Cross1Load + ((CrossDisp-
Cross1Disp)*((LoadCheck)-Cross1Load))/2;
        UnderArea=TotalArea-TopArea-PrevArea-BotArea;
        OverArea=SumAreas - PrevArea - BotArea - (Disp(Num,1)-
CrossDisp)*LoadCheck;
    end

    if ((j~=0) & (k~=0)) %It cuts both ascending and descending parts
        CrossDisp=(LoadCheck - b(j,1))/Slope(j,1);
        TotalArea=(CrossDisp*CrossDisp*SlopeInit)/2;
        TopArea=((CrossDisp-x)*(CrossDisp*SlopeInit-LoadCheck))/2;
        PrevArea=TotArea(j);
        BotArea=(CrossDisp-Cross1Disp)*Cross1Load + ((CrossDisp-
Cross1Disp)*((LoadCheck)-Cross1Load))/2;
        UnderArea1=TotalArea-TopArea-PrevArea-BotArea;


        CrossDisp2=(LoadCheck - b(k,1))/Slope(k,1);
        if (k==(Num-1)) %Last segment
            UnderArea2=((Cross2Disp2-CrossDisp2)*(LoadCheck-Cross2Load2))/2;
            UnderArea=UnderArea1+UnderArea2;
            BotArea2=(Cross2Disp2-CrossDisp2)*Cross2Load2 + ((Cross2Disp2-
CrossDisp2)*((LoadCheck)-Cross2Load2))/2;
            OverArea=SumAreas - PrevArea - BotArea - LoadCheck*(CrossDisp2-
CrossDisp) - TotArea2(k+1,1) -  BotArea2;
        else %Not the last segment
            for m=k+1:Num-1
                UnderArea2=Triangles(m,1) + (Disp(m+1,1)-
Disp(m,1))*(LoadCheck-Load(m,1));
            end
            UnderArea=UnderArea1+UnderArea2;
            BotArea2=(Cross2Disp2-CrossDisp2)*Cross2Load2 + ((Cross2Disp2-
CrossDisp2)*((LoadCheck)-Cross2Load2))/2;
            OverArea=SumAreas - PrevArea - BotArea - LoadCheck*(CrossDisp2-
CrossDisp) - TotArea2(k+1,1) -  BotArea2;
        end
    end

    X(1,1)=0;
```

```
    Y(1,1)=0;
    X(2,1)=x;
    Y(2,1)=LoadCheck;
    X(3,1)=Disp(Num,1);
    Y(3,1)=LoadCheck;

    if (((abs(OverArea - UnderArea)) < 50) & (UnderArea ~= 0))
       Test='End'
       break
    end
    x=x+0.00005;

end
plot(Disp,Load,X,Y)
X
Y
```

APPENDIX H

This appendix presents load-displacement curves obtained from Xtract or from experiments for Eikanas's walls and Snook's walls.

Wall 1: Aspect ratio: 0.93 – No confinement – 4#5@16

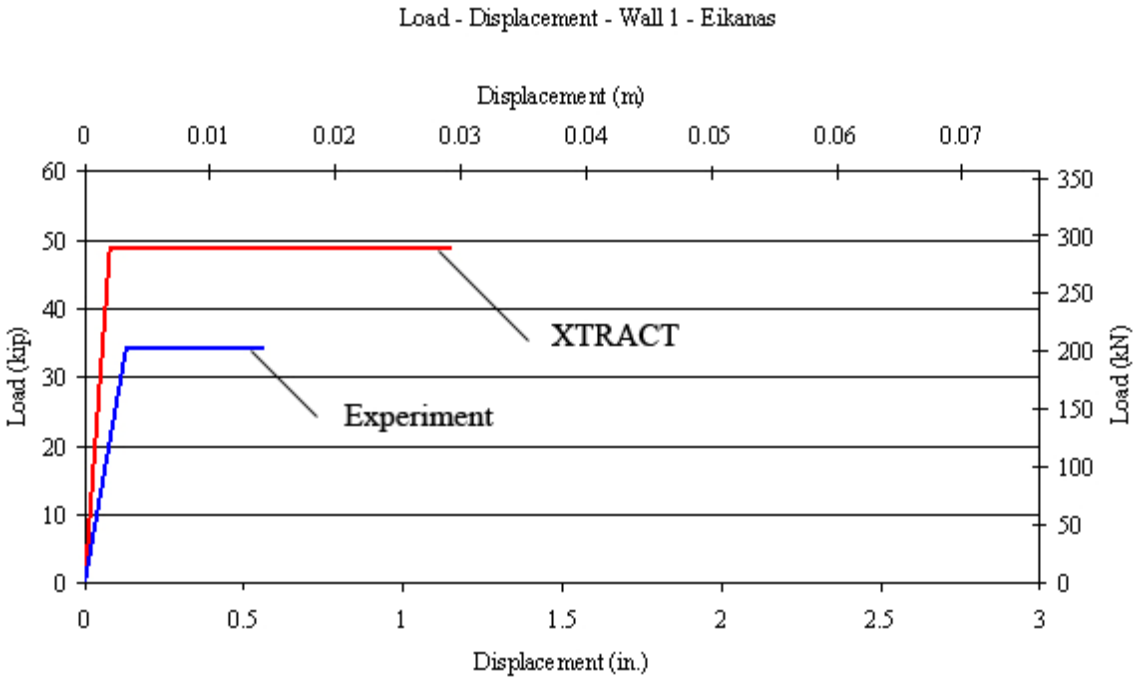

Wall 2: Aspect ratio: 1.51 – No confinement – 4#5@16

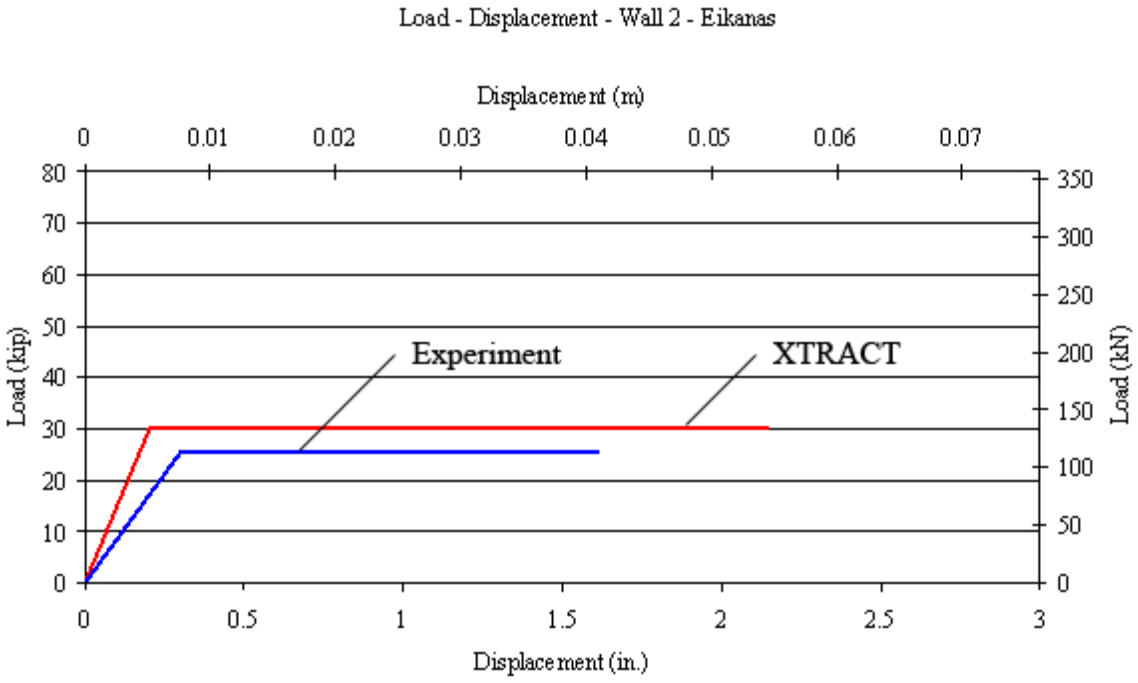

Wall 4: Aspect ratio: 0.93 – No confinement – 7#5@8

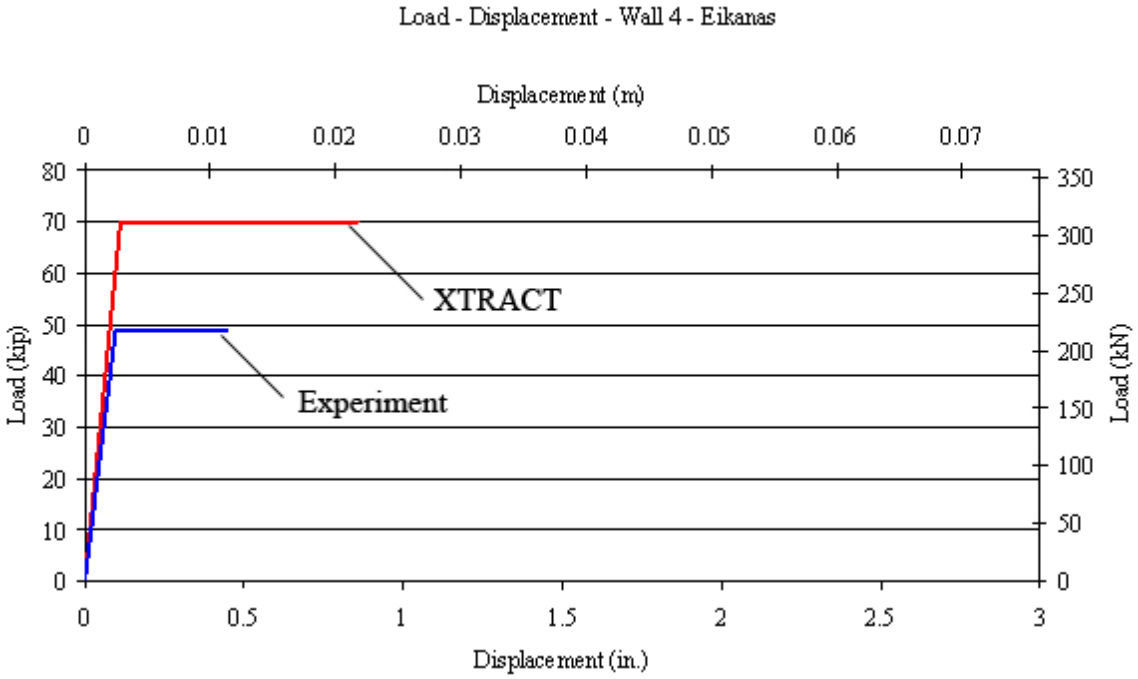

Wall 5: Aspect ratio: 1.51 – No confinement – 7#5@8

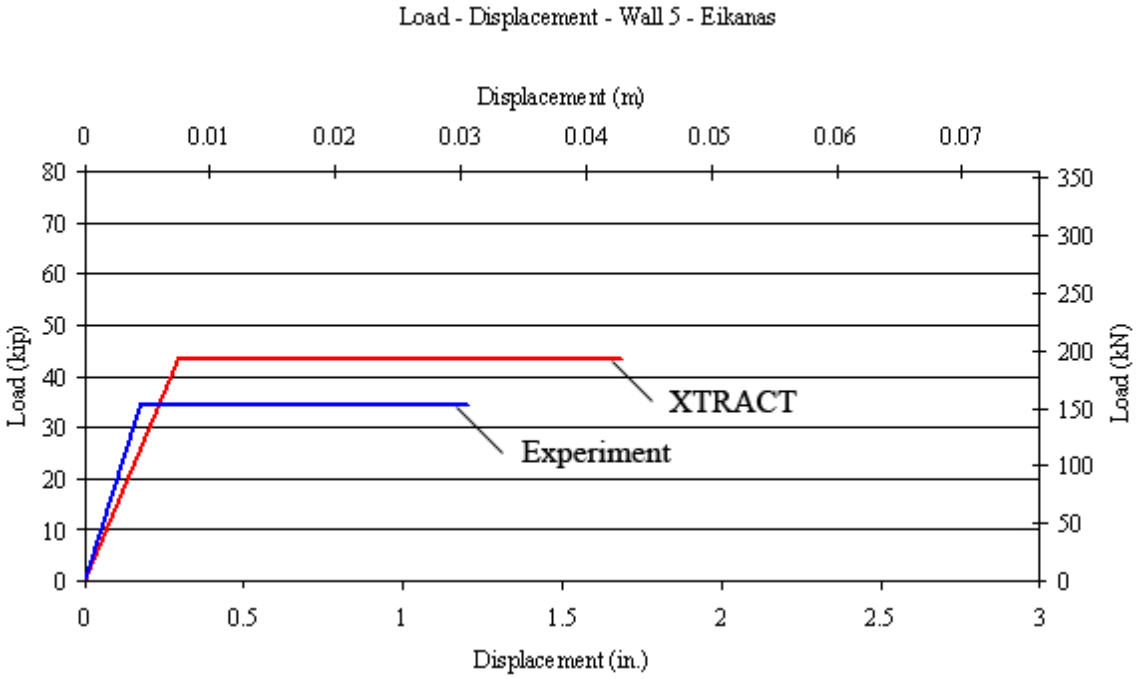

Wall 6: Aspect ratio: 2.12 – No confinement – 5#5@8

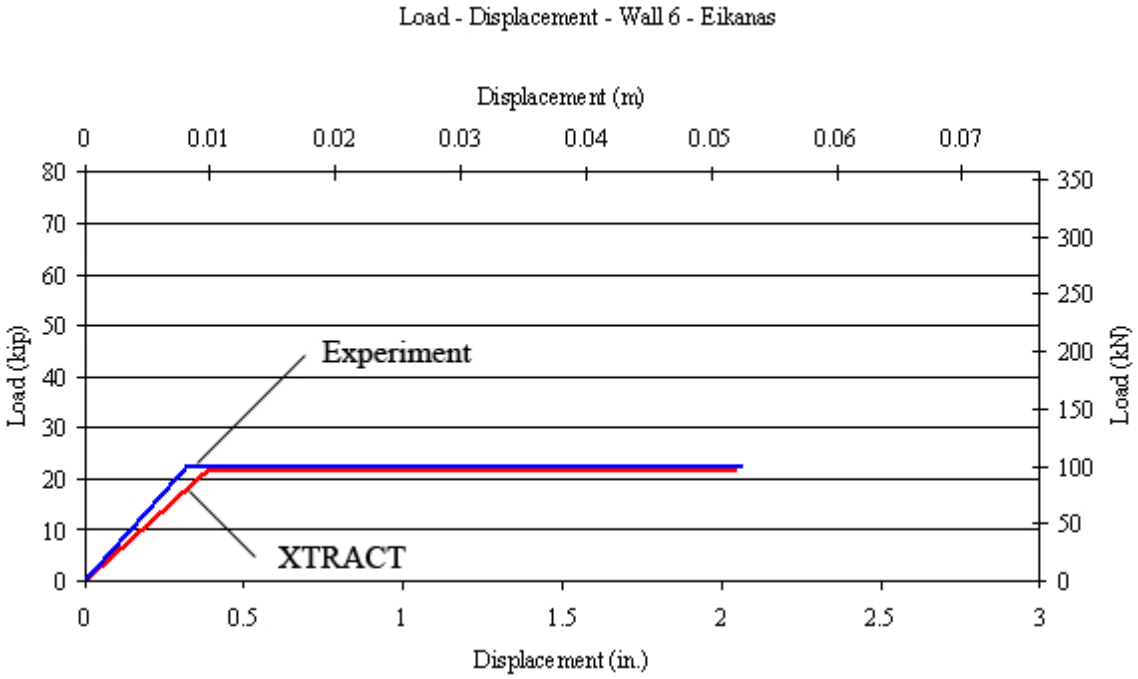

Wall 7: Aspect ratio: 0.73 – No confinement – 5#5@16

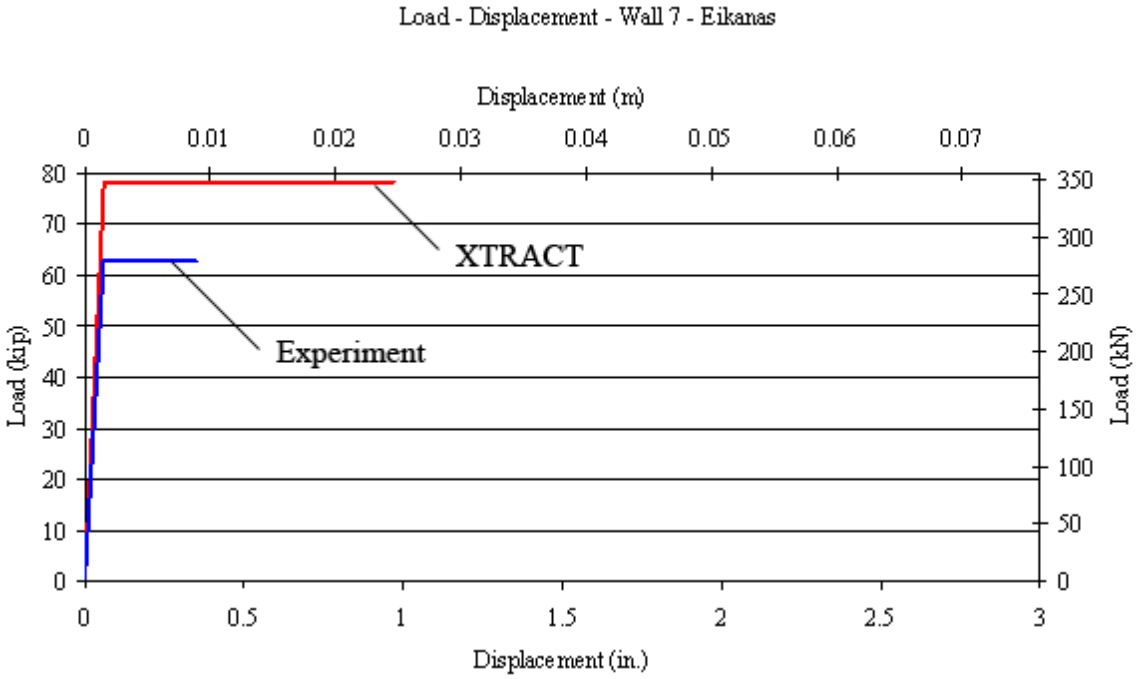

Wall 1: Aspect ratio: 0.93 – No confinement – 7#5@8

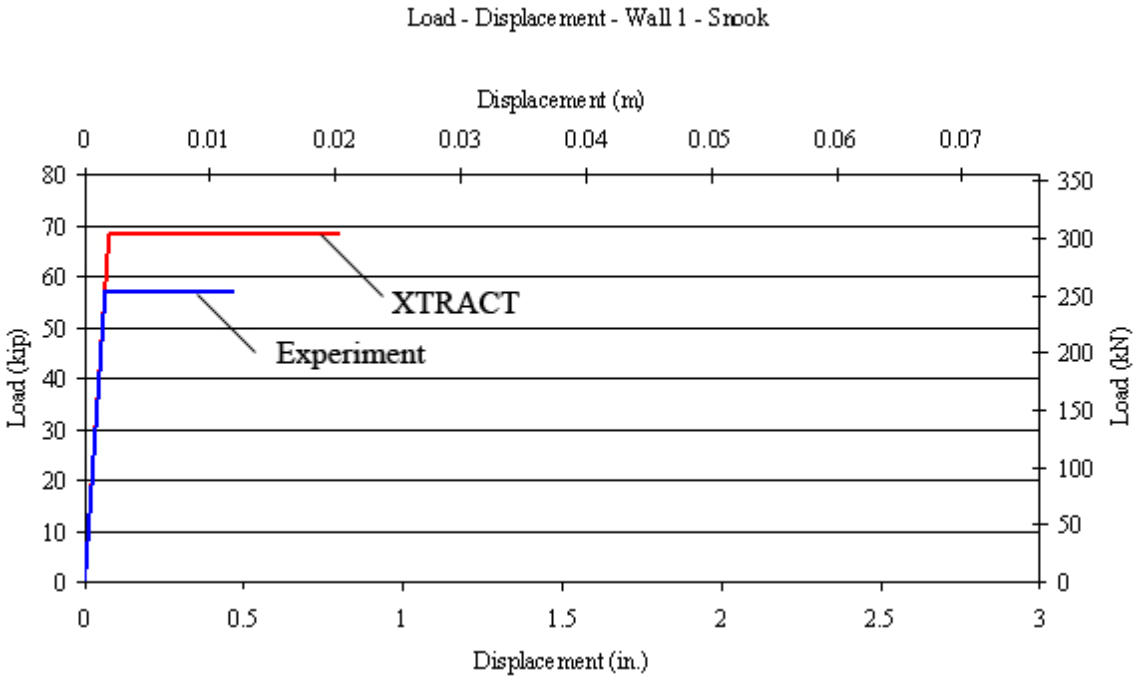

Wall 2: Aspect ratio: 0.93 – Steel plates – 7#5@8

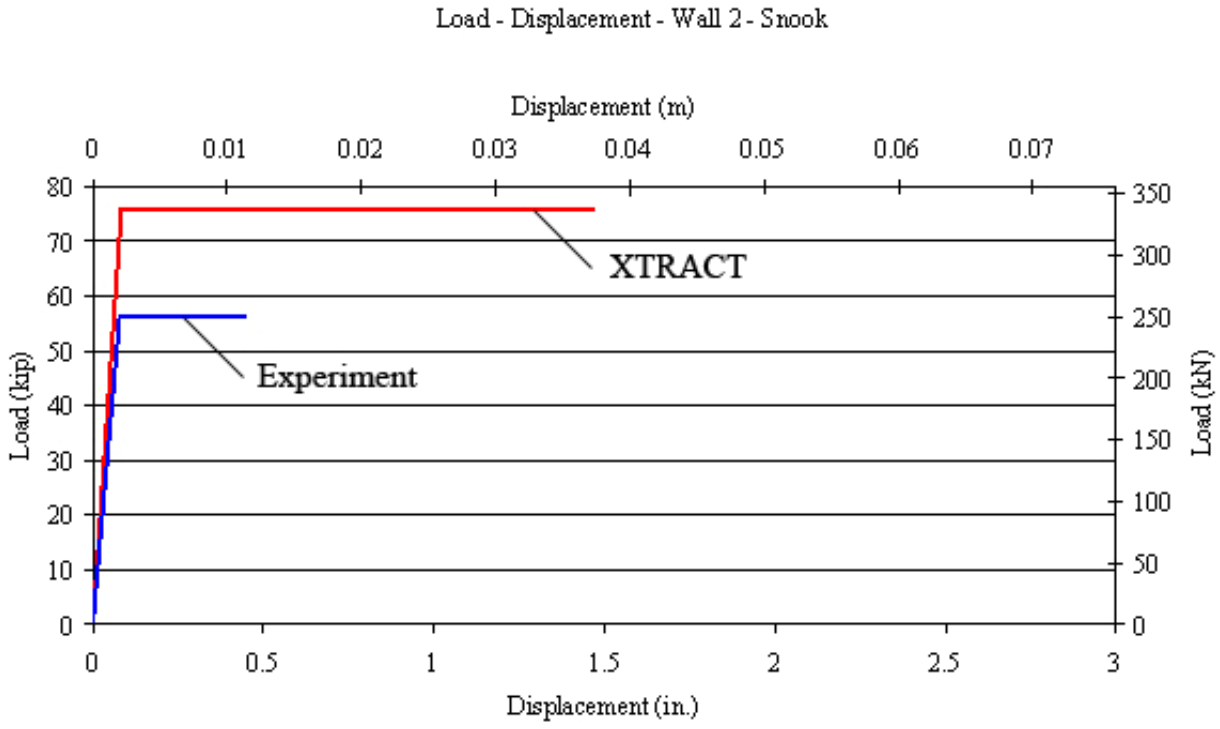

Wall 3: Aspect ratio: 0.93 – Seismic combs – 7#5@8

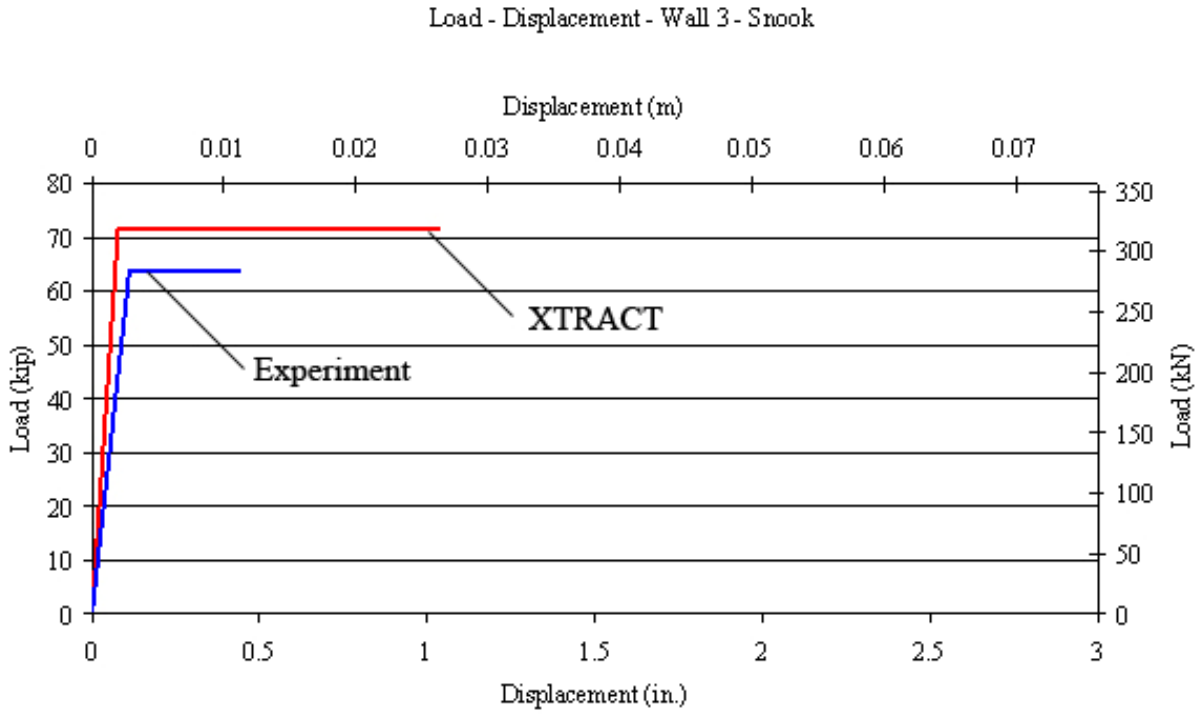

Wall 4: Aspect ratio: 0.93 – Fiber 1 = 5 lbs/yd^3 (2.97 kg/m^3) – 7#5@8

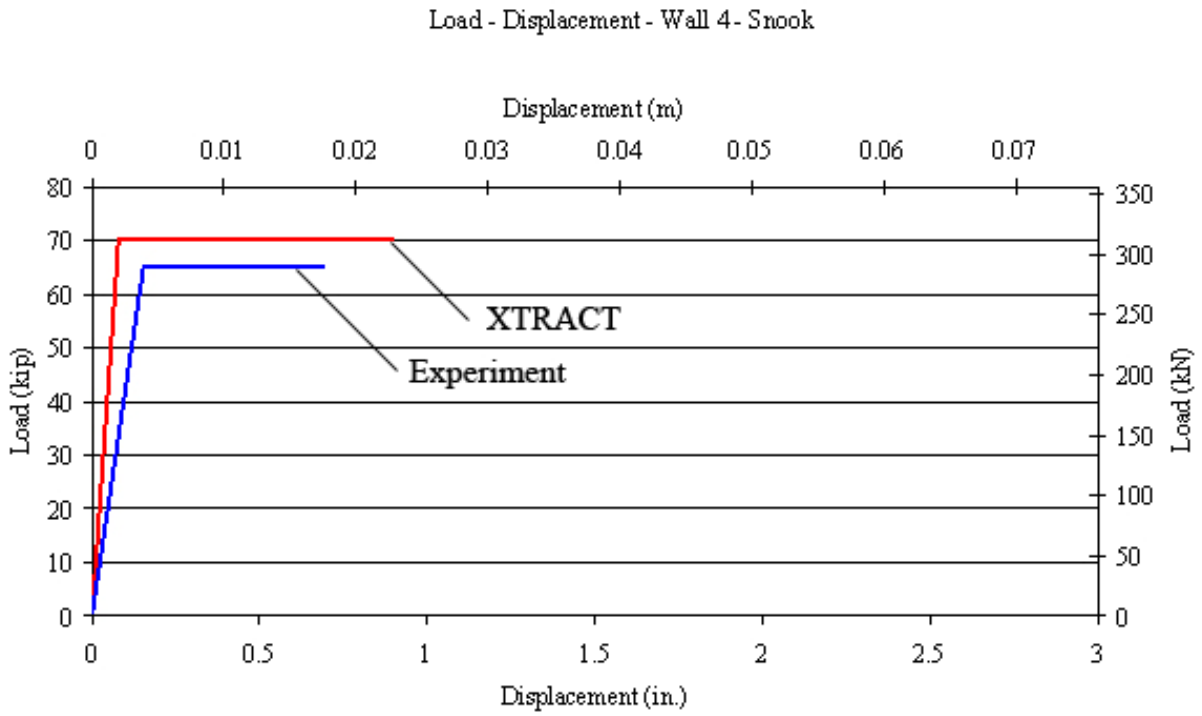

Wall 5: Aspect ratio: 1.51 – No Confinement – 7#5@8

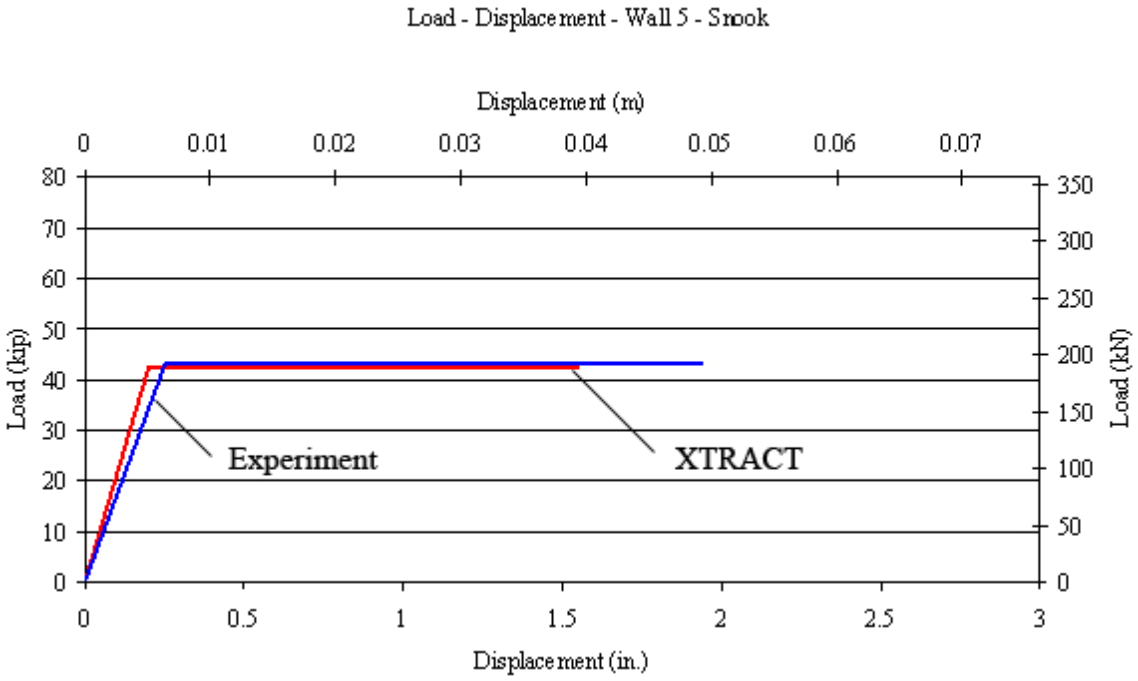

Wall 6: Aspect ratio: 1.51 – Steel Plates – 7#5@8 – (Note that the scale has changed)

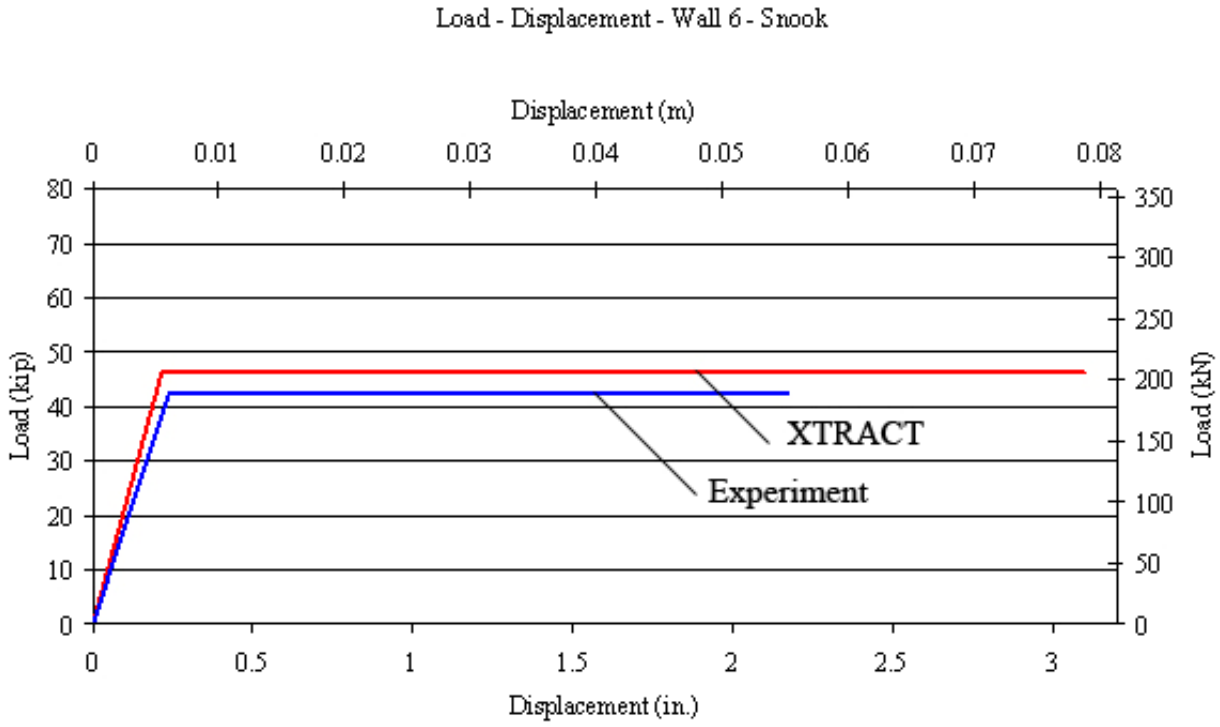

Wall 7: Aspect ratio: 1.51 – Seismic combs – 7#5@8

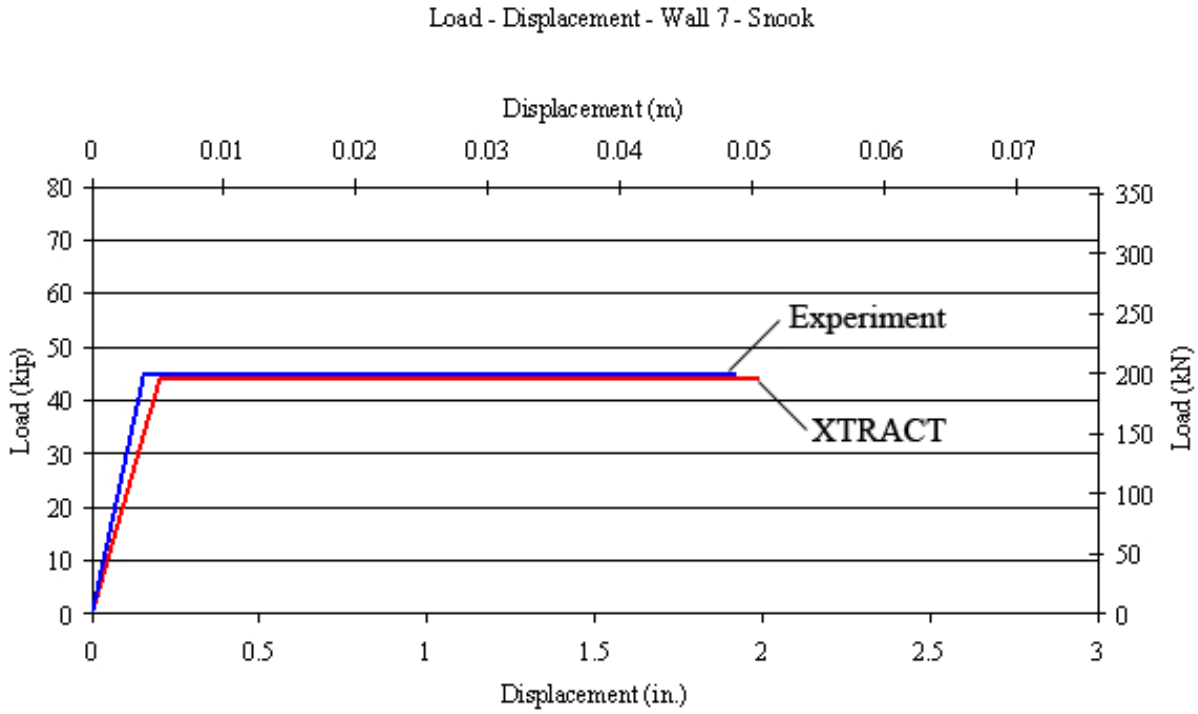

Wall 8: Aspect ratio: 1.51 – Fiber 1 = 5 lbs/yd^3 (2.97 kg/m^3) – 7#5@8

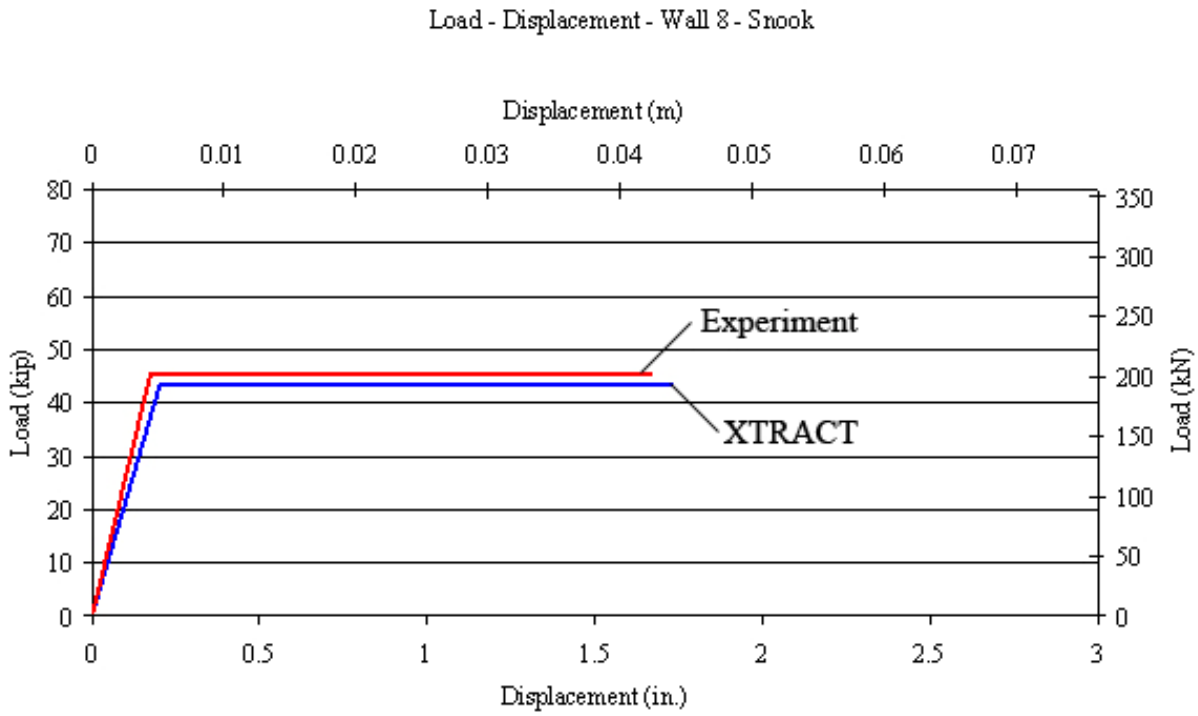

Wall 9: Aspect ratio: 1.51 – Fiber 2 = 8 lbs/yd^3 (4.76 kg/m^3) – 7#5@8

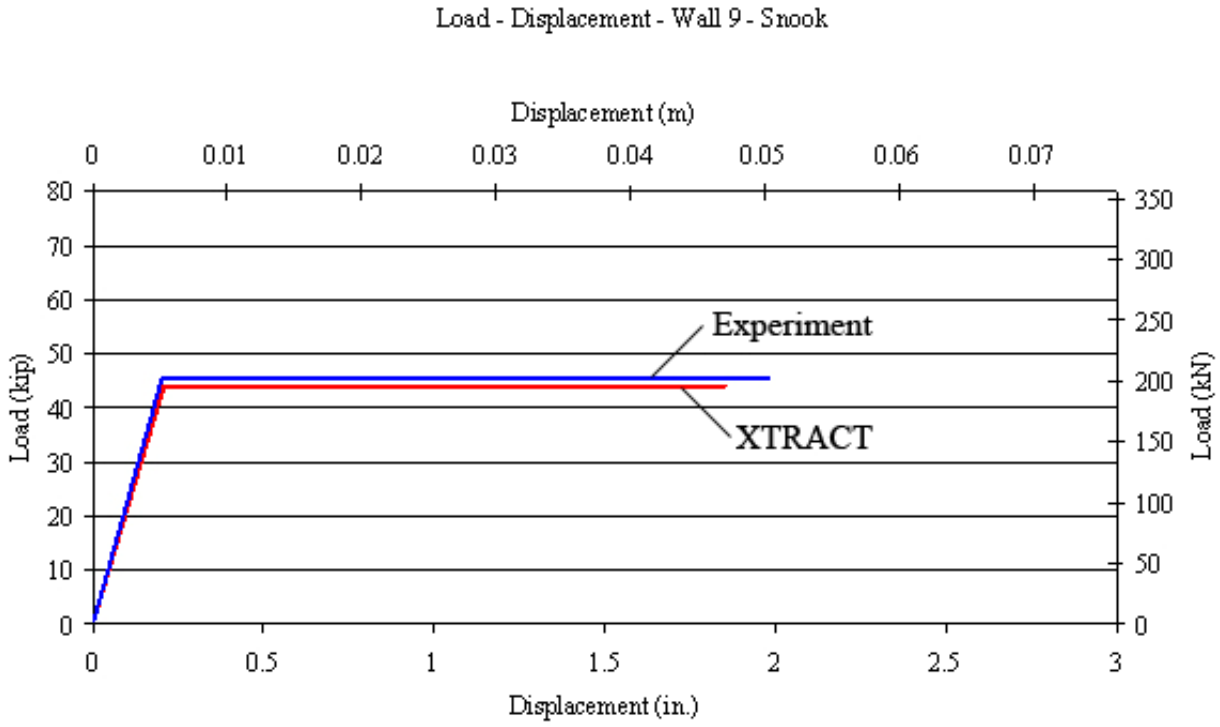

APPENDIX I

This appendix presents a comparison of the stress-strain curves of the confined masonry piers with once or twice the amount of confinement reinforcement. For fibers reinforced piers, the dosages studied were the original ones and twice the latter.ρ

Modified Kent-Park models adjusted for f'$_m$ for steel plates before and after increasing ρ:

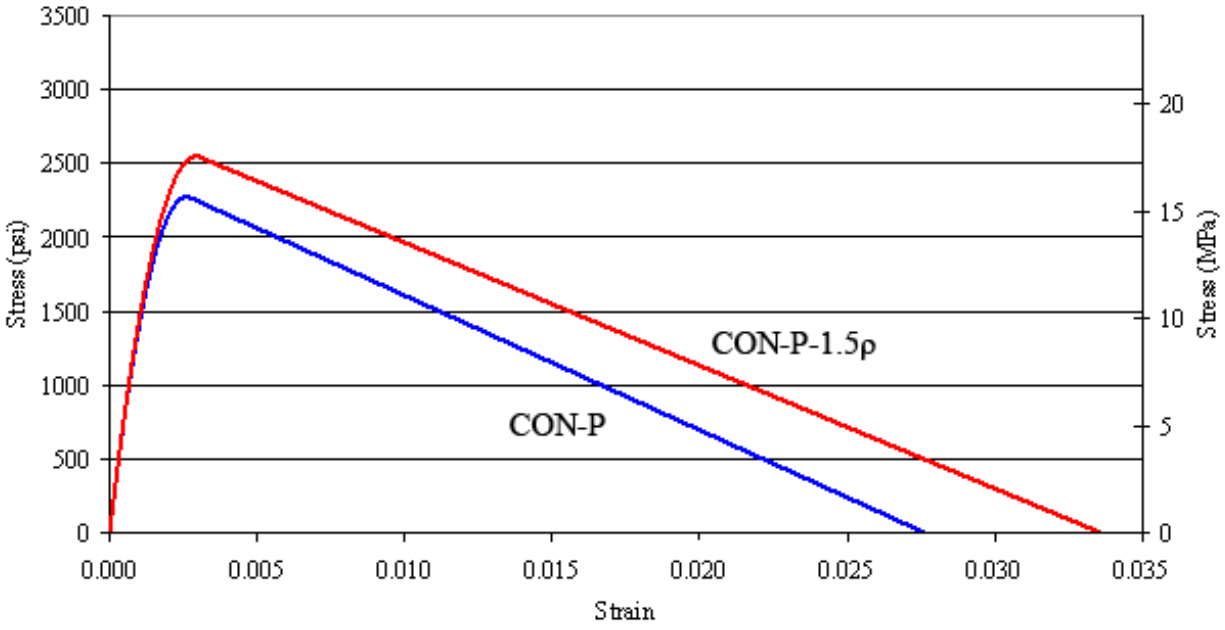

Modified Kent-Park models adjusted for f'$_m$ for seismic combs before and after increasing ρ:

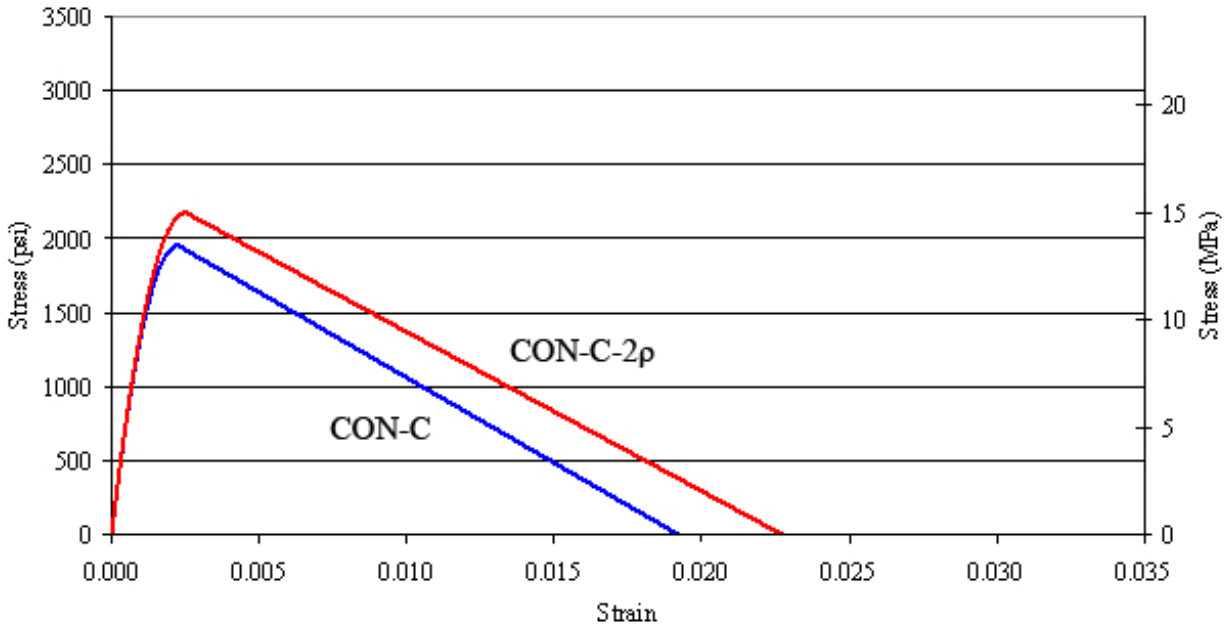

Modified Kent-Park models adjusted for f'$_m$ for Fiber 1 before and after increasing the dosages:

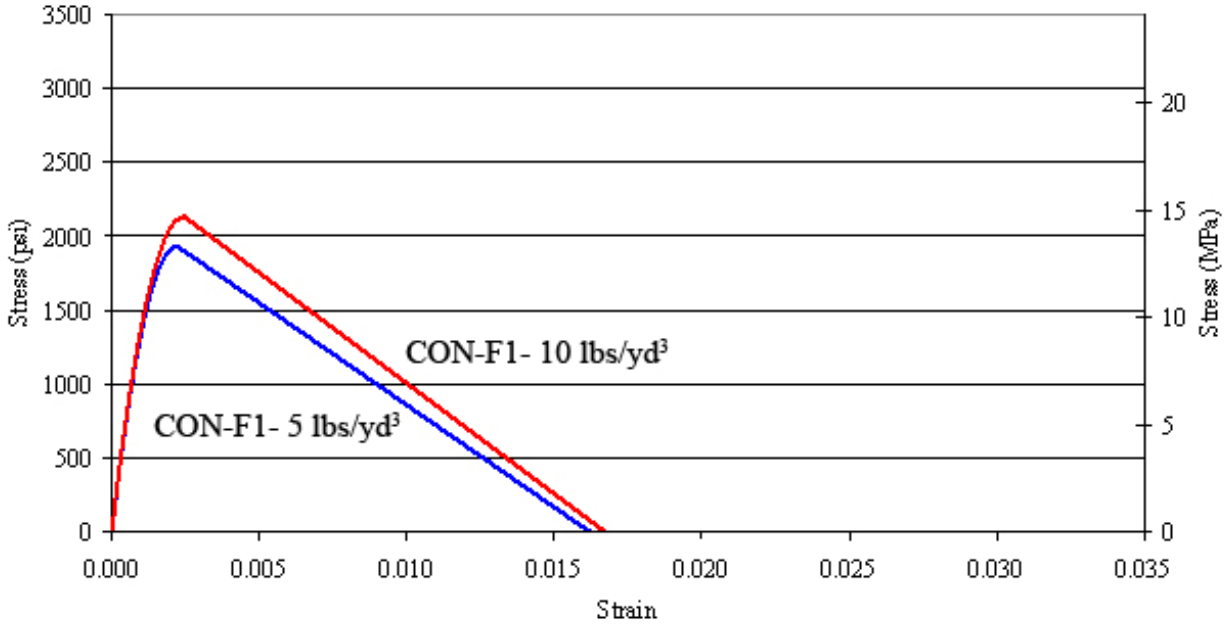

Modified Kent-Park models adjusted for f'$_m$ for Fiber 2 before and after increasing the dosages:

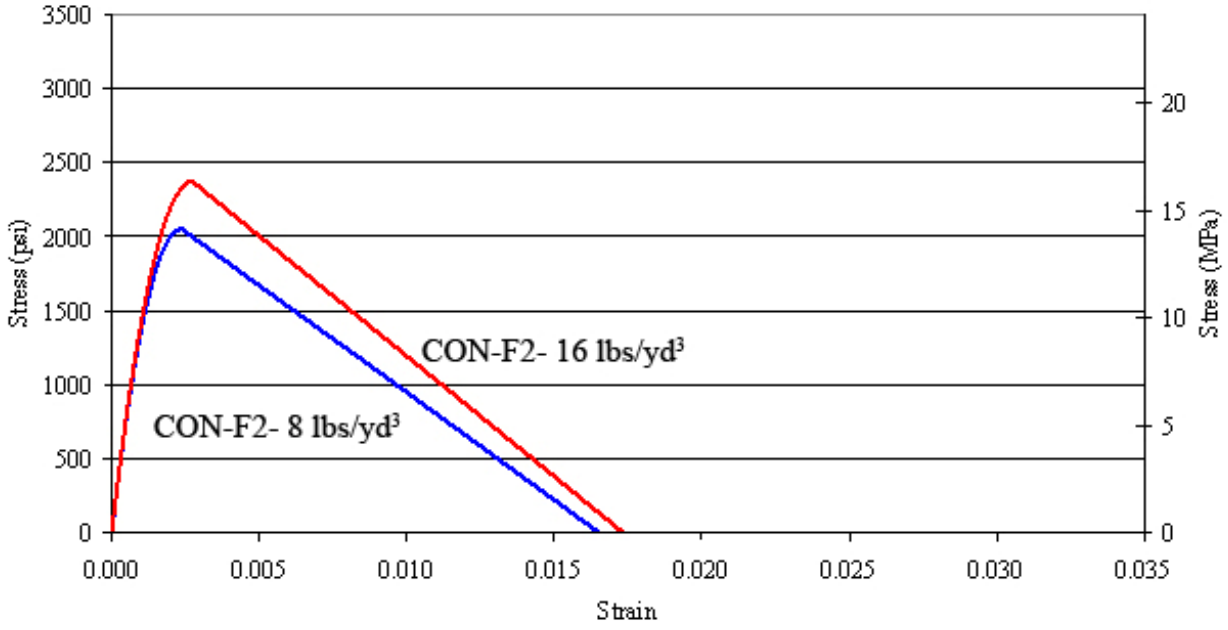

APPENDIX J

This appendix presents Xtract results for Snook's walls where the confinement reinforcement ratio has doubled.

XTRACT Analysis Report - Educational

Thomas Hervillard
Washington State University
10/30/2005

Section Name: Section1
Loading Name: Loading
Analysis Type: Moment Curvature

Section Details:

X Centroid:	27.81 in
Y Centroid:	3.813 in
Section Area:	424.2 in^2

Loading Details:

Constant Load - P:	14.42E+3 lbs
Incrementing Loads:	Myy Only
Number of Points:	80
Analysis Strategy:	Displacement Control

Analysis Results:

Failing Material:	Steel-Matt
Failure Strain:	.1200 Tension
Curvature at Initial Load:	-.2844E-19 1/in
Curvature at First Yield:	57.29E-6 1/in
Ultimate Curvature:	3.028E-3 1/in
Moment at First Yield:	2.392E+6 lb-in
Ultimate Moment:	3.963E+6 lb-in
Centroid Strain at Yield:	.8078E-3 Ten
Centroid Strain at Ultimate:	47.46E-3 Ten
N.A. at First Yield:	14.10 in
N.A. at Ultimate:	15.68 in
Energy per Length:	12.16E+3 lbs
Effective Yield Curvature:	97.78E-6 1/in
Effective Yield Moment:	4.083E+6 lb-in
Over Strength Factor:	.9707
Plastic Rotation Capacity:	39.30E-3 rad
EI Effective:	4.18E+7 kip-in^2
Yield EI Effective:	0 kip-in^2
Bilinear Harding Slope:	0 %
Curvature Ductility:	30.96

Comments:

User Comments

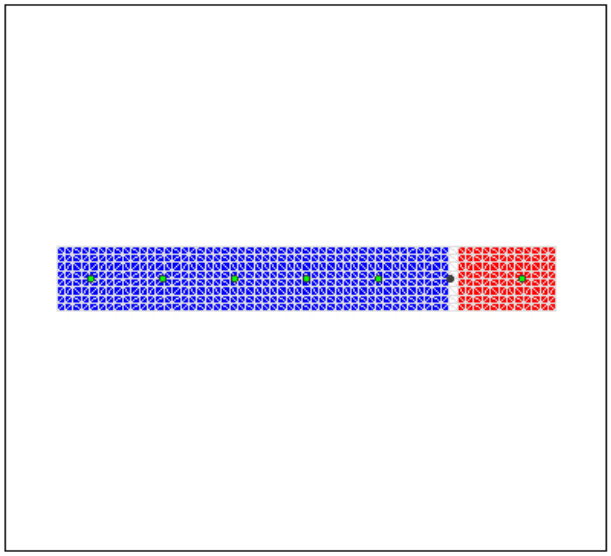

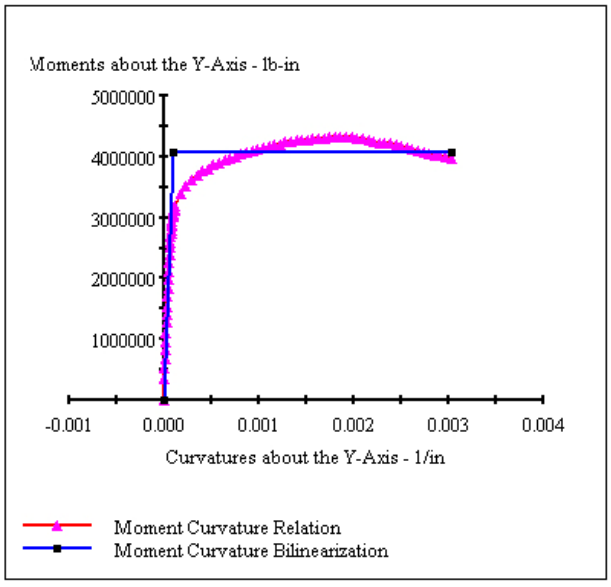

XTRACT Analysis Report - Educational

Thomas Hervillard
Washington State University
10/30/2005

Section Name: Section1
Loading Name: Loading
Analysis Type: Moment Curvature

Matt - Wall 3 - Con-C-2Rho

Section Details:

X Centroid:	27.81 in
Y Centroid:	3.813 in
Section Area:	424.2 in^2

Loading Details:

Constant Load - P:	14.42E+3 lbs
Incrementing Loads:	Myy Only
Number of Points:	80
Analysis Strategy:	Displacement Control

Analysis Results:

Failing Material:	Con-C-2Rho
Failure Strain:	32.00E-3 Compression
Curvature at Initial Load:	-.8031E-20 1/in
Curvature at First Yield:	57.42E-6 1/in
Ultimate Curvature:	2.081E-3 1/in
Moment at First Yield:	2.381E+6 lb-in
Ultimate Moment:	3.102E+6 lb-in
Centroid Strain at Yield:	.8047E-3 Ten
Centroid Strain at Ultimate:	18.25E-3 Ten
N.A. at First Yield:	14.01 in
N.A. at Ultimate:	8.769 in
Energy per Length:	7878 lbs
Effective Yield Curvature:	93.38E-6 1/in
Effective Yield Moment:	3.872E+6 lb-in
Over Strength Factor:	.8010
Plastic Rotation Capacity:	26.66E-3 rad
EI Effective:	4.15E+7 kip-in^2
Yield EI Effective:	0 kip-in^2
Bilinear Harding Slope:	0 %
Curvature Ductility:	22.29

Comments:

User Comments

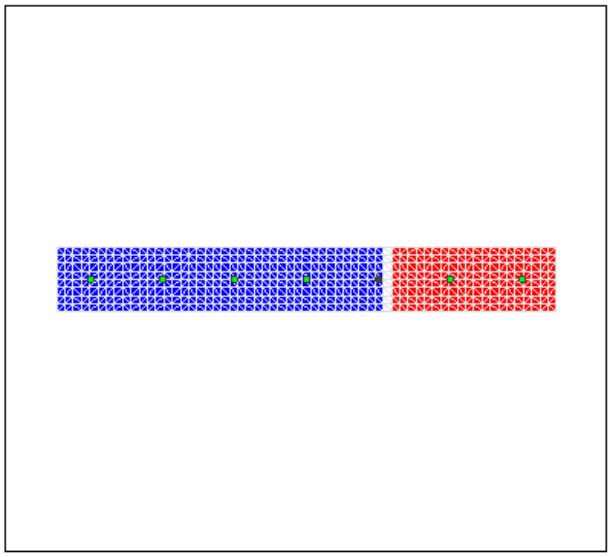

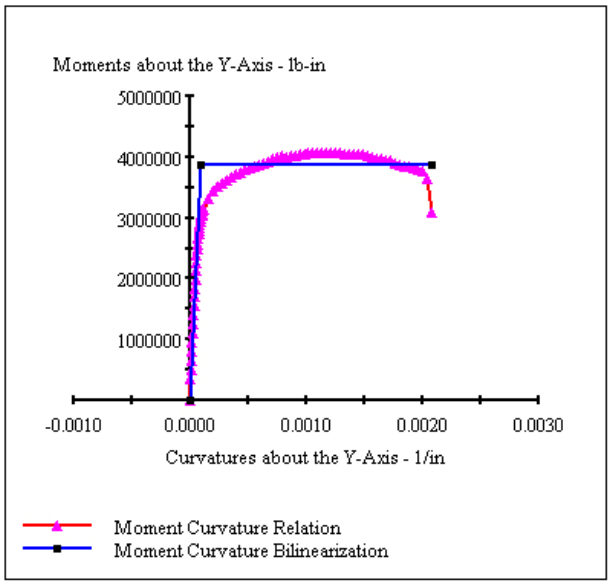

XTRACT Analysis Report - Educational

Thomas Hervillard
Washington State University
10/30/2005

Section Name: Section1
Loading Name: Loading
Analysis Type: Moment Curvature

Matt - Wall 4 - Con-F1-2Rho

Section Details:

X Centroid:	27.81 in
Y Centroid:	3.813 in
Section Area:	424.2 in^2

Loading Details:

Constant Load - P:	14.42E+3 lbs
Incrementing Loads:	Myy Only
Number of Points:	80
Analysis Strategy:	Displacement Control

Analysis Results:

Failing Material:	Con-F1-2Rho
Failure Strain:	23.00E-3 Compression
Curvature at Initial Load:	-.1317E-19 1/in
Curvature at First Yield:	52.07E-6 1/in
Ultimate Curvature:	1.573E-3 1/in
Moment at First Yield:	2.204E+6 lb-in
Ultimate Moment:	3.399E+6 lb-in
Centroid Strain at Yield:	.7224E-3 Ten
Centroid Strain at Ultimate:	20.25E-3 Ten
N.A. at First Yield:	13.87 in
N.A. at Ultimate:	12.87 in
Energy per Length:	5720 lbs
Effective Yield Curvature:	88.43E-6 1/in
Effective Yield Moment:	3.743E+6 lb-in
Over Strength Factor:	.9083
Plastic Rotation Capacity:	19.91E-3 rad
EI Effective:	4.23E+7 kip-in^2
Yield EI Effective:	0 kip-in^2
Bilinear Harding Slope:	0 %
Curvature Ductility:	17.78

Comments:

User Comments

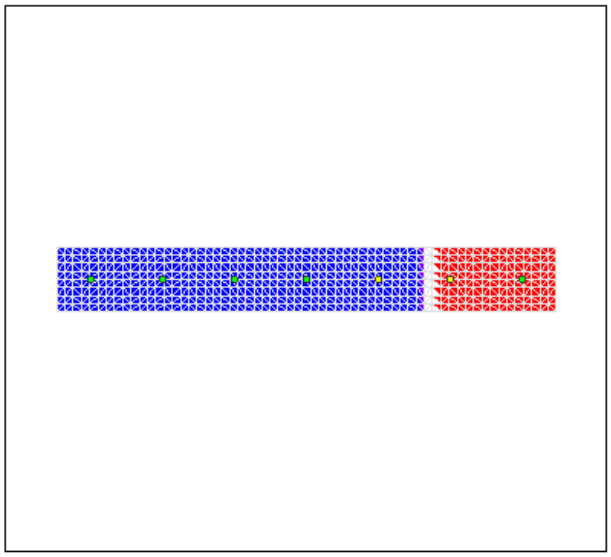

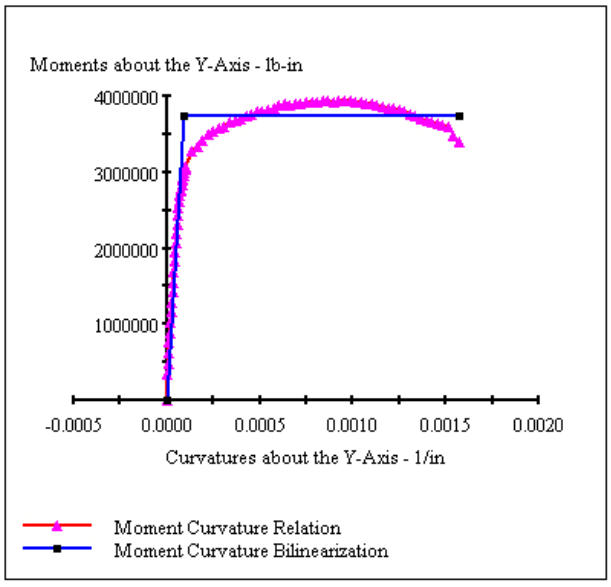

XTRACT Analysis Report - Educational

Thomas Hervillard
Washington State University
10/30/2005

Section Name: Section1
Loading Name: Loading
Analysis Type: Moment Curvature

Section Details:

X Centroid:	27.81 in
Y Centroid:	3.813 in
Section Area:	424.2 in^2

Loading Details:

Constant Load - P:	14.42E+3 lbs
Incrementing Loads:	Myy Only
Number of Points:	80
Analysis Strategy:	Displacement Control

Analysis Results:

Failing Material:	Steel-Matt
Failure Strain:	.1200 Tension
Curvature at Initial Load:	-.2844E-19 1/in
Curvature at First Yield:	57.29E-6 1/in
Ultimate Curvature:	3.028E-3 1/in
Moment at First Yield:	2.392E+6 lb-in
Ultimate Moment:	3.963E+6 lb-in
Centroid Strain at Yield:	.8078E-3 Ten
Centroid Strain at Ultimate:	47.46E-3 Ten
N.A. at First Yield:	14.10 in
N.A. at Ultimate:	15.68 in
Energy per Length:	12.16E+3 lbs
Effective Yield Curvature:	97.78E-6 1/in
Effective Yield Moment:	4.083E+6 lb-in
Over Strength Factor:	.9707
Plastic Rotation Capacity:	43.43E-3 rad
EI Effective:	4.18E+7 kip-in^2
Yield EI Effective:	0 kip-in^2
Bilinear Harding Slope:	0 %
Curvature Ductility:	30.96

Comments:

User Comments

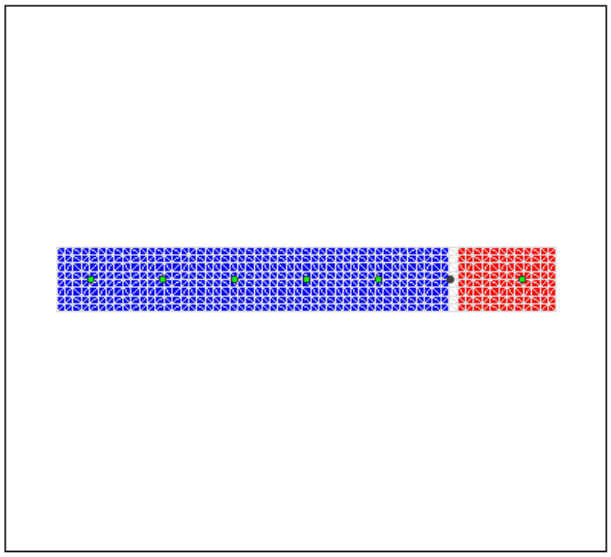

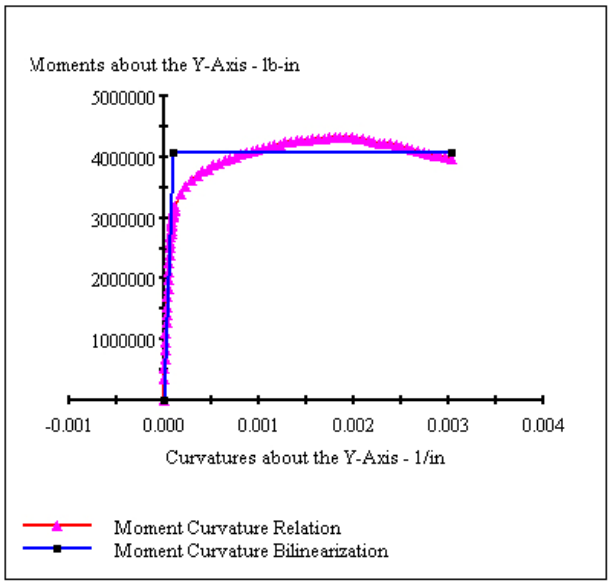

XTRACT Analysis Report - Educational

Thomas Hervillard
Washington State University
10/30/2005

Section Name: Section1
Loading Name: Loading
Analysis Type: Moment Curvature

Matt - Wall 7 - Con-C-2Rho

Section Details:

X Centroid:	27.81 in
Y Centroid:	3.813 in
Section Area:	424.2 in^2

Loading Details:

Constant Load - P:	14.42E+3 lbs
Incrementing Loads:	Myy Only
Number of Points:	80
Analysis Strategy:	Displacement Control

Analysis Results:

Failing Material:	Con-C-2Rho
Failure Strain:	32.00E-3 Compression
Curvature at Initial Load:	-.8031E-20 1/in
Curvature at First Yield:	57.64E-6 1/in
Ultimate Curvature:	2.145E-3 1/in
Moment at First Yield:	2.385E+6 lb-in
Ultimate Moment:	3.362E+6 lb-in
Centroid Strain at Yield:	.7994E-3 Ten
Centroid Strain at Ultimate:	23.40E-3 Ten
N.A. at First Yield:	13.87 in
N.A. at Ultimate:	10.91 in
Energy per Length:	8165 lbs
Effective Yield Curvature:	94.06E-6 1/in
Effective Yield Moment:	3.892E+6 lb-in
Over Strength Factor:	.8637
Plastic Rotation Capacity:	30.40E-3 rad
EI Effective:	4.14E+7 kip-in^2
Yield EI Effective:	0 kip-in^2
Bilinear Harding Slope:	0 %
Curvature Ductility:	22.80

Comments:

User Comments

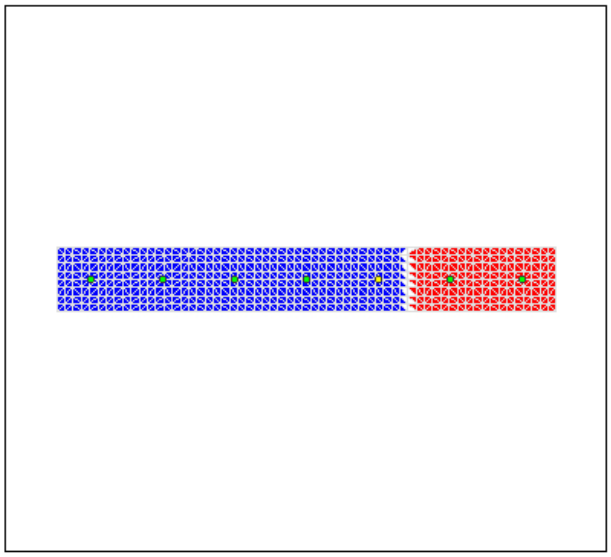

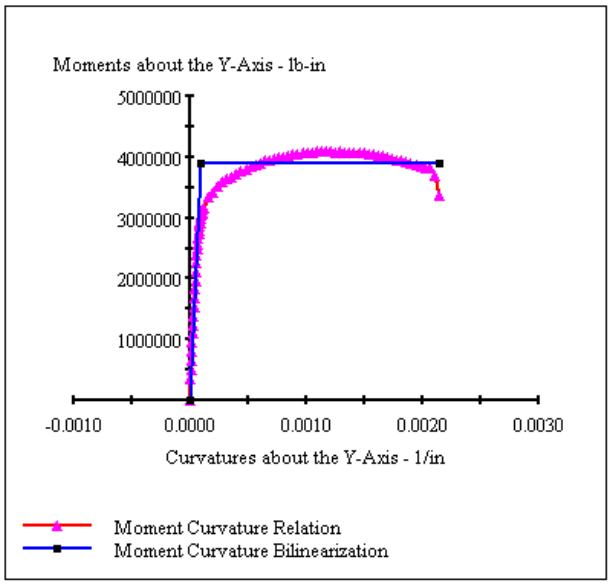

XTRACT Analysis Report - Educational

Thomas Hervillard
Washington State University
10/30/2005

Section Name: Section1
Loading Name: Loading
Analysis Type: Moment Curvature

Matt - Wall 8 - Con-F1-2Rho

Section Details:

X Centroid:	27.81 in
Y Centroid:	3.813 in
Section Area:	424.2 in^2

Loading Details:

Constant Load - P:	14.42E+3 lbs
Incrementing Loads:	Myy Only
Number of Points:	80
Analysis Strategy:	Displacement Control

Analysis Results:

Failing Material:	Con-F1-2Rho
Failure Strain:	23.00E-3 Compression
Curvature at Initial Load:	-.1317E-19 1/in
Curvature at First Yield:	52.07E-6 1/in
Ultimate Curvature:	1.573E-3 1/in
Moment at First Yield:	2.204E+6 lb-in
Ultimate Moment:	3.399E+6 lb-in
Centroid Strain at Yield:	.7224E-3 Ten
Centroid Strain at Ultimate:	20.25E-3 Ten
N.A. at First Yield:	13.87 in
N.A. at Ultimate:	12.87 in
Energy per Length:	5720 lbs
Effective Yield Curvature:	88.43E-6 1/in
Effective Yield Moment:	3.743E+6 lb-in
Over Strength Factor:	.9083
Plastic Rotation Capacity:	22.00E-3 rad
EI Effective:	4.23E+7 kip-in^2
Yield EI Effective:	0 kip-in^2
Bilinear Harding Slope:	0 %
Curvature Ductility:	17.78

Comments:

User Comments

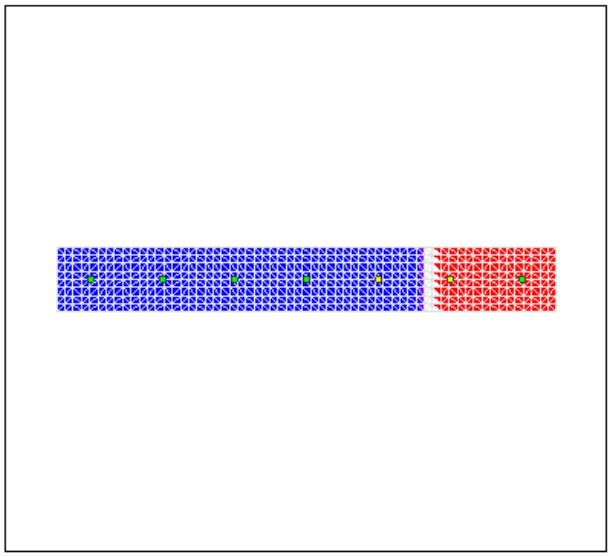

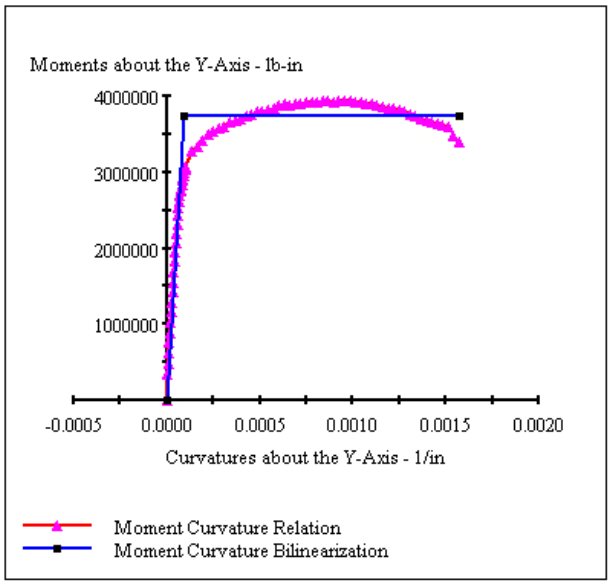

XTRACT Analysis Report - Educational

Thomas Hervillard
Washington State University
10/30/2005

Section Name: Section1
Loading Name: Loading
Analysis Type: Moment Curvature

Matt - Wall 9 - Con-F2-2Rho

Section Details:

X Centroid:	27.81 in
Y Centroid:	3.813 in
Section Area:	424.2 in^2

Loading Details:

Constant Load - P:	14.42E+3 lbs
Incrementing Loads:	Myy Only
Number of Points:	80
Analysis Strategy:	Displacement Control

Analysis Results:

Failing Material:	Con-F2-2Rho
Failure Strain:	26.00E-3 Compression
Curvature at Initial Load:	.2736E-19 1/in
Curvature at First Yield:	57.40E-6 1/in
Ultimate Curvature:	1.779E-3 1/in
Moment at First Yield:	2.404E+6 lb-in
Ultimate Moment:	3.470E+6 lb-in
Centroid Strain at Yield:	.8052E-3 Ten
Centroid Strain at Ultimate:	23.30E-3 Ten
N.A. at First Yield:	14.03 in
N.A. at Ultimate:	13.10 in
Energy per Length:	6651 lbs
Effective Yield Curvature:	91.63E-6 1/in
Effective Yield Moment:	3.838E+6 lb-in
Over Strength Factor:	.9043
Plastic Rotation Capacity:	25.01E-3 rad
EI Effective:	4.19E+7 kip-in^2
Yield EI Effective:	0 kip-in^2
Bilinear Harding Slope:	0 %
Curvature Ductility:	19.41

Comments:

User Comments

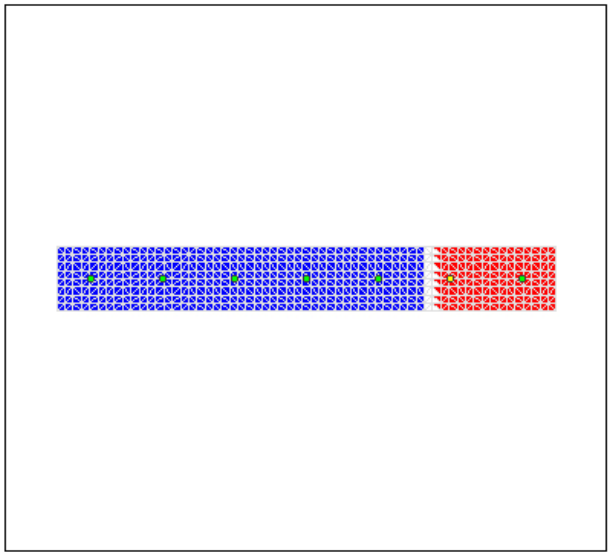

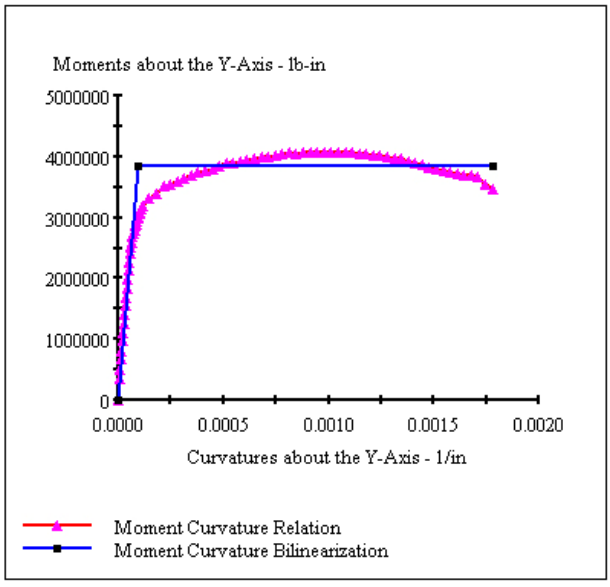

APPENDIX K

This appendix compares load-displacement curves based on Xtract results for walls confined with once or twice the confinement reinforcement ratio ρ.

Wall 2: Aspect ratio: 0.93 – Steel plates – 7#5@8

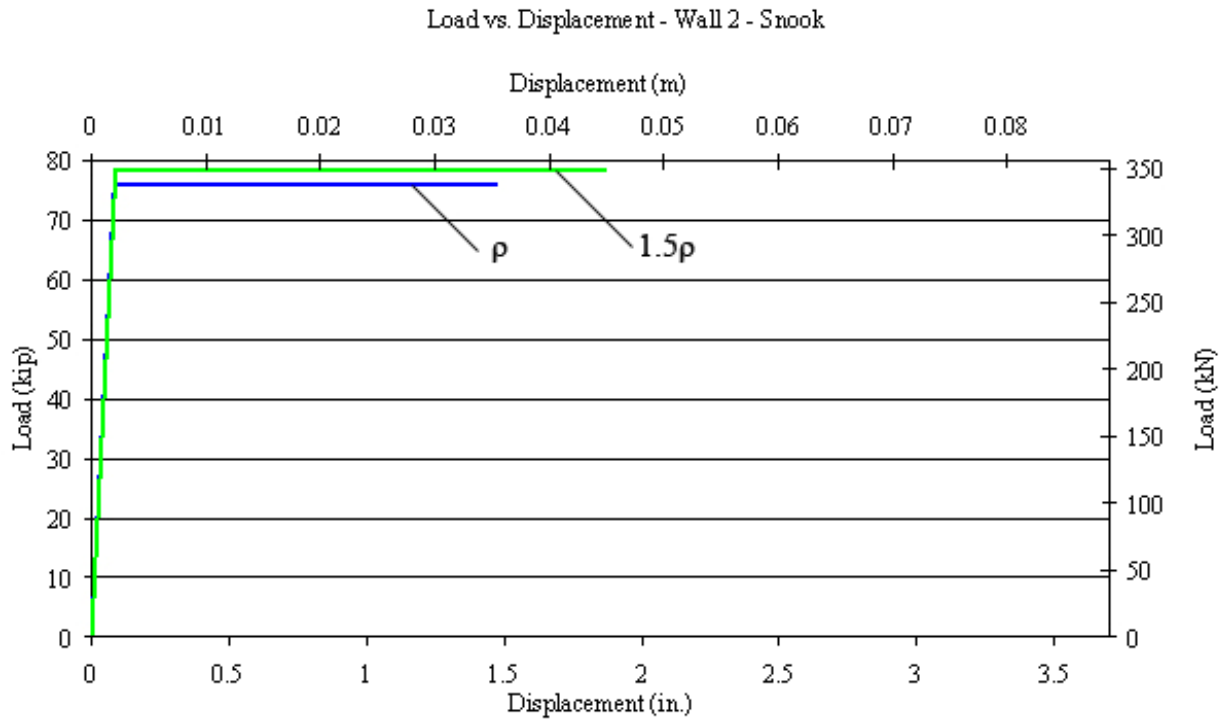

Wall 3: Aspect ratio: 0.93 – Seismic combs – 7#5@8

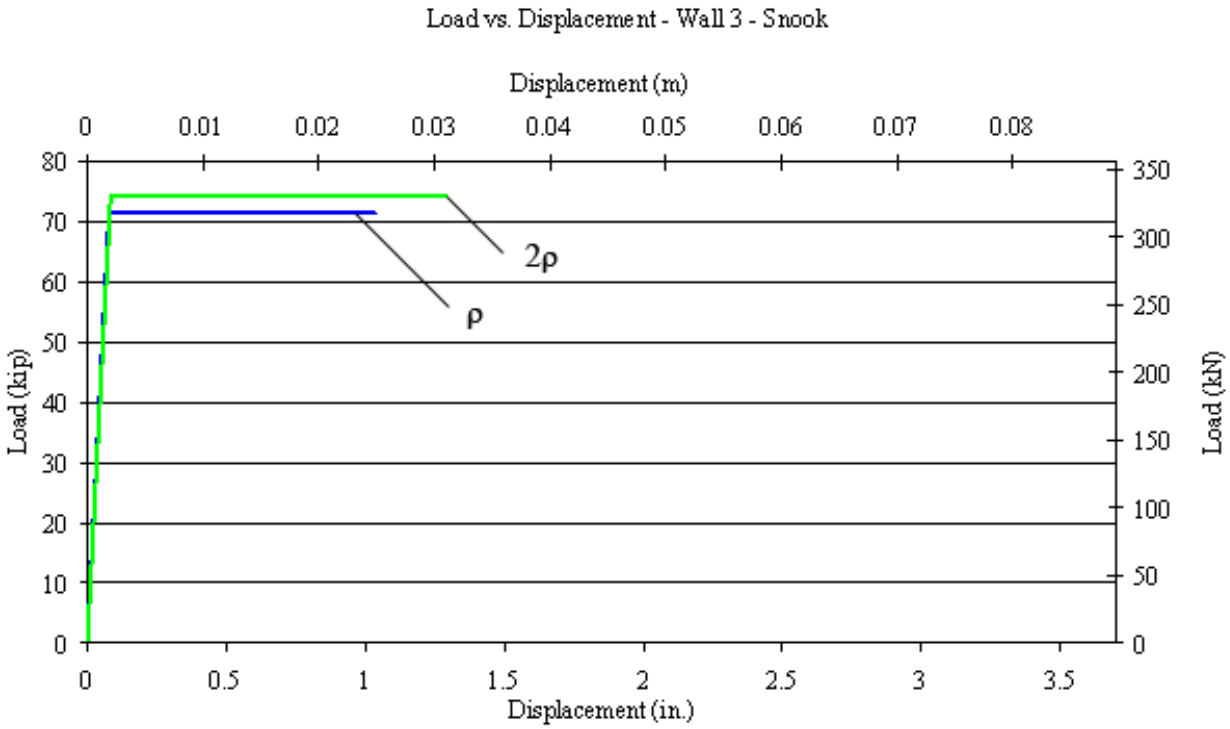

Wall 4: Aspect ratio: 0.93 – Fiber 1 – 7#5@8

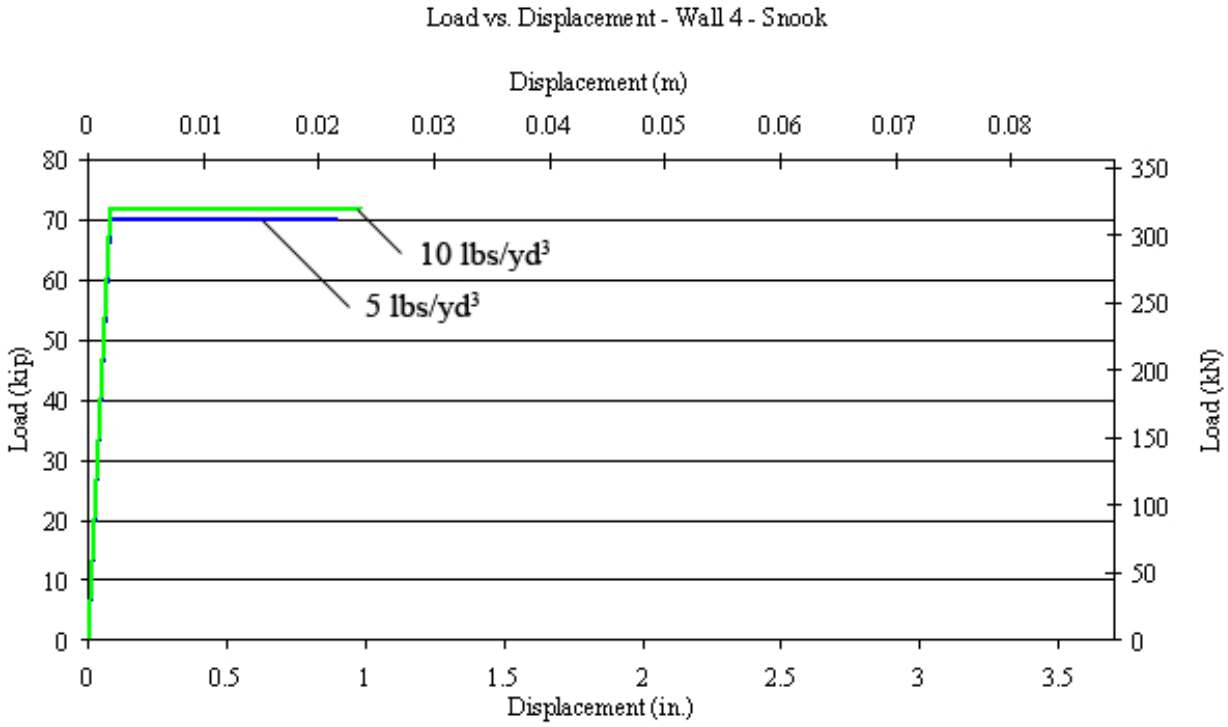

Wall 6: Aspect ratio: 1.51 – Steel plates – 7#5@8

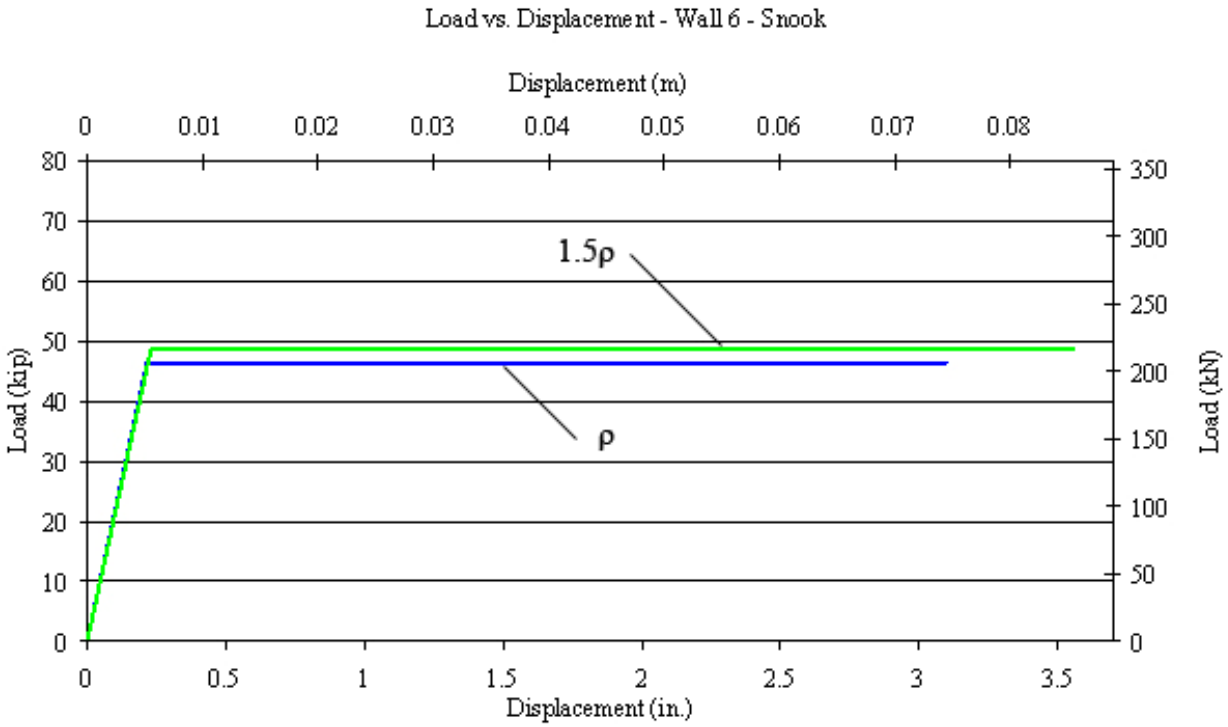

Wall 7: Aspect ratio: 1.51 – Seismic combs – 7#5@8

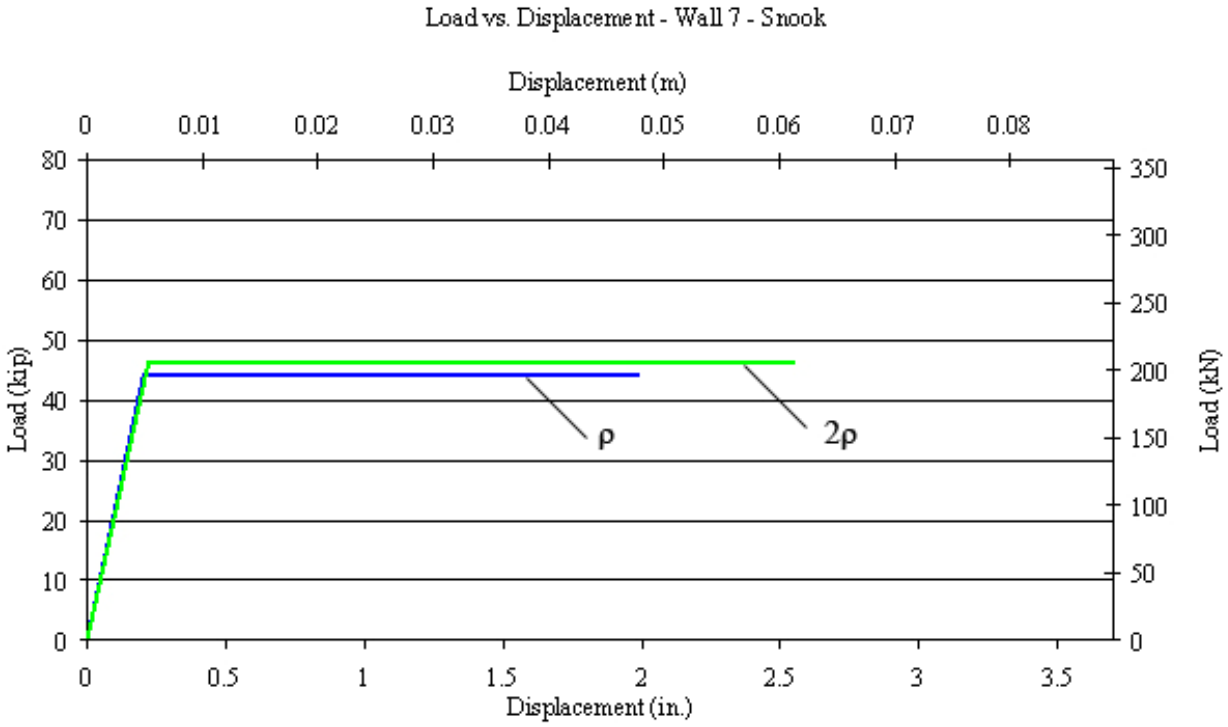

Wall 8: Aspect ratio: 1.51 – Fiber 1 – 7#5@8

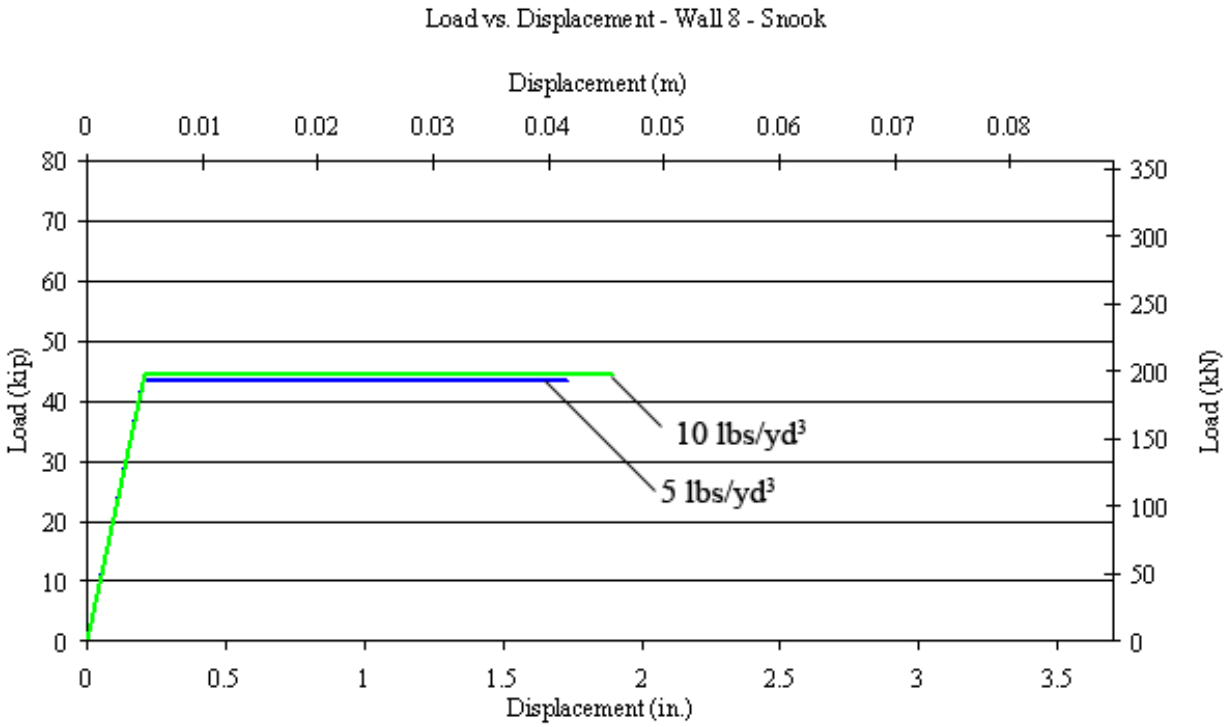

Wall 9: Aspect ratio: 1.51 – Fiber 2 – 7#5@8